This is to certify that the

thesis entitled

PRINCIPAL COMPONENT ANALYSIS OF RAPID SCANNING SPECTROSCOPY EXPERIMENTS IN CHEMICAL KINETICS

presented by

Robert N. Cochran

has been accepted towards fulfillment
of the requirements for

Ph.D. degree in Chemistry

Frederick W. Dorne

Major professor

Date 8/4/77

PRINCIPAL COMPONENT ANALYSIS OF RAPID SCANNING SPECTROSCOPY EXPERIMENTS IN CHEMICAL KINETICS

By

Robert N. Cochran

A DISSERTATION

Submitted to

Michigan State University

in partial fulfillment of the requirements

for the degree of

DOCTOR OF PHILOSOPHY

Department of Chemistry

1977

ABSTRACT

PRINCIPAL COMPONENT ANALYSIS OF RAPID SCANNING SPECTROSCOPY EXPERIMENTS IN CHEMICAL KINETICS

By

Robert N. Cochran

Principal component analysis is used to develop a procedure for extracting spectral and kinetic information from rapid scanning kinetics experiments. The procedure is applied to a rapid scanning stopped flow study of the horse liver alcohol dehydrogenase (LADH) catalyzed reduction of the substrate analog, p-nitroso-N,N-dimethylaniline (NDMA) by reduced nicotinamide adenine dinucleotide (NADH).

The first step of the procedure is to determine, independently of any mechanistic assumptions and of any assumptions about the spectral shapes of light absorbing species, the minimum number of light absorbing species (absorbers) in each scanning experiment. Two kinds of principal component analysis, M analysis and S analysis, yield, respectively, the minimum number m of absorbers in the experiment and the minimum number s of absorbers whose concentrations must have changed during the experiment. Errors caused by variations of the experimental signal-to-noise ratio with wavelength and time are

eliminated by statistically weighting the principal component calculations according to a general model of error variances. Further steps in the principal component procedure use the eigenvectors and eigenvalues from the weighted M and S analyses as tools for extracting from each scanning experiment the static spectra and concentration profiles of its absorbers without invoking mechanistic assumptions.

Analysis of the LADH-NDMA-NADH experiments reveals that the reaction has at least seven absorbers over the wavelength range 250 nm - 614 nm. The static spectra and concentration profiles extracted by principal component analysis show that at least three of these absorbers are transient intermediates in the sense that their concentrations grow and then decay in each experiment. The resolved concentration profiles of these absorbers give a set of qualitative observations that should be accounted for by mechanisms proposed for the reaction. In particular, the resolved concentration profile of the substrate NDMA in these experiments is incompatible with the mechanism proposed for the reaction by Dunn and Bernhard (1971). Some mechanisms that might be consistent with the qualitative observations are discussed.

In addition, the rate equations for the reversible Michaelis-Menten mechanism are integrated to first order in a singular perturbation scheme. The solutions, which hold for the entire time course of the reaction reveal

the range of validity of the steady state assumption in enzyme kinetics, and they suggest the experimental conditions necessary for extracting rate constants from pre-steady state data.

To Jane

ACKNOWLEDGMENTS

I wish to thank the National Science Foundation and the Department of Chemistry for financial support in the form of research and teaching assistantships.

I am most grateful to Dr. Frederick H. Horne, whose perceptive guidance, enthusiasm, and active participation made this thesis possible. I am also indebted to Drs. James L. Dye and Clarence H. Suelter, for including me in their enzyme kinetics project and for their encouragement and active participation in the research reported here.

I would like to thank Dr. James V. Beck for his excellent course on parameter estimation in engineering and science, which started my interest in the statistical design and analysis of experiments. I thank Dr. J. Sutherland Frame for his stimulating seminar series on matrix modeling, and for helpful discussions concerning the matrix models in this thesis.

I would like to thank Dr. Joseph Ceraso for his assistance in performing the stopped flow experiments in Chapter 4. I am grateful to Dr. William Waller for helpful discussion about the computer aspects of this work, and especially for providing his matrix diagonalization subrouting DIAG1. I wish to thank Dr. Tom Atkinson for providing programs that transferred our data from the minicomputer to the CDC-6500 computer, and for helping me use his two-dimensional multiple curve plotting package MULPLT

to prepare many of the figures in Chapter 4, and Mr. David Cox, who pointed out the usefulness and availability of the three dimensional plotting package GEOSYS.

Finally, I am grateful to my wife Jane for her patience and encouragement during the completion of this thesis, and for her art work which appears in Chapter 4.

TABLE OF CONTENTS

LIST OF TABLES

LIST OF FIGURES

Figure Page

CHAPTER 1

INTRODUCTION

The application of rapid scanning spectroscopic measurements to chemical kinetics experiments has been accelerated by the development of computer assisted data acquisition systems. (Dye and Feldman, 1966; Santini, Milano, and Pardue, 1973; Papadakis, Coolen, and Dye, 1975; Coolen, et al., 1975; Milano and Pardue, 1975; Miller, et al., 1975; and Hollaway and White, 1975.) A single rapid scanning kinetics experiment gives a three dimensional surface of a spectrophotometric response, such as absorbance, versus wavelength and time (see Figure 4.3). Each surface is the result of contributions from absorbing reactants, products, catalysts, and transient intermediates. Thus, rapid scanning spectroscopy can be a powerful tool for spectrally and kinetically characterizing complex reacting systems, if we can extract the spectral and kinetic information from each surface.

In Chapters 2 and 3 we develop the methodology for extracting the static spectra and concentration-time profiles of each absorber in a rapid scanning kinetics experiment, and in Chapter 4 we illustrate this methodology by applying it to a rapid scanning stopped flow study of a reaction catalyzed by the enzyme horse liver alcohol dehydrogenase (LADH). In this introductory chapter, we

present an overall view of the analysis of rapid scanning kinetics data.

Figure 1.1 shows in flow-diagram form, the steps involved in a rapid scanning kinetics study. First, we measure absorbance versus time and wavelength for a variety of initial conditions - the more the better. The varied initial conditions may be initial concentration, pH, temperature, and any other variables that might affect the course of the reaction. The chosen wavelength range should include all suspected absorbers whose spectral and kinetic properties are to be characterized in the study. Each experiment should, if possible, extend in time until absorbance is not changing at any wavelength in the scanning range of the experiment.

Each surface measured in Step 1 contains information about the static spectrum and concentration-time profile of each absorber in the reaction. The ultimate goal of a rapid scanning kinetics study is to identify one or more kinetic mechanisms that satisfactorily explain the concentration-time profiles of each absorber. However, we must first extract these concentration profiles from the experiments. Moreover, we need to be able to extract the static spectra and concentration profiles before proposing a specific kinetic mechanism since a kinetic mechanism presupposes that the concentration profiles are already known. Therefore, in Steps 2 and 3 of Figure 1.1 we extract the static spectra and concentration profiles

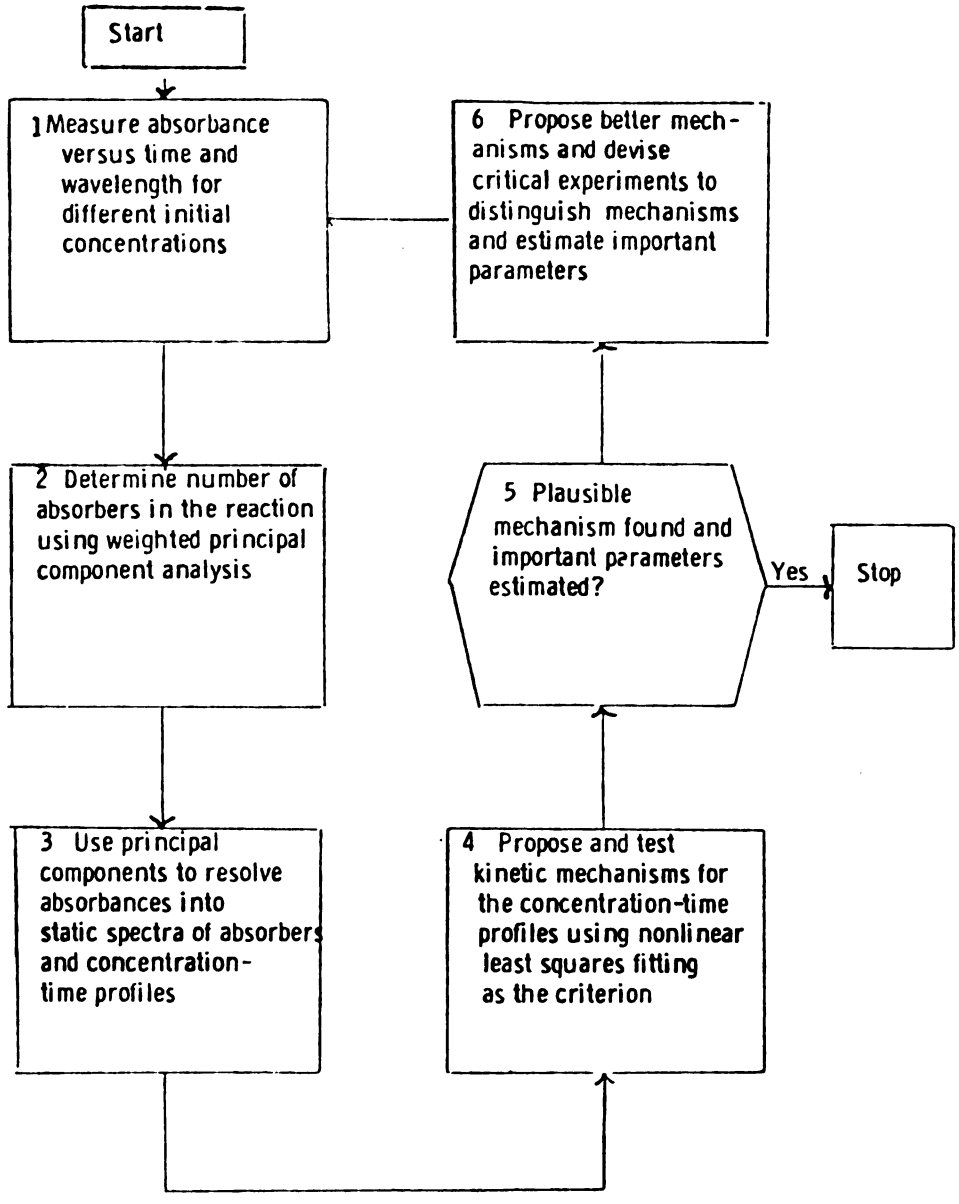

Figure 1.1. Strategy for a rapid scanning kinetics study.

before proposing kinetic mechanisms in Step 4.

We do not know how many absorbers occur in an experiment before we analyze it. Although we usually know which of the chemicals initially mixed are absorbers, and although we sometimes know which products are absorbers, we usually do not know how many light absorbing transient intermediates occur in the reaction. In Step 2, we determine by the method of weighted principal component analysis (Cochran and Horne, 1977) the minimum number of absorbers required to explain each scanning experiment and how many of these change concentrations. This method, presented in Chapter 2, requires no assumptions about the spectral shapes of the absorbers or the kinetic mechanism of the reaction.

In Step 3, we use an extension of the weighted principal component analysis method presented in Chapter 3 to resolve each scanning experiment into the static spectra and concentration profiles of its absorbers. Again, we avoid proposing a particular kinetic mechanism to extract this information. Instead we resolve the whole experiment by using the measured static spectra of suspected absorbers (reactants, products, and catalysts) plus information obtained by analyzing subspaces of wavelength and time that have been shown to contain fewer absorbers than the whole experiment.

In Chapter 4 we apply Steps 1 through 3 of Figure 1.1 to characterize spectrally and kinetically a complex

reaction catalyzed by the enzyme horse liver alcohol dehydrogenase. Weighted principal component analysis reveals that in the wavelength range 250 nm - 614 nm this reaction has at least seven absorbers. The static spectra and concentration profiles determined in Step 3 show that at least three of these absorbers are transient intermediates in the sense that their concentrations grow and then decay in each experiment.

Steps 4 through 6 are the advanced stages of a kinetics study. Armed with the static spectra and concentration profiles determined in Steps 1 through 3, we propose and test kinetic mechanisms. Each proposed mechanism contains adjustable parameters (rate constants, activation energies, and equilibrium constants.) The criterion for whether a proposed kinetic mechanism explains the experiments is to determine how well its predicted concentrations fit the concentrations extracted from the experiments when the parameters are adjusted by weighted nonlinear least squares. This step can be performed with a nonlinear least squares program such as KINFIT (Dye and Nicely, 1971). However, a typical mechanism for four or more absorbers in a single experiment may contain eight or more adjustable rate constants. A frequently encountered problem with so many adjustable parameters is that they cannot all be determined since some of them are coupled to each other. Insights into the solution of this common and troublesome problem can be found in the theory of sensitivity analysis applied

to parameter estimation, discussed in Box and Lucas (1959), Atkinson and Hunter (1968), Hill and Hunter (1974), Beck and Arnold (1975), Himmelblau (1970), Cukier, et al. (1973), Schaibly and Shuler (1973), and Cukier, et al. (1975).

If Step 5 indicates that our mechanism describes the experiments and that we have estimated its important parameters, we may terminate the study. However, if we have several mechanisms all of which describe the data, or if the important parameters in our mechanism are estimated poorly from fitting the available data, we proceed to Step 6.

In Step 6 we design critical experiments to distinguish between competing mechanisms and estimate parameters. Sensitivity analysis gives a criterion that can be used to design optimal experiments for estimating all the parameters or subgroups of parameters (Beck and Arnold, 1975; Hill and Hunter, 1974). Hunter and Reiner (1965), Box and Hill (1967), and Hill, Hunter, and Wichern (1968) have devised methods for the optimal design of critical experiments to distinguish between two or more rival mechanisms. Ultimately, we return to Step 1 to repeat the cycle by performing the critical experiments devised in Step 6.

The research reported in this dissertation is complete through Steps 1, 2, and 3. In the last section of Chapter 4, we discuss critically some mechanistic hypotheses

proposed by others for this enzyme system, and we speculate on mechanisms which might conform to our experimental results. Steps 4 through 6 have not been taken.

In Chapter 5 we treat the reversible, simple Michaelis-Menten mechanism, the simplest kinetic mechanism used to describe an enzyme catalyzed reaction. In particular, we present a singular perturbation solution of the nonlinear, stiff differential equations that occur. The singular perturbation method gives explicit algebraic solutions to these differential equations. In general, numerical solutions such as obtained with Gear's algorithm (Gear, 1971) are more practical than algebraic solutions because the numerical methods are easier to apply. However, the singular perturbation solution presented in Chapter 5 is instructive in revealing through its dimensional analysis the justification of the steady state assumption in enzyme kinetics. The explicit solutions also suggest experimental conditions necessary for extracting rate constants from pre-steady state data.

CHAPTER 2

STATISTICALLY WEIGHTED PRINCIPAL COMPONENT ANALYSIS OF RAPID SCANNING WAVELENGTH KINETICS EXPERIMENTS

A. INTRODUCTION

The development of sophisticated computer interfaced data collection systems has made scanning wavelength kinetics experiments practical for times as short as the stopped flow time scale (Santini, Milano, and Pardue, 1973; Papadakis, Coolen and Dye, 1975; Coolen et al., 1975; Milano and Pardue, 1975; Miller et al., 1975; Holloway and White, 1975). In a typical scanning wavelength kinetics experiment a spectral region is rapidly and repeatedly scanned while a spectrophotometric response such as absorbance, fluorescence, or chemiluminescence is measured at a fixed number of wavelength channels across the spectrum during each scan. If the time duration of each scan is short compared to the fastest spectrophotometrically detectable process in the reaction, the data can be regarded as a series of N consecutive, instantaneous spectra measured at p wavelength channels and can be represented by a (pxN) matrix $\underline{A}$, where A_{ij} is the spectrophotometric response measured at wavelength channel i at the time of scan j.

The reason for sampling this three dimensional space of response-wavelength-time instead of the simpler two dimensional space obtained in a fixed wavelength experiment is the need to characterize kinetic systems that contain more than one absorbing, fluorescing, or chemiluminescent solute. Whether the ultimate goal is to assay simultaneously several such solutes in a kinetic system with a known rate law, or to propose and test mechanisms for a complex reaction such as an enzyme system with detectable substrates, products, enzymes and enzyme-bound intermediates, a necessary first step in data analysis is to determine how many detectable solutes occur in the reaction. The multivariate statistical method of principal component analysis, which has been applied to spectral studies of multicomponent equilibrium systems (Kankare, 1970; Hugus and El-Awady, 1971; Lawton and Sylvestre, 1971; Sylvestre, Lawton and Maggio, 1974), band resolution of IR spectra (Bulmer and Shurvell, 1973), analysis of potentiometric data (Vadasdi, 1974), and analysis of mass spectra (Rozett and Petersen, 1975; Ritter, Lowry, Isenhour and Wilkins, 1976), is ideally suited for determining the number of detectable solutes in rapid scanning wavelength kinetics experiments.

The analogy between spectral studies of multicomponent equilibrium systems and scanning wavelength kinetics experiments and the applicability of principal component analysis to both was pointed out and demonstrated by

Sylvestre, Lawton, and Maggio (1974). In this chapter we extend the application to kinetics experiments and show that two kinds of principal component analysis are useful for kinetics experiments. Each requires only the matrix A, and each gives a lower bounds estimate of q, the number of solutes in the reaction with a spectrophotometric response. Second moment matrix principal component analysis, hereinafter called M analysis, gives for q a lower bounds estimate that is sensitive to the linear dependence of the concentrations of the detectable species. Sample covariance matrix principal component analysis, hereinafter called S analysis, gives an estimate that is sensitive to the linear dependence of the time rates of the concentrations. These two estimates of q are not necessarily the same, and we show that application of both analyses enables discrimination between mechanistic alternatives that would be indistinguishable with either analysis alone.

We first develop rules for the application of M and S analyses to errorless data. With this simplification the M and S estimates of q are the ranks of, respectively, the second moment matrix and the sample covariance matrix. We then discuss the effect of random measurement errors, and in particular the case in which the variance of the measurement errors is not constant throughout the experiment. The goal is to infer the essential ranks of the two matrices; i.e., the ranks that would obtain if

measurement errors could be eliminated. After demonstrating with a simple example that the usual procedure for inferring the two ranks gives incorrect results, we utilize a general error variance model to develop a weighting scheme that gives (i) correct estimates of the essential ranks, (ii) a low variance estimate of the errorless chemical reaction contribution to the data matrix, and (iii) a simple criterion for interpreting the eigenvalues of $\underline{M}$ and $\underline{S}$ in terms of their essential ranks. The weighting scheme is applicable to both kinetic and non-kinetic chemical applications of principal component analysis.

The starting point for both M and S analyses is the matrix model of the spectrophotometric data. The applicability of principal component analyses requires only that the response at each wavelength channel be a linear function of the concentration of each detectable species. We discuss in this thesis the analysis of absorbance data, where the linearity requirement is satisfied if Beer's Law holds. Similar linear laws occur for fluorescence and chemiluminescence, and the extension to these systems is straightforward. For errorless absorbance data in which Beer's Law holds, and from which the solvent baseline has been subtracted, the matrix model is

$$\underline{A} = \underline{F}\,\underline{C}^{T}, \qquad (2.1)$$

where $\underline{A}$ is a (pxN) matrix whose i, j element A_{ij} is the absolute absorbance measured at wavelength channel i in the spectrum scanned at time j. $\underline{F}$ is a (pxq) matrix defined by $\underline{F} = (\underline{f}_1, \underline{f}_2, \ldots, \underline{f}_q)$, where $\underline{f}_j$, hereinafter called the static spectrum of absorber j is a p component column vector whose i'th element is the product of the cell path length with the molar absorptivity of absorber j at wavelength channel i. $\underline{C}$ is a (Nxq) matrix defined $\underline{C} = (\underline{c}_1, \underline{c}_2, \ldots, \underline{c}_q)$, where $\underline{c}_j$, hereinafter called the concentration vector of absorber j, is an N component column vector whose i'th element is $c_j\ (t_i)$, the molarity of absorber j during spectrum i. Principal component analysis requires that the number of wavelength channels p and the number of consecutive spectra N are both larger than the number of absorbers q.

B. The Principal Component Method

The following example illustrates the application of M and S analyses to errorless data. Consider a three absorber reaction that follows the simple kinetic mechanism I,

$$A_1 \xrightarrow{k_1=3\ \text{sec}^{-1}} A_2, \qquad A_3 \xrightarrow{k_2=35\ \text{sec}^{-1}} A_2, \qquad \text{(I)}$$

where A_1, A_2, and A_3 represent absorbers one, two, and three. Suppose that over the wavelength range of the

experiment these three absorbers have the static spectra shown in Figure 2.1. An errorless experiment with 50 wavelength channels, 60 scans at 10 msec/scan, and initial concentrations $c_1(0) = c_3(0) = 0.001M$, would yield the absolute absorbance surface shown in Figure 2.2. The goal of the principal component analyses is to determine from just the information in Figure 2.2, with no prior information about the kinetic mechanism or the shapes of the static spectra, the minimum number of absorbers required to model the experiment, and of these absorbers, the minimum number that must change concentration during the experiment.

Since the mathematical details of principal component analysis are well documented (Anderson, 1963), we merely summarize the procedure here. The second moment matrix of $\underline{A}$ is the (pxp) matrix $\underline{M}$, defined by the equation

$$\underline{M} = (1/N)\ \underline{A}\ \underline{A}^T \qquad (2.2)$$

For an errorless experiment, the goal of M analysis is to obtain r_M, the rank of M, which by a standard matrix theorem (Bellman, 1970) equals r_A, the rank of $\underline{A}$. Since $r_A \leq q$, r_M is a lower limit to the number of absorbers in the reaction. We solve the eigenvalue problem

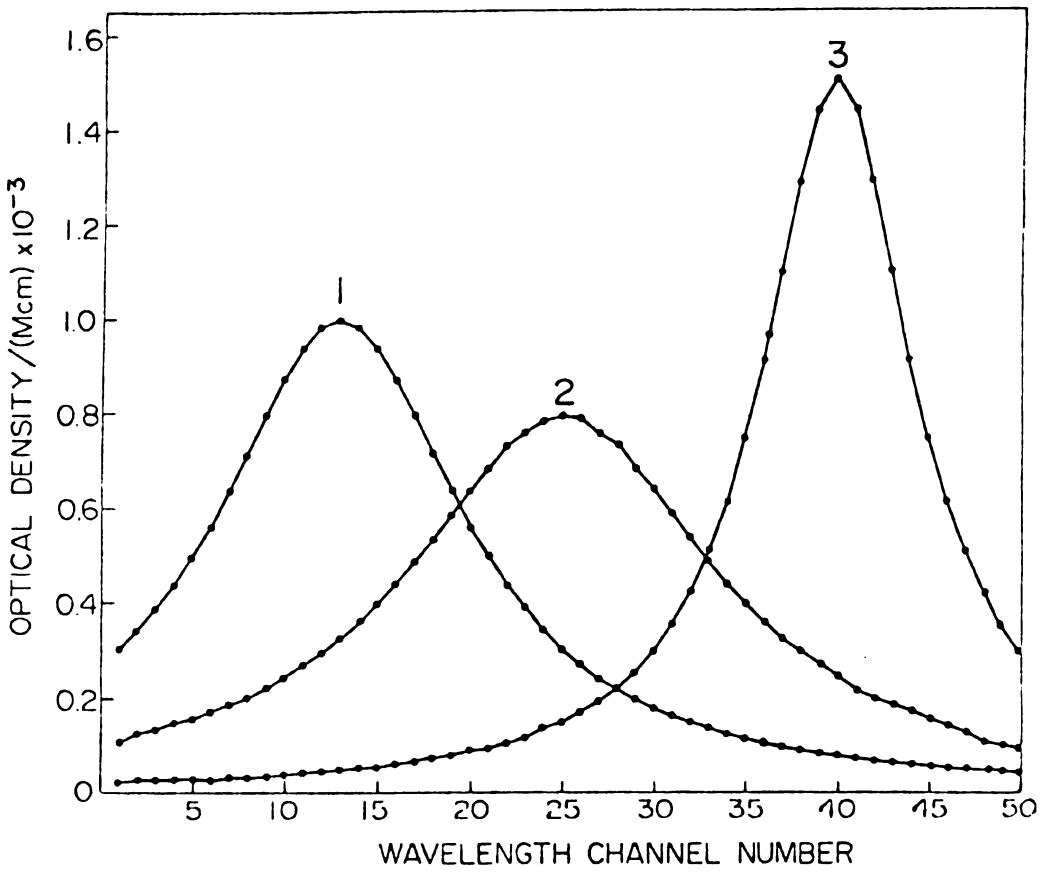

Figure 2.1. Static spectra of absorbers 1, 2, and 3 for the Mechanism I example.

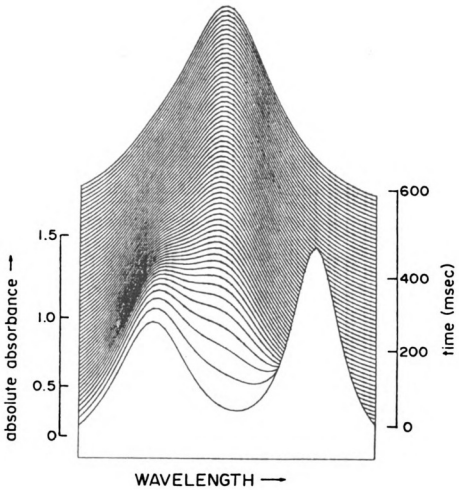

Figure 2.2. Errorless absolute absorbance surface A for Mechanism I.

$$\underline{M}\,\underline{\Phi} = \underline{\Phi}\,\underline{\Delta},\ \underline{\Phi}^T\underline{\Phi} = \underline{I},$$

$$\underline{\Delta} = \text{diag}\,(\delta_1,\delta_2,\ldots,\delta_p),$$

$$\delta_1 \geq \delta_2 \geq \delta_3 \geq ,\ldots, \geq \delta_p, \qquad (2.3)$$

where $\underline{\Delta}$ is the eigenvalue matrix and $\underline{\Phi}$ is a (pxp) matrix whose columns are the p orthonormal eigenvectors. For errorless data, there are two ways of obtaining r_M: (i) The rank of $\underline{M}$ equals the number of nonzero eigenvalues $\delta_1,\delta_2,\ldots,\delta_{r_M}$; (ii) Also, r_M is the lowest value of r for which $\hat{\underline{A}}_{(r)}$, defined by

$$\hat{\underline{A}}_{(r)} \equiv \underline{\Phi}_{(r)}\underline{\Phi}^T_{(r)}\underline{A} \qquad (2.4)$$

is exactly equal to $\underline{A}$, where $\underline{\Phi}_{(r)}$ is the (pxr) matrix whose r columns are the first r eigenvectors of $\underline{M}$. $\hat{\underline{A}}_{(r)}$ is called principal component estimate of $\underline{A}$. We demonstrate in Appendix A that $\hat{\underline{A}}_{(r_M)} = \underline{A}$ for an errorless experiment.

The sample covariance matrix of $\underline{A}$ is defined by

$$\underline{S} = [1/(N-1)](\underline{A}-\bar{\underline{A}})(\underline{A}-\bar{\underline{A}})^T, \qquad (2.5)$$

where $\bar{A}_{ij} = (1/N)\sum_{k=1}^{N} A_{ik}$. An S analysis gives r_S, the rank of $\underline{S}$, which is also the rank of $(\underline{A}-\bar{\underline{A}})$. Figure 2.3 is the $(\underline{A}-\bar{\underline{A}})$ surface for our example. The data plotted

in Figure 2.2 are plotted in Figure 2.3 after first subtracting the average of all 60 spectra from each spectrum. Figure 2.3 is thus a <u>difference surface</u>.

Given Beer's Law and errorless measurements, the matrix model of $(\underline{A}-\overline{\underline{A}})$ is

$$(\underline{A}-\overline{\underline{A}}) = \underline{F}\ \underline{H}^T, \qquad (2.6)$$

where $\underline{H}$ is an (Nxq) matrix defined by $\underline{H} = (\underline{h}_1, \underline{h}_2, \ldots \underline{h}_q)$, where

$$\underline{h}_i = \underline{c}_i - \overline{c}_i\underline{1},\ \overline{c}_i = 1/N \sum_{j=1}^{N} \overline{c}_i(t_j),$$

and where $\underline{1}$ is an N component column vector each of whose elements equals one. Equation (3.6) requires that $r_{(A-\overline{A})} \leq q$, and thus, r_S, like r_M, is a lower bounds estimate of the number of absorbers.

The rank of $\underline{S}$ has a further significance for kinetics, as follows. If we assume that the concentration of each absorber follows an arbitrary mass action rate law,

$$c_i(t_j) = c_i(o) + \int_o^{t_j} (dc_i/dt)dt,$$

then $h_i(t_j)$ is given by

$$h_i(t_j) = \int_o^{t_j} (dc_i/dt)dt - (1/N) \sum_{k=1}^{N} \int_o^{t_k} (dc_i/dt)dt. \qquad (2.7)$$

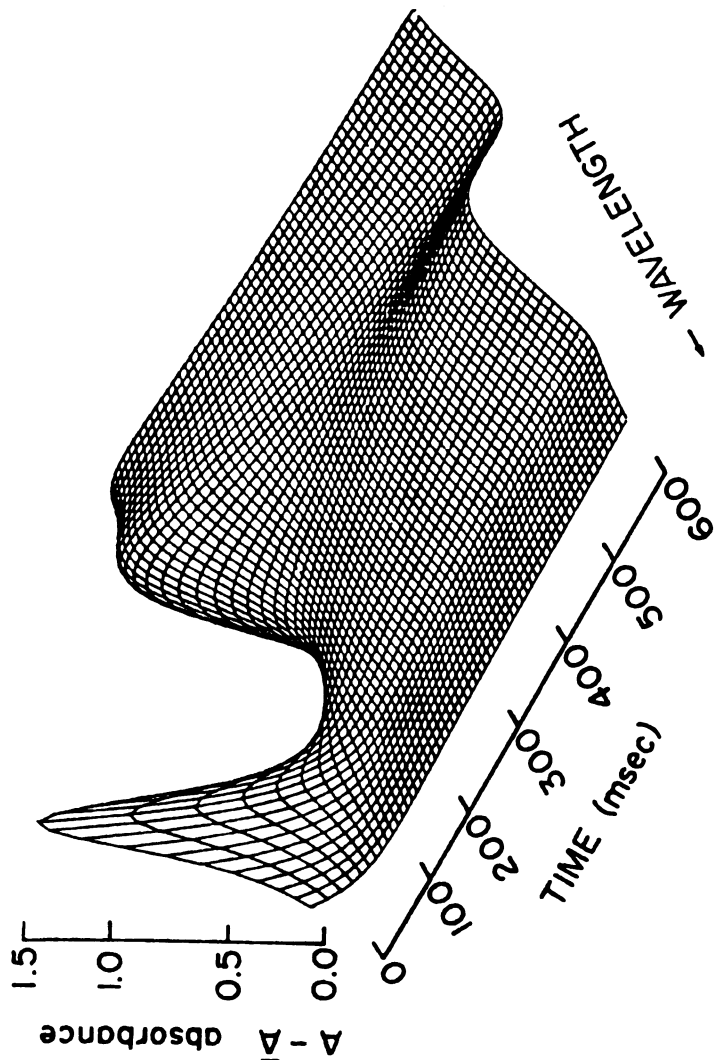

Figure 2.3. Errorless difference surface ($\underline{A}-\overline{\underline{A}}$) for Mechanism I.

Therefore, the rank of $\underline{H}$ equals the rank of $(d\underline{C}/dt)$, and for an errorless experiment, the rank of $\underline{S}$ equals the rank of $\underline{F}(d\underline{C}/dt)$. The rank of $\underline{S}$ is thus not only a lower limit to the number of absorbers in the reaction, but also a lower limit to the number of absorbers whose concentrations change independently of one another during the reaction.

In an S analysis we solve the eigenvalue problem

$$\underline{S}\ \underline{B} = \underline{B}\ \underline{A}, \qquad \underline{B}^T\underline{B} = \underline{I},$$

$$\underline{\Lambda} = \mathrm{diag}(\lambda_1,\lambda_2,\ldots,\lambda_p), \tag{2.8}$$

$$\lambda_1 \geq \lambda_2 \geq \lambda_3 \geq ,\ldots, \geq \lambda_p.$$

The rank of $\underline{S}$ equals the number of nonzero eigenvalues of $\underline{S}$ and is also the lowest value of r for which $(\hat{\underline{A}}_{(r)}-\overline{\underline{A}})$, defined

$$(\hat{\underline{A}}_{(r)}-\overline{\underline{A}}) \equiv \underline{B}_{(r)}\ \underline{B}^T_{(r)}(\underline{A}-\overline{\underline{A}}) \tag{2.9}$$

is an exact r principal component estimate of the experimental $(\underline{A}-\overline{\underline{A}})$ difference surface.

We apply these analyses to the errorless data in Figures 2.2 and 2.3. Table 2.1 lists the first four eigenvalues of $\underline{M}$ and $\underline{S}$; the remaining 46 eigenvalues of $\underline{M}$ and $\underline{S}$ are zero. Since there are three and two

Table 2.1

The First Four Eigenvalues of $\underline{M}$ and $\underline{S}$, Mechanism I

	M		S
1	35.58929	1	0.62866
2	0.55750	2	0.17361
3	0.16755	3	0.00000
4	0.00000	4	0.00000

nonzero eigenvalues of $\underline{M}$ and $\underline{S}$, respectively, we conclude that $r_M = 3$ and $r_S = 2$. Figure 2.4 shows the one principal component estimate of the $(\underline{A}-\overline{\underline{A}})$ data surface using Equation (2.9). We note that Figure 2.4 is not an exact reconstruction of the data surface shown in Figure 2.3. However, the two principal component estimate, $(\hat{\underline{A}}_{(2)}-\overline{\underline{A}})$, using Equation (2.9) is an exact reconstruction of the data surface in Figure 2.3, confirming that $r_S = 2$. Similarly, by observing that three is the lowest value of r for which $\hat{\underline{A}}_{(r)}$ given by Equation (2.4) is an exact reconstruction of the absolute absorbance surface in Figure 2.2, we confirm that $r_M = 3$.

From the data alone, without assuming a specific kinetic mechanism or anything about the static spectra, we have determined that three absorbers are required to

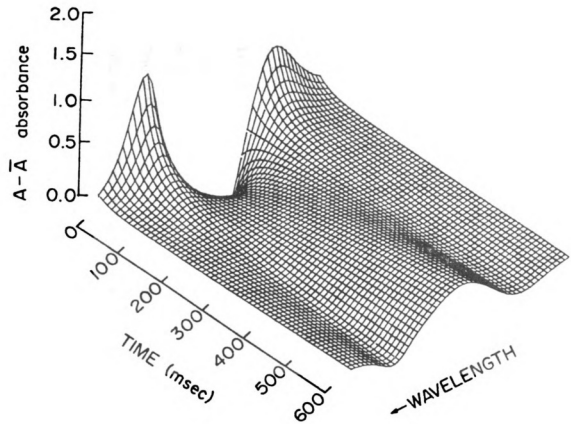

Figure 2.4. One principal component estimate ($\hat{\underline{A}}_{(1)}-\underline{\bar{A}}$) of the errorless difference surface.

explain the absolute absorbance surface in Figure 2.2 and that there are at least two absorbers whose concentrations change independently of one another during the reaction. Since this was a simulated experiment, we can check these answers against the known facts. There are three absorbers in the reaction and all three change concentration with time. However, Mechanism I has the constraint

$$dc_1/dt + dc_2/dt + dc_3/dt = 0.$$

Since this constraint says that the rate of one absorber depends on the rates of the other two, there are only two absorbers changing concentration independently. Thus, for this example, the equality holds in $r_M \leq q$, the inequality holds in $r_S \leq q$, and r_S equals the number of absorbers changing concentration independently during the reaction.

The goal of an actual experiment is of course the determination of a mechanism and its rate constants. When proposing mechanisms to explain an experiment, we can eliminate those mechanisms that do not give the (r_M, r_S) pair obtained from the M and S analyses of the experimental data. In the next section we give rules for deducing without numerical computation what (r_M, r_S) pair would occur for an errorless experiment given a kinetic mechanism, a set of rate constants, a set of

static spectra, and a set of initial concentrations. In the final two sections, we discuss estimation of the essential ranks of $\underline{M}$ and $\underline{S}$ from data containing varying amounts of random experimental error. These essential ranks follow the rules given for the actual ranks of $\underline{M}$ and $\underline{S}$ in errorless experiments.

C. Rules for the Ranks of M and S

From Equation (2.1), the rank of $\underline{A}$ depends on r_F, the rank of $\underline{F}$, and r_C, the rank of $\underline{C}$. This dependence is summarized in Table 2.2, which is obtained from standard theorems on matrices.

Table 2.2

Rules for the Rank of $\underline{M}$ for Errorless Experiments

	Conditions	Resulting r_M = Rank of $\underline{M}$
1	$r_F = r_C = q$	q
2	$r_F < r_C = q$	r_F
3	$r_C < r_F = q$	r_C
4	$r_C \leq r_F < q$	$\leq r_C$
5	$r_F \leq r_C < q$	$\leq r_F$

To use Table 2.2, we need rules for deducing r_F and r_C. The rank of $\underline{F}$ is given by

$$r_F = q - w, \tag{2.10}$$

where w is the number of linearly independent homogeneous equations that can be written among the static spectra of the q absorbers,

$$\sum_{j=1}^{q} a_{ij}\underline{f}_j = \underline{0}, \; i = 1,2,\ldots,w. \tag{2.11}$$

Similarly, the rank of $\underline{C}$ is given by

$$r_C = q - u, \tag{2.12}$$

where u is the number of linearly independent homogeneous equations that can be written among the concentration vectors of the q absorbers,

$$\sum_{j=1}^{q} b_{ij}\underline{c}_j = \underline{0}, \; i = 1,2,\ldots,u. \tag{2.13}$$

We use these rules to predict r_M for the example in the previous section. Since no equations of the form of Equation (2.11) exist, we have $r_F = 3 - 0 = 3$. Mass balance requires that

$$\underline{c}_1 + \underline{c}_2 + \underline{c}_3 = (c_1(0) + c_3(0))\,\underline{1} \tag{2.14}$$

where $c_1(0)$ and $c_3(0)$ are the initial concentrations of absorbers one and three, respectively. However, Equation (2.14) is an inhomogeneous linear equation, and is not of the form of Equation (2.13). Thus, we have $r_C = 3 - 0 = 3$, and, by Row 1 of Table 2.2, r_M is correctly predicted to be three.

Table 2.3

Rules for the Rank of $\underline{S}$ for Errorless Experiments

	Conditions	Resulting r_M = Rank of $\underline{M}$
1	$r_F = r_{\dot{C}} = q$	q
2	$r_F < r_{\dot{C}} = q$	r_F
3	$r_{\dot{C}} < r_F = q$	$r_{\dot{C}}$
4	$r_{\dot{C}} \leq r_F < q$	$\leq r_{\dot{C}}$
5	$r_F \leq r_{\dot{C}} < q$	$\leq r_F$

For errorless data the rank of $\underline{S}$ depends on the rank of $\underline{F}$ and the rank of $\dot{\underline{C}} = d\underline{C}/dt$. This dependence is summarized in Table 2.3. The rank of $\dot{\underline{C}}$ is given by

$$r_{\dot{C}} = q - v \tag{2.15}$$

where v is the number of linearly independent homogeneous

equations of the form

$$\sum_{j=1}^{q} g_{ij}\dot{\underline{c}}_j = \underline{0} \qquad i = 1,2,\ldots,v. \tag{2.16}$$

and where $\dot{\underline{c}}_j$ is an N component row vector whose k'th element is the rate (dc_j/dt) of increase of concentration of absorber j at the time of scan k.

To predict r_S for the example in the previous section, we note that Mechanism I leads to the constraint $\dot{\underline{c}}_1 + \dot{\underline{c}}_2 + \dot{\underline{c}}_3 = \underline{0}$. Thus, $r_C^{\cdot} = 3 - 1 = 2$, and since r_F is 3, we correctly observe from Row 2 of Table 2.3 that r_S is 2.

When modeling an experiment, we might propose a mechanism and a set of static spectra for which Row 4 or 5 of Table 2.2 or 2.3 occurs. We predict r_M or r_S for such a case by forming a rank factorization of, respectively, Equation (2.1) or Equation (2.6). For example, consider Mechanism I in a case where the static spectrum of the product A_2 is half the sum of the static spectra of the reactants A_1 and A_3. Because of this constraint on the static spectra, r_F is 2, and because of the constraint on the rates, $r_C^{\cdot}$ is also 2. From Row 4 or 5 of Table 2.3, we have $r_S \leq 2$. To determine r_S, we first note that by Equation (2.7) any constraint among the rates implies a corresponding constraint among the vectors $\underline{h}_i$. Thus, the constraint $\dot{\underline{c}}_1 + \dot{\underline{c}}_2 + \dot{\underline{c}}_3 = \underline{0}$ implies the constraint

$$\underline{h}_1 + \underline{h}_2 + \underline{h}_3 = \underline{0} \tag{2.17}$$

We substitute the two constraints $\underline{f}_1 - 2\underline{f}_2 + \underline{f}_3 = \underline{0}$ and Equation (2.17) into Equation (2.6), and rearrange the results to obtain

$$(\underline{A}-\overline{\underline{A}}) = (\underline{f}_3-\underline{f}_2)(\underline{h}_2^T+2\underline{h}_3^T). \tag{2.18}$$

Since $(\underline{A}-\overline{\underline{A}})$ is the product of two matrices of full rank 1, we conclude that r_S equals 1.

From the two examples of Mechanism I discussed so far, it is clear that more than one ordered pair (r_M,r_S) can occur for one kinetic mechanism. In fact, by following the procedures described above, we can predict all of the pairs that can occur for a given mechanism. For example, Table 2.4 lists every (r_M,r_S) pair that can occur for Mechanism I assuming three absorbers. At least two sets of constraints are listed that lead to each (r_M,r_S) pair.

Several important and general points are illustrated by this table. There is more discriminating power in the combination (r_M,r_S) than in r_M or r_S alone. For example, an experiment that gives an (r_M,r_S) pair (3,3), but for which only r_M is calculated could be incorrectly thought to follow Mechanism I. Moreover, of the cases that can occur given Mechanism I, r_M by itself distinguishes the three categories r_M = 3,2,1, and r_S by itself distinguishes

Table 2.4. Possible Combinations of r_M and r_S for Mechanism I.

r_M	r_S	Constraints in Addition to $\dot{\underline{c}}_1 + \dot{\underline{c}}_2 + \dot{\underline{c}}_3 = \underline{0}$	r_F	r_C	$r_{\dot{C}}$
3		A. No additional constraints	3	3	2
	2	B. $\underline{f}_1 + \alpha\underline{f}_2 + \gamma\underline{f}_3 = \underline{0}$, α and γ not both zero, $\gamma \neq -(1+\alpha)$	2	3	2
		C. $\underline{f}_2 + \alpha\underline{f}_3 = \underline{0}$, $\alpha \neq 0$, $\alpha \neq -1$	2	3	2
2		D. $\underline{f}_1 + \alpha\underline{f}_2 - (1+\alpha)\underline{f}_3 = \underline{0}$	2	3	2
		E. $k_1 = k_2$	3	2	1
		F. $e^{-k_1 t} = 1-k_1 t$, $e^{-k_2 t} = 1-k_2 t$	3	2	1
	1	G. $\underline{f}_1 + \alpha\underline{f}_2 = \underline{0}$, $\underline{f}_1 + \gamma\underline{f}_3 = \underline{0}$ α and γ not both zero	1	3	2
1		H. $k_1 = k_2$, $\underline{f}_1 + \alpha\underline{f}_2 + [c_3(0)/c_1(0)]\underline{f}_3 = \underline{0}$ $\alpha \neq -[1+c_3(0)/c_1(0)]$	2	2	1
	0	I. $k_1 = k_2$ $\underline{f}_1 - [1+c_3(0)/c_1(0)]\underline{f}_2 + [c_3(0)/c_1(0)]\underline{f}_3 = \underline{0}$	2	2	1
		J. $k_1 = k_2$ $\underline{f}_1 + \gamma[c_1(0)+c_2(0)]/[c_3(0)-\gamma c_1(0)]\underline{f}_2 = \underline{0}$ $\underline{f}_1 + \gamma\underline{f}_3 = \underline{0}$, $\gamma \neq 0$	1	2	1

the three categories r_S = 2,1,0, whereas the (r_M,r_S) pair distinguishes the five categories (r_M,r_S) = (3,2), (2,2), (2,1), (1,1), and (1,0).

Entry F in Table 2.4 illustrates that by collecting data over only a short time where the concentration-time curves are linear, as is done in most initial rate determinations, one can introduce a constraint that reduces r_M and r_S. Thus, when devising an assay method based on initial rates, one should first measure the reaction over its entire time range to increase the chance that r_M and r_S are close to the number of absorbers in the reaction.

Finally, it should be noted that any set of constraints that leads to $r_S = 0$, as in Entires I and J, represents an extreme. Since $(\underline{A}-\overline{\underline{A}})$ must then be the null matrix, every wavelength channel is an isosbestic point, and from the absorbance data the occurrence of a reaction is undetectable.

D. Effect of Random Measurement Errors

Each experimentally measured absorbance has associated with it a random measurement error. A more realistic model for $\underline{A}$ than Equation (2.1) should therefore include measurement errors:

$$\underline{A} = \underline{F}\,\underline{C}^T + \underline{\varepsilon}, \qquad (2.19)$$

where $\underline{A}$ is the matrix of measured absorbances, $\underline{F}$ and $\underline{C}$ are the same as before and are regarded as errorless, and $\underline{\varepsilon}$ is a (pxN) matrix whose i, j element ε_{ij} is the random measurement error of the absorbance measurement A_{ij}.

The inclusion of $\underline{\varepsilon}$ in Equation (2.19) implies that, in general, the matrices $\underline{M}$ and $\underline{S}$ have no zero eigenvalues and are of full rank p. Thus, r_M and r_S do not obey the rules summarized in Tables 2.2 and 2.3. These rules are still appropriate, however, if we replace r_M and r_S with the essential ranks m and s, respectively, where m is the rank of $\underline{M}$ and s is the rank of $\underline{S}$ for errorless measurements. The goal is to infer the essential ranks m and s from absorbances that obey Equation (2.19).

To complete this model, we must make some reasonable statistical assumptions about the error matrix $\underline{\varepsilon}$. We assume that the expected value of $\underline{\varepsilon}$, denoted $E(\underline{\varepsilon})$, is the null matrix, and that ε_{ij} is uncorrelated to any other measurement error; thus,

$$\text{cov}(\varepsilon_{ij},\varepsilon_{k\ell}) = 0, \text{ if } i\neq k \text{ or } j\neq \ell \qquad (2.20)$$

It is also necessary to assume a model for the variance of each measurement error, defined by

$$\text{var}(\varepsilon_{ij}) = E(\varepsilon_{ij}^2) = \sigma_{ij}^2 \qquad (2.21)$$

where σ_{ij} is the standard deviation of ε_{ij}. In the most

general model, each measurement would have its own arbitrary measurement error variance. To use this model, we would therefore need to specify (pxN) variances. On the other hand, the most restrictive model would require only one measurement error variance, $var(\varepsilon_{ij}) = \sigma^2$. Sylvestre, Lawton, and Maggio (1974) have developed statistical criteria for M analysis on the single variance model. We show by an example that deviation of experimental results from the single variance model can lead to incorrect estimates of the essential ranks m and s. To correct this error, we develop a weighted principal component analysis that accommodates the model

$$var(\varepsilon_{ij}) = x_i z_j \tag{2.22}$$

in which it is assumed that the variance of each measurement error is approximately factorable into x_i, a function of the wavelength channel number, times z_i, a function of the spectrum number. The model given by Equation (2.22) has (p + N) degrees of freedom, and although it is not as general as the (pxN) model, it should hold as an approximation for many experimental situations.

For example, in the application of Equation (2.22) to the scanning wavelength stopped flow absorbance spectrometer described by Papadikis, Coolen and Dye (1975) and Coolen, et al. (1975), the x_i contribution occurs because the measurement error variances change with

wav
ver
of
600
ban
wit
and
fil
spe
fro
ler

Nea
ney
ra

to
de
to
st
a
Mo
co
spe
ea

wavelength. Figure 2.5 shows a typical plot of $x_i^{1/2}$ versus wavelength from the low to high wavelength ends of the photomultiplier tube response curve (250 nm to 600 nm). The points were determined by measuring absorbance at 0.0133 sec/scan, 50 wavelength channels/scan, with distilled water in the sample and reference cells and a 0.7 nominal absorbance quartz neutral density filter in the sample optical path. Sixty successive spectra were recorded, and the variances were estimated from the scatter about the mean absorbance for each wavelength channel with the equation

$$x_i = (1/59) \sum_{k=1}^{60} (A_{ik}-\bar{A}_i)^2. \qquad (2.23)$$

Nearly identical data were obtained with four different neutral density filters over the 0.0 to 1.0 absorbance range.

The z_i contribution in this instrument is attributable to a feature of its data collection scheme, which is described in detail by Coolen, et al. (1975). In order to optimize the allocation of a finite number of computer storage locations and to sample the full dynamic range of a reaction with a fixed scanning rate setting of the monochromator, this instrument averages a number of consecutive scans and stores the average as a single spectrum. The number of measured scans averaged into each stored spectrum is increased with time during the

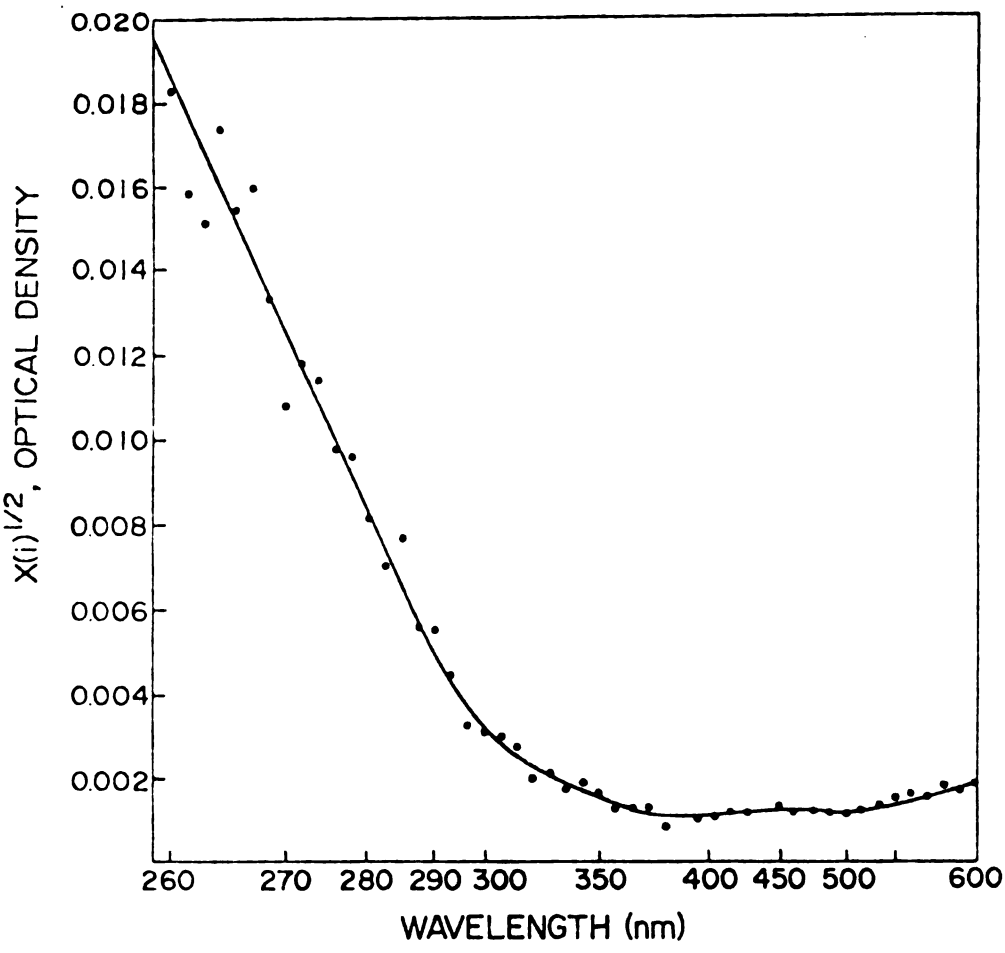

Figure 2.5. Typical Plot of $x_i^{1/2}$ versus wavelength for a 50 wavelength channel experiment.

reaction, so that at early times, where fast changes occur in the reaction, there is little or no averaging, while at long times, when the changes are slow, the signal to noise is greatly improved by increased averaging with little or no cost in curve distortion. In terms fully defined by Coolen et al. (1975), the z_j contribution for this instrument is given by the equation $z_i = g^{(1-n_j)}$, where g is the grouping factor (modulus for increasing the averaging), and n_j is the number of the consecutive group in which stored spectrum j occurs.

For an experiment that contains random measurement errors, as in Equation (2.19), $\hat{\underline{A}}_{(r)}$ given by Equation (2.4) no longer exactly equals $\underline{A}$ when r = m, and $(\hat{\underline{A}}_{(r)}-\overline{\underline{A}})$ given by Equation (2.9) no longer exactly equals $(\underline{A}-\overline{\underline{A}})$ when r = s. However, as we mathematically demonstrate in Appendix B, $\hat{\underline{A}}_{(r)}$ in Equation (2.4) is the ordinary least squares estimate of the experimental surface $\underline{A}$ constructed as a linear combination of the first r eigenvectors of $\underline{M}$, and $(\hat{\underline{A}}_{(r)}-\overline{\underline{A}})$ in Equation (2.9) is the ordinary least squares estimate of the experimental surface $(\underline{A}-\overline{\underline{A}})$ constructed as a linear combination of the first r eigenvectors of $\underline{S}$.

Given this least squares significance of Equations (2.4) and (2.9), it has been suggested in previous applications of principal component analysis (Kankare 1970; Lawton and Sylvestre 1971; Sylvestre, Lawton and Maggio 1974) that, when the experiment contains random errors,

we can determine m, the essential rank of $\underline{M}$, as the lowest value of r for which $\underline{\hat{A}}_{(r)}$ in Equation (2.4) fits the experimental surface $\underline{A}$ to within its random errors. Likewise, s, the essential rank of $\underline{S}$ would be the lowest r for which $(\underline{\hat{A}}_{(r)}-\underline{\bar{A}})$ in Equation (2.9) fits the experimental surface $(\underline{A}-\underline{\bar{A}})$ to within its random errors The reasoning is that, since only the first m eigenvectors of $\underline{M}$ are required to exactly reconstruct $\underline{A}$ for an errorless experiment, the first m eigenvectors of $\underline{M}$ in an experiment with random errors should primarily reflect the non-random, Beer's Law contribution, $\underline{F}\,\underline{C}^T$, in Equation (2.19). However, as the following simulated example shows, if $\text{var}(\varepsilon_{ij})$ changes significantly with i and j, the above procedure using Equations (2.4) and (2.9) can fail because the first few eigenvectors of $\underline{M}$ and $\underline{S}$ are dominated by the random error term $\underline{\varepsilon}$, in Equation (2.19).

Consider an M analysis of a two absorber reaction that follows Mechanism II

$$A_1 \xrightarrow{k_1=20\ \text{sec}^{-1}} A_2 \xrightarrow{k_2=10\ \text{sec}^{-1}} D \qquad \text{(II)}$$

where D is a non-absorbing product. Suppose that A_1 and A_2 have the 20 wavelength channel static spectra shown in Figure 2.6. Figure 2.7 shows the absolute absorbance surface that would be obtained in an errorless experiment under the following conditions: 20 wavelength channels, 36 consecutive spectra, 10 msec/scan, and

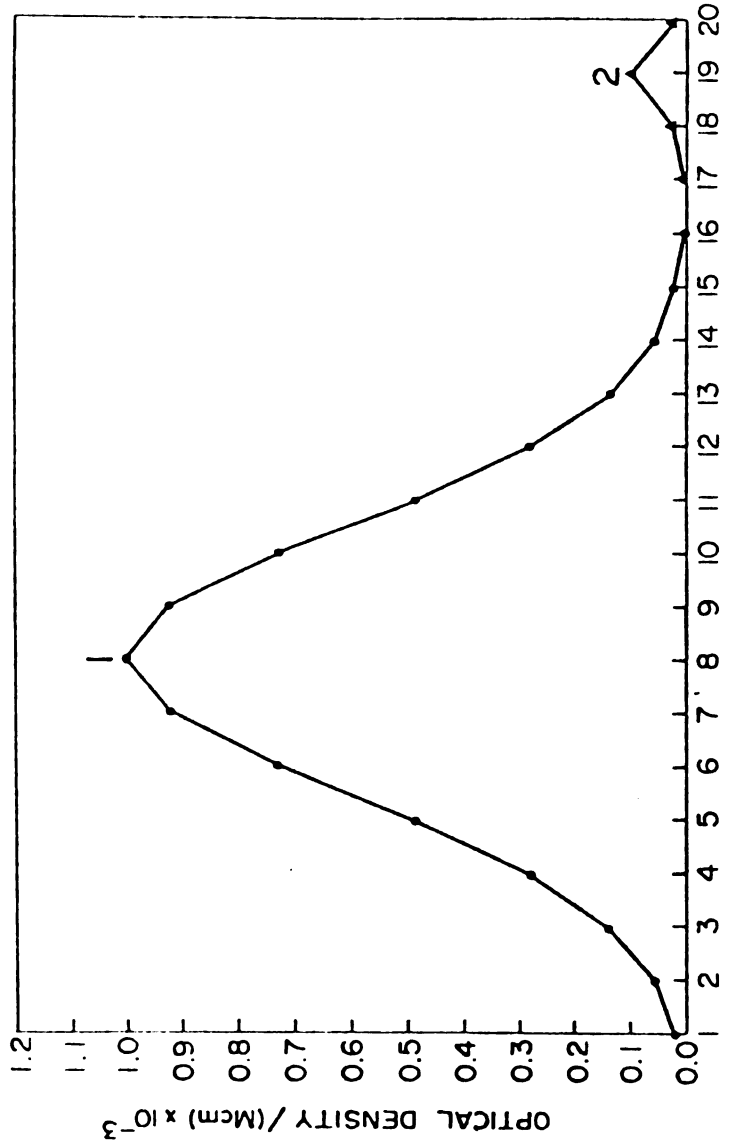

Figure 2.6. Static spectra of absorbers 1 and 2 for the Mechnism II example.

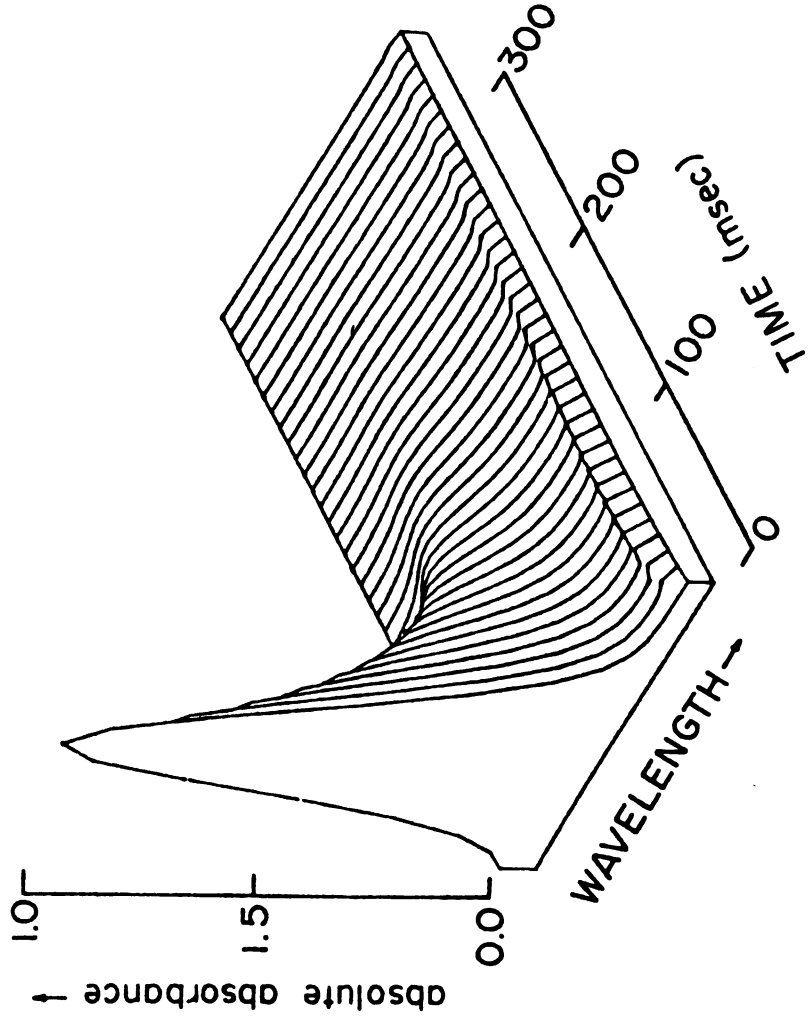

Figure 2.7. Errorless absolute absorbance surface A for Mechanism II.

$c_1(0) = 0.001$ M.

Now consider an experiment under these conditions that also contains normal random noise whose variance follows Equation (2.22) with the x_i factor shown in Figure 2.8. Let the 36 spectra occur in 3 groups of 12 consecutive spectra each, and let z_j be given by $z_j = 2^{(1-n_j)}$, where n_j is the number of the group in which scan j occurs. The resulting noisy absorbance surface is shown in Figure 2.9.

For this example, $r_F = 2$ and $r_C = 2$. Thus, according to Table 2.2, an M analysis of this noisy data should give an essential rank m = 2; that is, $\hat{\underline{A}}_{(2)}$ in Equation (2.4) should fit the data to within its random noise. Figure 2.10 shows the surface $\hat{\underline{A}}_{(2)}$. Figure 2.11 is a two-dimensional plot of the noisy data points and the estimated absorbances $\hat{\underline{A}}_{(2)}$ versus time at wavelength channel 19. It is clear from Figure 2.11 that $\hat{\underline{A}}_{(2)}$ does not fit $\underline{A}$ to within the random noise. Thus, we would incorrectly conclude from this analysis of the noisy data that m > 2. In fact, the noisy data at channel 19 are not fit to within random error until m = 13.

E. Statistically Weighted Principal Component Analysis

We can avoid this incorrect result by using the variance model of Equation (2.22) to weight the absorbance matrix before performing the principal component calculations.

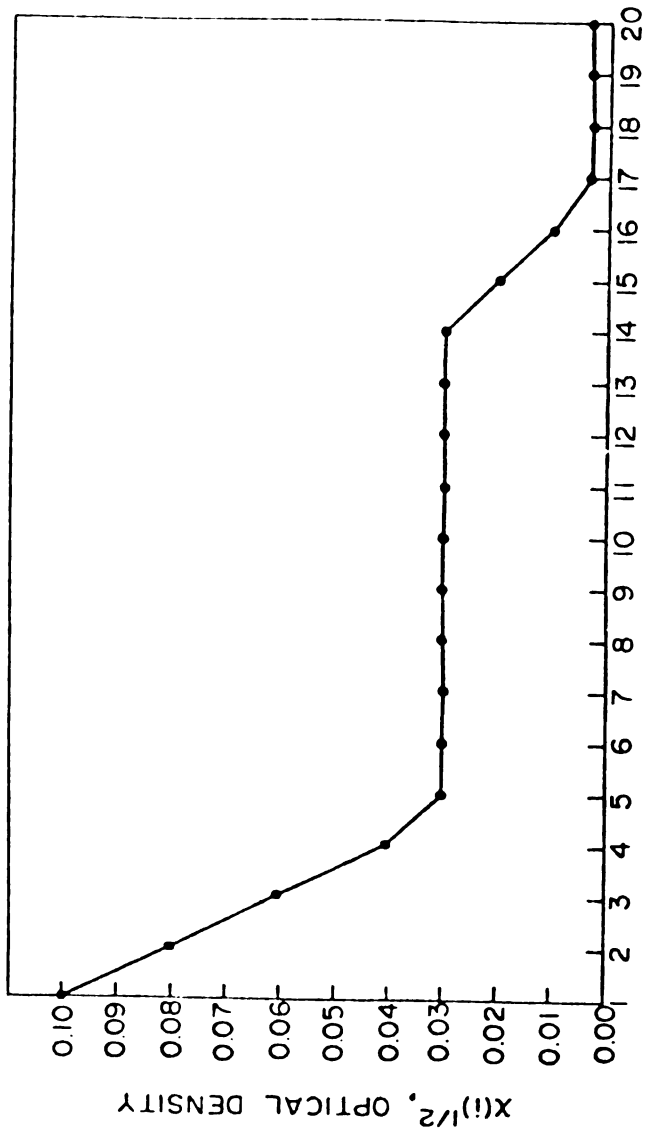

Figure 2.8. $x_1^{1/2}$ versus channel number for the simulated noisy data for Mechanism II.

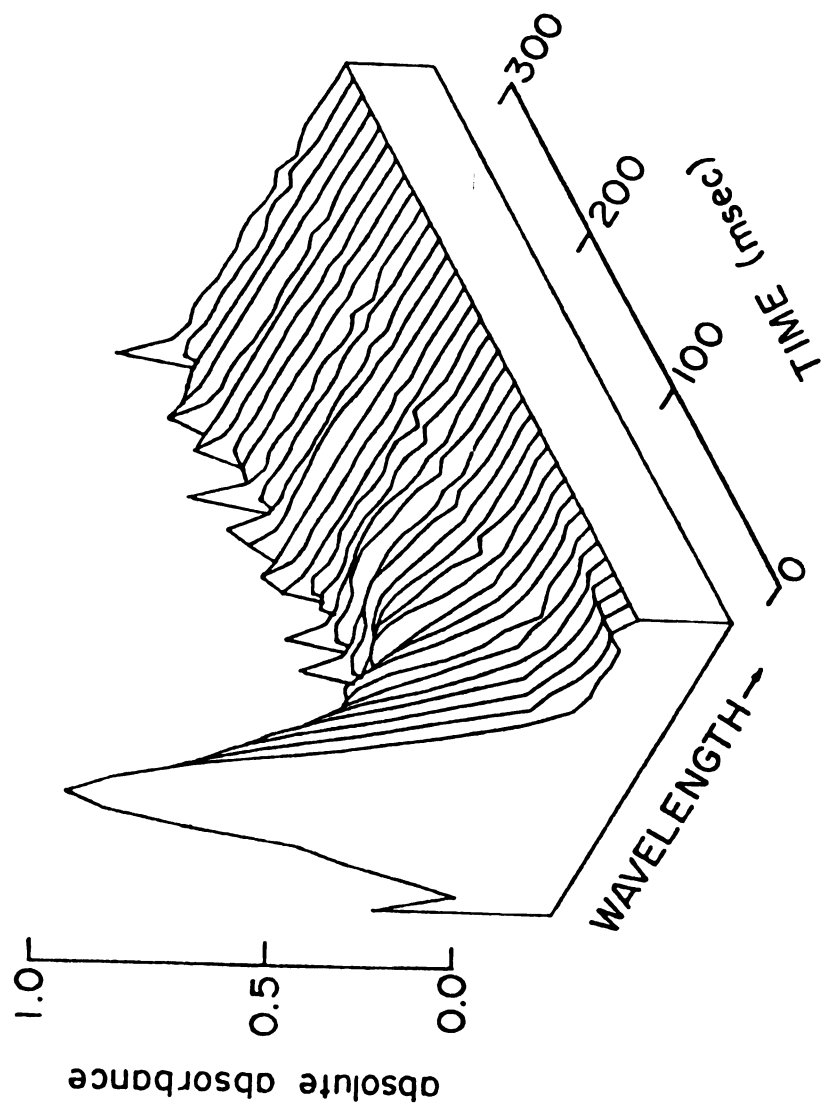

Figure 2.10. Unweighted two principal component estimate $\hat{\underline{A}}_{(2)}$ of the absolute absorbance surface taken from the noisy absorbance surface.

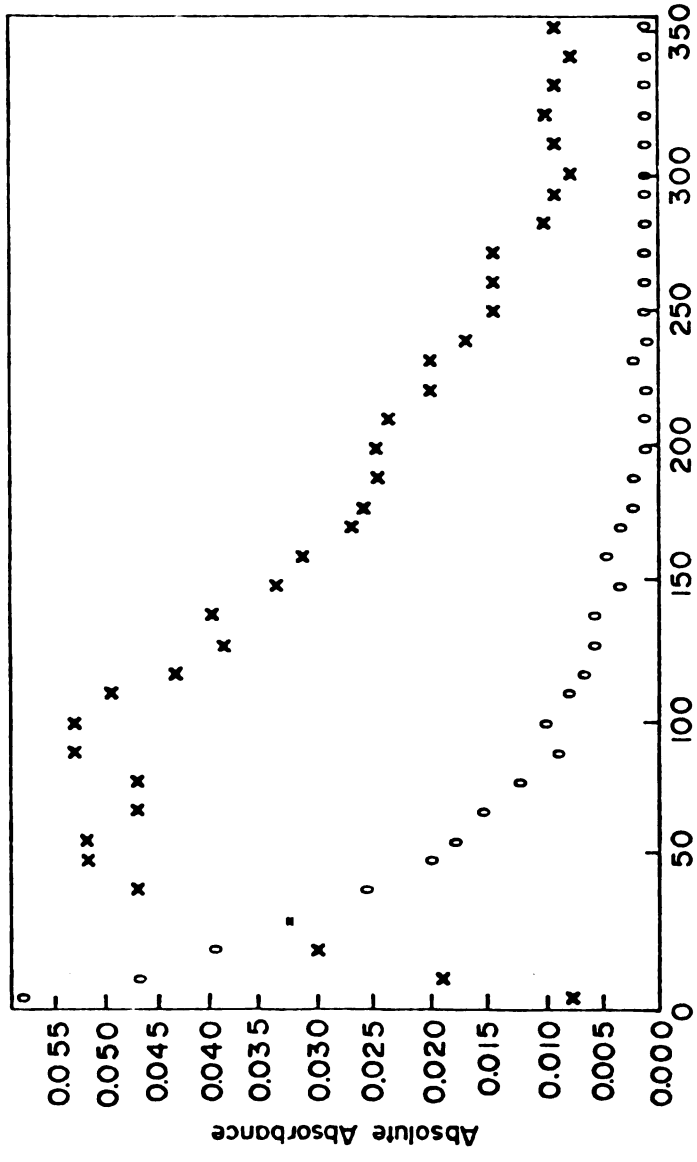

Figure 2.11. Comparison of the unweighted estimate $\hat{\underline{A}}_{(2)}$ with the noisy data $\underline{A}$ at wavelength channel 19. X = noisy data $\underline{A}$, 0 = unweighted estimate $\hat{\underline{A}}_{(2)}$.

We define two nonsingular diagonal weighting matrices, $\underline{L}$, and $\underline{T}$, as follows:

$$\underline{L} \equiv \text{diag } (L_1, L_2, \ldots, L_p)$$
$$\underline{T} \equiv \text{diag } (T_1, T_2, \ldots, T_N), \tag{2.24}$$

with the values of L_i and T_j yet to be chosen. We define the weighted absorbance matrices as $\underline{A}_W \equiv \underline{L}\ \underline{A}\ \underline{T}$ and $\underline{\bar{A}}_W \equiv \underline{L}\ \underline{\bar{A}}\ \underline{T}$, replace $\underline{M}$ with $\underline{M}_W = (1/N)\ \underline{A}_W \underline{A}_W^T$ and $\underline{S}$ with $\underline{S}_W = [1/(N-1)]\ (\underline{A}_W - \underline{\bar{A}}_W)(\underline{A}_W - \underline{\bar{A}}_W)^T$, and perform principal component analyses using $\underline{M}_W$ and $\underline{S}_W$. Equations (2.4) and (2.9) become, respectively,

$$\underline{\hat{A}}_{(r)} = \underline{L}^{-1}\ \underline{\Phi}_{(r)}\ \underline{\Phi}_{(r)}^T\ \underline{L}\ \underline{A} \tag{2.25}$$

$$(\underline{\hat{A}}_{(r)} - \underline{\bar{A}}) = \underline{L}^{-1}\ \underline{B}_{(r)}\ \underline{B}_{(r)}^T\ \underline{L}\ (\underline{A} - \underline{\bar{A}}) \tag{2.26}$$

where in Equations (2.25) and (2.26) $\underline{\Phi}$ and $\underline{B}$ are the eigenvector matrices of $\underline{M}_W$ and $\underline{S}_W$, respectively.

We shall assign values to $\underline{L}$ and $\underline{T}$ so that, given the variance model of Equation (2.22), the eigenvectors of $\underline{M}_W$ and $\underline{S}_W$ are minimally perturbed by the random measurement errors from the values they would have in an errorless experiment. Consider the expected value of $\underline{M}_W$, denoted $E(\underline{M}_W)$, which is the value $\underline{M}_W$ approaches asymptotically as N, the number of spectra in the experiment, increases.

Following procedures given by Anderson (1963) we have, for the model described by Equations (2.19) and (2.22),

$$E(\underline{M}_W) = (1/N)\ \underline{L}\ E(\underline{A})\ \underline{T}^2 E\ (\underline{A}^T)\ \underline{L} \tag{2.27}$$

$$+ (1/N)\mathrm{tr}\ (\underline{T}^2\underline{Z})\ \underline{L}^2\underline{X}$$

where

$$E\ (\underline{A}) = \underline{F}\ \underline{C}$$

$$\underline{Z} \equiv \mathrm{diag}\ (z_1, z_2, \ldots, z_N)$$

and

$$\underline{X} \equiv \mathrm{diag}\ (x_1 x_2, \ldots, x_p)$$

Equation (2.27) is derived in Appendix C. The first term on the R.H.S. of Equation (2.27) is the contribution of $\underline{F}\ \underline{C}$, and is $E(\underline{M}_W)$ for an errorless experiment. The contribution from the measurement errors is isolated in the second term,

$$(1/N)\mathrm{tr}(\underline{T}^2\underline{Z})\ \underline{L}^2\underline{X}$$

Our goal in choosing $\underline{L}$ and $\underline{T}$ is to have the eigenvectors

of $E(\underline{M}_W)$ the same as the eigenvectors of $(1/N)\ \underline{L}\ E(\underline{A})\ \underline{T}^2\ E(\underline{A}^T)\ \underline{L}$. We achieve this goal by choosing

$$\underline{L} = a^{1/2}\ \underline{X}^{-1/2}$$
$$\underline{T} = b^{1/2}\ \underline{Z}^{-1/2} \qquad (2.28)$$

where a and b are arbitrary constants. With this choice Equation (2.27) becomes

$$E(\underline{M}_W) = (ab/N)\ \underline{X}^{-1/2}\ E(\underline{A})\ \underline{Z}^{-1}\ E(\underline{A}^T)\ \underline{X}^{-1/2} + ab\ \underline{I}. \qquad (2.29)$$

Since any vector is an eigenvector of $\underline{I}$, the eigenvectors of $E(\underline{M}_W)$ are the eigenvectors of the first term,

$$(ab/N)\ \underline{X}^{-1/2}\ E(\underline{A})\ \underline{Z}^{-1}\ E(\underline{A}^T)\underline{X}^{-1/2}$$

An analogous derivation shows that Equation (2.28) is also the best assignment of $\underline{L}$ and $\underline{T}$ for weighted $\underline{S}$ analysis.

Figure 2.12 compares the estimated absorbances given by Equation (2.25) to the noisy data at wavelength channel 19, where Equation (2.28) was used to define $\underline{L}$ and $\underline{T}$ with a=b=1. The data are fit to within the random noise for r = 2. By similarly observing that $\hat{\underline{A}}_{(1)}$ with Equation (2.25) does not fit the noisy data surface and that $\hat{\underline{A}}_{(2)}$ does, we correctly conclude that the essential rank m is two. Figure 2.13 is the surface estimated from the

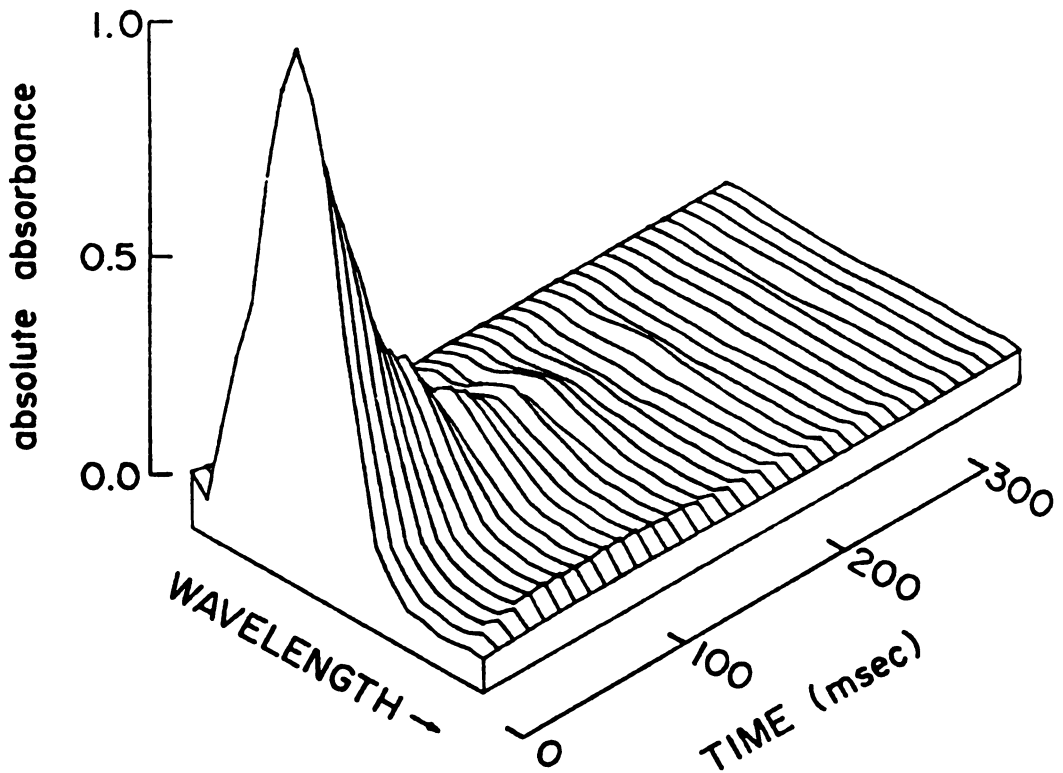

Figure 2.12. Comparison of the weighted estimate $\underline{\hat{A}}_{(2)}$ with the noisy data $\underline{A}$ at wavelength channel 19. X = noisy data $\underline{A}$, 0 = weighted estimate $\underline{\hat{A}}_{(2)}$.

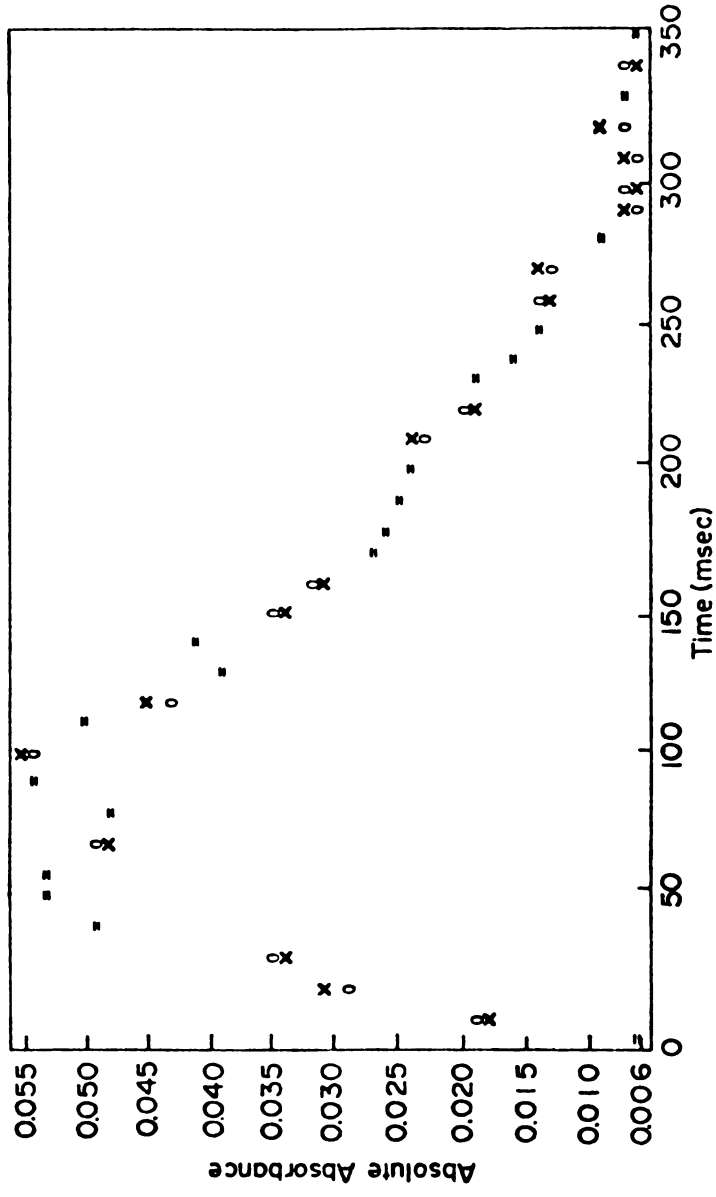

Figure 2.13. Weighted two principal component estimate $\hat{\underline{A}}_{(2)}$ of the absolute absorbance surface taken from the noisy absorbance surface.

noisy data in Figure 2.9 with Equation (2.25). It is clear that Figure 2.13 is a better reconstruction than Figure 2.10 of the errorless absorbance surface in Figure 2.7. Thus, weighted principal component analysis gives a lower variance estimate than unweighted analysis of the chemical reaction's contribution to the absorbance data.

With weighted principal component analysis and the variance model of Equation (2.22), we obtain convenient criteria for interpreting the eigenvalues of $\underline{M}_W$ and $\underline{S}_W$, and for determining when $\hat{\underline{A}}_{(r)}$ fits $\underline{A}$ to within experimental error. Using Equation (2.28) to define $\underline{L}$ and $\underline{T}$, and choosing a=b=1, we have

$$E(\underline{M}_W) = (1/N)\ \underline{X}^{-1/2}\ E(\underline{A})\ \underline{Z}^{-1}\ E(\underline{A}^T)\ \underline{X}^{-1/2} + \underline{I} \qquad (2.30)$$

The term

$$(1/N)\ \underline{X}^{-1/2}\ E(\underline{A})\ \underline{Z}^{-1}\ E(\underline{A}^T)\ \underline{X}^{-1/2}$$

has (p-m) zero eigenvalues. It follows that $E(\underline{M}_W)$ has (p-m) degenerate eigenvalues equal to 1. Therefore the mean of the last (p-m) eigenvalues of $\underline{M}_W$ should approach 1. Similar arguments show that the mean of the last (p-s) eigenvalues of $\underline{S}_W$ should approach 1. No such simple relationship holds for the eigenvalues of $\underline{M}$ and $\underline{S}$. Table 2.5 lists the mean of the last (p-r) eigenvalues of $\underline{M}_W$ with r=0, 1,2, and 3 for the analysis of the noisy data

Table 2.5

Mean of the Last (p-r) Eigenvalues of $\underline{M}_W$ for the Noisy Data

r	$[1/(p-r)] \sum_{i=r+1}^{p} \delta_i$
0	29.992
1	6.601
2	1.012
3	0.919

in Figure 2.9. Note that the mean of the last (p-r) eigenvalues approaches 1.0 for r = 2, which confirms that the essential rank m = 2.

The most straightforward procedure for determining when $\hat{\underline{A}}_{(r)}$ fits $\underline{A}$ to within experimental error is to examine plots similar to Figure 2.12. When $\hat{\underline{A}}_{(r)}$ and $\underline{A}$ are close, one can examine a plot of the residuals $(\hat{\underline{A}}_{(r)}-\underline{A})$. The residuals should not be highly patterned when plotted versus time or wavelength if the measurement errors are truly uncorrelated and we have chosen the value of r equal to the essential rank. Sylvestre, Lawton, and Maggio (1974) have given an equation describing the sum of the squares of the residuals for r = m and single variance measurement

errors. With statistically weighted principal component analysis we can extend their equation to the nonuniform variance error model of Equation (2.22). When r = m for weighted M analysis, the function $Q_r/(N-r)(p-r)$ approaches the value ab, where Q_r is given by

$$Q_r = \sum_{i=1}^{p} \sum_{j=1}^{N} [(\underline{\Phi}_{(r)}\underline{\Phi}_{(r)}^T - \underline{I})\underline{A}_W]_{ij}^2 \qquad (2.31)$$

and $\hat{\underline{A}}_{(r)}$ is defined by Equation (2.25). This function also approaches the value ab for weighted S analysis when r = s, and $\underline{\Phi}_{(r)}$ and $\underline{A}_W$ in Equation (2.28) are replaced with $\underline{B}_{(r)}$ and $(\underline{A}_W - \bar{\underline{A}}_W)$, respectively. Table 2.6 lists the values of $Q_r/(N-r)(p-r)$ for weighted M analysis of the noisy data in Figure 2.9, where a=b=1. Since 4=2 is the lowest value for r for which $Q_r/(N-r)(p-r)$ is close to 1.0, we would infer that the essential rank m = 2.

In conclusion, we emphasize that the weighting matrices $\underline{L}$ and $\underline{T}$ are not fudge factors, especially when the variance model of Equation (2.22) holds as an approximation. The improved results obtained with the weights require additional measurements like those in Figure 2.5 to determine the elements of $\underline{L}$ and $\underline{T}$. Moreover, unweighted principal component analysis can be regarded as a special case of weighted analysis where $\underline{L}$ and $\underline{T}$ are arbitrarily set equal to identity matrices. Even when Equation (2.22) does not accommodate the error variances, a judicious approximate choice of $\underline{L}$ and $\underline{T}$ should be preferred to the arbitrary

Table 2.6

$Q_r/(N-r)(p-r)$ for Weighted M Analysis of the Noisy Data

r	$Q_r/(N-r)(p-r)$
1	6.790
2	1.071
3	1.003

choice of identity matrices. As with any statistical treatment of experimental measurements containing random errors, the reliability of the results increases with sample size, i.e., the number of wavelength channels and the number of consecutive spectra.

The rules given in Tables 2.2 and 2.3 for the essential ranks of $\underline{M}_W$ and $\underline{S}_W$ are not restricted to absorbance kinetic experiments, and are applicable to any scanning wavelength kinetics experiment where the response is a linear function of the concentrations. The weighting scheme is not restricted to kinetics experiments. It is applicable to any principal component analysis where the measurement error variance can be approximated by Equation (2.22) where x_i and z_j are each a function of one of the two independent measurement variables (the analogs of wavelength and time in the scanning wavelength kinetics application).

CHAPTER 3

ESTIMATION OF STATIC SPECTRA AND CONCENTRATION PROFILES VIA WEIGHTED PRINCIPAL COMPONENT ANALYSIS

Rapid scanning spectroscopy is a powerful experimental tool for characterizing the progress of reactions that have more than one light absorbing species. In rapid scanning wavelength absorbance kinetics experiment, absorbance is measured at p wavelength channels across a spectral region that is rapidly and repeatedly scanned as the reaction progresses. If the scanning rate is fast compared to the fastest absorbance change in the reaction, the resulting N consecutive spectra may be regarded as instantaneous and the absorbance-wavelength-time surface may be represented by the (pxN) matrix $\underline{A}$, where A_{ij} is the absorbance measured at wavelength channel i at the time of scan j. Since multicomponent reactions in general produce unstable intermediates as well as unanticipated products, the number of absorbers in a rapid scanning experiment is generally unknown before the experiment is analyzed. Moreover, the spectra of these intermediates and products are generally unknown.

The preceding chapter dealt with the use of statistically weighted principal component analysis to determine the number of absorbers in a rapid scanning kinetics

experiment. The two kinds of principal component analysis, M analysis and S analysis, yield, respectively, the minimum number m of absorbers required to interpret the experiment and the minimum number s of absorbers whose concentrations must have changed during the experiment. In this chapter, we develop further tools and propose a strategy for inferring from a rapid scanning experiment the spectral and kinetic properties of its absorbers.

The first step in the strategy is the determination of m and s for the whole experiment. If the measured static spectra of known reactants, products, and catalysts fit and account for the m required absorbers, then we have resolved the experiment. If, however, we are still left with intermediates and products whose static spectra and concentrations are unknown, we examine subspaces of wavelength and time to find parts of the experiment where the number q of absorbers is small. When q is small, the analysis is considerably simplified, and further information about static spectra and concentrations is obtained for each subspace. The final step is to reassemble the information from the subspaces in order to estimate the static spectra and the concentrations for the whole experiment.

As before, we assume that $\underline{A}$ satisfies the model given by

$$\underline{A} = \underline{F}\,\underline{C}^T + \underline{\varepsilon} = \left(\sum_{j=1}^{q} \underline{f}_j \underline{c}_j^T\right) + \underline{\varepsilon}, \qquad (3.1)$$

where q is the number of absorbers, $\underline{F}\,\underline{C}^T$ is the errorless contribution of Beer's Law, and $\underline{\varepsilon}$ is the matrix of uncorrelated random measurement errors. The static spectrum matrix $\underline{F}$ is defined by $\underline{F} = (\underline{f}_1, \underline{f}_2, \ldots, \underline{f}_q)$, where $\underline{f}_j$, the static spectrum of absorber j, is a p component column vector whose i'th element is the product of the absorbance cell path length and the molar absorptivity of absorber j at wavelength channel i. The concentration matrix $\underline{C}$ is defined by $\underline{C} = (\underline{c}_1, \underline{c}_2, \ldots, \underline{c}_q)$ where $\underline{c}_j$, the concentration vector of absorber j, is an N component column vector whose i'th element is the molarity of absorber j during spectrum i. The i,j'th element of $\underline{\varepsilon}$ is assumed to have expected value zero and variance satisfying the model

$$\mathrm{var}(\varepsilon_{ij}) = \sigma_{ij}^2 = x_i z_j. \qquad (3.2)$$

From the eigenvectors and eigenvalues of the M analysis, we develop criteria for estimating $\underline{F}$ and $\underline{C}$ to within arbitrary multiplicative constants. We find that q^2 elements of $\underline{F}$ and/or $\underline{C}$ suffice for estimating the (N+p)q elements of $\underline{F}$ and $\underline{C}$. This is a great reduction in the arbitrariness of these matrices since (N+P)q is generally much larger than q^2. Moreover, we find a least squares criterion for deciding, independently of any assumptions about other absorbers or kinetic mechanisms, whether a single suspected absorber's static spectrum or concentration vector fits the experimental data. Each suspected static spectrum

or concentration vector that fits provides q of the q^2 numbers required to estimate $\underline{F}$ and $\underline{C}$.

The problem of estimating $\underline{F}$ and $\underline{C}$ takes simpler forms when q is small. We present the simplifications for an experiment or any part of an experiment that contains only one, two, or three absorbers. For experiments containing only two absorbers, we present equations that require no additional information to define the upper and lower bounds of the static spectra and concentration vectors. These equations are extensions of those presented by Lawton and Sylvestre (1971) for the individual spectra in two absorber equilibrium systems, and are similar to those presented by Warner, et al. (1977) for emission and excitation spectra in two component fluorescence data.

From the eigenvectors and eigenvalues of the S analysis, we develop a least squares criterion for determining if a suspected absorber whose static spectrum fits the data has a rate in the reaction that is linearly independent of the rates of the other (q-1) absorbers.

Finally, these new tools are utilized in a seven-step strategy proposed for resolving rapid-scanning kinetics experiments by principal component analysis. In the following chapter, the strategy is applied to a reaction catalyzed by the enzyme horse liver alcohol dehydrogenase. The analysis shows that there are at least seven absorbers, of which four are transient intermediates.

A. M Analysis Estimates of $\underline{F}$ and $\underline{C}$

In M analysis we form the weighted second moment matrix $\underline{M}_W$, defined by

$$\underline{M}_W = (1/N)\ \underline{A}_W \underline{A}_W^T,\ \underline{A}_W = \underline{L}\ \underline{A}\ \underline{T}$$

$$\underline{L} = a^{1/2}\ \text{diag}\ (x_1^{-1/2},\ x_2^{-1/2},\ldots,x_p^{-1/2})$$

$$T = b^{1/2}\ \text{diag}\ (z_1^{-1/2},\ z_2^{-1/2},\ldots,z_N^{-1/2}) \qquad (3.3)$$

where a and b are arbitrary positive constants. The eigenvalue equation to be solved is

$$\underline{M}_W \underline{\Phi} = \underline{\Phi}\ \underline{\Delta}$$

$$\underline{\Phi} = (\underline{\phi}_1, \underline{\phi}_2, \ldots, \underline{\phi}_p)$$

$$\underline{\Delta} = \text{diag}\ (\delta_1, \delta_2, \ldots, \delta_p),\ \delta_1 \geq \delta_2 \geq \ldots \geq \delta_p \qquad (3.4)$$

The essential rank m is the minimum number of absorbers required to interpret the experiment and is determined by finding the lowest value of r for which $\hat{\underline{A}}_{(r)}$, defined by

$$\hat{\underline{A}}_{(r)} = (\underline{L}^{-1} \underline{\Phi}_{(r)} \underline{\Phi}_{(r)}^T \underline{L})\ \underline{A},\ \underline{\Phi}_{(r)} = (\underline{\phi}_1, \underline{\phi}_2, \ldots \underline{\phi}_r), \qquad (3.5)$$

fits the experimental matrix $\underline{A}$ to within its random errors. An identical but more useful equation for $\hat{\underline{A}}_{(r)}$ is

$$\hat{\underline{A}}_{(r)} = \underline{L}^{-1}\underline{\Phi}_{(r)}\underline{\Omega}_{(r)}\underline{\Psi}^{T}_{(r)}\underline{T}^{-1},$$

$$\underline{\Omega}_{(r)} = \text{diag}\ (\omega_1,\omega_2,\ldots,\omega_r), \quad \omega_j = +N\delta_j^{1/2}$$

$$\underline{\Psi}_{(r)} = (\underline{\psi}_1,\underline{\psi}_2,\ldots,\underline{\psi}_r) = \underline{\Omega}^{-1}_{(r)}\underline{A}^{T}_{W}\underline{\Phi}_{(r)} \tag{3.6}$$

It can be shown (Appendix A) that the r columns of $\underline{\Psi}_{(r)}$ contain the first r eigenvectors of $\underline{M}'_W$, defined by $\underline{M}'_W = (1/p)\ \underline{A}^{T}_{W}\underline{A}_{W}$.

The essential rank m is not only the <u>minimum</u> number of absorbers, but is also the <u>maximum</u> number of absorbers whose spectral and kinetic properties can be determined by analyzing a particular experiment. In some experiments there may be extra absorbers that cannot be distinguished because their concentrations or their static spectra are linearly coupled. Additional experiments, in which conditions are varied, are required to detect and characterize such additional absorbers. We assume, for a particular experiment, that m is the total number of absorbers, <u>i.e.</u>, that q equals m.

The model for M analysis estimates of $\underline{F}$ and $\underline{C}$ is

$$\hat{\underline{A}}_{(m)} = \hat{\underline{F}}\ \hat{\underline{C}}^{T} = \sum_{j=1}^{m} \hat{\underline{f}}_j\hat{\underline{c}}^{T}_{j}, \tag{3.7}$$

where $\hat{\underline{A}}_{(m)}$ is given by Equation (3.6), and $\hat{\underline{F}}\ \hat{\underline{C}}^T$ is an estimate of $\underline{F}\ \underline{C}^T$ in Equation (3.1). We use Equation (3.7) to estimate for each absorber the shape of its static spectrum, the shape of its concentration profile, and its contribution to the measured absorbance-wavelength-time surface. $\hat{\underline{F}}$ is defined by $\hat{\underline{F}} = (\hat{\underline{f}}_1, \hat{\underline{f}}_2, \ldots, \hat{\underline{f}}_m)$, where $\hat{\underline{f}}_j$ is an estimate of $\alpha_j \underline{f}_j$, with α_j an arbitrary constant. $\hat{\underline{C}}$ is defined by $\hat{\underline{C}} = (\hat{\underline{c}}_1, \hat{\underline{c}}_2, \ldots, \hat{\underline{c}}_m)$, where $\hat{\underline{c}}_j$ is an estimate of $(1/\alpha_j)\underline{c}_j$. The vector product $\hat{\underline{f}}_j \hat{\underline{c}}_j^T$ is then an estimate of $\underline{f}_j \underline{c}_j^T$, the contribution of the j'th absorber to the measured absorbance surface.

Whereas $\underline{F}$ and $\underline{C}$ are errorless, $\hat{\underline{F}}$ and $\hat{\underline{C}}$ are not, in general, errorless. To see this, define the residual absorbance matrix for m absorbers as $\underline{R}_{(m)} = \underline{A} - \hat{\underline{A}}_{(m)}$. The terms $\underline{F}\ \underline{C}^T$ and $\hat{\underline{F}}\ \hat{\underline{C}}^T$ are then related by $\hat{\underline{F}}\ \hat{\underline{C}}^T = \underline{F}\ \underline{C}^T + (\underline{\varepsilon} - \underline{R}_{(m)})$. In an errorless experiment, where $\underline{\varepsilon}$ is zero, the term $(\underline{\varepsilon} - \underline{R}_{(m)})$ is also zero, and $\hat{\underline{F}}\ \hat{\underline{C}}^T$ equals $\underline{F}\ \underline{C}^T$. In an experiment with errors, where $\underline{\varepsilon}$ is nonzero, $(\underline{\varepsilon} - \underline{R}_{(m)})$ is in general also nonzero, and $\hat{\underline{F}}\ \hat{\underline{C}}^T$ does not equal $\underline{F}\ \underline{C}^T$. However, it can be shown (Appendix C) that $(\underline{\varepsilon} - \underline{R}_{(m)})$ vanishes in a properly weighted M analysis as either N, the number of consecutive spectra, or p, the number of wavelength channels, becomes very large. Therefore, we take $\hat{\underline{F}}\ \hat{\underline{C}}^T$ to be an error-containing estimate of $\underline{F}\ \underline{C}^T$.

Equations (3.6) and (3.7) together give

$$\hat{\underline{F}}\ \hat{\underline{C}}^T = \underline{L}^{-1} \underline{\Phi}_{(m)} \underline{\Omega}_{(m)} \underline{\Psi}_{(m)}^T \underline{T}^{-1} \qquad (3.8)$$

Solved for $\hat{\underline{F}}$, Equation (3.8) gives

$$\hat{\underline{F}} = (\underline{L}^{-1}\underline{\Phi}_{(m)})\underline{U}, \tag{3.9}$$

where $\underline{U}$ is an (mxm) matrix defined by

$$\underline{U} = \underline{\Omega}_{(m)}\underline{\Psi}_{(m)}^{T}\underline{T}^{-1}\hat{\underline{C}}(\hat{\underline{C}}\ \hat{\underline{C}}^{T})^{-1}. \tag{3.10}$$

Solved for $\hat{\underline{C}}$, Equation (3.10) gives

$$\hat{\underline{C}} = (\underline{T}^{-1}\underline{\Psi}_{(m)})\ \underline{V}, \tag{3.11}$$

where $\underline{V}$ is an (mxm) matrix defined by

$$\underline{V} = \underline{\Omega}_{(m)}\underline{\Phi}_{(m)}^{T}\underline{L}^{-1}\hat{\underline{F}}(\hat{\underline{F}}\ \hat{\underline{F}}^{T})^{-1} \tag{3.12}$$

Note that Equations (3.9) and (3.11) assume, respectively, the existence of the inverses $(\hat{\underline{C}}\ \hat{\underline{C}}^{T})^{-1}$ and $(\hat{\underline{F}}\ \hat{\underline{F}}^{T})^{-1}$. These inverses are guaranteed since m is the essential rank of $\underline{M}_{W}$. Resubstitution of Equations (3.9) and (3.11) into Equation (3.8) gives the following condition on $\underline{U}$ and $\underline{V}$

$$\underline{U}\ \underline{V}^{T} = \underline{\Omega}_{(m)} \tag{3.13}$$

Equations (3.9) through (3.13) considerably reduce the arbitrariness of $\hat{\underline{F}}$ and $\hat{\underline{C}}$. $\hat{\underline{F}}$ is a rotation of $\underline{L}^{-1}\underline{\Phi}_{(m)}$ by the rotation matrix $\underline{U}$, and $\hat{\underline{C}}$ is a rotation of $\underline{T}^{-1}\underline{\Psi}_{(m)}$ by

the rotation matrix $\underline{V}$. If the m^2 elements of either $\underline{U}$ or $\underline{V}$ are known, the unknown rotation matrix is given by Equation (3.13), and $\hat{\underline{F}}$ and $\hat{\underline{C}}$ can be computed directly from Equations (3.9) and (3.11), respectively.

Thus, the strategy for obtaining $\hat{\underline{F}}$ and $\hat{\underline{C}}$ is to estimate enough elements of $\underline{U}$ and $\underline{V}$ separately so that all of $\underline{U}$ and $\underline{V}$ are given by Equation (3.13). To this end, we partition $\underline{U}$ and $\underline{V}$,

$$\underline{U} = (\underline{u}_1, \underline{u}_2, \ldots, \underline{u}_m)$$

$$\underline{V} = (\underline{v}_1, \underline{v}_2, \ldots, \underline{v}_m) \qquad (3.14)$$

where each $\underline{u}_j$ and each $\underline{v}_j$ is an m component column vector. Then Equations (3.9) and (3.11) become

$$\hat{\underline{f}}_j = (\underline{L}^{-1}\underline{\Phi}_{(m)})\ \underline{u}_j, \qquad j = 1,2,\ldots m,$$

$$\hat{\underline{c}}_j = (\underline{T}^{-1}\underline{\Psi}_{(m)})\ \underline{v}_j, \qquad j = 1,2,\ldots m, \qquad (3.15)$$

which show that the j'th columns of $\underline{U}$ and $\underline{V}$ depend only on the j'th static spectrum and concentration vector, respectively.

For a given reaction there is usually a set of suspected absorbers. For example, in an enzyme-catalyzed reaction the suspected absorbers are any light absorbing substrates, inhibitors, and enzymes that were mixed to initiate the

reaction. Equations (3.15) are models against which spectral and kinetic information about suspected absorbers can be tested. If a suspected absorber is one of the m linearly independent absorbers in the experiment, its static spectrum and concentration vector must satisfy Equations (3.15).

We now present least squares equations, based on Equations (3.15) for determining whether a suspected absorber fits as one of the m linearly independent absorbers in the experiment. Suppose there are proposed values for k wavelength channels of $\underline{\hat{f}}_j$, with $m \leq k \leq p$. These proposed values may come from the measured static spectrum of a suspected absorber. Define the proposed static spectrum as the p component column vector $\underline{\hat{f}}_{jprop}$, where the k channels for which there are proposed values contain those values, and where the remaining (p-k) wavelength channels contain zeroes. The least squares loss function for using $\underline{\hat{f}}_{jprop}$ to estimate $\underline{u}_j$ in the first of Equations (3.15) is given by

$$Q_{LS} = (\underline{\hat{f}}_{jprop} - \underline{L}^{-1}\underline{\Phi}_{(m)}\underline{u}_j)^T \underline{W}_f (\underline{\hat{f}}_{jprop} - \underline{L}^{-1}\underline{\Phi}_{(m)}\underline{u}_j),$$

$$\underline{W}_f = \text{diag}\,(W_{f_1}, W_{f_2}, \ldots, W_{f_p}), \qquad (3.16)$$

where W_{f_i} is unity if there is a proposed value for channel i and is zero otherwise. The least squares estimate of $\underline{u}_j$ is the value for which Q_{LS} is minimized with respect to $\underline{u}_j$ and is given by

$$\hat{\underline{u}}_{jLS} = \underline{P}_f^{-1}\underline{\Phi}_{(m)}\underline{L}^{-1}\underline{W}_f\,\hat{\underline{f}}_{jprop}$$

$$\underline{P}_f = \underline{\Phi}_{(m)}^T\underline{L}^{-2}\underline{W}_f\underline{\Phi}_{(m)}. \qquad (3.17)$$

Then the M analysis estimate of $\hat{\underline{f}}_j$ on the assumption that the suspected absorber fits as one of the m absorbers in the experiment, is given by

$$\hat{\underline{f}}_{jLSM} = (\underline{L}^{-1}\underline{\Phi}_{(m)})\hat{\underline{u}}_{jLS} \qquad (3.18)$$

Note that whereas $\hat{\underline{f}}_{jprop}$ contains proposed values for only k wavelength channels, $\hat{\underline{f}}_{jLSM}$ contains estimated values for all p channels. If $\hat{\underline{f}}_{jLSM}$ fits $\hat{\underline{f}}_{jprop}$ to within random error at the k wavelength channels for which both contain values, then $\hat{\underline{f}}_{jprop}$ satisfies the first of Equations (3.15), and we conclude that the suspected absorber fits as one of the m linearly independent absorbers in the experiment. Moreover, $\hat{\underline{u}}_{jLS}$ is then taken to be an estimate of the j'th column of $\underline{U}$. If $\hat{\underline{f}}_{jLSM}$ and $\hat{\underline{f}}_{jprop}$ do not fit each other to within random error, then $\hat{\underline{f}}_{jprop}$ does not satisfy the first of Equations (3.15) and we conclude that the suspected absorber does not fit as one of the m linearly independent absorbers.

The second of Equations (3.15) gives a similar least squares equation for using proposed values for k elements of $\underline{e}_j$ to determine whether a suspected absorber fits as one of the m linearly independent absorbers in the

experiment. Define the proposed concentration vector as $\underline{c}_{jprop}$, where the k times for which there are proposed values contain those values, and where the remaining (N-k) times contain zeroes. The least squares estimate of $\hat{\underline{v}}_j$ in the second of Equations (3.15) is given by

$$\hat{\underline{v}}_{jLS} = \underline{P}_c^{-1}\underline{\Psi}_{(m)}\underline{T}^{-1}\underline{W}_c\hat{\underline{c}}_{jprop},$$

$$\underline{P}_c = \underline{\Psi}_{(m)}^T\underline{T}^{-2}\underline{W}_c\underline{\Psi}_{(m)},$$

$$\underline{W}_c = \text{diag}\,(W_{c_1}W_{c_2},\ldots,W_{c_N}), \tag{3.19}$$

Where W_{c_i} is unity if there is a proposed value for time i and is zero otherwise. The M analysis estimate of $\underline{c}_j$ on the assumption that the suspected absorber fits as one of the m linearly independent absorbers in the experiment is given by

$$\hat{\underline{c}}_{jLSM} = (\underline{T}^{-1}\underline{\Psi}_{(m)})\,\hat{\underline{v}}_{jLS} \tag{3.20}$$

If $\hat{\underline{c}}_{jLSM}$ fits $\hat{\underline{c}}_{jprop}$ at the k times for which both contain values, we conclude that the suspected absorber fits as one of the m linearly independent absorbers, and we take $\hat{\underline{v}}_{jLS}$ to be the j'th column of $\underline{V}$.

Two notes of caution are necessary regarding the correct interpretation of these least squares criteria. First, the fit of a suspected absorber as one of the m

linearly independent absorbers shows that the experiment can be interpreted using the suspected absorber as one of the absorbers, but does not prove that the suspected absorber is an absorber in the experiment. Secondly, if a suspected absorber does not fit as one of the m linearly independent absorbers, it may still be an absorber in the experiment if there are actually more than m absorbers and if the static spectrum or concentration vector of the suspected absorber is linearly dependent on the static spectra or concentration vectors of other absorbers.

Example 1. As an example of the effect of linear dependence, consider a two absorber reaction that follows the simple kinetic mechanism

$$A_1 + A_2 \xrightarrow{k_1} \text{non absorbing products} \qquad \text{(I)}$$

where the initial concentrations of A_1 and A_2 in the experiment are equal

$$c_1(0) = c_2(0)$$

Mechanism (I) imposes the constraint

$$\underline{\dot{c}}_1 = \underline{\dot{c}}_2,$$

where $\underline{\dot{c}}_j = d/dt\ (\underline{c}_j)$, and Equations (3.A) and (3.B) together give the constraint

$$\underline{c}_1 = \underline{c}_2 \qquad (3.C)$$

so that $\underline{c}_1$ and $\underline{c}_2$ are linearly dependent. Although there are two absorbers, m is unity. Even if the static spectra $\underline{f}_1$ and $\underline{f}_2$ are linearly independent, they do not individually satisfy the first of Equations (3.15), and by testing them as proposed static spectra we would correctly conclude that A_1 and A_2 are not linearly independent absorbers in the reaction. The information in the experiment lumps A_1 and A_2 together as one absorber. This can be seen by noting that the Beer's Law contribution to this experiment may be written as

$$\underline{F}\ \underline{C}^T = (\underline{f}_1+\underline{f}_2)\ \underline{c}_1^T \qquad (3.D)$$

from which it can be shown that the combination $\hat{\underline{f}}_{jprop} = (\underline{f}_1+\underline{f}_2)$ would fit as the proposed static spectrum for an absorber.

The problem of estimating $\underline{F}$ and $\underline{C}$ simplifies when the number of absorbers is small. In the next three sections we review the simplifications for one, two, and three absorber experiments. These simplifications apply also to any subspace of wavelength and time that contains only one, two or three absorbers, even though the overall experiment contains more than three absorbers.

B.

is

Eq

Si

pl

of

fr

To

ce

no

ex

of

sc

C.

th

B. One Absorber Simplifications

The estimation of $\underline{F}$ and $\underline{C}$ in a one absorber experiment is trivial. The matrices $\underline{U}$ and $\underline{V}$ reduce to scalars. Equations (3.15) and (3.13) become

$$\hat{\underline{f}}_1 = (\underline{L}^{-1}\underline{\phi}_1)u_{11},\ \hat{\underline{c}}_1 = (\underline{T}^{-1}\underline{\psi}_1)v_{11},\ u_{11}v_{11} = \omega_1. \qquad (3.21)$$

Since $\hat{\underline{f}}_1$ is an estimate of $\underline{f}_1$ to within an arbitrary multiplicative constant α_1, we may take $\hat{\underline{f}}_1$ to be any multiple of $\underline{L}^{-1}\underline{\phi}_1$. Arbitrarily setting u_{11} equal to one, we obtain from Equations (3.21)

$$\hat{\underline{f}}_1 = \underline{L}^{-1}\underline{\phi}_1,\ \hat{\underline{c}}_1 = (1/\omega_1)\ \underline{T}^{-1}\underline{\psi}_1. \qquad (3.22)$$

To determine α_1 so that the molar absorptivities and concentrations of absorber one are known requires either the nonzero molarity of absorber one at any time during the experiment, or the product of the nonzero molar absorptivity of absorber one at any wavelength channel times the absorbance cell path length.

C. Two Absorber Simplifications

The simplifications for two absorber experiments give the following three results:

1. When the shape of one absorber's static spectrum

is known, the shape of the other absorber's concentration profile can be computed directly.

2. When the shape of one absorber's concentration profile is known, the shape of the other absorber's static spectrum can be computed directly.

3. Even when there is no outside information about the static spectra and concentration profiles, their upper and lower bounds can be computed directly from the M analysis eigenvectors and eigenvalues.

In a two absorber experiment $\underline{U}$ and $\underline{V}$ are the (2x2) matrices

$$\underline{U} = (\underline{u}_1, \underline{u}_2) = \begin{pmatrix} u_{11} & u_{12} \\ u_{21} & u_{22} \end{pmatrix}$$

$$\underline{V} = (\underline{v}_1, \underline{v}_2) = \begin{pmatrix} v_{11} & v_{12} \\ v_{21} & v_{22} \end{pmatrix} \qquad (3.23)$$

The following relationships between the vectors in $\underline{U}$ and $\underline{V}$ can be derived from Equation (3.13)

$$\underline{v}_1 = [1/\det(\underline{U})]\underline{\Omega}_{(2)}\underline{K}\,\underline{u}_2,\ \underline{v}_2 = -[1/\det(\underline{U})]\underline{\Omega}_{(2)}\,\underline{K}\,\underline{u}_1$$

$$\underline{u}_1 = [1/\det(\underline{V})]\underline{\Omega}_{(2)}\underline{K}\,\underline{v}_2,\ \underline{u}_2 = -[1/\det(\underline{V})]\underline{\Omega}_{(2)}\,\underline{K}\,\underline{v}_1$$

$$\underline{K} = \begin{pmatrix} 0 & 1 \\ -1 & 0 \end{pmatrix} \tag{3.24}$$

We assume that absorbers one and two are assigned so that $\det(\underline{U})$ and $\det(\underline{V})$ are positive. (Switching absorbers merely changes the signs of these determinants.) If the static spectrum of absorber two is known, $\underline{u}_2$ can be estimated via Equation (3.17). Then, the first of Equations (3.24) gives $\underline{v}_1$ to within the arbitrary multiplicative constant $[1/\det(\underline{U})]$. This is sufficient to estimate $\hat{\underline{c}}_1$ since $\hat{\underline{c}}_1$ itself is defined with the arbitrary multiplicative constant $(1/\alpha_1)$. Arbitrarily setting $[1/\det(\underline{U})] = 1$, we have, from Equations (3.15) and (3.24),

$$\hat{\underline{c}}_1 = (\underline{T}^{-1}\underline{\Psi}_{(2)})\underline{\Omega}_{(2)}\underline{K}\,\underline{u}_2. \tag{3.25}$$

Hence, we obtain $\hat{\underline{c}}_1$ from $\hat{\underline{f}}_2$. Likewise the next three of Equations (3.24) yield, respectively, $\hat{\underline{c}}_2$ from $\hat{\underline{f}}_1$, $\hat{\underline{f}}_1$ from $\hat{\underline{c}}_2$, and $\hat{\underline{f}}_2$ from $\hat{\underline{c}}_1$. Note from Equations (3.24) that in a two absorber experiment the shapes of a single absorber's concentration profile and static spectrum can be varied independently of one another and therefore, contain no information about each other.

Physically sensible static spectra and concentration vectors must contain only nonnegative numbers. By a derivation similar to the one presented by Lawton and Sylvestre (1971), we can use the nonnegative definiteness of the elements of $\underline{\hat{f}}_1$, $\underline{\hat{f}}_2$, $\underline{\hat{c}}_1$ and $\underline{\hat{c}}_2$ to define solution bands that contain the shapes of these vectors. Since we are interested in only the shapes of the static spectra and concentration profiles, we normalize these vectors to unit length. Hence, define $\underline{\hat{f}}'_1$, $\underline{\hat{f}}'_2$, $\underline{\hat{c}}'_1$, and $\underline{\hat{c}}'_2$ whose elements satisfy the following normalization equations and inequalities

$$\sum_{i=1}^{P} \hat{f}'_{i1} = 1, \quad \hat{f}'_{i1} \geq 0$$

$$\sum_{i=1}^{P} \hat{f}'_{i2} = 1, \; \hat{f}'_{i2} \geq 0, \; i = 1,2,\ldots,p$$

$$\sum_{i=1}^{N} \hat{c}'_{i1} = 1, \quad \hat{c}'_{i1} \geq 0,$$

$$\sum_{i=1}^{N} \hat{c}'_{i2} = 1, \; \hat{c}'_{i2} \geq 0, \quad i = 1,2,\ldots,N \qquad (3.26)$$

The results are displayed in Tables 3.1 and 3.2. Note that $\underline{\hat{f}}'_{iL}$ and $\underline{\hat{f}}'_{iH}$ delineate regions of acceptability of $\underline{\hat{f}}'_i$. In general, $\underline{\hat{f}}'_{iL}$ and $\underline{\hat{f}}'_{iH}$ cross over i.e., $\underline{\hat{f}}'_{iL}$ is not always less than $\underline{\hat{f}}'_{iH}$. The same situation obtains for $\underline{\hat{c}}'_{iL}$ and $\underline{\hat{c}}'_{iH}$. Examples may be found in Chapter 4.

These solution bands are particularly useful since

Table 3.1. Solution Bands for Normalized Static Spectra.

$\hat{\underline{f}}'_1$ must fall on or between $\hat{\underline{f}}'_{1L}$ and $\hat{\underline{f}}'_{1H}$.

$$\hat{\underline{f}}'_{1L} = (\underline{L}^{-1}\,\underline{\Phi}_{(2)})\underline{u}'_{1L}, \quad \hat{\underline{f}}'_{1H} = (\underline{L}^{-1}\,\underline{\Phi}_{(2)})\underline{u}'_{1H}$$

$$\hat{\underline{f}}'_{2L} = (\underline{L}^{-1}\,\underline{\Phi}_{(2)})\underline{u}'_{2L}, \quad \hat{\underline{f}}'_{2H} = (\underline{L}^{-1}\,\underline{\Phi}_{(2)})\underline{u}'_{2H}$$

$$\underline{u}'_{1L} = (a_1 - a_2 a_3)^{-1}\begin{pmatrix} 1 \\ -a_3 \end{pmatrix}, \quad \underline{u}'_{1H} = (a_1\omega_1 + a_2 a_4 \omega_2)^{-1}\begin{pmatrix} \omega_1 \\ a_4\omega_2 \end{pmatrix}$$

$$\underline{u}'_{2L} = (a_1\omega_1 + a_2 a_5 \omega_2)^{-1}\begin{pmatrix} \omega_1 \\ a_5\omega_2 \end{pmatrix}, \quad \underline{u}'_{2H} = (a_1 + a_2 a_6)^{-1}\begin{pmatrix} 1 \\ a_6 \end{pmatrix}$$

$$a_1 = \sum_{i=1}^{p} L_i^{-1}\,\phi_{i1}, \quad a_2 = \sum_{i=1}^{p} L_i^{-1}\,\phi_{i2}$$

$$a_3 = \min_{\phi_{i2}>0} (\phi_{i1}/\phi_{i2}), \quad a_4 = \min(\psi_{j2}/\psi_{j1})$$

$$a_5 = \max(\psi_{j2}/\psi_{j1}), \quad a_6 = \min_{\phi_{i2}<0} \left|\phi_{i1}/\phi_{i2}\right|$$

Table 3.2. Solution Bands for Normalized Concentration Vectors.

$\hat{\underline{c}}_i'$ must fall on or between $\hat{\underline{c}}_{iL}'$ and $\hat{\underline{c}}_{iH}'$.

$$\hat{\underline{c}}_{1L}' = (\underline{T}^{-1}\ \underline{\Psi}_{(2)})\underline{v}_{1L}', \quad \hat{\underline{c}}_{1H}' = (\underline{T}^{-1}\ \underline{\Psi}_{(2)})\underline{v}_{1H}'$$

$$\hat{\underline{c}}_{2L}' = (\underline{T}^{-1}\ \underline{\Psi}_{(2)})\underline{v}_{2L}', \quad \hat{\underline{c}}_{2H}' = (\underline{T}^{-1}\ \underline{\Psi}_{(2)})\underline{v}_{2H}'$$

$$\underline{v}_{1L}' = (b_1 - b_2 b_3)^{-1} \begin{pmatrix} 1 \\ -b_3 \end{pmatrix}, \quad \underline{v}_{1H}' = (b_1\omega_1 + b_2 b_4 \omega_2)^{-1} \begin{pmatrix} \omega_1 \\ b_4\omega_2 \end{pmatrix}$$

$$\underline{v}_{2L}' = (b_1\omega_1 + b_2 b_5 \omega_2)^{-1} \begin{pmatrix} \omega_1 \\ b_5\omega_2 \end{pmatrix}, \quad \underline{v}_{2H}' = (b_1 + b_2 b_6)^{-1} \begin{pmatrix} 1 \\ b_6 \end{pmatrix}$$

$$b_1 = \sum_{j=1}^{N} T_j^{-1}\ \psi_{j1}, \quad b_2 = \sum_{j=1}^{N} T_j^{-1}\ \psi_{j2}$$

$$b_3 = \min_{\psi_{j2}>0} (\psi_{j1}/\psi_{j2}), \quad b_4 = \min\ (\phi_{i2}/\phi_{i1})$$

$$b_5 = \max(\phi_{i2}/\phi_{i1}), \quad b_6 = \min_{\psi_{j2}<0} \left|\psi_{j1}/\psi_{j2}\right|$$

they define the range of acceptable static spectra and concentration vectors without requiring any assumptions about the identities of the absorbers or the kinetic mechanism of the reaction. In general, as the static spectra and concentration profiles become less linearly dependent (less overlapping), their solution bands become narrower, and the experiment thus more clearly defines their shapes.

D. Three Absorber Simplifications

Simplifications for three absorber experiments give the following results:

1. When the shapes of two absorbers' static spectra are known, the shape of the remaining absorber's concentration profile can be computed directly.

2. When the shapes of two absorbers' concentration profiles are known, the shape of the remaining absorber's static spectrum can be computed directly.

Assume that absorbers one through three are assigned so that det($\underline{U}$) and det($\underline{V}$) are positive. Equation (3.13) gives the following relationships between the vectors in $\underline{U}$ and $\underline{V}$.

$$\underline{v}_\alpha = [1/\det(\underline{U})]\, \underline{\Omega}_{(3)}\, (\underline{u}_\beta \times \underline{u}_\gamma)$$

$$\underline{u}_\alpha = [1/\det(\underline{V})]\, \underline{\Omega}_{(3)}\, (\underline{v}_\beta \times \underline{v}_\gamma) \qquad (3.27)$$

where the subscripts (α,β,γ) are taken in the order

$$(1,2,3), \quad (2,3,1), \quad \text{or } (3,1,2).$$

If the static spectra of absorbers two and three are known, the first of Equations (3.27) gives $\underline{v}_1$ to within the arbitrary constant $[1/\det(\underline{U})]$. As in the two absorber case, we may arbitrarily set $[1/\det(\underline{V})] = 1$, so that from Equations 3.15) and (3.27) $\hat{\underline{c}}_1$ is given by

$$\hat{\underline{c}}_1 = (\underline{T}^{-1}\underline{\Psi}_{(3)})\underline{\Omega}_{(3)} \ (\underline{u}_2 \times \underline{u}_3) \tag{3.28}$$

Thus, the first of Equations (3.27) gives the concentration profile of any absorber from the static spectra of the other two absorbers. Likewise, the second of Equations (3.27) gives the static spectrum of any absorber from the concentration profiles of the other two absorbers. As in the two absorber case, the shapes of a single absorber's static spectrum and concentration profile can be varied independently of one another, and hence contain no information about each other.

E. S. Analysis Estimates of F

Suppose that the proposed static spectrum $\hat{\underline{f}}_{j\text{prop}}$ for a suspected absorber fits as belonging to one of the m absorbers in the experiment. In this section we present

a least squares equation that uses the S analysis eigenvectors and $\underline{\hat{f}}_{jprop}$ to characterize the rate behavior of absorber j in the experiment.

In weighted S analysis we are concerned with the experimentally measured matrix $(\underline{A}-\underline{\bar{A}})$, where $\bar{A}_{ij} = (1/N) \sum_{k=1}^{N} A_{ik}$, and for which we assume the model

$$(\underline{A}-\underline{\bar{A}}) = \underline{F}\,\underline{H}^T + (\underline{\varepsilon}-\underline{\bar{\varepsilon}}) = \left(\sum_{j=1}^{q} \underline{f}_j \underline{h}_j^T\right) + (\underline{\varepsilon}-\underline{\bar{\varepsilon}})$$

$$\underline{H} = (\underline{h}_1, \underline{h}_2, \ldots, \underline{h}_q)$$

$$\underline{h}_j = \underline{c}_j - \underline{1}(1/N) \sum_{k=1}^{N} c_j(t_k)$$

$$\bar{\varepsilon}_{ij} = (1/N) \sum_{k=1}^{N} \varepsilon_{ik}$$

We form the weighted sample covariance matrix $\underline{S}_W$, defined by

$$\underline{S}_W = [1/(N-1)]\ (\underline{A}_W-\underline{\bar{A}}_W)(\underline{A}_W-\underline{\bar{A}}_W)^T \qquad (3.30)$$

where

$$\underline{\bar{A}}_W + \underline{L}\,\underline{A}\,\underline{T},$$

and we solve the eigenvalue equation

$$\underline{S}_W\underline{B} = \underline{B}\ \underline{\Lambda}$$

$$\underline{\Lambda} = \text{diag}(\lambda_1,\lambda_2,\ldots,\lambda_p), \quad \lambda_1 \geq \lambda_2 \geq,\ldots,\geq \lambda_p \tag{3.31}$$

The essential rank s is the minimum number of absorbers whose concentrations must have changed during the experiment. It is determined by finding the lowest value of r for which $(\hat{\underline{A}}_{(r)}-\overline{\underline{A}})$, defined by

$$(\hat{\underline{A}}_{(r)}-\overline{\underline{A}}) = (\underline{L}^{-1}\underline{B}_{(r)}\underline{B}_{(r)}{}^{T}\underline{L})\ (\underline{A}-\overline{\underline{A}}) \tag{3.32}$$

fits the experimental matrix $(\underline{A}-\overline{\underline{A}})$ to within its random errors. By the same reasoning that was applied to M analysis, we take from Equation (3.32) the following model for estimating $\underline{F}$ and $\underline{H}$

$$(\hat{\underline{A}}_{(s)}-\overline{\underline{A}}) = \hat{\underline{F}}\ \hat{\underline{H}}^{T} = \sum_{j=1}^{q} \hat{\underline{f}}_j\hat{\underline{h}}_j^{T} = (\underline{L}^{-1}\underline{B}_{(s)}\underline{B}_{(s)}^{T}\underline{L})\ (\underline{A}-\overline{\underline{A}}) \tag{3.33}$$

Now s cannot exceed m; <u>i.e.</u>, there cannot be more absorbers changing concentration than there are absorbers in the experiment. If we assume, as before, that m is the number of absorbers in the experiment, there are only two cases to consider:

<u>Case 1.</u> If s equals m, the concentrations of all m absorbers have changed during the experiment. Moreover, the rate vectors $(\dot{\underline{c}}_j,\ j = 1,2,\ldots,m)$ form a linearly independent set.

Case 2. If s is less than m, then at least (m-s) absorbers have either not changed concentration during the experiment or have rate vectors that are linearly dependent on the rate vectors of other absorbers in the experiment.

If absorber j has a nonzero, linearly independent rate vector $\underline{\dot{c}}_j$, then $\underline{\hat{f}}_j$ must satisfy the equation

$$\underline{\hat{f}}_j = (\underline{L}^{-1}\underline{B}_{(s)})\underline{g}_j, \tag{3.34}$$

where $\underline{g}_j$ is an s component column vector. If absorber j has a zero or linearly dependent rate vector, then $\underline{\hat{f}}_j$ does not in general satisfy Equation (3.34).

Moreover, we can use the proposed static spectrum to determine whether or not absorber j satisfies Equation (3.34). Given $\underline{\hat{f}}_{jprop}$, the least squares estimate of $\underline{g}_j$ is $\underline{\hat{g}}_{jLS}$, defined by

$$\underline{\hat{g}}_{jLS} = \underline{P}_s^{-1}\underline{B}_{(s)}\ \underline{L}^{-1}\underline{W}_s\ \underline{\hat{f}}_{jprop},$$

$$\underline{P}_s = \underline{B}_{(s)}^T\underline{L}^{-2}\underline{W}_W\underline{B}_{(s)},$$

$$\underline{W}_s = \text{diag}(W_{s1}, W_{s2}, \ldots, W_{sN}), \tag{3.35}$$

where W_{si} is unity if there is a proposed value for channel i and is zero otherwise. The S analysis estimate of $\underline{\hat{f}}_j$ is given by

$$\hat{\underline{f}}_{jLSS} = (\underline{L}^{-1}\underline{B}_{(s)})\hat{\underline{g}}_{jLS} \qquad (3.36)$$

If absorber j has a nonzero, linearly independent rate vector, then $\hat{\underline{f}}_{jLSS}$ and $\hat{\underline{f}}_{jprop}$ must be equal to within random error. Otherwise, they do not in general fit each other. If $\dot{\underline{c}}_j$ is linearly dependent on the rate vectors of other absorbers in the reaction, then an appropriate linear combination of $\underline{f}_j$ and the static spectra of these other absorbers satisfies Equation (3.34). We give two simple examples to illustrate S-analysis testing of linear independence.

Example 2. Consider a two absorber system where absorber one decays to non-absorbing products via the mechanism

$$A_1 \overset{k_1}{\rightarrow} \text{non-absorbing products} \qquad (II)$$

and where absorber two does not change concentration during the experiment. If $\underline{f}_1$ and $\underline{f}_2$ are linearly independent, then m=q=2. The constraint $\dot{\underline{c}}_2 = \underline{0}$ implies that $\underline{h}_2 = 0$. Therefore, $\underline{H}$ is of rank one, and s=1. With $\underline{h}_2 = 0$, Equation (3.33) for this system becomes

$$(\hat{\underline{A}}_{(1)}-\bar{\underline{A}}) = \hat{\underline{f}}_1\hat{\underline{h}}_1^T = (\underline{L}^{-1}\underline{B}_{(1)}\underline{B}_{(1)}^T\underline{L})\ (\underline{A}-\bar{\underline{A}}),$$

which gives

$$\hat{\underline{f}}_1 = (\underline{L}^{-1}\underline{B}_{(1)})\ \underline{g}_1$$

$$\underline{g}_1 = \underline{B}_{(1)}^T\underline{L}(\underline{A}-\bar{\underline{A}})\ \underline{h}_1(\underline{h}_1\underline{h}_1^T)^{-1}.$$

Thus, $\hat{\underline{f}}_1$ satisfies Equation (3.34), as expected, and absorber one fits as having linearly independent rates. $(\hat{\underline{A}}_{(1)}-\bar{\underline{A}})$ contains no information about absorber two. Thus, $\hat{\underline{f}}_2$, as expected, does not satisfy Equation (3.34), and absorber two does not fit as having linearly independent rates.

Example 3. Consider a two absorber system that reacts via the mechanism

$$A_1 \overset{k_1}{\rightarrow} A_2 \qquad \text{(III)}$$

where $\underline{f}_1$ and $\underline{f}_2$ are linearly independent. For this case, m=q=2. Mechanism (III) has the constraint

$$\dot{\underline{c}}_1 + \dot{\underline{c}}_2 = \underline{0}$$

which implies the constraint

$$\hat{\underline{h}}_1 + \hat{\underline{h}}_2 = \underline{0}$$

$\underline{H}$ is thus of rank one, and s = 1. Equation (3.33) for this system is

$$(\hat{\underline{A}}_{(1)}-\bar{\underline{A}})=\hat{\underline{F}}\ \hat{\underline{H}}^T=\hat{\underline{f}}_1\hat{\underline{h}}_1^T + \hat{\underline{f}}_2\hat{\underline{h}}_2^T = (\underline{L}^{-1}\underline{B}_{(1)}\underline{B}_{(1)}^T\underline{L}),$$

which cannot be solved for $\hat{\underline{F}}$ since $\hat{\underline{H}}$ is of rank one and the inverse $(\hat{\underline{H}}\ \hat{\underline{H}}^T)^{-1}$ does not exist. Therefore, $\hat{\underline{f}}_1$ and $\hat{\underline{f}}_2$ do not satisfy Equation (3.34) and absorbers one and two do not fit as having linearly independent rates.

S analysis lumps absorbers one and two together. To see this, note that with $\underline{h}_1 + \underline{h}_2 = \underline{0}$, $\underline{F}\ \underline{H}^T$ can be expressed as

$$\underline{F}\ \underline{H}^T = (\underline{f}_1-\underline{f}_2)\underline{h}_1$$

$(\underline{f}_1-\underline{f}_2)$ satisfies Equation (3.34) and, therefore, the combination $\underline{f}_{jprop} = (\underline{f}_1-\underline{f}_2)$ would fit as an "absorber" with linearly independent rates.

F. Strategy for Resolving a Rapid Scanning Kinetics Experiment

In this section we present a seven step strategy for applying the tools discussed in Chapter 2 and the preceding sections of this Chapter to resolve a rapid scanning kinetics experiment into the static spectra and concentration vectors of its absorbers. We assume that the kinetic mechanism of the reaction is not already known. Indeed, the proposal and testing of kinetic mechanisms and estimation of their rate constants are advanced goals of a

rapid scanning kinetics study, and should not be undertaken until the static spectra and concentration vectors have first been extracted from each experiment.

Most of the external information with which the experiment is to be resolved comes from measured or proposed static spectra of suspected absorbers. Little is assumed to be known already about the concentration vectors, except perhaps the initial concentrations of reactants and catalysts, a degree of knowledge usually too small to be of much value in resolving the experiment.

Step 1. Use weighted M and S analyses to determine the essential ranks m and s for the whole experiment. There must be at least m absorbers in the experiment, and of these, at least s must change concentration.

Step 2. Assume that there are m absorbers in the experiment. Fit to the M analysis eigenvectors for the whole experiment the measured static spectrum of each light absorbing reactant, catalyst, and known product. Each spectrum that fits may be counted as belonging to an absorber in the experiment. Each spectrum that does not fit is either not present in the experiment, or represents an absorber whose concentration is linearly dependent on the other absorbers' concentrations. In the latter case, the experiment has more than m absorbers. Unless there are strong reasons to suspect linear dependence among the concentrations or static spectra, maintain the assumption that m is the number of absorbers in the experiment.

Step 3. Fit each measured static spectrum that fits in Step 2 to the S analysis eigenvectors. Each spectrum that fits the S analysis eigenvectors may be counted as belonging to an absorber whose concentration changed and whose rate is linearly independent of the rates of the other absorbers. Each spectrum that does not fit represents an absorber whose concentration did not change, or whose rate is linearly dependent on the rates of the other absorbers.

Step 4. If the number of measured static spectra that fit the M analysis eigenvectors equals m, then all m columns of $\underline{U}$ have been estimated. Form $\underline{U}$ and obtain $\underline{V}$ from Equation (3.13). Use $\underline{V}$ to obtain the concentration vectors of the m absorbers. The experiment has been resolved.

If the number of measured static spectra that fit the M analysis eigenvectors is less than m, there is insufficient information to resolve the experiment at this point. Some of the m absorbers must be intermediates or unknown products of the reaction. Although there are no measured static spectra for these, we may infer some of their spectral and kinetic properties in Step 5.

Step 5. Perform principal component analyses on subspaces of wavelength and time in hopes of finding parts of the experiment with fewer absorbers than the whole experiment.

Step 6. Partially or completely resolve subspaces that contain one, two, or three absorbers by using the one, two and three absorber simplifications plus information

from absorbers whose measured static spectra fit the M analysis eigenvectors for these subspaces.

Step 7. Each concentration vector obtained from a subspace of wavelengths in Step 6 can be fit to the M analysis eigenvectors for the whole experiment to give one column of $\underline{V}$ for the whole experiment. Likewise, each static spectrum obtained from a subspace of time gives one column of $\underline{U}$ for the whole experiment. If enough information has been obtained in Step 6 to give either the static spectra or concentration vectors of the required minimum number of absorbers m for the whole experiment, fit this new information to the M analysis eigenvectors for the whole experiment to obtain either all the columns of $\underline{U}$ or $\underline{V}$. The remaining unknown rotation matrix may be obtained from Equation (3.13). Use $\underline{U}$ and $\underline{V}$ to obtain $\underline{F}$ and $\underline{C}$. The experiment has been resolved.

The following Chapter applies this seven step strategy in a rapid scanning kinetics study of an enzyme-catalyzed reaction.

CHAPTER 4

A RAPID SCANNING STOPPED FLOW STUDY OF THE LADH-CATALYZED REDUCTION OF NDMA BY NADH

A. Introduction

In this chapter we apply the method of principal component analysis described in the two preceding chapters to a scanning stopped flow study of the horse liver alcohol dehydrogenase (LADH) catalyzed reduction of the substrate analog p-nitroso-N,N-dimethylaniline (NDMA) by reduced nicotinamide adenine dinucleotide (NADH). Previous studies of this reaction by Dunn and Bernhard (1971), Schack and Dunn (1972), and Suelter, et al. (1975) have indicated that the reaction is spectrally complex. It is thus particularly suitable for a scanning kinetics study. The purpose of the research reported here was to map out for the first time the static spectra and concentration profiles of the light absorbing substrates, products, and transient intermediates that occur in this reaction.

LADH is an extensively studied enzyme that catalyzes the metabolism of ingested ethanol to acetaldehyde via the overall reaction (Bränden, et al., 1975)

$$\text{Ethanol} + \text{NAD}^+ \rightleftarrows \text{Acetaldehyde} + \text{NADH} + \text{H}^+ \qquad \text{(I)}$$

where NAD^+ is oxidized nicotinamide adenine dinucleotide. NADH and NAD^+ belong to a special class of substrates and products called coenzymes. They are the oxidizing and reducing agents in reactions catalyzed by many dehydrogenase enzymes besides LADH. The reactions and properties of NADH and NAD^+ have been reviewed by Kaplan (1960).

The review articles by Sund and Theorell (1960), Bränden, et al., (1975), and Dalziel (1975) discuss the structural and kinetic aspects of LADH. LADH is a dimer with two catalytic sites per molecule and a molecular weight of 84000 (Sund and Theorell, 1960). Pietrusko, et al. (1966) showed that there are two types of protein chains for LADH, which they called the E and S subunits. These give three possible dimeric forms (called isozymes) of LADH: EE, SS, and ES. The E subunit occurs more frequently and is active in the oxidation of ethanol (i.e., Reaction I). The less frequently occurring subunit S, is active in the oxidation of stercids (Pietrusko and Theorell, 1969). However, S has some ethanol activity and E has some steroid activity (Bränden, et al., 1975). Theorell et al., (1970) studied the binding of NADH to EE, SS, and ES, and found no evidence for interaction between the subunits. Pietrusko et al. (1966) determined that commercially available preparations of LADH contain predominantly the EE isozyme with 2-5% ES isozyme. Shore (private communication) claims that the LADH preparation

available from the Boehringer Mannheim Corporation (the preparation used in our study) is of sufficiently high EE purity for use in kinetic studies without risk of measurable interference from the ES isozyme.

Since the concentration of H^+ is usually buffered to be nearly constant in kinetic studies, Reaction I is viewed as a two-substrate, two-product reaction. Cleland and colleagues have developed a method of steady-state-initial-rate analysis for two substrate enzyme reactions [Cleland (1970)] that has been extensively applied to LADH catalyzed reactions of aliphatic alcohols and aldehydes in reactions analogous to I, [Wratten and Cleland (1963), Dalziel and Dickinson (1965)]. These studies, reviewed by Dalziel (1975), are consistent with the conclusion that in the most likely mechanism for Reaction I, NAD^+ binds to the active side of LADH before the alcohol binds, and that the aldehyde dissociates from the active site before NADH dissociates. This concept is called the "ordered mechanism" of LADH [Cleland (1970)] since the substrates and products enter and leave in a fixed order.

In steady-state-initial-rate kinetics studies, the total enzyme concentration is much smaller than the initial substrate concentrations, so that enzyme-bound transient intermediates of substrates and products are in general not spectrophotometrically detectable. In these experiments one observes only the overall conversion of enzyme-free substrates to enzyme-free products. However, in

experiments where the total enzyme concentration is of magnitude comparable to the initial substrate concentrations, the enzyme bound intermediates are spectrophotometrically detectable, providing their spectra are different from those of the free enzyme, substrates, and products. Moreover, a significant portion of the time course in a high enzyme concentration experiment involves the binding of substrates to the enzyme to form these transient intermediates. Studies with high enzyme concentrations are called "transient phase studies" [Dalziel (1975)], and in general require fast reaction techniques (e.g., stopped flow). The application of fast reaction techniques to transient phase enzyme studies is reviewed by Hammes and Schimmel (1970).

LADH catalyzed reactions have been extensively studied by the stopped flow technique under conditions of high enzyme concentrations by Shore (1969), Shore and Gutfreund (1970), Bernhard, et al. (1970), Dunn and Bernhard (1971), Brooks, Shore, and Gutfreund (1972), Luisi and Favilla (1972), Dunn (1972), McFarland and Bernhard (1972), Dunn and Hutchison (1973), Shore, et al (1974), Dunn, Biellman, and Branlandt (1975), Shore and Santiago (1975) and Suelter, et al. (1975). Some of these studies have been reviwed by Holbrook and Gutfreund (1973), Dalziel (1975), and Bränden, et al. (1975). The studies of Shore, Gutfreund and colleagues have focused primarily on the oxidation of ethanol (Reaction I), and the studies of Dunn, Bernhard,

and colleagues have focused primarily on the reduction of analogs of acetaldehyde in Reaction I.

The substrate NDMA that is the subject of our study is an acetaldehyde analog substrate first studied by Dunn and Bernhard (1971). They proposed the following overall reaction for the LADH catalyzed reduction of NDMA by NADH

$$NDMA + NADH + H^+ \rightarrow P + NAD^+ \qquad (II)$$

where NDMA is p-nitroso-N,N-dimethylaniline, and where P was tentatively assigned as p-N,N-dimethylaminophenyl-hydroxylamine. NDMA was used because of its intense chromophore at 440 nm ($_{440}$ = 3.54×10^4 O.D. $M^{-1}cm^{-1}$) and was intended to be an analog of the non-absorber acetaldehyde in the biological Reaction I [Dunn and Bernhard (1971)]; i.e., Reaction II involves reduction of the carbonyl group of acetaldehyde.

Dunn and Bernhard (1971) measured in single wavelength stopped flow experiments the absorbance-time profiles at 330 nm and 440 nm under a variety of initial concentrations. Their interpretation of the reaction focused primarily on the 440 nm results. They report that when $[NDMA]_0 > [LADH]_0 > [NADH]_0$ (where $[LADH]_0$ is the initial concentration of active sites assuming two active sites per LADH molecule), then the absorbance decay at 440 nm is biphasic, with equal amplitude absorbance changes in the fast and slow portions. On the assumption

that NDMA is the only absorber at 440 nm, they calculated that each portion of the biphasic decay corresponds to the disappearance of NDMA equal to 1/2 $[NADH]_0$. They observed biphasic absorbance decay at 440 nm to a final value of zero optical density under the conditions $[LADH]_0 < [NDMA]_0 < [NADH]_0$. With the assumption that NDMA is the only absorber at 440 nm, they calculated that the amount of NDMA that disappeared in the fast portion was equal to 1/2 $[LADH]_0$. For the conditions $[NDMA]_0 < [LADH]_0 << [NADH]_0$, they report a single rapid first order decay of absorbance at 440 nm to zero optical density.

To explain their calculated results for the disappearance of NDMA, Dunn and Bernhard (1971) proposed the following mechanism, where E = LADH, S = NDMA, and X = (NAD^+-Product) complex,

$$E(NADH)_2(S) \overset{\text{fast}}{\rightleftarrows} E(NADH)_2(S)_2 \overset{\text{fast}}{\rightleftarrows}$$
$$E(NADH)(S)(X) \overset{\text{slow}}{\rightarrow} \ldots E + 2NAD^+ + 2P \qquad \text{(III)}$$

They assume that only species containing S have absorbance at 440 nm, and that the spectral contribution of each S is the same as free NDMA. III has been named the "half-of-the-sites reactivity mechanism" [Bränden, et al. (1975)]. It predicts that when one of the two sites on an LADH molecule contains the NAD^+-Product complex X, conversion to NAD^++Product of the NADH-S complex occupying

the other site becomes very slow; i.e., the presence of X on one site lowers the activity of the other site. III also assumes that both sites must be occupied by NADH before either site can reduce S. This feature is required to account for Dunn and Bernhard's calculation that, when $[NDMA]_0 > [NADH]_0$, the amount of S converted to X in the fast portion of the biphasic decay is 1/2 $[NADH]_0$, with another amount 1/2 $[NADH]_0$ converted to P in the slow portion. Dunn and Bernhard (1971) proposed that NDMA can dissociate rapidly from E(NADH)(S)X. Therefore, when $[NDMA]_0 < [LADH]_0 << [NADH]_0$ the NDMA is free to bind to an enzyme molecule that does not contain X, and III predicts a single rapid decay of NDMA.

In proposing III, Dunn and Bernhard (1971) did not assume that the two sites of LADH are different; there is strong structural evidence that the free EE isozyme of LADH is a symmetric dimer [Bränden, et al. (1975)]. Rather, they assume that the two sites interact with each other when they are occupied by substrates and products. Note that III requires interaction between the sites in two senses:

(i) Both sites must be occupied by NADH and NDMA before any product complex is formed.

(ii) The presence of X on one site lowers the catalytic activity of the other site.

In earlier studies of the LADH catalyzed reduction

of benzaldehyde, β-napthaldehyde, and 4-(2'-imidazolylazo) benzaldehyde, Bernhard, et al. (1970) reported biphasic decays of NADH and each aldehyde which they interpreted in terms of Mechanism III. However, Shore and Gutfreund (1970) studied the transient phase kinetics of Reaction I with ethanol as the substrate and with acetaldehyde as the substrate and found no evidence for any interaction between the sites of LADH. In a review article on transient phase kinetic studies of dehydrogenases, Holbrook and Gutfreund (1973) express the view that the biphasic decays reported by Dunn and Bernhard (1971) reflect two distinct steps in the mechanism rather than different reaction rates for the individual sites.

The purpose of the research reported here is the spectral and kinetic characterization of the substrates, products and transient intermediates in the spectrally rich LADH-NDMA-NADH reaction system, rather than the resolution of the "half-of-the-sites reactivity" issue. The broad-banded absorbance spectra of substrates enzyme and products in Reaction II make this reaction spectrally rich: NDMA (λ_{max} = 440 nm), NADH (λ_{max_1} = 260 nm, λ_{max_2} = 340 nm), NAD^+ (λ_{max} = 260 nm), LADH (λ_{max} = 280 nm), and P (λ_{max} = 255 nm (Dunn and Bernhard, 1971)). Dunn and Bernhard (1971) observed that the decay of absorbance at 330 nm, which they attributed to the 340 nm band of NADH, was not correlated to the decay of absorbance at 440 nm, which they attributed to NDMA. Since the decay at 330 nm

was much slower than at 440 nm, they hypothesized an absorbing intermediate at 330 nm. Schack and Dunn (1972) observed absorbance growth and decay at 540 nm, which they attributed to yet another intermediate. Suelter, et al. (1975) observed in four replicate scanning stopped flow experiments that the decay portions of the absorbance-time profiles at 330 nm, 350 nm, and 360 nm, had different first order decay parameters. They hypothesized two intermediates plus the 340 nm band of NADH as absorbers at these wavelengths. Suelter, et al. (1975) also observed the growth and decay of absorbance at 540 nm reported previously by Schack and Dunn (1972). These hints of spectral complexity and the occurrence of possible transient intermediates, plus the previous lack of a systematic, mechanism-independent means of sorting out these intermediates, indicated to us that the LADH-NDMA-NADH reaction was ripe for a scanning kinetics study coupled with principal component analysis.

Figure 4.1 shows a simplified block diagram of the scanning stopped flow absorbance spectrometer used in this study. The design, construction, and characterization of the stopped flow spectrometer were executed and reported by Ho (1976). This instrument is a modification of the stopped flow system reported by Papadakis, Coolen and Dye (1975) and was specifically designed for enzyme studies. It features low holding volumes to minimize the required quantities of enzyme solutions

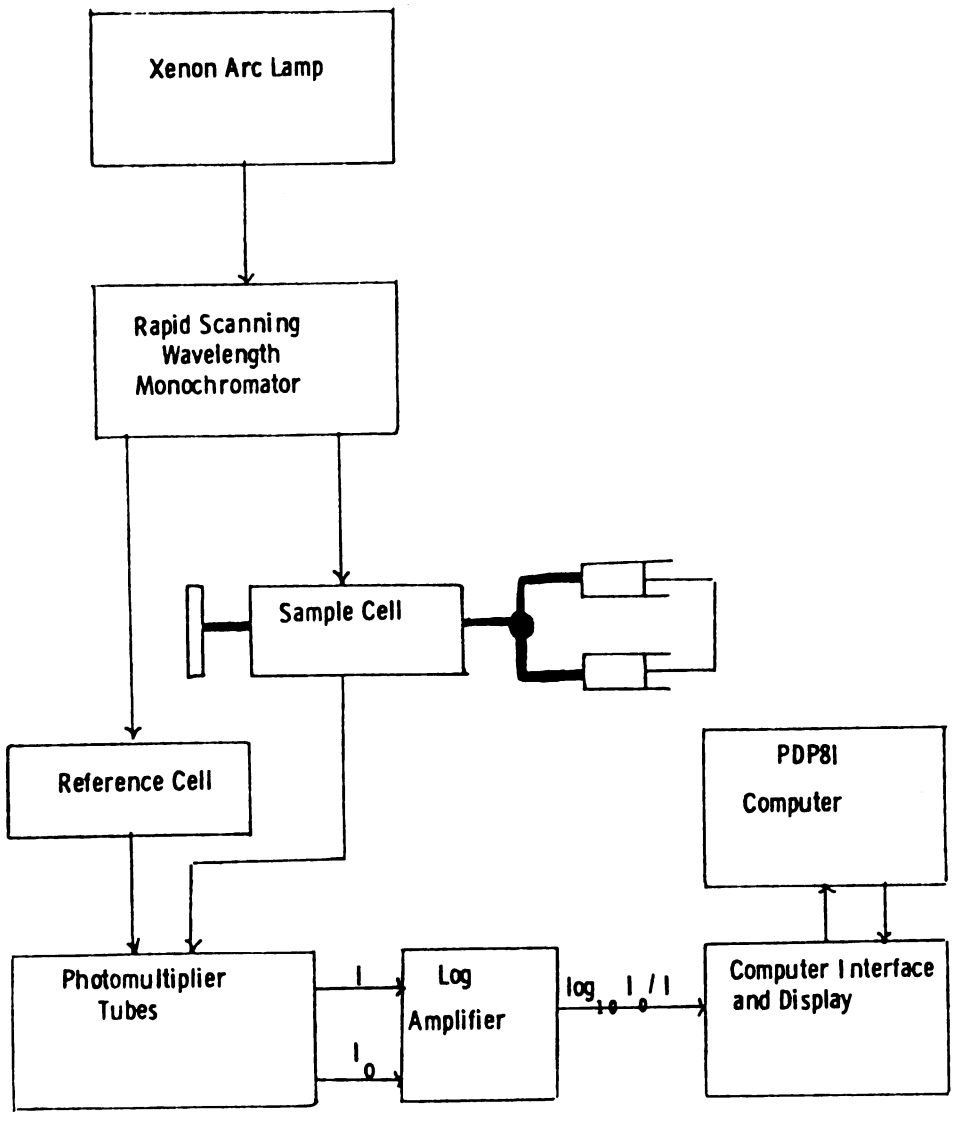

Figure 4.1. Schematic diagram of the scanning stopped flow spectrometer.

and is convertible into a scanning stopped flow fluorescence spectrometer. The data collection interface and software are described by Coolen, et al. (1975), Papadakis (1974), and Coolen (1974).

B. Materials

The solvent for all solutions in this study was 0.05 M $Na_2P_2O_7$ (Mallinckrodt Analytical Reagent) made with quartz distilled H_2O and titrated to pH 8.75 with 6N HCl (Mallinckrodt Analytical Reagent).

Horse liver alcohol dehydrogenase (1.1.1.1) was purchased from the Boehringer Mannheim Corporation. According to the label, the sample contained a crystallized suspension of ∿100 mg LADH in 0.02 M phosphate buffer, pH 7.0, with 10% ethanol. As preparation for kinetics measurements, the entire LADH sample was centrifuged, the supernatant was discarded, the precipitate was dissolved in 10 ml of pH 8.75 buffer, and this 10 ml solution was dialized against three 2000 ml portions of pH 8.75 buffer to remove the ethanol and other low molecular weight impurities. The dialized 10 ml LADH solution was diluted to 30 ml with pH 8.75 buffer to make the LADH stock solution, which was stored at 0°C until used in the kinetics measurements.

NADH (Nicotinamide adenine dinucleotide) was purchased from P. L. Biochemicals as ChromatoPure™ Coenzyme-1

(DPNH) (DPNH is an older abbreviation used instead of NADH.) NDMA was purchased from the Aldrich Chemical Company as Aldrich Analyzed N,N-dimethyl-4-Nitrosoaniline. NADH and NDMA were used without further purification.

The concentrations of the LADH, NADH, and NDMA stock solutions determined from absorbances measured with a Cary 17 spectrometer and literature values of molar absorptivities are given in Table 4.1. The specific activity of the LADH stock solution in the reduction of NDMA by NADH was determined to be 8.5±0.1 (moles NDMA/sec equiv LADH) at pH 8.75, 24°C, under assay conditions, and with saturation of LADH by NADH and NDMA and where one equivalent of LADH is defined as one mole of active sites, on the assumption of two active sites per molecule of LADH (Branden et al., 1975). Dunn and Bernhard (1971) report a specific activity of 24±2 (moles NDMA/sec equiv. LADH) for the same conditions.

C. Rapid Scanning Experiments from 275 nm to 614 nm

The purpose of these experiments was to characterize spectrally and kinetically the substrates, products, and transient intermediates of the LADH-NADH-NDMA reaction over a wide spectral range. The wavelength range 275 nm - 614 nm was chosen for two reasons: (1) This is the widest range that can be scanned in a single experiment with adequate signal to noise ratio across the spectrum

Table 4.1

Molar Absorptivities of LADH, NADH, and NDMA and Concentrations of Stock Solutions

	$\varepsilon_{max}/10^{-3}$ O.D. $M^{-1}cm^{-1}$	λ_{max}/nm	Concentration of Stock Solution/uM
LADH	35.3[a]	280	31.4
NADH	6.22[b]	340	120.
NDMA	35.4[c]	440	107.

[a]Sund and Theorell (1960).

[b]P. L. Biochemicals (1973).

[c]Dunn and Bernhard (1971).

with the current stopped flow spectrometer. (ii) The range 275 nm - 614 nm includes the wavelengths of maximum absorbance for LADH (280 nm), for the NADH nicotinamide absorbance band (340 nm), and for NDMA (440 nm), and extends beyond 540 nm, where absorbance changes observed by two other groups of investigators (Schack and Dunn, 1972; Suelter et al., 1975) have been attributed to a transient intermediate.

Table 4.2 summarizes the initial conditions of the rapid scanning kinetics experiments. Four sets of initial conditions were tested. The first digit of each experiment number has possible values one through four, indicating which of the four sets of initial conditions was employed. The second digit represents replicates for a particular set of initial conditions. Table 4.2 also introduces the abbreviation system used in this chapter. LADH is represented by E, NADH by N, and NDMA by S. The abbreviation for an experiment gives the symbol for each species subscripted with its initial micromolarity in the experiment. The initial concentration of LADH is reported as micromolarity of active sites (micronormality), on the assumption of two active sites per molecule of LADH (Brändén, et al., 1975).

In a scanning stopped flow experiment, the reaction is initiated by mixing solutions from two pushing syringes. Thus, in each experiment, two of the three reactants LADH, NADH, and NDMA must be premixed in one of the

Table 4.2. Initial Conditions of the 275 nm - 614 nm Experiments. E = LADH, N = NADH, S = NDMA.

Experiment Number	Abbreviation	Identification (File Name)	Mixing Order	$[LADH]_0/\mu N^a$	$[NADH]_0/\mu M$	$[NDMA]_0/\mu M$	N=Number of Spectra
1.1	$E_{7.39}N_{15.0}S_{13.4}$	GVAOAR.RC	(N) with (E+S)	7.39	13.4	13.4	61
1.2		GVAOAQ.RC					
2.1	$E_{7.39}N_{15.0}S_{13.4}$	GULVABV.RC	(N+S) with (E)	7.39	15.0	13.4	61
3.1	$E_{18.6}N_{15.0}S_{13.4}$	GULABD.RC	(N+S) with (E)	18.6	15.0	13.4	64
3.2		GULABF.RC					
3.3		GULABG.RC					
4.1	$E_{7.39}N_{6.0}S_{13.4}$	GVAOAF.RC	(N+S) with (E)	7.39	6.0	13.4	64
4.2		GVAOAG.RC					

[a]Normality, or (Active Site Concentration) using 2 active sites/mole enzyme.

pushing syringes. Experiments 1.1 through 4.2 cover three sets of initial concentrations. Experiment 2.1 repeats the initial concentrations of Experiments 1.1 and 1.2, but with NADH and NDMA premixed in one pushing syringe instead of LADH and NDMA. This was done in order to determine if LADH and NDMA react without NADH in a way that measurably alters the course of the reaction after NADH is added. Experiments 3.1 through 4.2 have the same mixing order as Experiment 2.1.

For use as proposed static spectra of suspected absorbers in the principal component analysis that follows, the individual static spectra of LADH (7.39 μN), NADH (18.6 μM), and NDMA (5.36 μM) were measured in the stopped flow spectrometer with the same instrumental settings as for the scanning kinetics experiments. Each static spectrum is the average of 256 scans.

All of the scanning experiments were performed with a scanning rate of 37.5 scans/sec (75 scans/sec with the backscan discarded), 54 wavelength channels per scan, and 5 samples per point. The number of consecutive spectra are listed for each kinetics experiment in Table 4.2. The temperature in each experiment was assumed to be the ambient temperature of the laboratory, which was 23-24°C over the course of the experiments.

With a given voltage applied to the photomultiplier tubes, the overall response curve of the stopped flow spectrometer has a higher signal in the 300 nm - 600 nm

range than below 300 nm. Therefore, the order to flatten the response curve so that the 275 nm - 614 nm range could be scanned in a single experiment, a liquid optical filter solution of 0.090 M $CoSO_4$ and 0.076 M $NiSO_4$ in a 4.2 cm path length quartz cell was inserted between the Xenon lamp and the entrance slit of the monochromator. Solutions of $CoSO_4$ and $NiSO_4$ have broad absorbance bands centered at 510 nm and 390 nm, respectively, so that the filter solution reduces the signal in the 300 nm - 600 nm range to match more closely the signal below 300 nm.

D. Calibrations and Corrections

The wavelength of each wavelength channel was estimated by fitting observed absorbance peaks of holmium oxide and didymium oxide glasses to an equation which is appropriate for the particular scanning monochromator and the data collection system used. The details of this procedure are given in Appendix E. Figure 4.2 shows the wavelength curve obtained from the calibration procedure, and Table 4.3 lists the estimated wavelengths of each channel.

Absorbances and times for each experiment were estimated by the program ABCAL from neutral density filter calibration data and the software collection parameters for each experiment. Appendix E describes these calibrations and gives instructions for using ABCAL.

Table 4.3. Wavelength Calibration of the 275 nm - 614 nm Experiments.

m=Wavelength Channel	λ/nm	m=Wavelength Channel	λ/nm
1	274.6	28	367.9
2	275.2	29	376.7
3	275.9	30	384.6
4	276.8	31	393.8
5	277.9	32	403.4
6	279.2	33	413.6
7	280.0	34	424.3
8	282.3	35	435.5
9	284.1	36	447.2
10	286.1	37	459.4
11	288.3	38	472.0
12	290.8	39	484.9
13	293.4	40	498.0
14	296.3	41	511.3
15	299.4	42	524.6
16	302.8	43	537.6
17	306.4	44	550.4
18	310.3	45	562.6
19	314.4	46	574.0
20	318.9	47	584.4
21	323.7	48	593.7
22	828.8	49	601.4
23	334.3	50	607.6
24	340.2	51	612.1
25	346.5	52	614.6
26	353.2	53	615.1
27	360.3	54	613.7

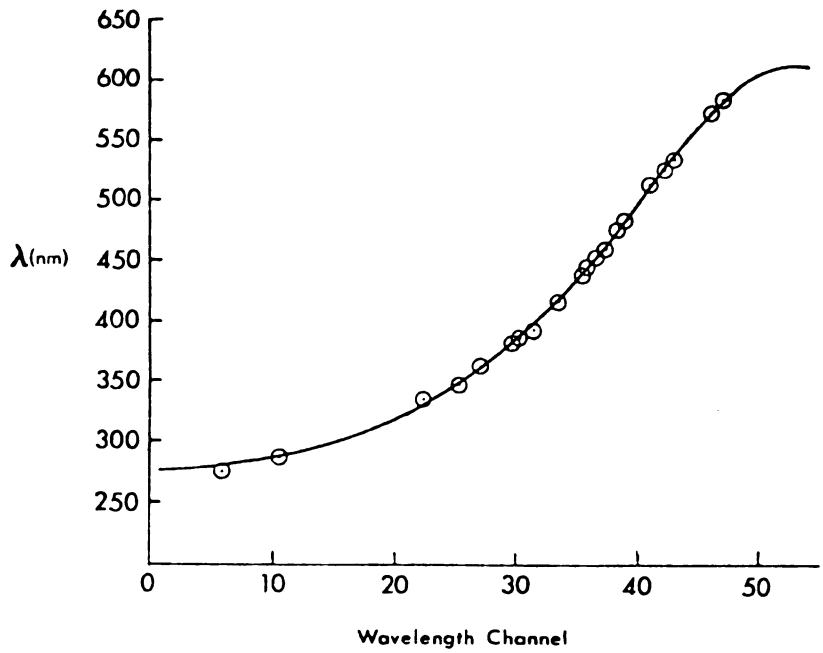

Figure 4.2. Wavelength calibration for the 275 nm - 614 nm experiments. Points are holmium oxide and didymium oxide calibration peaks.

The absorbance-wavelength-time data were corrected for two sources of systematic experimental error. The first source of systematic error is the finite scan speed of the monochromator. Recall from Chapter 2 that the model for the absorbance matrix $\underline{A}$ in principal component analysis assumes that each consecutive spectrum is measured instantaneously, whereas, in these experiments, each scan requires 0.0133 seconds. This difference between the experiment and the model is important in the first group of spectra, where the half-times of absorbance changes may have magnitudes comparable to the scanning period. The data were corrected for the finite scan speed error by interpolating the absorbances so that each wavelength channel in a corrected spectrum corresponds in time to the last wavelength channel of the spectrum. If A_{ij} is the absorbance measured at wavelength channel i in the spectrum j at time t_{ij}, then the absorbance corrected for finite scan speed is given by

$$A_{ij}(\text{corrected}) = \frac{(A_{ij+1}-A_{ij})(t_{pj}-t_{ij})}{(t_{ij+1}-t_{ij})} + A_{ij}$$

$$i = 1,2,\ldots,p$$

$$j = 1,2,\ldots(N-1)$$

where the p'th wavelength channel is the last channel in the spectrum (p=54). The N'th (or last) consecutive

spectrum is not corrected for finite scan speed.

The second source of systematic error is light of wavelength above ∿320 nm that is scattered by the monochromator and artificially depresses absorbances measured below 300 nm. Additional kinetics experiments were performed to obtain the data necessary to correct absorbances for scattered light. An experiment was performed with the same initial conditions as each experiment in Table 4.2, but with a Corning CS054 Color Filter in the sample path. The CS054 filter is a cutoff filter of absorbance greater than 2 for wavelengths below 300 nm. The absorbance corrected for scattered light is A_t,

$$A_t = \log_{10}[(1-10^{-A_f})/(10^{-A}-10^{-A_c})] \qquad (4.1)$$

where A is the measured absorbance, A_t is the true absorbance, A_c is the absorbance measured at the wavelength and time corresponding to A but with the CS054 filter in the sample path, and A_f is the absorbance of the CS054 filter at the same wavelength as A and A_c.

The absorbances are related to intensities by the equations

$$A = \log_{10}[I_o/(I_t+I_s)]$$

$$A_t = \log_{10}(I_o/I_t)$$

$$A_c = \log_{10}[I_o/(I_t 10^{-A_f} + I_s)],$$

where I_o is the light intensity from the reference cell, I_t is the true intensity from the sample cell (without scattered light), and I_s is the scattered light intensity from the sample cell. Absorbances for wavelength channels 1-15 (275 nm - 300 nm) were corrected for scattered light with Equation (4.1). The correction increased these absorbances by 0.1-0.2 optical density units but did not change the qualitative shape of the absorbance-time profile at each wavelength channel.

E. Absorbance-Wavelength-Time Surfaces

In Experiments 1.1-4.2, absorbances for wavelength channels 48 through 54 (594 nm - 614 nm) varied randomly about zero. Therefore, we omit these channels from the discussion of Experiments 1.1 - 4.2 in the remainder of this chapter.

Figure 4.3 shows two views of the corrected absolute absorbance surface A for wavelength channels 1 through 47 (275 nm - 584 nm) in Experiment 1.1. Note that the 61 consecutive spectra are equally spaced in Figure 4.3 and that the scale for the time axis is geometric in time. This is because the data collection software averages a number of measured scans and stores the average as a single consecutive spectrum. The number of measured scans averaged into each stored spectrum is increased with time during the reaction, so that, at early times where fast

Figure 4.3. Experimental absolute absorbance surface A, Experiment 1.1, $E_{7.39}N_{15.0}S_{13.4}$, (N) with (E+S). A. Front view. B. Rear view.

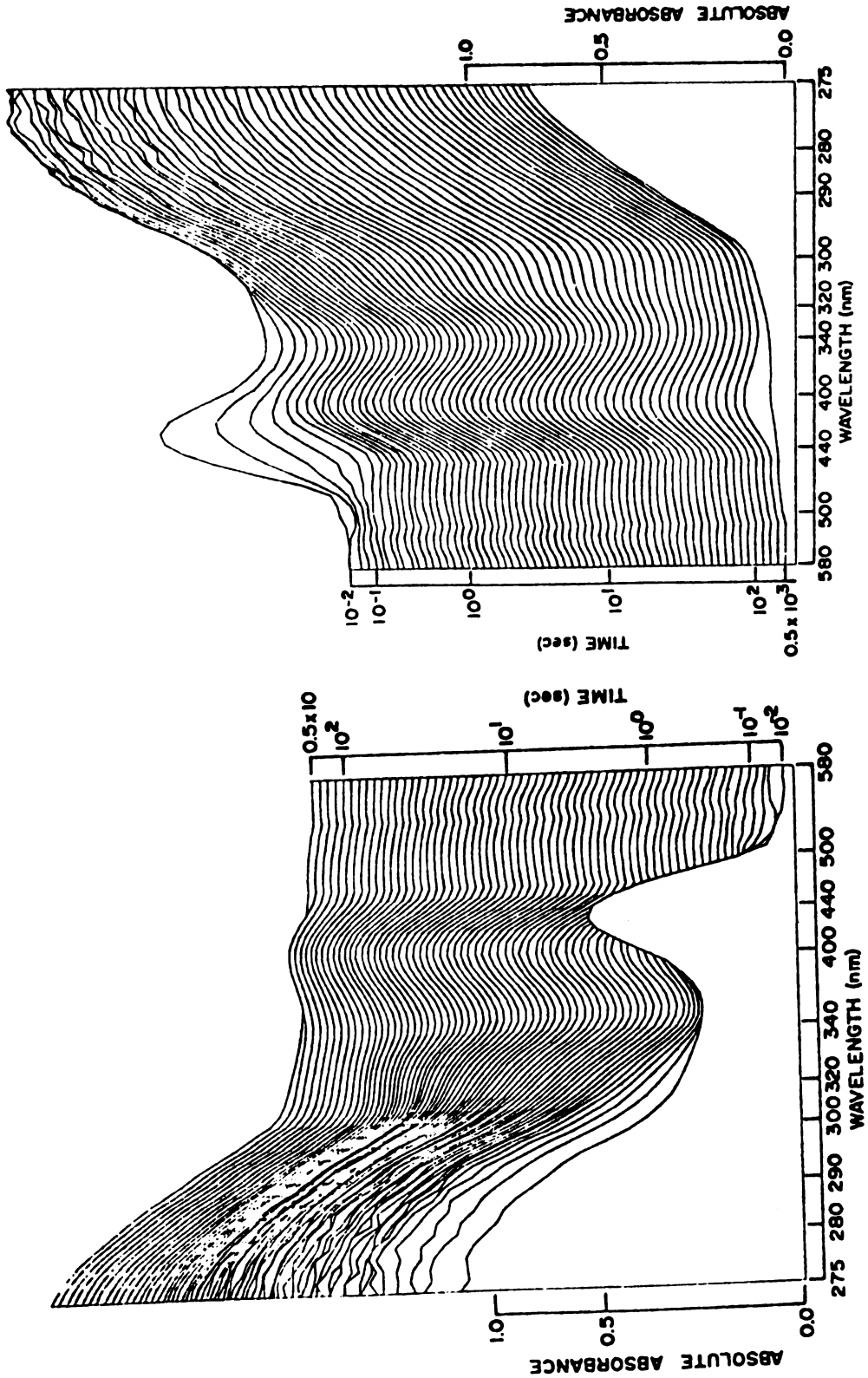
ABSOLUTE ABSORBANCE
1.0
0.5
0.0
275 280 290 300 320 340 400 440 500 580
WAVELENGTH (nm)
TIME (sec)
0.5x10
10^2
10^1
10^0
10^-1
10^-2
ABSOLUTE ABSORBANCE
1.0
0.5
0.0
275 280 290 300 320 340 400 440 500 580
WAVELENGTH (nm)
TIME (sec)
10^-2
10^-1
10^0
10^1
10^2
0.5x10^3

Figure 4.3

changes occur in the reaction, there is little or no averaging, while at late times when changes are slow, there are many measured scans per stored spectrum. (See Coolen et al. (1975) for a detailed description of this averaging scheme.) The last spectrum of a given experiment is called the infinity spectrum. The operator manually triggers the measurement of the infinity spectrum when absorbance monitored on a storage oscilloscope has stopped changing with time. In Experiments 1.1 - 4.2, the time elapsed between the (N-1)'th spectrum and the infinity spectrum is at least 300 seconds.

Figure 4.3 is dominated by large constant absorbances that obscure the progress of the reaction. The dynamics of absorbance changing with time at different wavelengths are better illustrated for Experiment 1.1 by the difference surface ($\underline{A}-\overline{\underline{A}}$), two views of which are shown in Figures 4.4 and 4.5. Data plotted in Figure 4.3 are plotted in Figures 4.4 and 4.5 after first subtracting the average of all 61 consecutive spectra from each spectrum. Note that, if absorbance did not change with time during an experiment, the difference surface ($\underline{A}-\overline{\underline{A}}$) would be a horizontal plane. Figures 4.6, 4.7, and 4.8 show the difference surfaces ($\underline{A}-\overline{\underline{A}}$) for Experiments 2.1, 3.1, and 4.1, respectively. Each of the replicate experiments 1.2, 3.2, 3.3, and 4.2, not shown here, has a difference surface similar to that for the first experiment with the corresponding initial conditions.

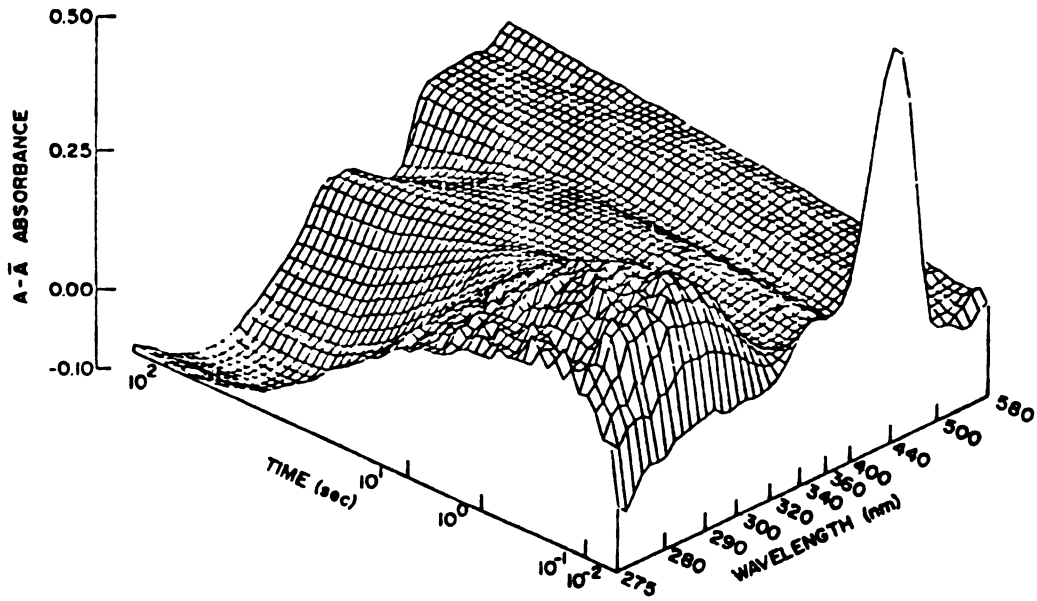

Figure 4.4. Experimental difference surface ($\underline{A}$-$\overline{\underline{A}}$), Experiment 1.1, $E_{7.39}N_{15.0}S_{13.4}$, (N) with (E+S), front view.

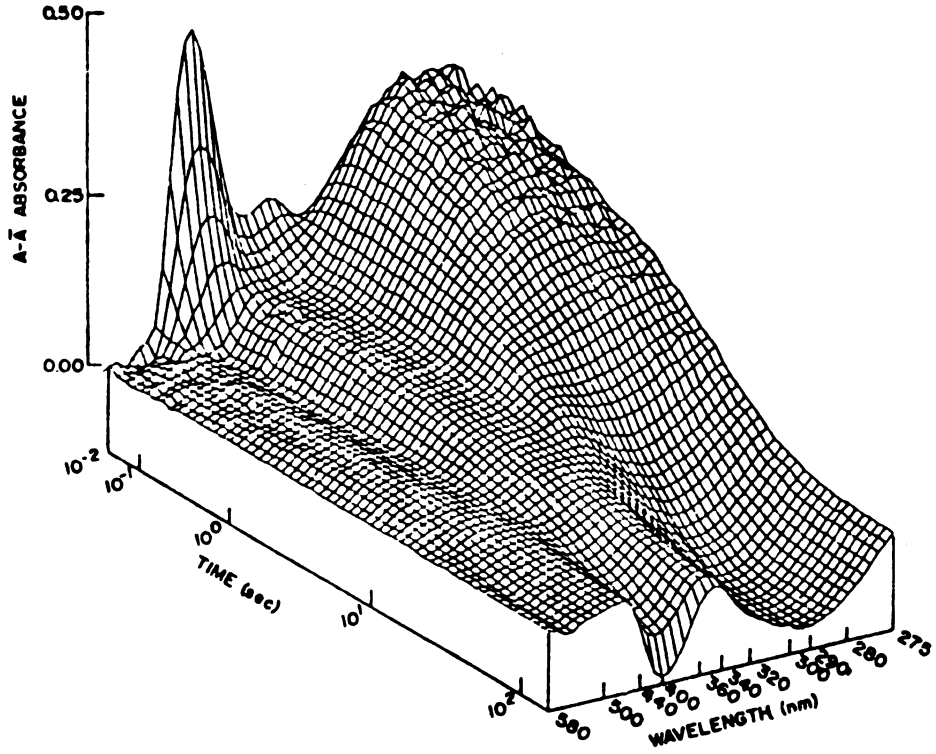

Figure 4.5. Experimental difference surface ($\underline{A}$-$\overline{\underline{A}}$), Experiment 1.1, $E_{7.39}N_{15.0}S_{13.4}$, (N) with (E+S), Rear view.

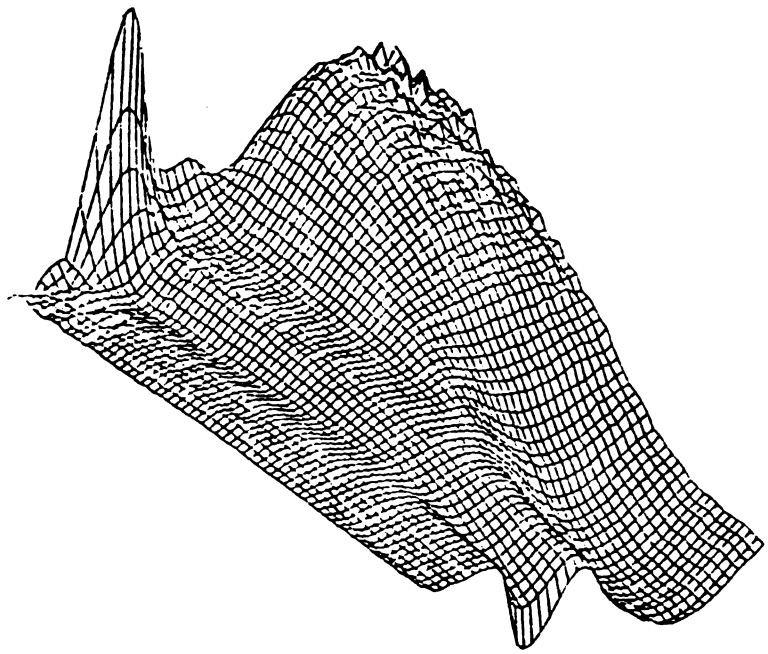

Figure 4.6. Experimental difference surface ($\underline{A}-\overline{\underline{A}}$), Experiment 2.1, $E_{7.39}N_{15.0}S_{13.4}$, (N+S) with (E), Rear view.

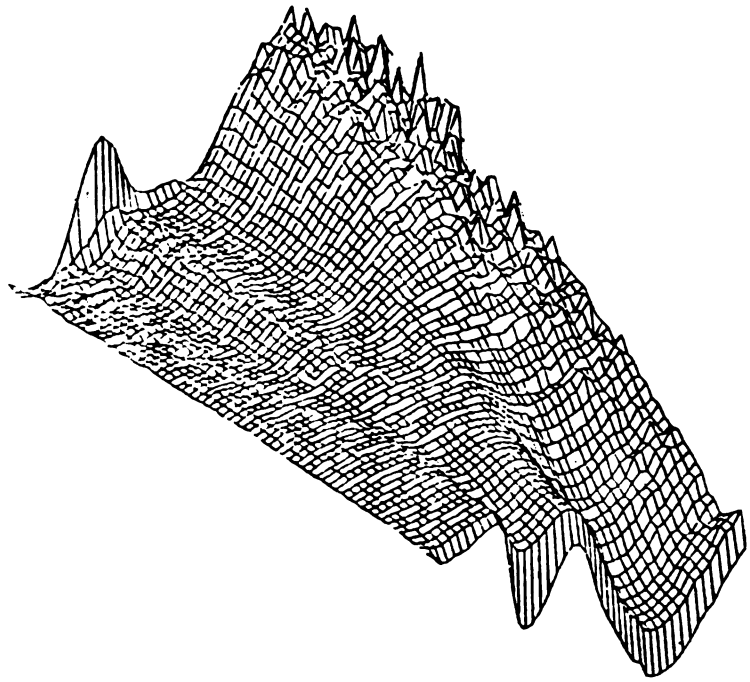

Figure 4.7. Experimental difference surface ($\underline{A}-\overline{\underline{A}}$), Experiment 3.1, $E_{18.6}N_{15.0}S_{13.4}$, (N+S) with (E), Rear view.

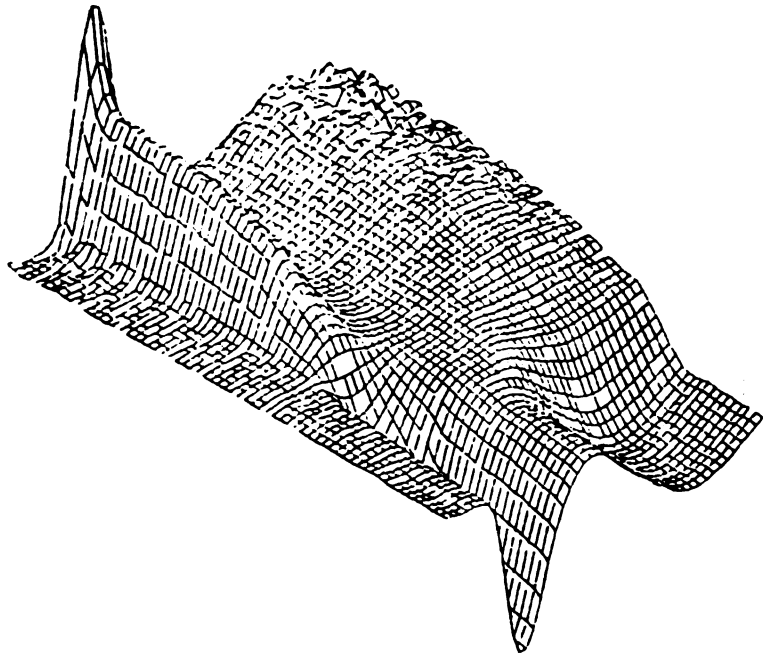

Figure 4.8. Experimental difference surface (A-A), Experiment 4.1, $E_{7.39}N_{6.0}S_{13.4}$, (N+S) with (E), Rear view.

F. Weights for Principal Component Analysis

Note in Figures 4.4 - 4.8 that each experiment has considerably more random noise at low wavelengths and early times than at high wavelengths and late times. Recall from Chapter 2 that, to account for the imbalance of signal/noise in principal component analysis, we devised a weighting scheme which assumes that σ_{ij}^2, the variance of the i,j'th measurement error, is given by

$$\sigma_{ij}^2 = x_i z_j$$

where x_i and z_j describe the change of noise with wavelength and time, respectively.

The contribution of x_i in Experiments 1.1 - 4.2 was estimated from the following separate series of experiments. In each experiment, 63 consecutive scans were collected with buffer solution in both the sample and reference cells, and with a neutral density filter in the sample path to give a nominal absorbance level. The variance x_i was estimated from scatter about the mean absorbance for each wavelength channel with the equation

$$x_i = (1/62) \sum_{k=1}^{63} (A_{ik} - \bar{A}_i)^2$$

The variation of experimental noise with wavelength was

determined for the following nominal absorbance levels: 0.0, 0.3, 0.7, 1.0, and 1.3 optical density units. Figure 4.9 shows $x_i^{1/2}$ versus wavelength channel i at three absorbance levels covering this range of absorbances. For a given absorbance level, the highest error variance occurs at channel one. The peaks of $x_i^{1/2}$ at channels 32 and 41 correspond respectively to the $NiSO_4$ and $CoSO_4$ absorbances bands at 390 nm and 510 nm, which reduce the signal and thus increase the absorbance noise at these wavelengths.

Note that $x_i^{1/2}$ varies with absorbance as well as with wavelength channel i. Although the weighting scheme does not have enough degrees of freedom explicitly to account for the variation of noise with three independent variables (wavelength, time, and absorbance), we can approximately include the variation with absorbance by choosing for $x_i^{1/2}$ the value for the nominal absorbance level closest to the mean absorbance measured at channel i in the kinetics experiment. With this approximation, L_i, the wavelength weight for the i'th wavelength channel, was assigned by the equation

$$L_i = a^{1/2} x_i^{-1/2} \qquad (2.28)$$

with the arbitrary constant a set to unity (see Chapter 2). Table 4.4 lists the wavelength weights for Experiment 1.1.

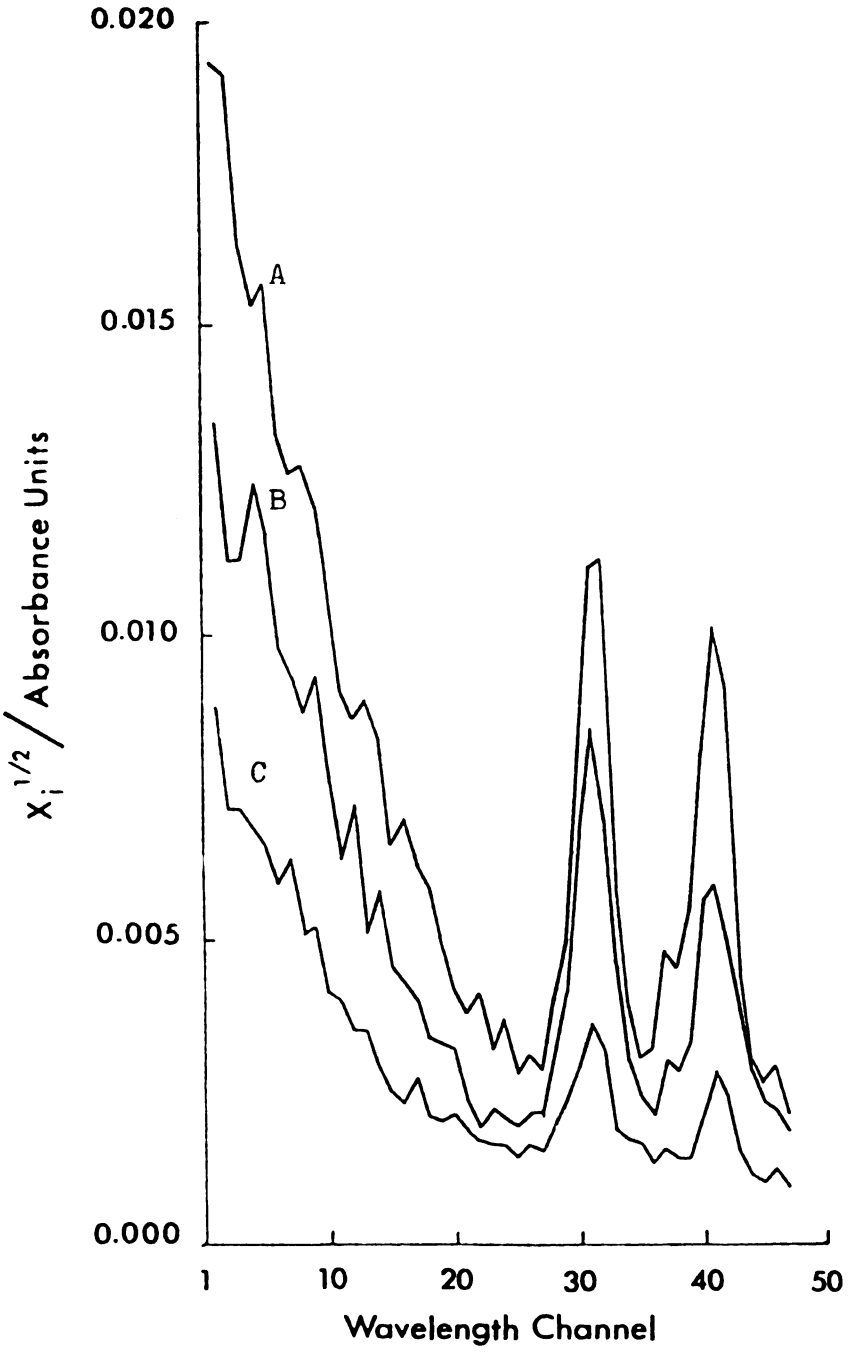

Figure 4.9. $x_1^{1/2}$ (standard deviation of random errors) versus wavelength channel for Experiments 1.1 - 4.2. A. 1.3 O.D. neutral density filter. B. 0.7 O.D. neutral density filter. C. Buffer versus buffer.

Table 4.4. Wavelength Weights, Li, for Experiment 1.1.

Wavelength Channel i	Li	Wavelength Channel i	Li
1	65.5	25	620.1
2	72.0	26	581.7
3	79.3	27	638.1
4	63.8	28	475.0
5	88.4	29	392.8
6	90.1	30	265.3
7	94.0	31	228.1
8	93.1	32	275.6
9	107.6	33	467.9
10	125.1	34	547.9
11	158.2	35	704.4
12	141.1	36	750.4
13	192.4	37	702.1
14	311.7	38	698.8
15	357.0	39	488.9
16	375.0	40	458.5
17	324.1	41	359.1
18	384.0	42	316.9
19	386.5	43	639.5
20	445.2	44	989.3
21	521.4	45	917.0
22	468.0	46	903.4
23	482.7	47	1132.4
24	555.2		

The number of measured scans averaged and stored as the j'th consecutive spectrum of the experiment is $g^{(n_j-1)}$, where g is the grouping factor and n_j is the group number of spectrum j. (See Coolen, et al. (1975) for a detailed explanation of these terms.) [In Experiments 1.1 - 3.3, g = 2, and for Experiments 4.1 = 4.2, g = 3.] The contribution of z_j to the error variance should be given by

$$z_j = g^{(1-n_j)}.$$

However, the absorbance data are stored in the PDP8I computer as four octal bit words, and the digital resolution of absorbances in Experiments 1.1 - 4.2 is $\sim\pm 0.001$ optical density units. To take account of this digital resolution limit, z_j was assigned as shown in Table 4.5, where increasing the spectral averaging beyond 8 or 9 (measured scans/stored spectrum) was assumed to give no further reduction of z_j. The time weights, T_j, listed in Table 4.5, were assigned by the equation

$$T_j = b^{1/2} z_j^{-1/2} \qquad (2.28)$$

with the arbitrary constant b set to unity (see Chapter 2).

In Sections G through N we apply the seven step strategy of Chapter 3 to resolve Experiments 1.1 - 4.2 into the static spectra and concentration vectors of their absorbers.

Table 4.5. Time Weights T_j for Experiments 1.1 - 4.2.

Number of Spectra Averaged	z_i	T_j (Optical Density
1	1.000	1.000
2	0.500	1.414
3	0.333	1.732
4	0.250	2.000
8[a]	0.125	2.828
9[b]	0.111	3.000

[a]Grouping factor = 2.

[b]Grouping factor = 3.

G. Principal Component Analysis, Step 1

In Step 1 we use weighted M and S analyses to determine for each complete experiment, m, the minimum number of absorbers, and s, the minimum number of absorbers whose concentrations change with time. The numbers m and s are determined by finding the minimum number of eigenvectors of $\underline{M}_W$ and $\underline{S}_W$, respectively, that are required to reconstruct the experimental absorbance surface to within its random experimental error. We illustrate this procedure with the M analysis of Experiment 1.1.

Figure 4.5 is the experimental difference surface $(\underline{A}-\overline{\underline{A}})$ for Experiment 1.1. Figure 4.10 is the reconstruction of $(\underline{A}-\overline{\underline{A}})$ using one eigenvector of $\underline{M}_W$ and is the best least squares fit of Figure 4.5 that can be obtained assuming that there is only one absorber in Experiment 1.1, regardless of what we assume for the kinetic mechanism or the static spectrum of the absorber. Since Figure 4.10 is a poor reconstruction of Figure 4.5, we conclude that Experiment 1.1 must have more than one absorber.

Figure 4.11 is the best reconstruction of $(\underline{A}-\overline{\underline{A}})$ assuming that Experiment 1.1 has only two absorbers. Again, Figure 4.11 is a poor reconstruction of the experimental difference surface in Figure 4.5, so we conclude that Experiment 1.1 must have more than two absorbers.

Figure 4.12 is the best reconstruction of $(\underline{A}-\overline{\underline{A}})$

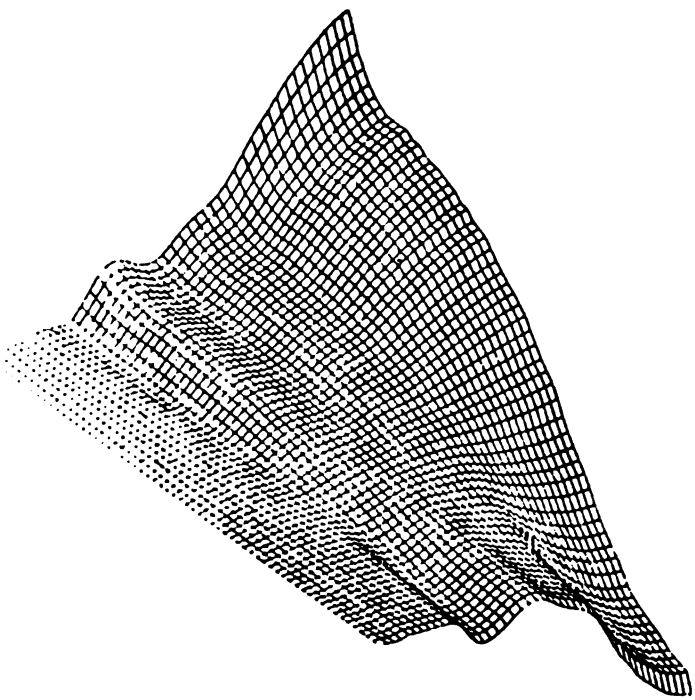

Figure 4.10. Reconstruction of experimental difference surface assuming one absorber in Experiment 1.1, Rear view.

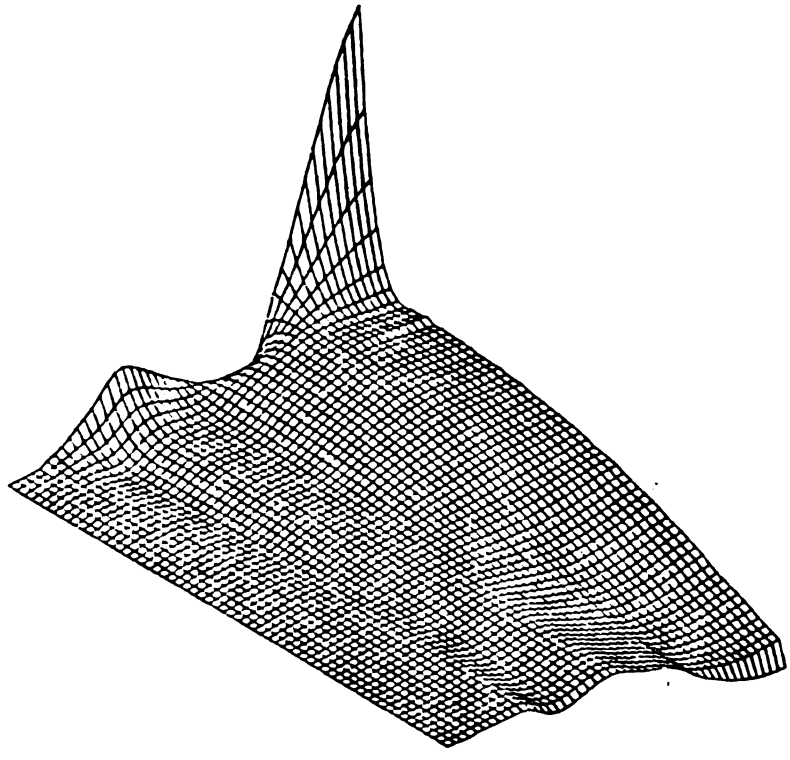

Figure 4.11. Reconstruction of experimental difference surface assuming two absorbers in Experiment 1.1, Rear view.

assuming that Experiment 1.1 has only three absorbers. We observe that it is qualitatively similar to the experimental difference surface in Figure 4.5. However, there are some systematic differences. We note particularly that the last spectrum (the infinity spectrum) is not correctly reconstructed in Figure 4.12. The incorrectness of this single spectrum is sufficient evidence for us to conclude that Experiment 1.1 must have more than three absorbers. However, there are other systematic differences between Figures 4.12 and 4.5 that can be seen with the aid of a weighted residual surface.

The weighted residual surface for r eigenvectors is defined by

$$\underline{R}_{W(r)} = \underline{L}(\underline{\hat{A}}_{(r)} - \underline{A})\underline{T}.$$

If the reconstructed and experimental difference surfaces agree to within their random errors, the weighted residual surface should be random. Moreover, when the error model $\sigma_{ij}^2 = x_i z_j$ exactly describes the experiment (it approximately describes Experiment 1.1) and when the weighting matrices $\underline{L}$ and $\underline{T}$ are assigned with their arbitrary constants a and b set equal to unity, then the sample variance of the weighted residuals, $Q_r/(N-r)(p-r)$, with Q_r defined by Equation (2.31), should approach unity for r equal to the essential rank m. Figure 4.13 is the weighted residual surface assuming there are only three

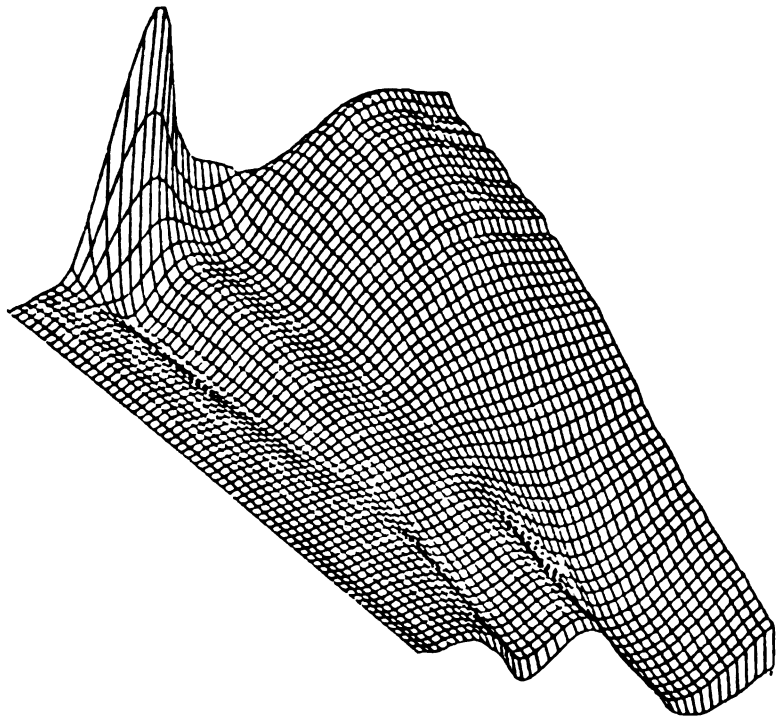

Figure 4.12. Reconstruction of experimental difference surface assuming three absorbers in Experiment 1.1, Rear view.

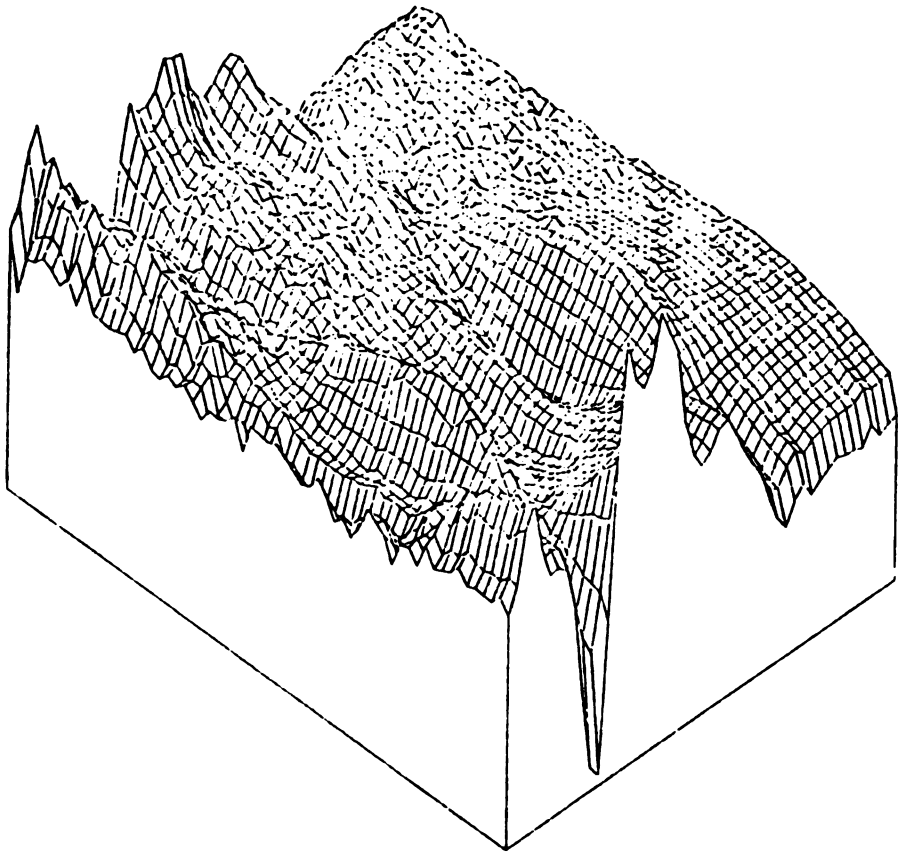

Figure 4.13. Weighted residual surface assuming three absorbers in Experiment 1.1, Rear view. Vertical scale from -450.0 to +500.0 weighted absorbance units.

absorbers in Experiment 1.1. The systematic appearance of the weighted residual surface and the fact that $Q_3/(N-3)(p-3)$ equals 84.08 support the conclusion that Experiment 1.1 must have more than three absorbers.

Figure 4.14 is the best reconstruction of ($\underline{A}$-$\overline{\underline{A}}$) assuming that Experiment 1.1 has only four absorbers. We note that the infinity spectrum is not a correct reconstruction of the experimental infinity spectrum in Figure 4.5, so we conclude that Experiment 1.1 must have more than four absorbers. Figure 4.15 is the weighted residual surface assuming there are only four absorbers in Experiment 1.1. We note that the weighted residuals are more random for four absorbers than for three absorbers, but that they are still systematic at late time, and that the weighted residuals across the infinity spectrum are much larger than across the other spectra. $Q_4/(N-4)(p-4)$ is 10.57, and the weighted residuals thus support the conclusion that Experiment 1.1 has more than four absorbers.

Figure 4.16 is the best reconstruction of ($\underline{A}$-$\overline{\underline{A}}$) assuming that Experiment 1.1 has only five absorbers. We note that the experimental infinity spectrum is correctly reconstructed in Figure 4.16. Figure 4.17 is the weighted residual surface for five absorbers, which appears to have few if any systematic patterns. $Q_5/(N-5)(p-5)$ equals 2.24, which is close to unity, especially considering that the error model $\sigma_{ij}^2 = x_i z_j$ only approximately describes Experiment 1.1.

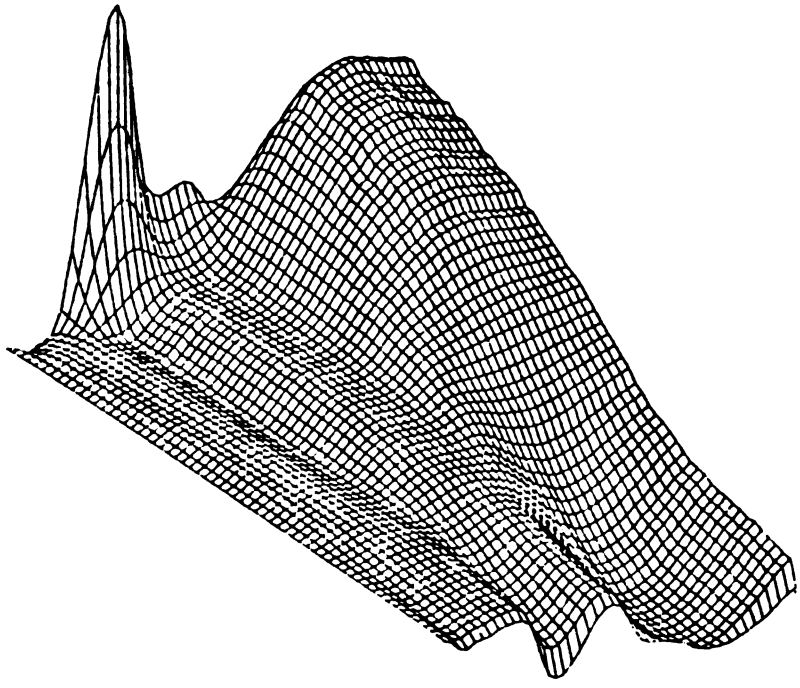

Figure 4.14. Reconstruction of experimental difference surface assuming four absorbers in Experiment 1.1, Rear view.

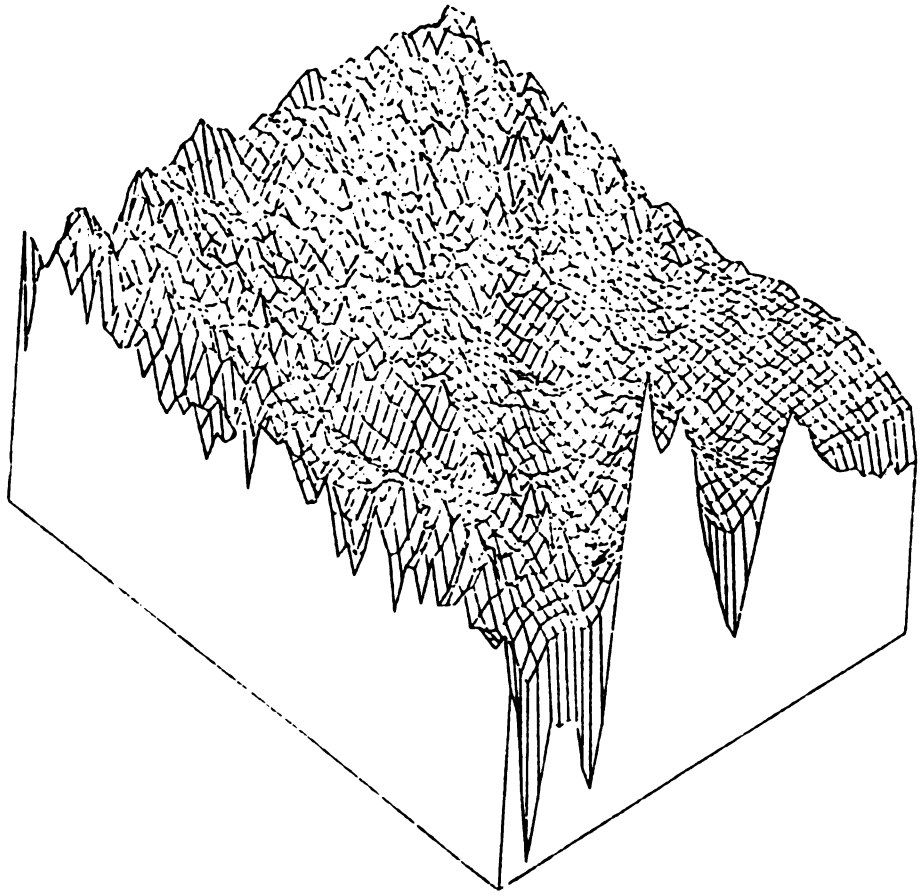

Figure 4.15. Weighted residual surface assuming four absorbers in Experiment 1.1, Rear view. Vertical scale from -30.0 to +10.0 weighted absorbance units.

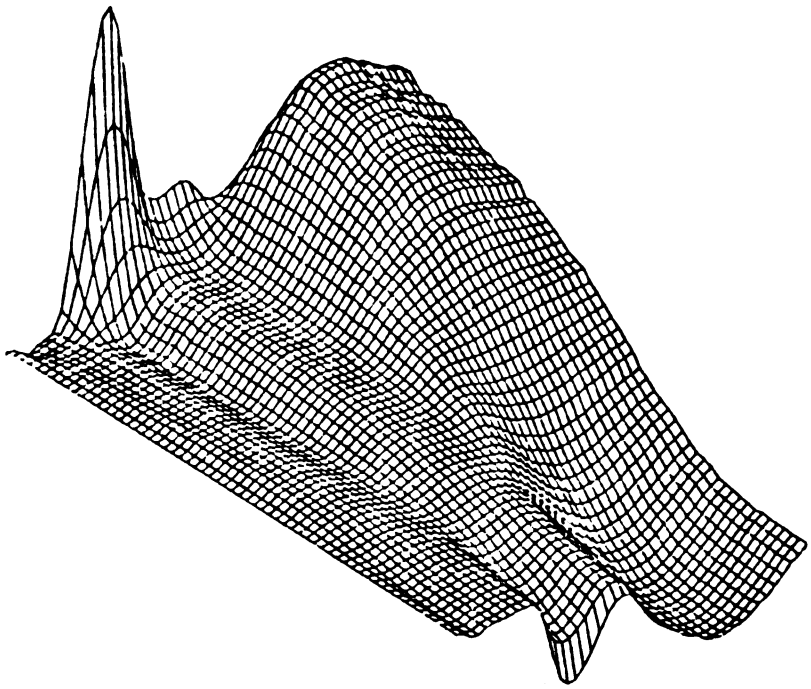

Figure 4.16. Reconstruction of experimental difference surface assuming five absorbers in Experiment 1.1, Rear view.

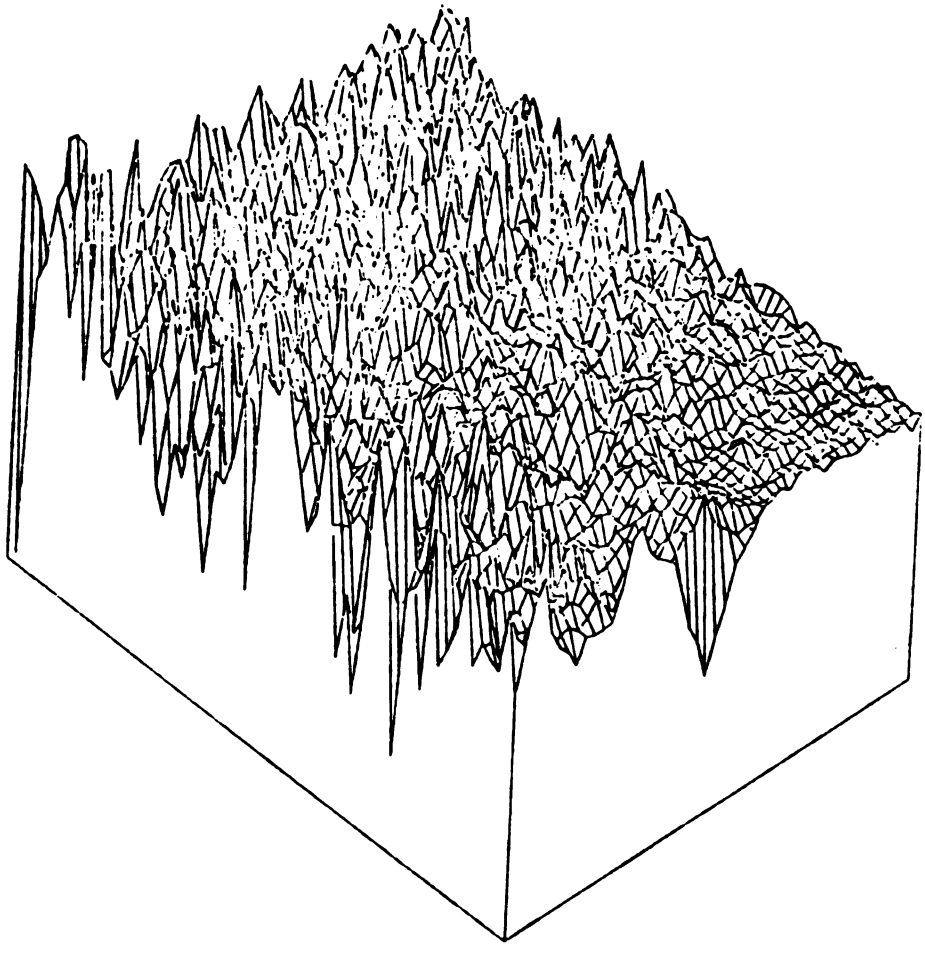

Figure 4.17. Weighted residual surface assuming five absorbers in Experiment 1.1, Rear view. Vertical scale from -10.0 to +5.0 weighted absorbance units.

Before concluding that five eigenvectors of $\underline{M}_W$ are sufficient to reconstruct the experimental absorbances to within random errors, we examine the two dimensional plots of the experimental and reconstructed absorbances versus time for all 47 wavelength channels. Figure 4.18A shows the comparison of $\underline{\hat{A}}_{(5)}$ and $\underline{A}$ for wavelength channel 1. Similar plots show that $\underline{\hat{A}}_{(5)}$ fits $\underline{A}$ equally well for wavelength channels 2 through 47. Now, m, the essential rank of $\underline{M}_W$, is defined as the <u>minimum</u> number of eigenvectors required to reconstruct the experimental absorbances to within their random errors. Therefore, we conclude that m equals five in Experiment 1.1 from the observations that one, two, three, or four eigenvectors do not reconstruct the absorbances to within random errors, whereas five eigenvectors reconstruct the absorbances to within random errors. The only improvement in reconstructing the absorbances with more than five eigenvectors is to reconstruct the random errors themselves. Figure 4.18B shows the comparison of $\underline{\hat{A}}_{(6)}$ and $\underline{A}$ for wavelength channel 1. Note that $\underline{\hat{A}}_{(6)}$ gives no improvement over $\underline{\hat{A}}_{(5)}$ in reconstructing $\underline{A}$, except at the level of the random errors. Thus, we conclude that Experiment 1.1 has five linearly independent absorbers.

Recall from Chapter 2 and Appendix C that for an infinitely large experiment described by the error variance model $\sigma_{ij}^2 = x_i z_i$, the mean of the nonessential eigenvalues of $\underline{M}_W$, defined by

Figure 4.18. (A) $\underline{\hat{A}}_{(5)}$ and $\underline{A}$ for wavelength channel 1 (275 nm), Experiment 1.1. X = $\underline{A}$, O = $\underline{\hat{A}}_{(5)}$.

(B) $\hat{A}_{(6)}$ and $\underline{A}$ for wavelength channel 1 (275 nm), Experiment 1.1. X = $\underline{A}$, O = $\underline{\hat{A}}_{(6)}$.

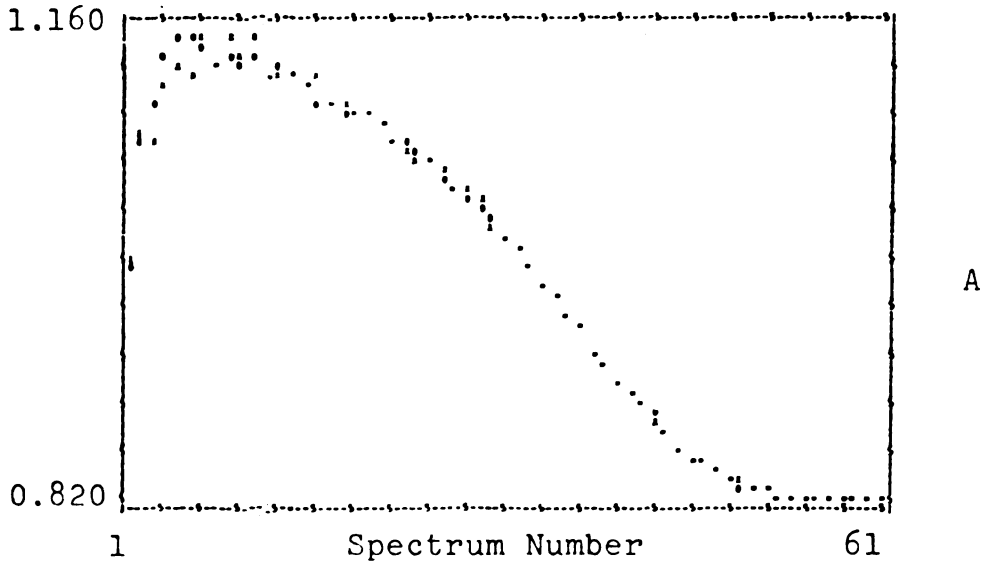
1.160
0.820
1
Spectrum Number
61
A

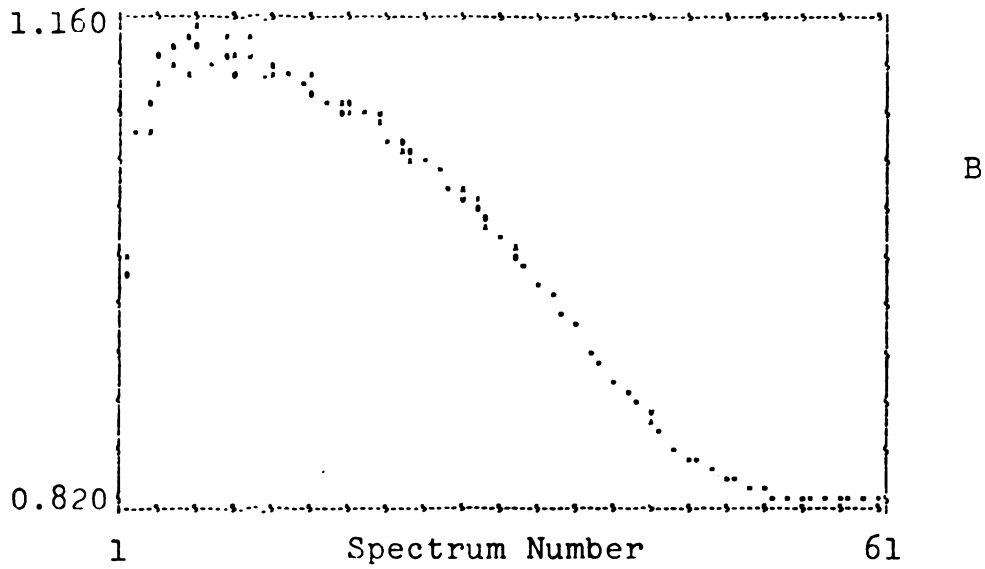
1.160
0.820
1
Spectrum Number
61
B

Figure 4.18.

$$\bar{\delta}_r = [1/(p-r)] \sum_{i=r+1}^{p} \delta_i$$

equals one for r=m,m+1,...,p. Therefore, the first value of r for which $\bar{\delta}_r$=1 is m, the essential rank of $\underline{M}_W$. This suggests that for a finite size experiment described by the error variance model $\sigma_{ij}^2 = x_i z_j$, m is the first value of r for which $\bar{\delta}_r$ approaches unity. The same rule applies to the mean of the nonessential eigenvalues of $\underline{S}_W$ when r equals s, the essential rank of $\underline{S}_W$.

Since the variance model $\sigma_{ij}^2 = x_i z_j$ only approximately describes Experiments 1.1 - 4.2., we do not use the mean of the nonessential eigenvalues as a strict criterion for determining m and s. Instead, we use as the criterion the reconstruction of the experimental absorbances to within random errors, as illustrated above for the determination of m in Experiment 1.1. Nevertheless, we list the mean of the nonessential eigenvalues for M and S analyses of Experiments 1.1 - 4.2 in Tables 4.6 and 4.7, respectively. In these tables, the mean of the nonessential eigenvalues is underscored for the minimum number of eigenvectors required to reconstruct the experimental absorbances to within random errors. Thus, Experiments 1.1 through 3.3 have five linearly independent absorbers (m=5), of which at least four change concentration (s=4), whereas Experiments 4.1 and 4.2 have six linearly independent absorbers (m=6), of which at least five change concentration (s=5). Note that in all these experiments,

Table 4.6. M Analysis Mean of Non-Essential Eigenvalues.

Experiment	Abbreviation	r = Number of Eigenvectors of $\underline{M}_W$					
		1	2	3	4	5	6
1.1	$E_{7.4}N_{15.0}S_{13.4}$	646.38	251.80	79.94	9.88	<u>2.06</u>[a]	1.21
1.2	$E_{7.4}N_{15.0}S_{13.4}$	782.71	307.91	85.14	10.55	<u>2.00</u>	1.22
2.1	$E_{7.4}N_{15.0}S_{13.4}$	552.46	202.61	71.22	8.96	<u>1.57</u>	0.93
3.1	$E_{18.6}N_{15.0}S_{13.4}$	233.58	59.69	15.72	3.97	<u>1.97</u>	1.42
3.2	$E_{18.6}N_{15.0}S_{13.4}$	425.61	89.02	9.53	3.87	<u>2.20</u>	1.35
3.3	$E_{18.6}N_{15.0}S_{13.4}$	453.05	126.95	36.44	5.12	<u>1.82</u>	1.05
4.1	$E_{7.4}N_{6.0}S_{13.4}$	2872.80	65.62	6.67	2.97	2.04	<u>1.43</u>
4.2	$E_{7.4}N_{6.0}S_{13.4}$	2964.84	67.65	13.32	3.07	2.18	<u>1.53</u>

[a]Underscored values indicate the minimum number of eigenvectors with which the experimental absorbance surface is reconstructed to within its random errors.

Table 4.7. S Analysis Mean of Non-Essential Eigenvalues.

Experiment	Abbreviation	r = Number of Eigenvectors of $\underline{S}_W$					
		1	2	3	4	5	6
1.1	$E_{7.4}N_{15.0}S_{13.4}$	377.97	90.75	11.21	<u>2.13</u>[a]	1.27	0.96
1.2	$E_{7.4}N_{15.0}S_{13.4}$	543.03	96.34	12.00	<u>2.07</u>	1.27	0.81
2.1	$E_{7.4}N_{15.0}S_{13.4}$	293.86	81.95	9.95	<u>1.72</u>	0.99	0.74
3.1	$E_{18.6}N_{15.0}S_{13.4}$	70.62	18.27	4.18	<u>2.02</u>	1.48	1.29
3.2	$E_{18.6}N_{15.0}S_{13.4}$	105.50	10.88	4.11	<u>2.30</u>	1.43	0.96
3.3	$E_{18.6}N_{15.0}S_{13.4}$	141.61	46.06	5.46	<u>1.98</u>	1.15	0.94
4.1	$E_{7.4}N_{6.0}S_{13.4}$	139.22	8.08	3.95	2.30	<u>1.65</u>	1.26
4.2	$E_{7.4}N_{6.0}S_{13.4}$	152.02	23.46	3.78	2.45	<u>1.59</u>	1.26

[a]Underscored values indicate the minimum number of components with which the experimental absorbance surface is reconstructed to within its random error.

the mean of the nonessential eigenvalues is within an order of magnitude of unity for the correct essential rank. Of course, the mean of the nonessential eigenvalues must either decrease or remain constant as r is increased beyond m, since the eigenvalues are arranged in decreasing order.

Tables 4.8 and 4.9 list the sample variance of the weighted residuals, $Q_r/(N-r)(p-r)$, for the M and S analyses of Experiments 1.1 - 4.2, with a format similar to Tables 4.6 and 4.7. Note that $Q_r/(N-r)(p-r)$ is within an order of magnitude of unity for the correct essential rank in each experiment.

We take as evidence of the precision of the scanning experiments the reproducibility of the (m,s) pairs for the replicate experiments and the similar appearance of their experimental absorbance surfaces. Therefore, in Steps 2 through 7 we shall discuss only the first experiment for each set of initial conditions, i.e., Experiments 1.1, 2.1, 3.1, and 4.1.

H. Principal Component Analysis, Step 2

In Step 2 we fit to the M analysis eigenvectors for each whole experiment the measured static spectra of NDMA, NADH, and LADH. A measured static spectrum that fits a particular experiment may be counted as belonging to one of the m absorbers in that experiment.

Table 4.8. $Q_r/[(N-r)(p-r)]$ M Analysis.

Experiment	Abbreviation	r = Number of Eigenvectors of $\underline{M}_W$					
		1	2	3	4	5	6
1.1	$E_{7.4}N_{15.0}S_{13.4}$	657.15	260.32	84.08	10.57	<u>2.24</u>[a]	1.34
1.2	$E_{7.4}N_{15.0}S_{13.4}$	795.75	318.34	89.54	11.29	<u>2.18</u>	1.35
2.1	$E_{7.4}N_{15.0}S_{13.4}$	561.67	209.48	74.90	9.59	<u>1.71</u>	1.03
3.1	$E_{18.6}N_{15.0}S_{13.4}$	237.28	61.61	16.50	4.23	<u>2.14</u>	1.56
3.2	$E_{18.6}N_{15.0}S_{13.4}$	432.37	91.89	10.00	4.12	<u>2.38</u>	1.49
3.3	$E_{18.6}N_{15.0}S_{13.4}$	460.24	131.04	38.23	5.46	<u>1.98</u>	1.16
4.1	$E_{7.4}N_{6.0}S_{13.4}$	2918.40	67.74	6.99	3.17	2.21	<u>1.58</u>
4.2	$E_{7.4}N_{6.0}S_{13.4}$	3011.90	69.84	13.97	3.27	2.37	<u>1.69</u>

[a]Underscored values indicate the minimum number of components with which the experimental absorbance surface can be reconstructed to within its random error.

Table 4.9. $Q_r/[(N-r)(p-r)]$ S-Analysis.

Experiment	Abbreviation	r = Number of Eigenvectors of $\underline{S}_W$					
		1	2	3	4	5	6
1.1	$E_{7.4}N_{15.0}S_{13.4}$	377.97	92.29	11.59	2.24[a]	1.36	1.05
1.2	$E_{7.4}N_{15.0}S_{13.4}$	543.03	97.97	12.41	2.18	1.36	0.88
2.1	$E_{7.4}N_{15.0}S_{13.4}$	293.86	83.34	10.29	1.81	1.06	0.81
3.1	$E_{18.6}N_{15.0}S_{13.4}$	70.62	18.57	4.31	2.13	1.58	1.40
3.2	$E_{18.6}N_{15.0}S_{13.4}$	105.50	11.06	4.24	2.42	1.53	1.04
3.3	$E_{18.6}N_{15.0}S_{13.4}$	141.61	46.81	5.64	2.08	1.23	1.02
4.1	$E_{7.4}N_{6.0}S_{13.4}$	139.22	8.21	4.08	2.42	1.77	1.37
4.2	$E_{7.4}N_{6.0}S_{13.4}$	152.02	23.83	3.90	2.57	1.70	1.37

[a]Underscored values indicate the minimum number of components with which the experimental absorbance surface can be reconstructed to within its random experimental error.

Figures 4.19 through 4.22 show the M analysis fits of the measured static spectrum of NDMA to Experiments 1.1, 2.1, 3.1, and 4.1, respectively. Only in Experiment 4.1 does the measured static spectrum of NDMA fit as one of the m linearly independent absorbers. In Experiments 1.1, 2.1, and 3.1, the static spectrum of NDMA fits except for a shoulder in the calculated spectrum centered approximately at wavelength channel 24 (340 nm). This suggests that in these experiments, the concentration of NDMA may be linearly dependent on the concentration of another absorber with an absorbance band at 340 nm. If so, then Experiments 1.1, 2.1, and 3.1 actually have six absorbers, of which only five are linearly independent.

Figures 4.23 and 4.24 show the M analysis fits of the measured static spectra of NADH and LADH to Experiment 1.1. Neither measured static spectrum fits as belonging to one of the five linearly independent absorbers. Similar poor M analysis fits were obtained for NADH and LADH in Experiments 2.1, 3.1, and 4.1. Since NADH and LADH are undoubtedly present as chemical species in all of these experiments, these results suggest that either different spectral forms for NADH and LADH occur in the reaction, with effectively instantaneous complete conversion to these forms, or that the static spectra or concentration profiles of NADH and LADH are linearly dependent on the static spectra or concentration profiles of the other absorbers in these experiments.

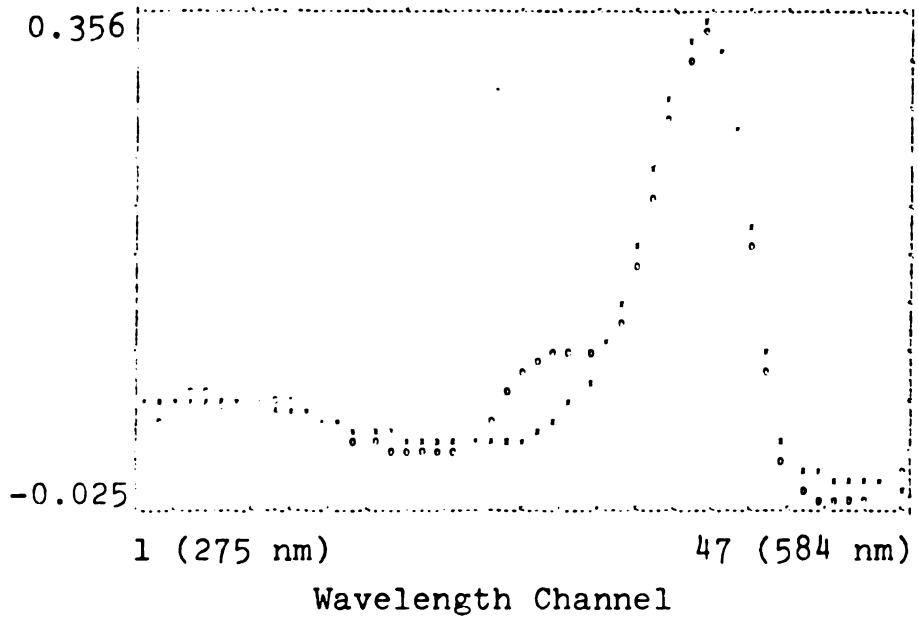

Figure 4.19. M analysis fit of the measured NDMA static spectrum to Experiment 1.1. X = measured, O = calculated. Vertical scale in arbitrary absorbance units.

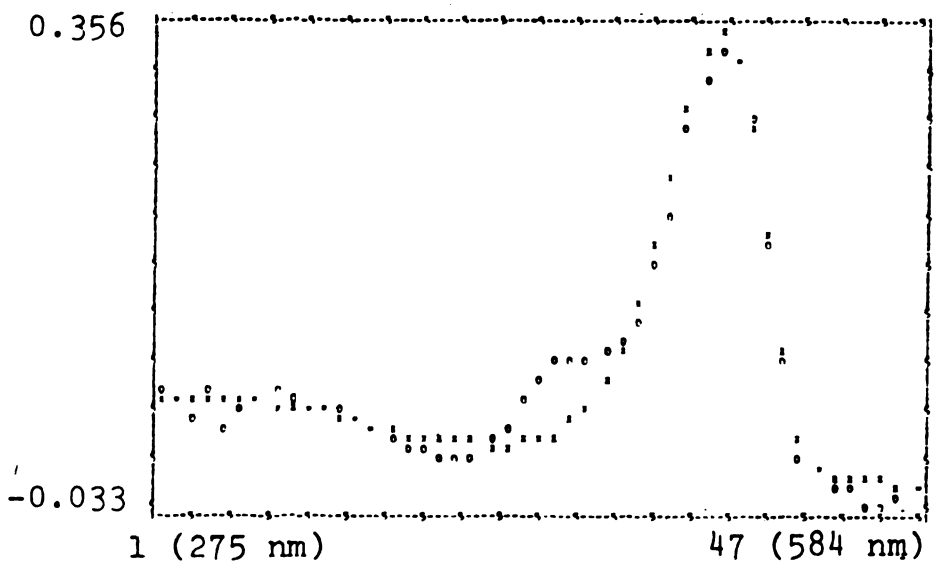

Figure 4.20. M analysis fit of the measured NDMA static spectrum to Experiment 2.1. X = measured, O = calculated. Vertical scale in arbitrary absorbance units.

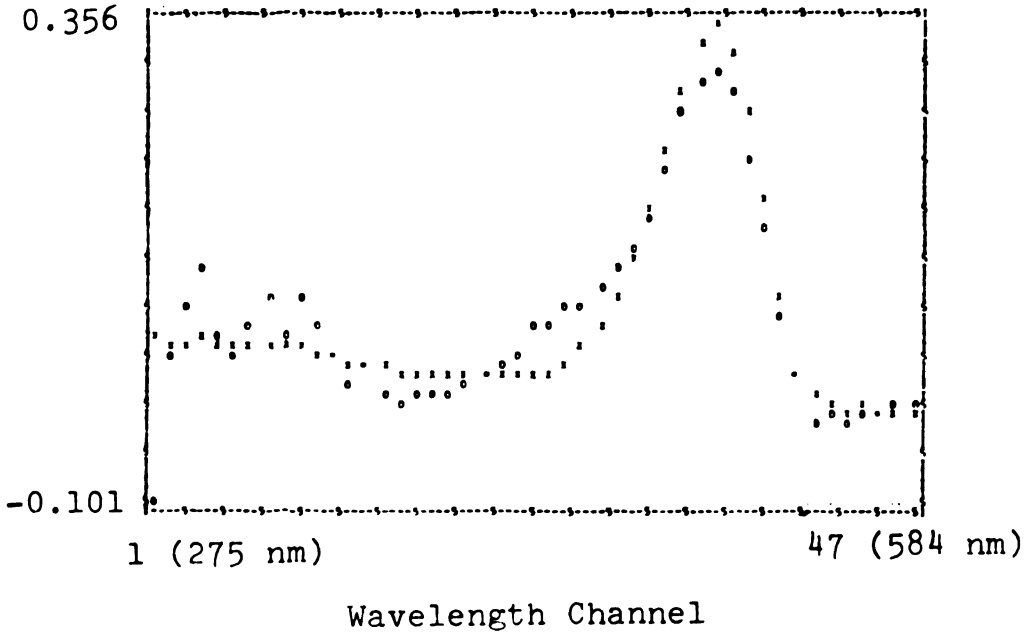

Figure 4.21. M analysis fit of the measured NDMA static spectrum to Experiment 3.1. X = measured, O = calculated. Vertical scale in arbitrary absorbance units.

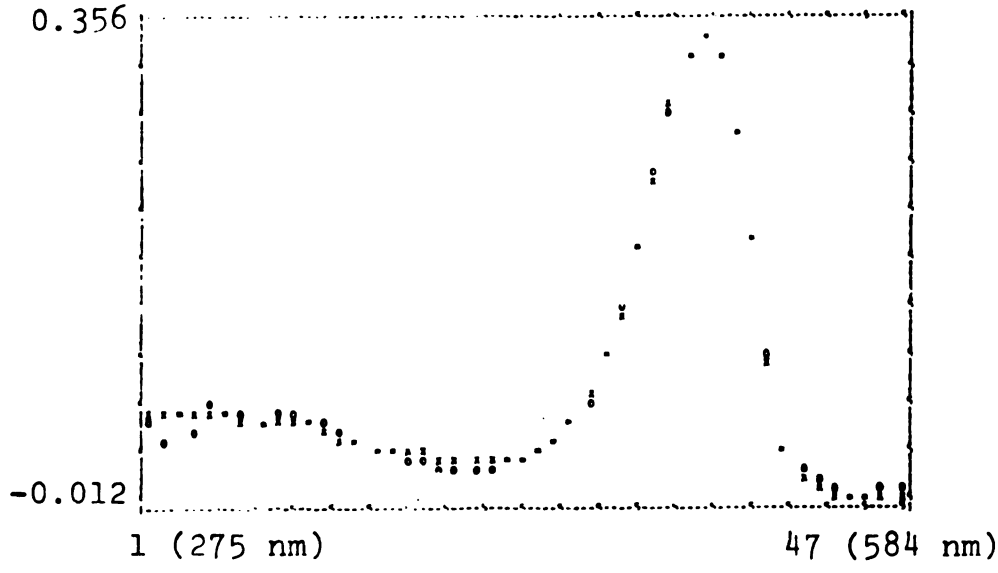

Figure 4.22. M analysis fit of the measured NDMA static spectrum to Experiment 4.1. X = measured, O = calculated. Vertical scale in arbitrary absorbance units.

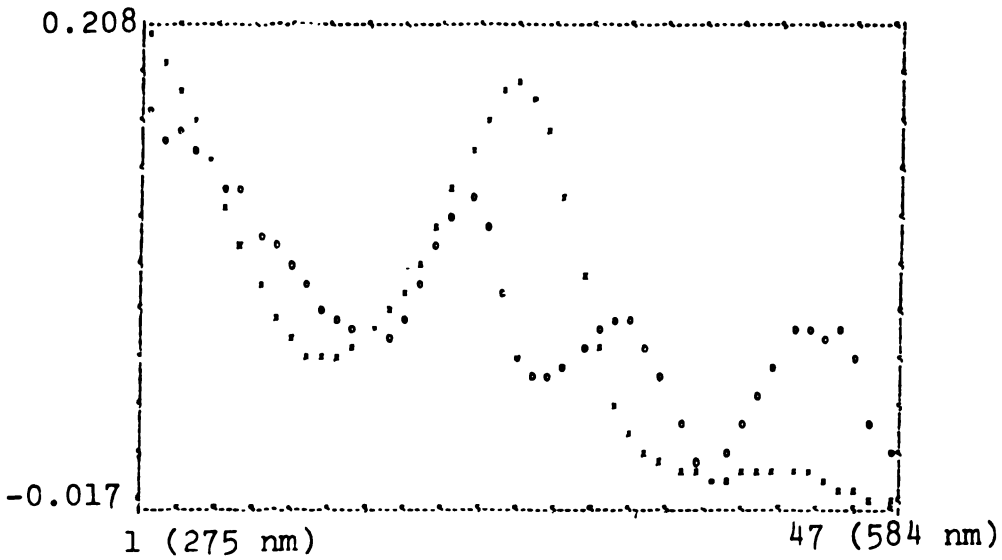

Figure 4.23. M analysis fit of the measured NADH static spectrum to Experiment 1.1. X = measured, O = calculated. Vertical scale in arbitrary absorbance units.

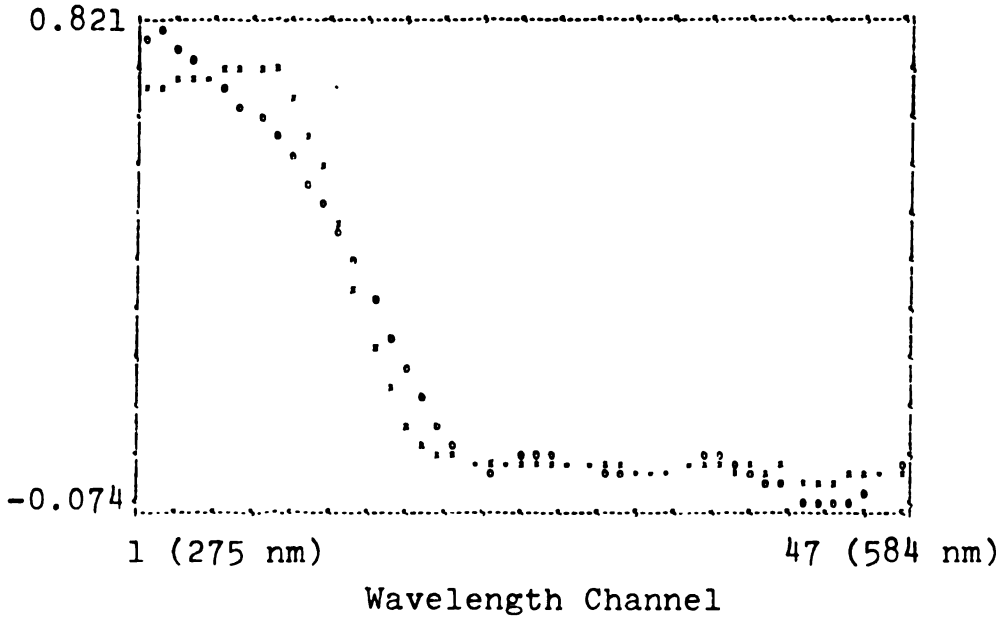

Figure 4.24. M analysis fit of the measured LADH static spectrum to Experiment 1.1. X = measured, O = calculated. Vertical scale in arbitrary absorbance units.

The NADH situation is partly resolved by considering the changes that occur when NADH is oxidized to NAD^+. Figure 4.25 shows the absorbance spectra of NADH and NAD^+ (P. L. Biochemicals, 1973). NADH has two absorbance bands, with peaks at 260 nm and 340 nm, respectively. The 340 nm absorption arises from the reduced nicotinamide portion of NADH (Kaplan, 1960) and disappears when NADH is oxidized to NAD^+. The 260 nm absorption arises from the adenine portion of NADH, and is enhanced but not changed in shape by an additional 260 nm absorption from the oxidized nicotinamide portion when NADH is oxidized to NAD^+ (Kaplan, 1960). Thus, the two absorbance peaks of NADH should make separate Beer's Law contributions to the absorbance surface. We therefore fit separately the 260 nm and 340 nm bands to the M analysis eigenvectors of Experiments 1.1 through 4.1.

Figure 4.26 shows the M analysis fit of the NAD^+ 260 nm absorbance band from Figure 4.25 to Experiment 1.1. The fit is too poor to conclude that the 260 nm absorbance band of NADH and NAD^+ fits as a linearly independent absorber in Experiment 1.1. The same negative result was obtained for Experiments 2.1, 3.1, and 4.1. (In Section O we analyze a special scanning experiment from 250 nm - 300 nm that includes the NADH-NAD^+ absorbance maximum at 260 nm.)

Figure 4.27 shows the M analysis fit of the 340 nm band of the measured static spectrum of NADH to Experiment

1.1, from which we condlude thattthe 340 nm band of NADH does not belong to one of the five linearly independent absorbers in Experiment 1.1. The 340 nm band of NADH fits equally poorly in Experiments 2.1 and 3.1. Figure 4.28 shows the M analysis fot of the 340 nm NADH band to Experiment 4.1. The fit is good except for the large random deviations in the baseline below 300 nm. This suggests that the 340 nm band of NADH may make a small absorbance contribution as the sixth absorber in Experiment 4.1, which would be consistent with the following observations:

1. $NADH_{340\ nm}$ fits Experiment 4.1, but not Experiments 1.1, 2.1, and 3.1.
2. Experiment 4.1 has six linearly independent absorbers, whereas Experiments 1.1, 2.1, and 3.1 have only five.
3. Experiments 1.1, 2.1, and 3.1 appear to have linear dependence between the concentrations of NDMA and an absorber with a peak near 340 nm.

Our interpretation of these observations is that in Experiment 4.1 NDMA and $NADH_{340\ nm}$ have linearly independent concentrations, whereas, in Experiments 1.1, 2.1, and 3.1 the concentrations of NDMA and $NADH_{340\ nm}$ are linearly dependent on each other. We note that Experiments 1.1, 2.1, and 3.1 have the same ratio of initial concentrations $([NDMA]_0/[NADH]_0) = 0.89$, nearly unity, whereas Experiment

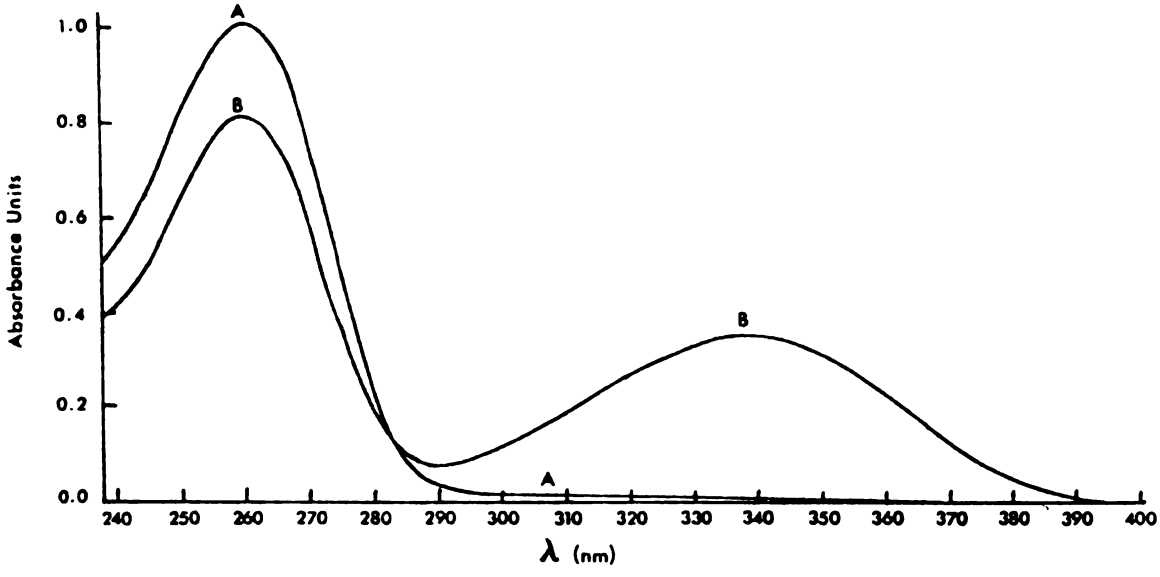

Figure 4.25. Absorbance of spectra of NADH and NAD^+ (P. L. Biochemicals, 1973).

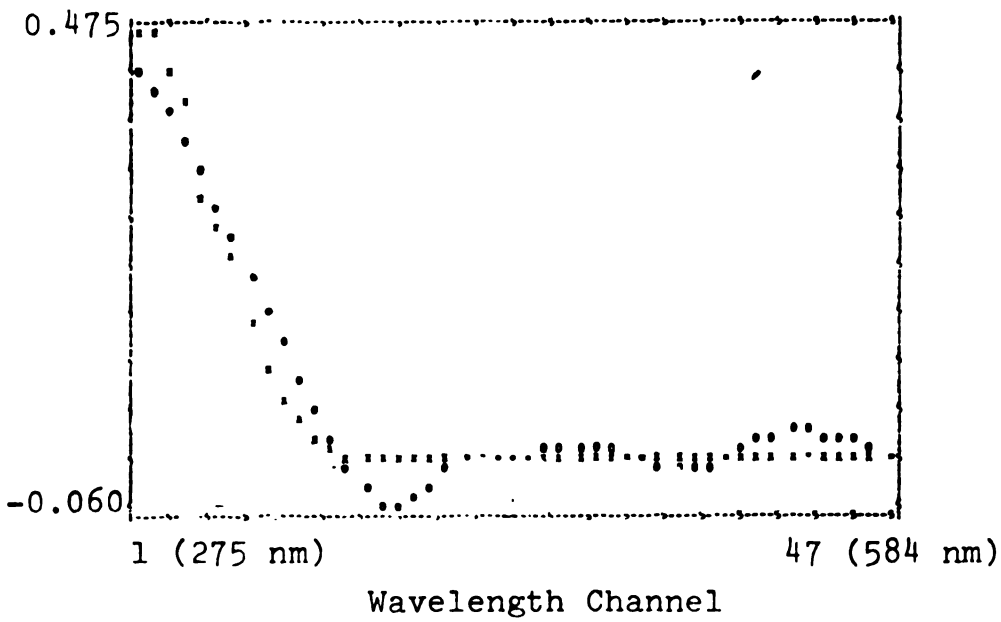

Figure 4.26. M analysis fit of the 260 nm NAD^+ absorbance band to Experiment 1.1. X = 260 nm NAD^+ band, O = calculated. Vertical scale in arbitrary absorbance units.

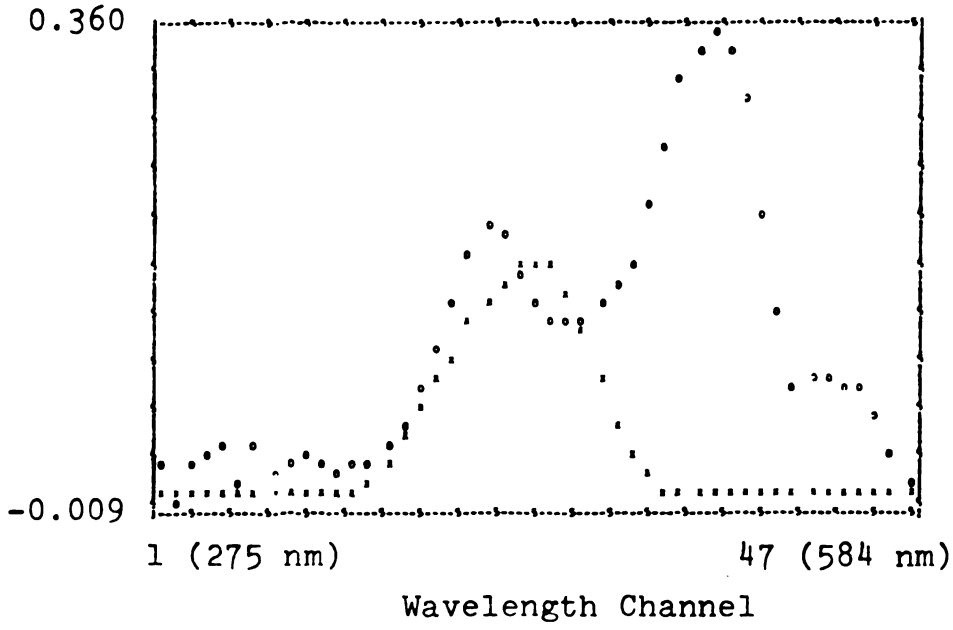

Figure 4.27. M analysis fit of the 340 nm NADH absorbance band to Experiment 1.1. X = 340 nm NADH band, O = calculated. Vertical scale in absolute absorbance units.

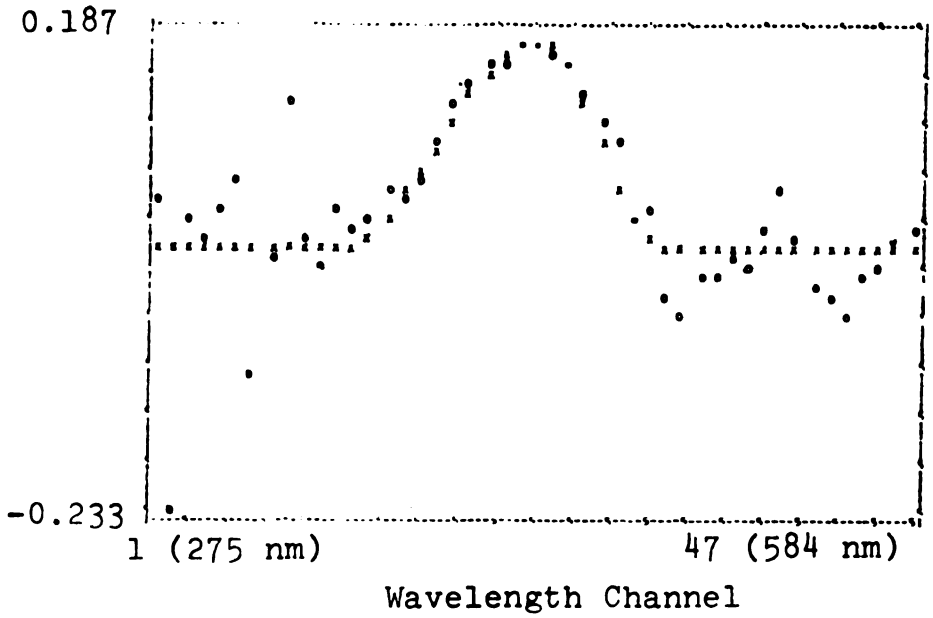

Figure 4.28. M analysis fit of the 340 nm NADH absorbance band to Experiment 4.1. X = 340 nm NADH band, O = calculated. Vertical scale in arbitrary absorbance units.

4.1 has the ratio $([NDMA)_0/[NADH]_0)$ = 2.3. This suggests (see Example 3.1) that the linear dependence of NDMA and NADH concentrations in Experiments 1.1, 2.1, and 3.1, may occur because the ratio of their initial concentrations is near the ratio of their stoichiometries in the reaction (assuming a 1:1 stoichiometry ratio.)

I. Principal Component Analysis, Step 3

In Step 3 we fit to the S analysis eigenvectors each measured static spectrum that fit as an absorber in Step 2. Each spectrum that fits the S analysis eigenvectors may be counted as belonging to an absorber whose concentration changed and whose rate is linearly independent of the rates of the other absorbers.

In Step 2, we showed that the measured static spectrum of NDMA and the 340 nm band of NADH fit as belonging to an absorber in Experiment 4.1. Figures 4.29 and 4.30 show the S analysis fits of NDMA and $NADH_{340\ nm}$ to Experiment 4.1, from which we conclude that NDMA and the 340 nm band of NADH have linearly independent rates in Experiment 4.1. There are no other static spectra from Step 2 to test in Step 3.

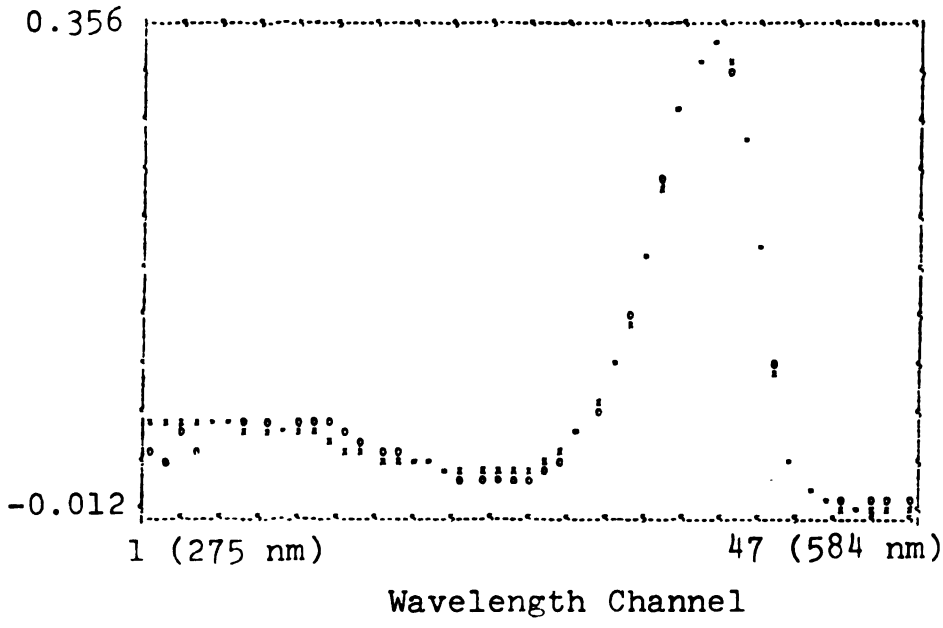

Figure 4.29. S analysis fit of the measured NDMA static spectrum to Experiment 4.1. X = measured, O = calculated. Vertical scale in arbitrary absorbance units.

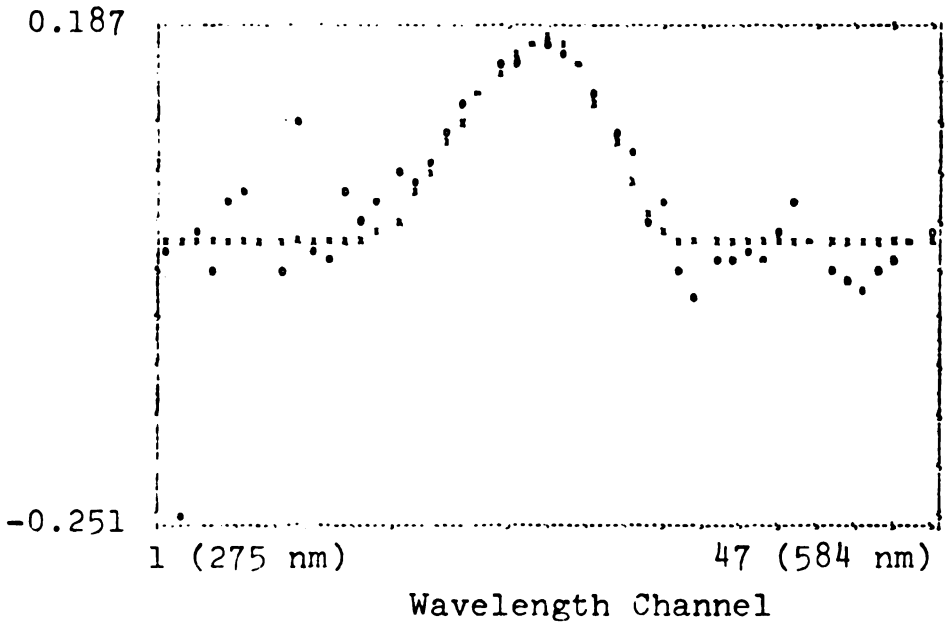

Figure 4.30. S analysis fit of the 340 nm NADH absorbance band to Experiment 4.1. X = 340 nm NADH band, O = calculated. Vertical scale in arbitrary absorbance units.

J. Principal Component Analysis, Step 4

Recall from Section B of Chapter 3 that each measured static spectrum that fits the M analysis eigenvectors of an experiment gives an estimate for one column of the rotation matrix $\underline{U}$. When m columns of $\underline{U}$ have been estimated, we can resolve the experiment into the static spectra and concentration vectors of its m linearly independent absorbers.

We have from Step 2 two columns of $\underline{U}$ for Experiment 4.1, corresponding to the successful M analysis fitting of the static spectra of NDMA and $NADH_{340\ nm}$. Four more columns of $\underline{U}$ are required to resolve Experiment 4.1. So far we have no estimates for the five columns of $\underline{U}$ in Experiments 1.1, 2.1, and 3.1 since no measured static spectra fit these experiments. In Step 2 we suggested that NDMA and $NADH_{340\ nm}$ may be linearly dependent absorbers in Experiments 1.1, 2.1, and 3.1. Even if they are, they count together as only one linearly independent absorber in these experiments, and we are still left with four linearly independent absorbers that must be either transient intermediates or unknown products. Although we have no measured static spectra for these absorbers, we can infer some of their spectral and kinetic properties in Steps 5 through 7, which we perform for Experiment 1.1. We then transfer the spectral properties determined for Experiment 1.1 to Experiments 2.1, 3.1, and 4.1.

K. Principal Component Analysis, Step 5

In Step 5 we perform M and S analysis on subspaces of wavelength and time to find parts of Experiment 1.1 that contain fewer than five absorbers.

Figure 4.31 shows a breakdown of Experiment 1.1 into four wavelength subspaces, I (channels 1-15), II (channels 16-29), III (channels 30-38), and IV (channels 39-47). We performed M and S analyses on each subspace, using all 61 consecutive spectra in each case. Figure 4.31 shows the (m,s) pairs thus obtained for each subspace and several combinations of subspaces.

We draw the following conclusions from Figure 31:

1. Either the concentration of one of the two absorbers in I does not change, or the rates of the two absorbers in I are linearly dependent on each other.
2. III and IV have one absorber in common, whereas the two absorbers in I do not absorb in III or IV.
3. I, III, and IV are two-absorber subspaces that together have all five of the linearly independent absorbers that are in the whole experiment.

Therefore, by separately resolving I, III, and IV with the two absorber simplifications of Chapter , Section D, we can obtain the concentration profiles of all five linearly independent absorbers. From these, we can resolve

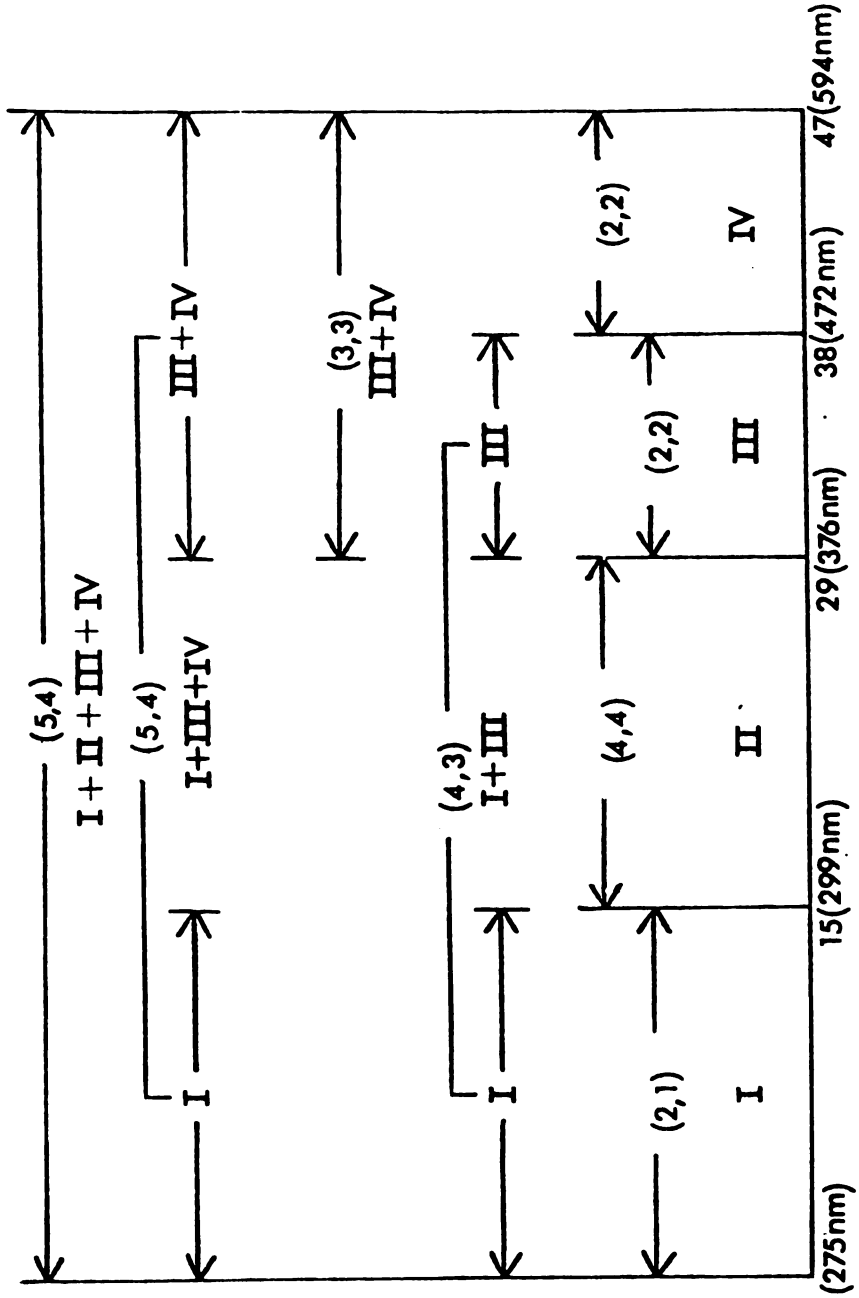

Figure 4.31. (m,s) pairs for Wavelength Subspaces I-IV of Experiment 1.1.

the whole experiment to obtain the static spectra of all five linearly independent absorbers.

L. Principal Component Analysis, Step 6

In Step 6 we use the two absorber simplifications of Chapter 3, Section D, to resolve partially or completely each of Subspaces I, III, and IV.

Subspace I (275 nm - 299 nm) In Step 2, we showed that LADH and NADH, which absorb between 275 nm and 299 nm, do not fit as linearly independent absorbers in Experiment 1.1. Therefore, we have no outside information about the static spectra or concentration profiles of the two absorbers in Subspace I. However, we can obtain the range of acceptable shapes for their static spectra and concentration profiles by applying the solution bands for two absorbers defined in Chapter 3, Section D. Recall that these solution bands use the nonnegative definiteness of the static spectra and concentration profiles and the M analysis eigenvectors to define the upper and lower bounds of the static spectra and concentration profiles, each normalized to unit length.

Figure 4.32A shows the solution bands for the first absorber's normalized static spectrum, which must fall on or between $\hat{\underline{f}}'_{1L}$ and $\hat{\underline{f}}'_{1H}$, symbolized by L and H, respectively. Note that L and H corss, and thus $\underline{f}'_{1L}$ is not

Figure 4.32. Solution bands for normalized static spectra in Subspace I, Experiment 1.1, L = $\hat{\underline{f}}'_{jL}$, H = $\hat{\underline{f}}'_{jH}$. A. First absorber. B. Second absorber.

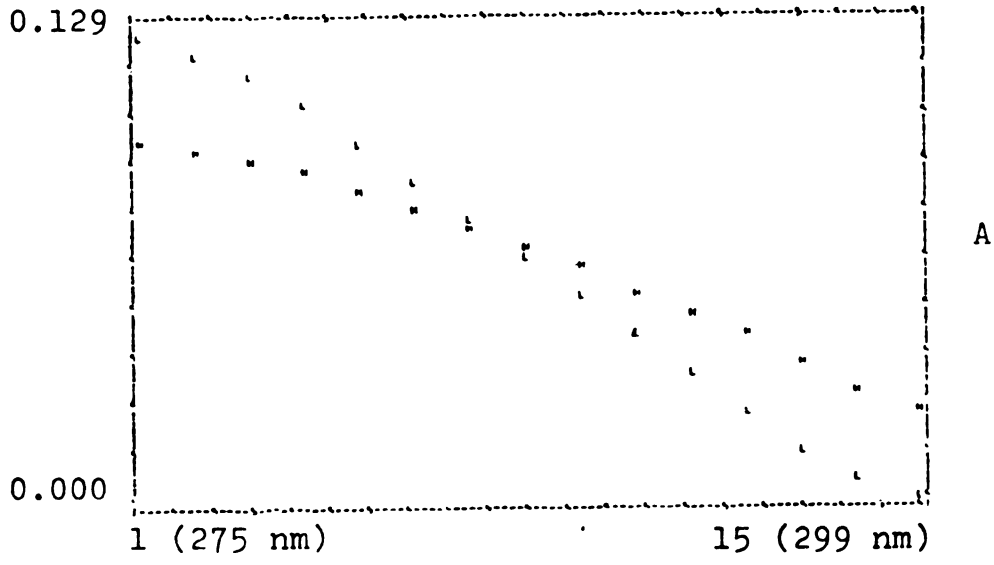
0.129
0.000
A
1 (275 nm)
15 (299 nm)
Wavelength Channel

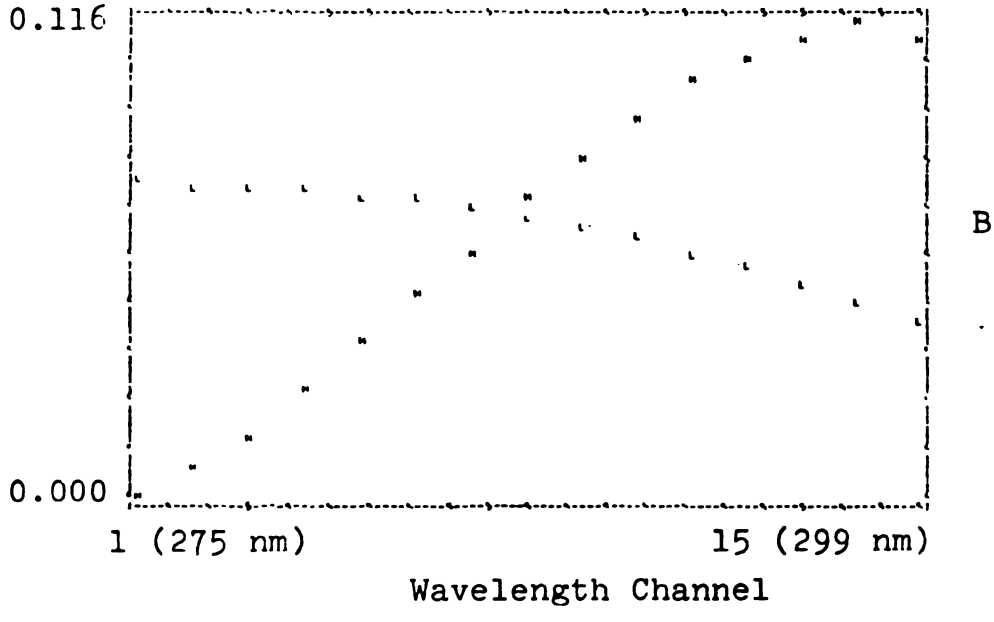
0.116
0.000
B
1 (275 nm)
15 (299 nm)
Wavelength Channel

Figure 4.32.

always less than $\hat{\underline{f}}'_{1H}$. This is a general situation that also obtains for the concentration solution bands $\hat{\underline{c}}'_{jL}$ and $\hat{\underline{c}}'_{jH}$. From Figure 4.32A we see that the absorbance of the first absorber in I is still increasing with decreasing wavelength between channels 2 and 1, and that this absorber thus has its maximum absorbance at a wavelength less than or equal to 275 nm.

Figure 4.32B shows the solution bands for the static spectrum of the second absorber in Subspace I. These solution bands are not as informative as those for the first absorber, since they give no indication of where the second absorber has its peak absorbance.

Figures 4.33A and 4.33B show the solution bands for the normalized concentration profile of the first and second absorbers, respectively, in Subspace I. (Note that in these figures the time axis is linear in spectrum number, and not in time.) The normalized concentration profiles must fall on or between $\hat{\underline{c}}'_{jL}$ and $\hat{\underline{c}}'_{1H}$, symbolized by L and H, respectively. According to Figure 4.33A, the first absorber's concentration may grow and then decay (H), decay and then grow (L), or remain constant (a possibility between L and H). According to Figure 4.33B, the second absorber's concentration must grow and then decay.

Subspace III (385 nm - 472 nm) Figures 4.34 and 4.35 show the solution bands for the normalized static spectra

Figure 4.33. Solution bands for normalized static spectra in Subspace I, Experiment 1.1, L = $\underline{\hat{c}}'_{jL}$, H = $\underline{\hat{c}}'_{jH}$. A. First absorber. B. Second absorber.

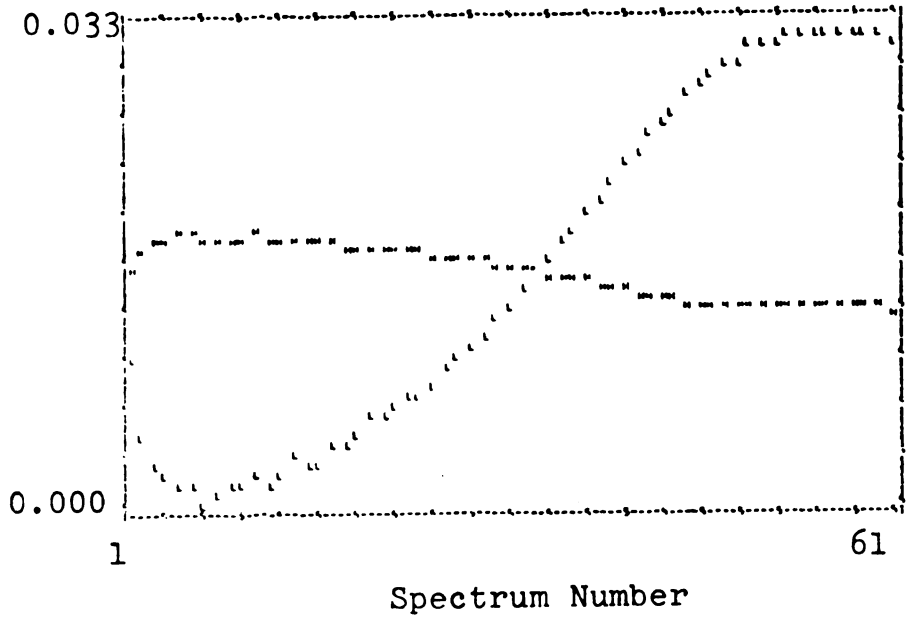
0.033
0.000
1
61
Spectrum Number
A

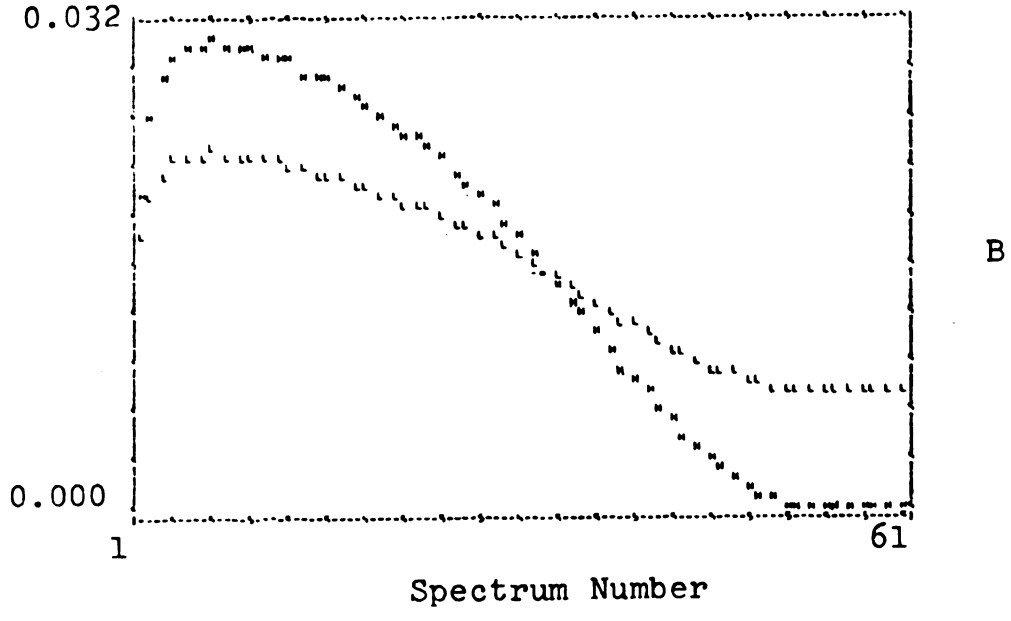
0.032
0.000
1
61
Spectrum Number
B

Figure 4.33.

and concentration profiles of the two absorbers in Subspace III. According to Figure 4.34A, the first absorber's absorbance maximum in thisssubspace is between 385 nm and 403 nm (wavelength channels 30-32), and according to Figure 4.34B, the second absorber's absorbance maximum is between 424 nm and 459 nm (wavelength channels 34-37). From Figure 4.35A we cannot determine whether the first absorber's concentration profile is a biphasic decay (H) or a growth followed by decay (L). Figure 4.35B shows that the second absorber's concentration profile is a rapid decay.

NDMA has an absorbance maximum at 440 nm, and as a substrate in the reaction, might be expected to decay rapidly. Therefore, NDMA is a likely candidate for the second absorber in Subspace III. Figure 4.36A shows the M analysis fit of the measured static spectrum of NDMA in Subspace III, and we conclude that NDMA is the second absorber in III.

Recall from Chapter 3, Section D, that in a two absorber subspace, when the shape of one absorber's static spectrum is known, the shape of the other absorber's concentration profile can be computed directly. By assuming that NDMA is the second absorber, we compute the shape of the first absorber's concentration profile shown in Figure 4.36B from the shape of its static spectrum and the M analysis eigenvectors. Thus, the first absorber is an intermediate that grows and decays.

Figure 4.34. Solution bands for normalized static spectra in Subspace III, Experiment 1.1, L = $\hat{\underline{f}}'_{jL}$, H = $\hat{\underline{f}}'_{jH}$. A. First absorber. B. Second absorber.

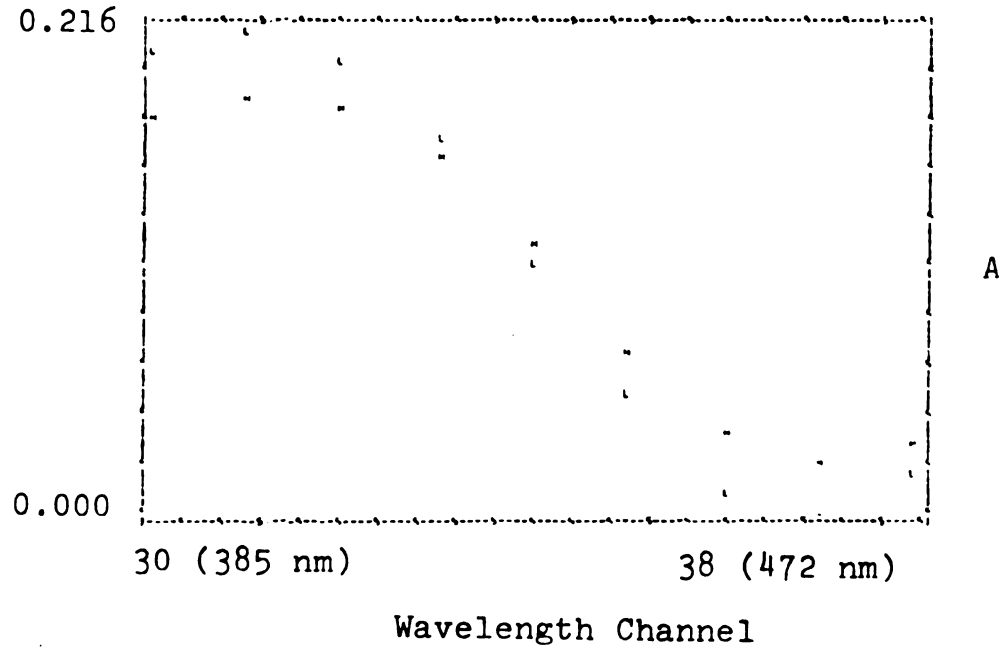
0.216
0.000
30 (385 nm)
38 (472 nm)
Wavelength Channel
A

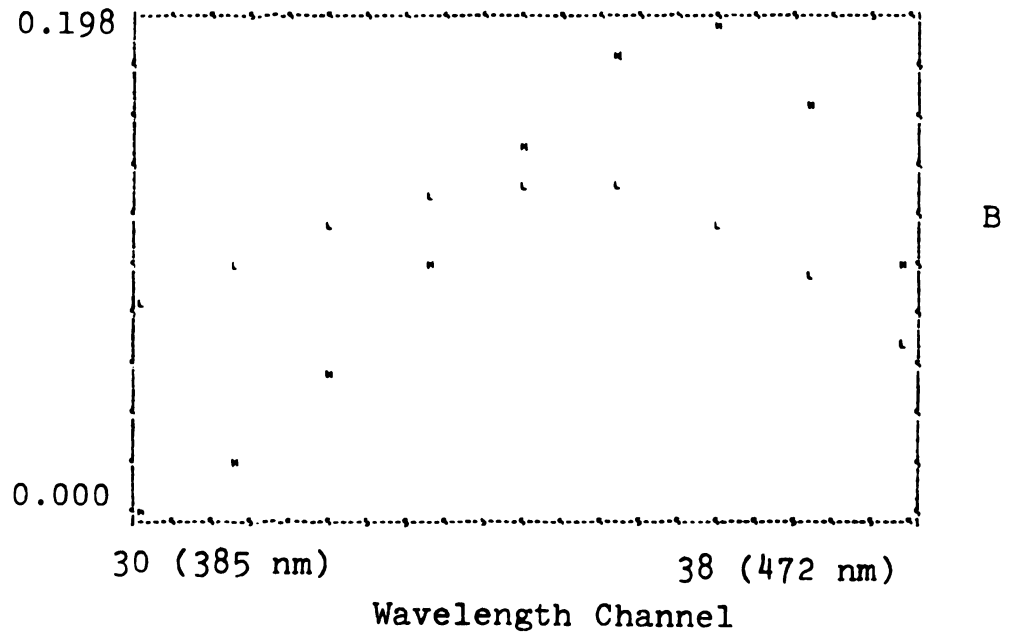
0.198
0.000
30 (385 nm)
38 (472 nm)
Wavelength Channel
B

Figure 4.34.

Figure 4.35. Solution bands for normalized concentration profiles in Subspace III, Experiment 1.1, L = $\underline{c}'_{jL}$, H = $\underline{\hat{c}}'_{jH}$. A. First absorber. B. Second absorber.

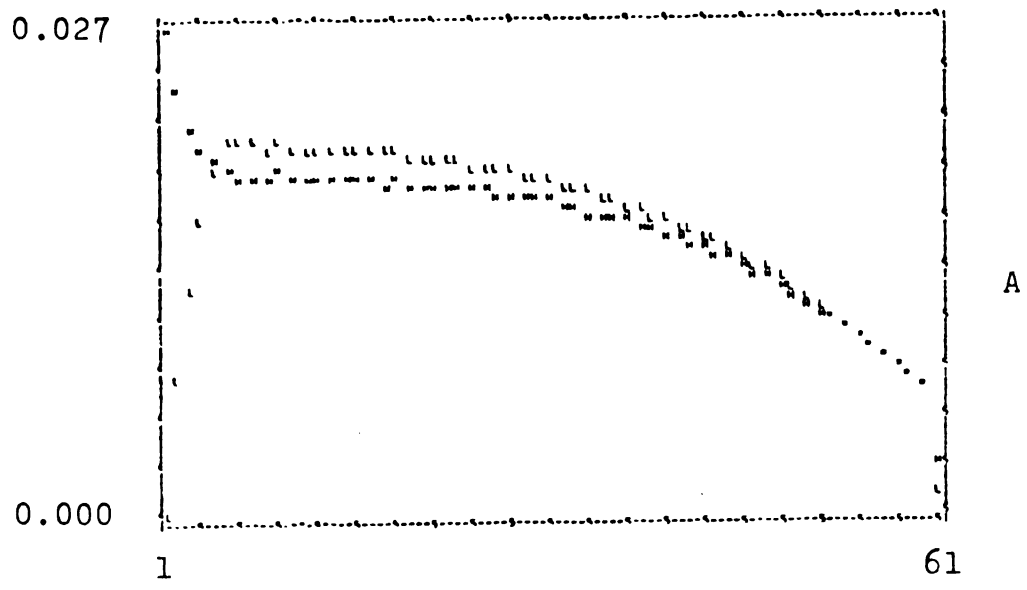

Spectrum Number

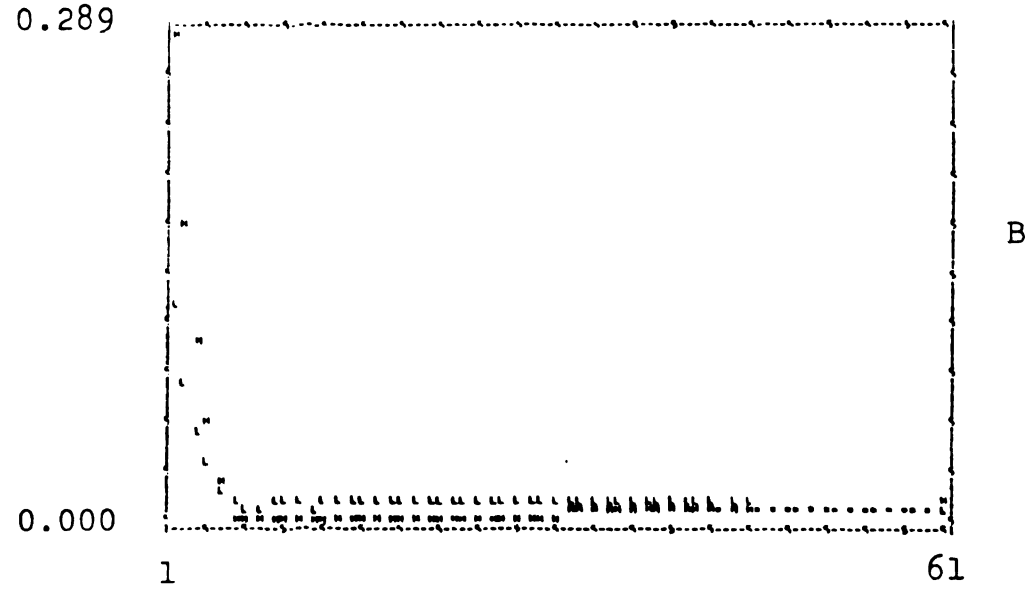

Spectrum Number

Figure 4.35.

Figure 4.36. A. M analysis fit of the measured NDMA static spectrum, Subspace III, Experiment 1.1, X = measured, O = calculated. Vertical scale in arbitrary absorbance units.

B. Concentration profile of the first absorber in Subspace III, Experiment 1.1. Vertical scale in arbitrary concentration units.

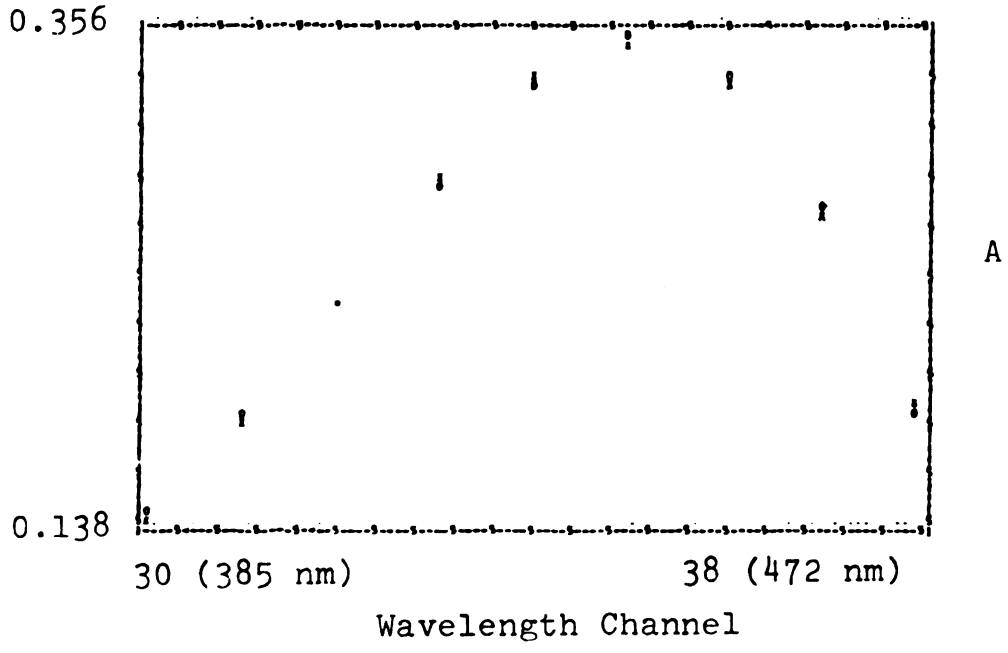
0.356
0.138
A
30 (385 nm)
38 (472 nm)
Wavelength Channel

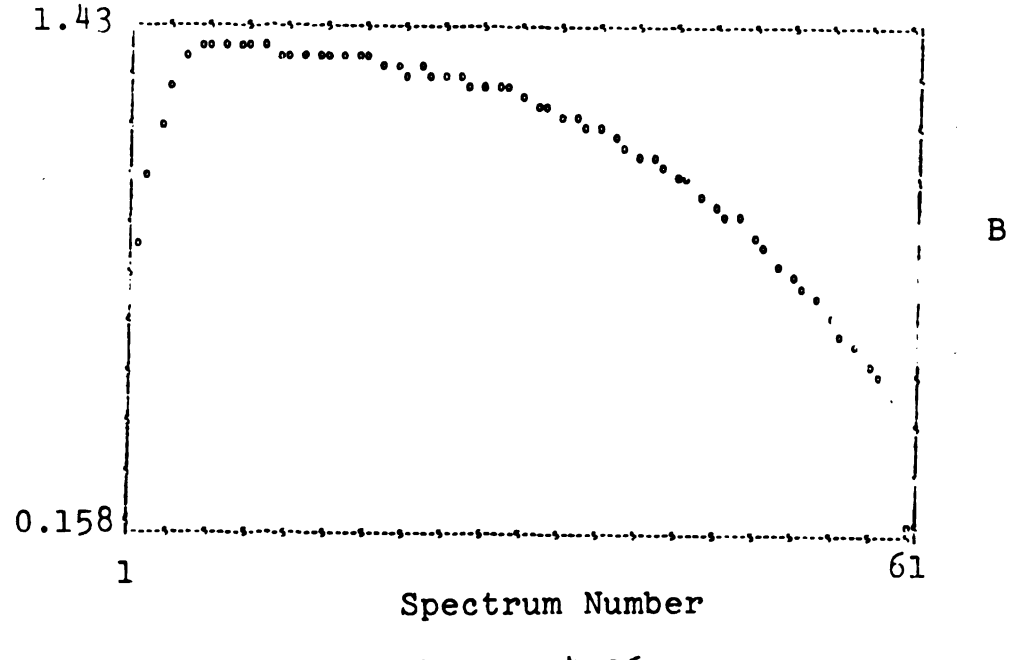
1.43
0.158
B
1
61
Spectrum Number

Figure 4.36.

We still do not have the shapes of the first absorber's static spectrum and the second absorber's (NDMA) concentration profile. We note, however, from Figure 4.35B that the second absorber's (NDMA) concentration does not significantly change during the last 16 consecutive spectra, whereas Figure 4.36B shows that the first absorber's concentration changes during the last 16 consecutive spectra. Furthermore, an S analysis of the last 16 spectra in Subspace III gives an essential rank s of one, which supports our observation that only one absorber changes concentration in these spectra. Assuming that the first absorber changes concentration during the last 16 spectra, we obtain its static spectral shape from the first eigenvector of $\underline{S}_W$ by the equation $\hat{\underline{f}}_1 = \underline{L}^{-1}\underline{B}_{(1)}$. We obtain the contribution of the first absorber to all of Subspace III by performing an M analysis fit of $\underline{L}^{-1}\underline{B}_{(1)}$ to all 61 consecutive spectra. The results are shown in Figure 4.37A. Note that the first absorber has its maximum absorbance at 394 nm (wavelength channel 31). The concentration profile of NDMA (the second absorber) can be computed directly from the static spectrum of the first absorber, and is shown in Figure 4.37B. Thus, we have used the two absorber simplifications to resolve Subspace III into the static spectra and concentration profiles displayed in Figures 4.36 and 4.37.

Subspace IV (385 nm - 584 nm) Subspace IV shares one of its two absorbers with Subspace III (see Figure 4.31).

Figure 4.37. A. M analysis fit of the first absorber's static spectrum, Subspace III, Experiment 1.1. $X = \underline{L}^{-1}\underline{B}_{(1)}$ from last 16 consecutive spectra, O = calculated M analysis fit using all 61 consecutive spectra. Vertical scale in arbitrary absorbance units.

B. Concentration profile of NDMA in Experiment 1.1. Vertical scale in arbitrary concentration units.

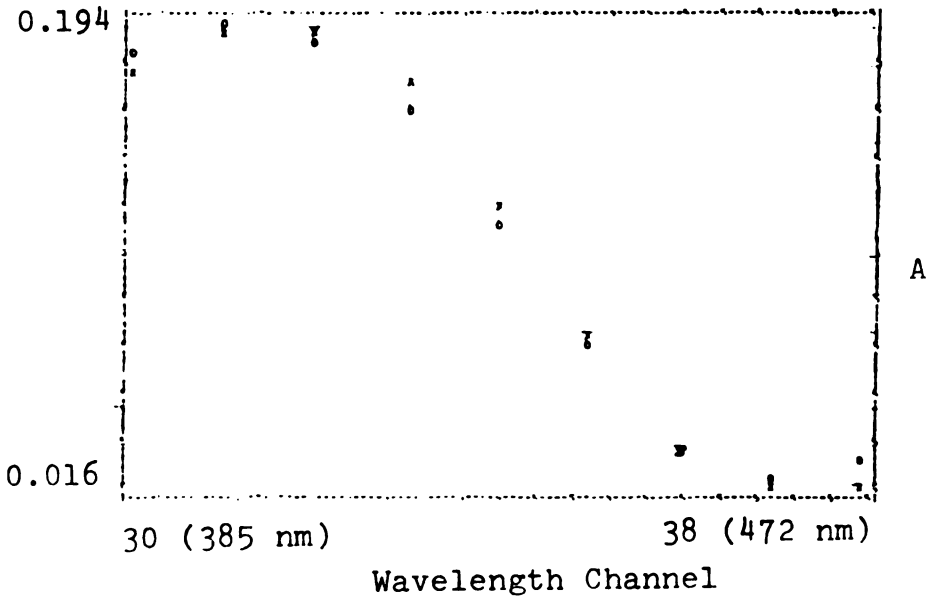
0.194
0.016
A
30 (385 nm)
38 (472 nm)
Wavelength Channel

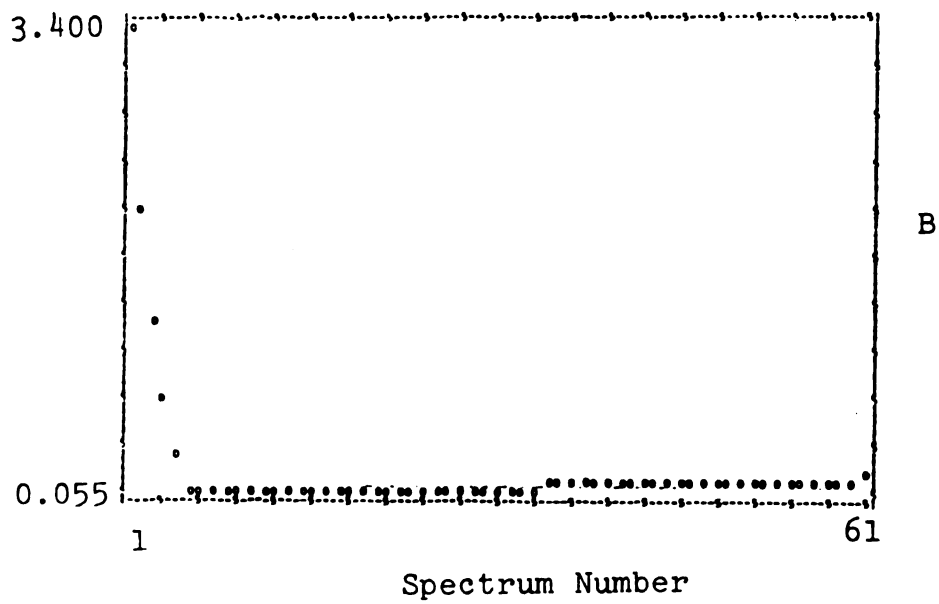
3.400
0.055
B
1
61
Spectrum Number

Figure 4.37.

Since we have obtained the concentration profiles of both absorbers in III, we need to obtain from IV only the concentration profile of the absorber it does not share with III. Wavelength channels 44 through 47 (550 nm - 584 nm) in Experiment 1.1 show the growth and decay of absorbance previously observed by two other groups of investigators (Schack and Dunn (1972), and Suelter et al. (1975)). Both groups attributed this to a transient intermediate. An M analysis of wavelength channels 44-47 shows that these channels have two linearly independent absorbers (m=2). However, the systematic errors are small for reconstructing the experimental absorbance at these wavelength channels with only one eigenvector of $\underline{M}_W$, and thus wavelength channels 44-47 have only a small contribution from the second absorber. Figure 4.38 shows the solution bands for the normalized concentration profiles of the two absorbers in channels 44-47. The normalized concentration profile of the first absorber is well defined in Figure 4.38A, but the normalized concentration profile of the second absorber, shown in Figure 4.38B, is poorly defined, and contains mostly random noise. Thus, the first absorber is the predominant absorber, and the second absorber in channels 44-47 absorbs barely above the level of the random experimental errors.

Figure 4.38. Solution bands for normalized concentration profiles in wavelength channels 44-47, Experiment 1.1, L = $\underline{\hat{c}}'_{jL}$, H = $\underline{\hat{c}}'_{jH}$. A. First absorber. B. Second absorber.

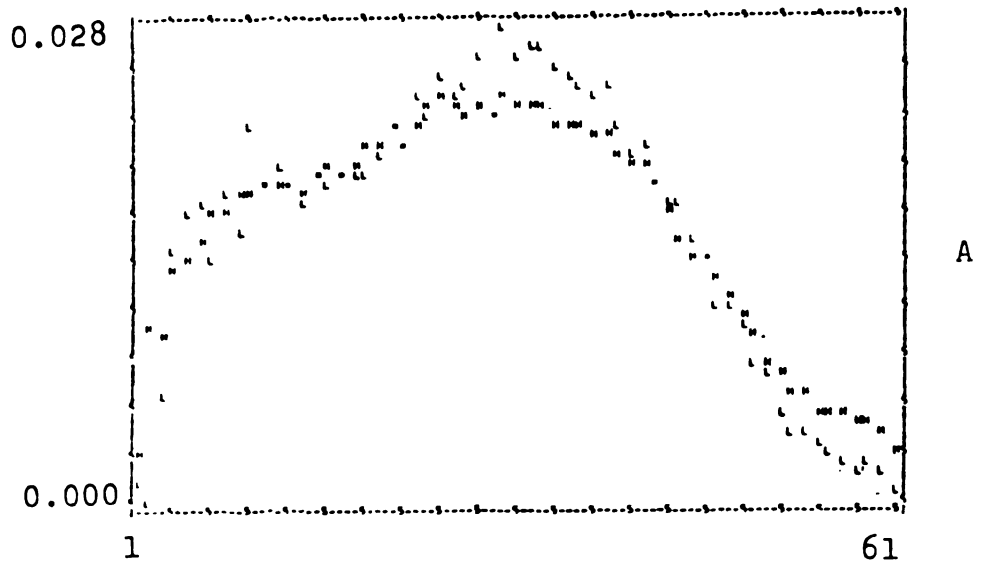
0.028
0.000
1
61
A
Spectrum Number

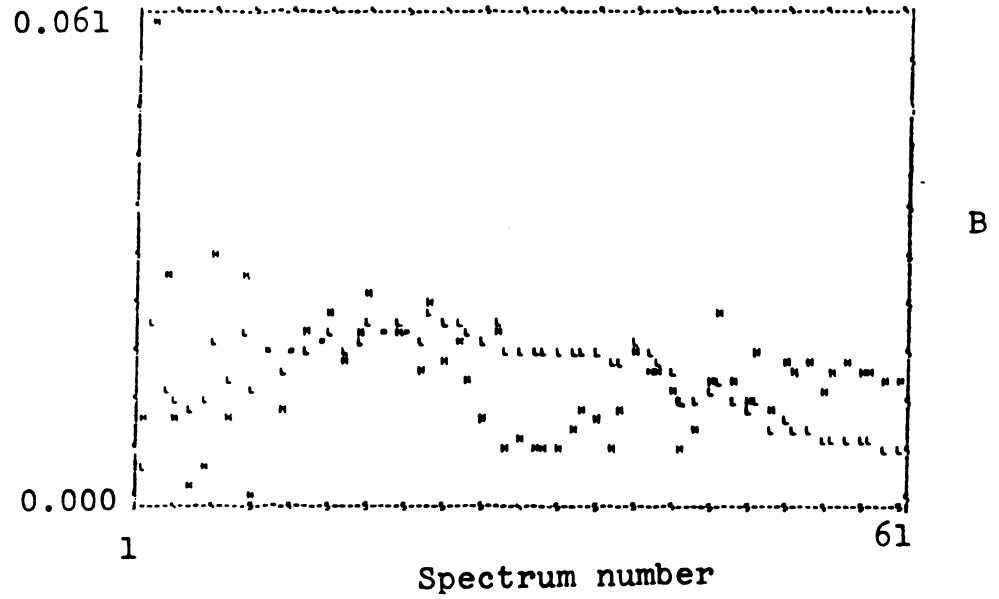
0.061
0.000
1
61
B
Spectrum number

Figure 4.38.

M. Principal Component Analysis, Step 7

In Step 7 we use the concentration profiles obtained in Step 6 from Subspaces I, III, and IV of Experiment 1.1 to resolve the whole experiment. Specifically, the goal is to estimate all five columns of the rotation matrix $\underline{V}$ for the whole experiment. The whole experiment is then resolved into the static spectra and concentration profiles of its five linearly independent absorbers. When fit to the M analysis eigenvectors for theewhole experiment, each concentration profile from Subspaces I, III, and IV gives one column of $\underline{V}$.

In Step 6 we resolved Subspace III to obtain the concentration profiles of NDMA and an intermediate with maximum absorbance at 394 nm. The solution bands for the first absorber in wavelength channels 44-47 of Subspace IV almost define its normalized concentration profile. We take the normalized concentration profile of the first absorber in channels 44-47 to be $\hat{\underline{c}}_{1L}$ in Figure 4.38A. From subspace I we have only the extrema shown in Figure 4.33 for the normalized concentration profiles of its two absorbers.

Figure 4.39 shows the static spectral information obtained to this point in the procedure for the five linearly independent absorbers in Experiment 1.1. The numbering system for the five absorbers is:

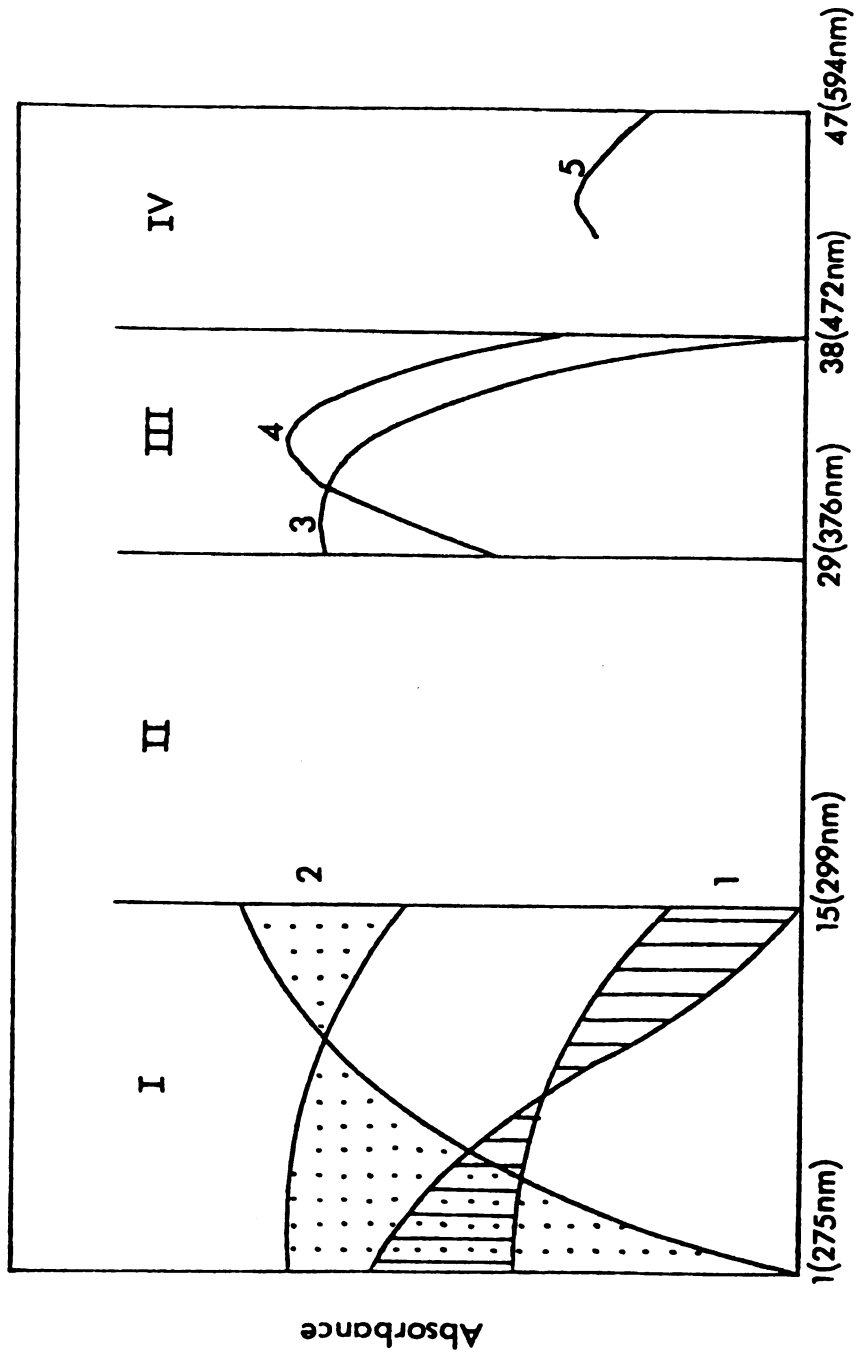

Figure 4.39. Summary of static spectral information obtained from Subspace I, III, and IV, Experiment 1.1.

Absorber 1--first absorber in Subspace I

Absorber 2--second absorber in Subspace I

Absorber 3--first absorber in Subspace III

Absorber 4--second absorber in Subspace III (NDMA)

Absorber 5--first absorber in wavelength channels 44-47

We use the known concentration profiles to estimate directly columns of $\underline{V}$ and consider only the extrema for the unknown concentration profiles. Thus, we fit the concentration profiles for Absorbers 3, 4, and 5 to the M analysis eigenvectors for the whole experiment to estimate columns 3, 4, and 5 of $\underline{V}$. From each of the extrema $\hat{\underline{c}}'_{1L}$ and $\hat{\underline{c}}'_{1H}$ $\underline{V}$ (Figure 4.33A) for the concentration profiles of Absorber 1 we estimate the corresponding extrema for column 1 of $\underline{V}$. Similarly, the two extrema for Absorber 2, $\hat{\underline{c}}'_{2L}$ and $\hat{\underline{c}}'_{2H}$ (Figure 4.33B) give two extrema for column 2 of $\underline{V}$. We have, then, four estimates of $\underline{V}$ corresponding to each of the four permutations of known concentration profiles with the extrema for Absorbers 1 and 2; i.e.,

$$(\hat{\underline{c}}'_{1L}, \hat{\underline{c}}'_{2L}, \hat{\underline{c}}_3, \hat{\underline{c}}_4, \hat{\underline{c}}_5), \quad (\hat{\underline{c}}'_{1L}, \hat{\underline{c}}'_{2H}, \hat{\underline{c}}_3, \hat{\underline{c}}_4, \hat{\underline{c}}_5),$$

$$(\hat{\underline{c}}'_{1H}, \hat{\underline{c}}'_{2H}, \hat{\underline{c}}_3, \hat{\underline{c}}_4, \hat{\underline{c}}_5), \text{ and } (\hat{\underline{c}}'_{1H}, \hat{\underline{c}}'_{2H}, \hat{\underline{c}}_3, \hat{\underline{c}}_4, \hat{\underline{c}}_5).$$

Equation (3.13) gives an estimate of the rotation matrix

$\underline{U}$ corresponding to each estimate of $\underline{V}$, and Equation (3.9) gives from each estimate of $\underline{U}$ an estimated static spectra matrix $\underline{F}$ for the whole experiment.

In summary, all four combinations of concentration profiles give the same static spectra for Absorbers 3, 4, and 5. Thus, our estimates for the static spectra and concentration profiles of Absorbers 3, 4, and 5 are insensitive to Absorbers 1 and 2 over the range of extrema for the concentration profiles of Absorbers 1 and 2. The combinations ($\underline{c}'_{1L}$, $\underline{c}'_{2H}$, $\underline{c}_3$, $\underline{c}_4$, $\underline{c}_5$) and ($\underline{c}'_{1H}$, $\underline{c}'_{2H}$, $\underline{c}_3$, $\underline{c}_4$, $\underline{c}_5$) give for Absorber 1 a physically unreasonable static spectrum that makes large contributions of negative absorbance (-0.2 O.D.) to wavelength channels 17-24 in Experiment 1.1. The combinations ($\underline{c}'_{1L}$, $\underline{c}'_{2L}$, $\underline{c}_3$, $\underline{c}_4$, $\underline{c}_5$) and ($\underline{c}'_{1H}$, $\underline{c}'_{2L}$, $\underline{c}_3$, $\underline{c}_4$, $\underline{c}_5$) give physically reasonable results (i.e., nonnegative static spectra). The static spectra for these two combinations are shown in Figure 4.40, where the static spectra of Absorbers 3, 4, and 5 are shown only once since they are the same for both combinations.

Table 4.10 lists the matrices $\underline{V}$ and $\underline{U}$ for the combination ($\underline{c}'_{1L}$, $\underline{c}'_{2L}$, $\underline{c}_3$, $\underline{c}_4$, $\underline{c}_5$) plus the eigenvalues used in Equation (3.13) to calculate $\underline{U}$ from $\underline{V}$. The j'th column of $\underline{V}$ was estimated from the concentration profile for the j'th absorber, and the j'th column of $\underline{U}$ corresponds to the resultant static spectrum of the j'th absorber. Table 4.11 lists $\underline{V}$ and $\underline{U}$ for the combination ($\underline{c}'_{1H}$, $\underline{c}'_{2L}$,

Table 4.10. Rotation Matrices $\underline{V}$, $\underline{U}$ and Eigenvalue Matrix $\underline{\Omega}_{(5)}$ Combination ($\hat{\underline{c}}'_{1L}$, $\hat{\underline{c}}'_{2L}$, $\hat{\underline{c}}_3$, $\hat{c}_4$, $\hat{c}_5$).

$\omega_1 = 1.07892\times10^4$ $\omega_4 = 4.34340\times10^2$

$\omega_2 = 1.05952\times10^3$ $\omega_5 = 1.43678\times10^2$

$\omega_3 = 6.90359\times10^2$

	$\underline{v}_1$	$\underline{v}_2$	$\underline{v}_3$	$\underline{v}_4$	$\underline{v}_5$
	9.42317	9.46059	15.3230	5.64134×10^{-1}	14.45586
	-7.91744	3.65331	-7.38177×10^{-1}	-7.75041×10^{-2}	5.78557×10^{-1}
$\underline{V}$ =	-5.38758	1.86465	-7.17083×10^{-1}	8.04911×10^{-1}	-1.57245×10^{-2}
	8.92297×10^{-2}	-4.60060×10^{-1}	1.44810	-5.00356×10^{-1}	3.18208
	5.56546×10^{-1}	2.49948×10^{-1}	5.92807×10^{-1}	-1.23918×10^{-1}	-1.10191

	$\underline{u}_1$	$\underline{u}_2$	$\underline{u}_3$	$\underline{u}_4$	$\underline{u}_5$
	223.802	571.788	145.631	314.782	59.615
	17.75367	200.812	-133.615	-462.142	16.6726
$\underline{U}$ =	-105.110	108.446	92.0657	491.824	22.7067
	-81.6546	-174.455	101.887	-580.121	60.9488
	-34.5174	-49.2396	110.523	-245.233	-61.2394

Table 4.11. Combination ($\hat{c}'_{1L}, \hat{c}'_{2H}, \hat{c}_3, \hat{c}_4, \hat{c}_5$) Experiment 1.1 Rotation Matrices $\underline{V}$ and $\underline{U}$.

	$\underline{v}_1$	$\underline{v}_2$	$\underline{v}_3$	$\underline{v}_4$	$\underline{v}_5$
$\underline{V}$ =	1.59748×10^{-1} -2.11383×10^{-2} -2.04340×10^{-2} -3.84456×10^{-3} -2.45776×10^{-1}	a	a	a	a
	$\underline{u}_1$	$\underline{u}_2$	$\underline{u}_3$	$\underline{u}_4$	$\underline{u}_5$
$\underline{U}$ =	b	267.438 176.667 34.493 -63.4121 -2.29941	a	a	a

[a]These columns are the same as in Table 4.10.

[b]$\underline{u}_1$ (Table 4.11) = 1.40114 $\underline{u}_1$ (Table 4.10).

$\underline{c}_3$, $\underline{c}_4$, $\underline{c}_5$). Note that columns 2 through 5 of $\underline{V}$ are the same in Tables 4.10 and 4.11 since the concentration profiles assumed for Absorbers 2 through 5 are the same for the two combinations. Note also that columns 3 through 5 of $\underline{U}$ are the same in Tables 4.10 and 4.11 since both combinations of concentration profiles give the same static spectra for Absorbers 3, 4, and 5. Changing the concentration profile of Absorber 1 from $\underline{c}'_{1L}$ in Table 4.10 to $\underline{c}'_{1H}$ in Table 4.11 changes the shape of the static spectrum of Absorber 2 ($\underline{u}_2$ is different), but changes $\underline{u}_1$ by only a constant multiple factor; i.e., the shape of the static spectrum for Absorber 1 is the same for both combinations.

Note in Figure 4.40 that Absorber 4 has, in addition to the 440 nm absorbance maximum of NDMA, a shoulder with a maximum near 340 nm. Thus, as discussed in Section H, Absorber 4 represents NDMA and $NADH_{340\ nm}$ in Experiment 1.1. Absorber 3 has a maximum absorbance at 403 nm and a shoulder with a maximum near 320 nm. Absorber 5 has two absorbance maxima, one at 320 nm, and another broad band centered near 550 nm.

Figure 4.41 shows the concentration profiles for the combinations ($\underline{c}'_{1L}$, $\underline{c}'_{2L}$, $\underline{c}_3$, $\underline{c}_4$, $\underline{c}_5$) and ($\underline{c}'_{1H}$, $\underline{c}'_{2L}$, $\underline{c}_3$, $\underline{c}_4$, $\underline{c}_5$). (Note that the time scale is linear with time.) Figure 4.42 shows the early time portion of these concentration profiles. Note that Absorber 4 (NDMA) rapidly decays to zero concentration and that during the same time Absorber 3 undergoes an initial burst to its maximum

Figure 4.40. Static spectra of Absorbers 1-5 in Experiment 1.1, $E_{7.39}N_{15.0}S_{13.4}$, (N) with (E+S), scaled to maximum absorbance in the experiment.

A. Absorbers 1 and 2 from $\hat{\underline{c}}'_{1L}$, $\hat{\underline{c}}'_{2L}$.

B. Absorbers 1 and 2 from $\hat{\underline{c}}'_{1H}$, $\hat{\underline{c}}'_{2L}$.

C. Absorbers 3, 4, and 5.

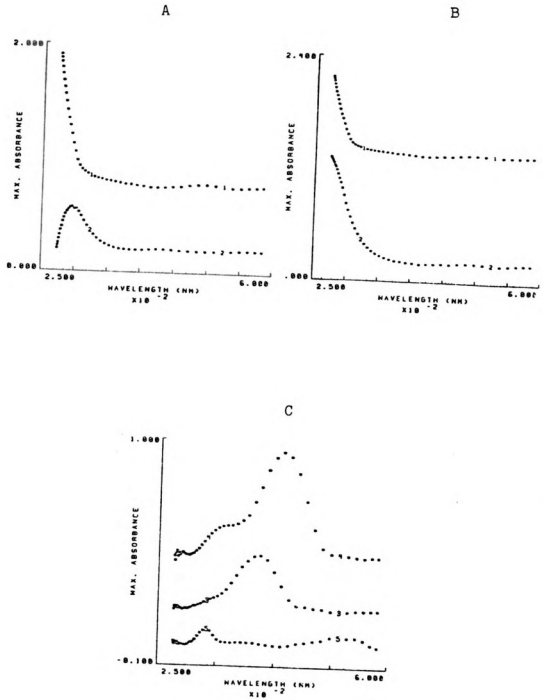

Figure 4.40.

Figure 4.41. Concentration profiles of Absorbers 1-5 in Experiment 1.1, $E_{7.39}N_{15.0}S_{13.4}$, (N) with (E+S), full time course.
A. Absorbers 1 and 2, $\underline{\hat{c}}'_{1L}$, $\underline{\hat{c}}'_{2L}$.
B. Absorbers 1 and 2, $\underline{\hat{c}}'_{1H}$, $\underline{\hat{c}}'_{2L}$.
C. Absorbers 3, 4, and 5.

A

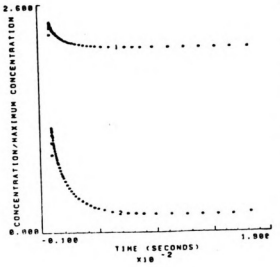

B

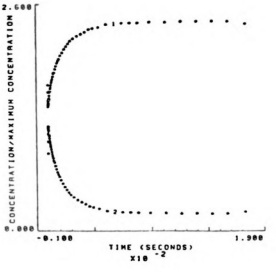

C

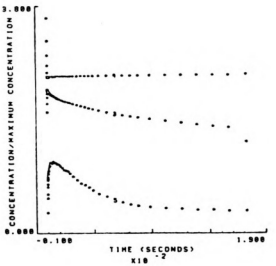

Figure 4.41.

Figure 4.42. Concentration profiles of Absorbers 1-5 in Experiment 1.1, $E_{7.39}N_{15.0}S_{13.4}$, (N) with (E+S), early time course.

A. Absorbers 1 and 2, $\underline{\hat{c}}'_{1L}$, $\underline{\hat{c}}'_{2L}$.

B. Absorbers 1 and 2, $\underline{\hat{c}}'_{1H}$, $\underline{\hat{c}}'_{2L}$.

C. Absorbers 3, 4, and 5.

A

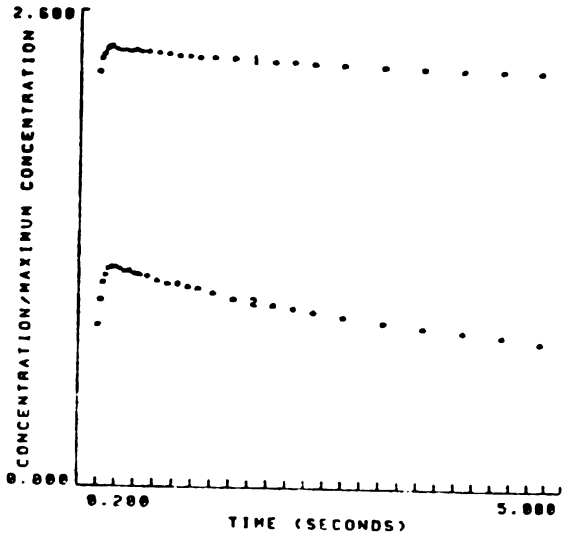

B

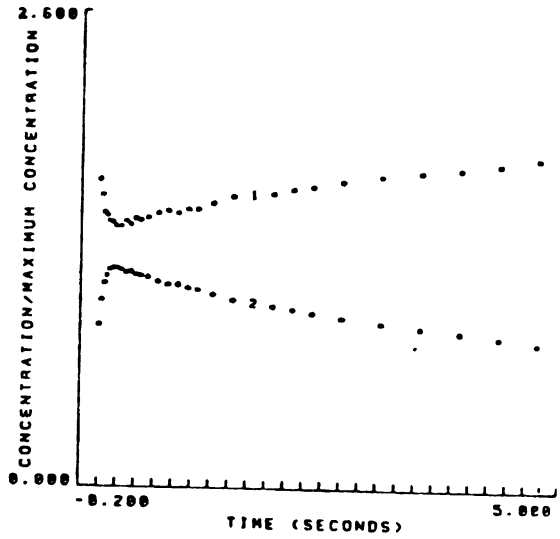

C

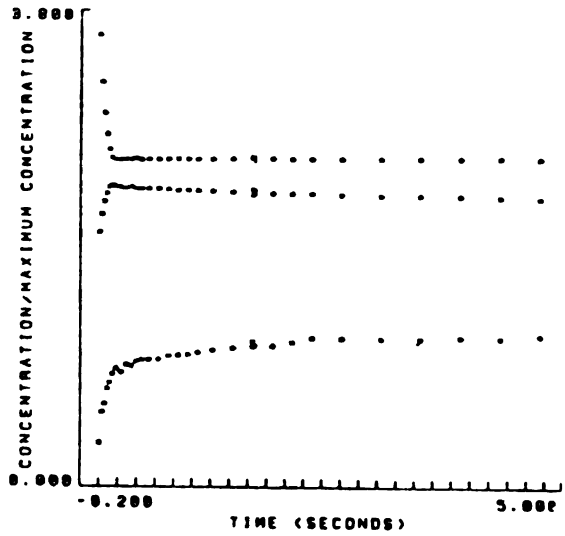

Figure 4.42.

concentration, from which it slowly decays to zero concentration. Absorber 5 is an intermediate with a fast growth corresponding to the rapid decay of NDMA, followed by a slower growth to its maximum concentration, from which it decays to zero concentration.

Thus, despite incomplete information about Absorbers 1 and 2, we have obtained the static spectra and concentration profiles of Absorbers 3, 4, and 5 across the entire spectral range of Experiment 1.1. Since Experiments 2.1, 3.1, and 4.1 are likely to have some absorbers in common with Experiment 1.1, we now resolve these Experiments using the static spectral information from Experiment 1.1.

N. Resolution of Experiments 2.1, 3.1, and 4.1

In this section we use the static spectra obtained for Absorbers 1 through 5 in Experiment 1.1 (Figure 4.40) to resolve Experiments 2.1, 3.1, and 4.1. Each static spectrum from Experiment 1.1 that fits the M analysis eigenvectors of one of these experiments may be counted as belonging to an absorber in that experiment.

Experiment 2.1. Figure 4.43 shows the M analysis fits of the static spectra of Absorbers 3, 4, and 5 obtained from the analysis of Experiment 1.1. The two combinations of static spectra for Absorbers 1 and 2 from

Figure 4.43. M analysis fits of Absorbers 3, 4, and 5 to Experiment 2.1, $E_{7.39}N_{15.0}S_{13.4}$, (N+S) with (E). Vertical scales in arbitrary absorbance units.

A. Absorber 3.

B. Absorber 4.

C. Absorber 5.

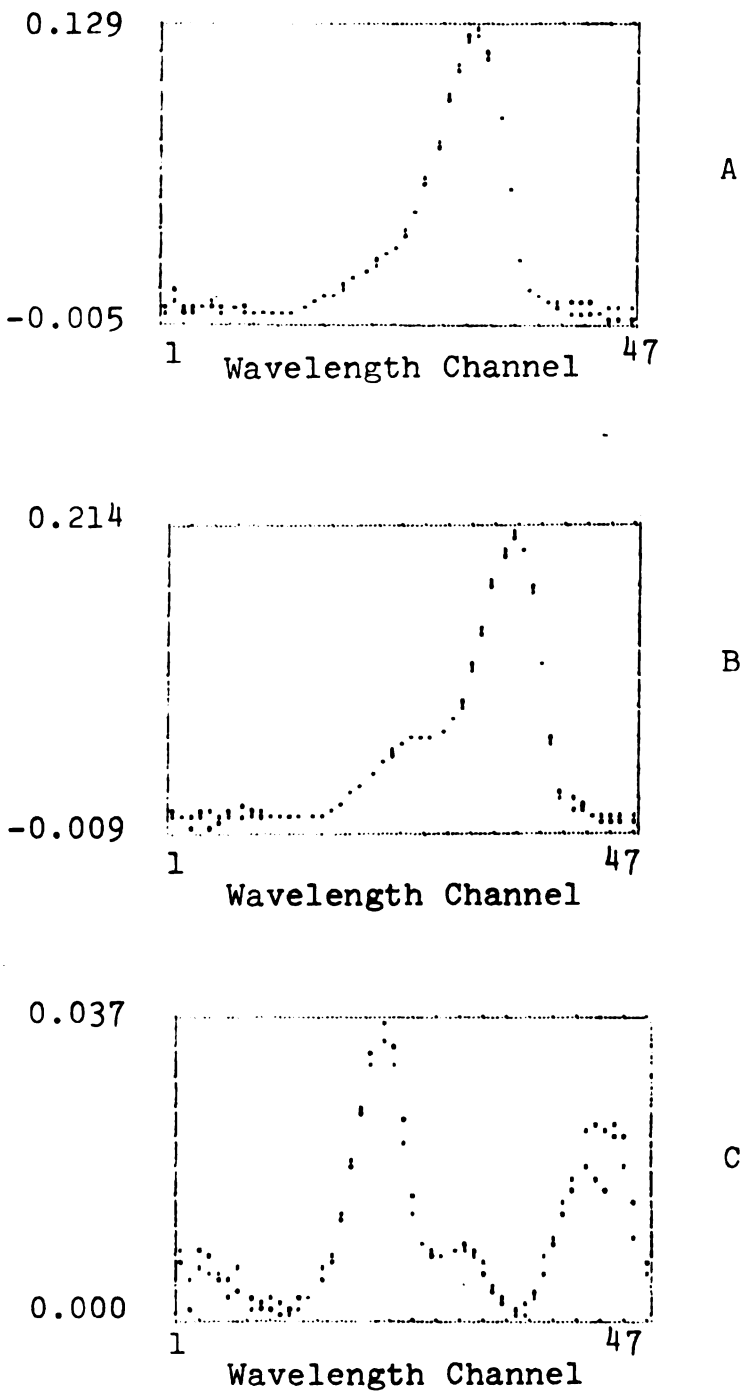
0.129
-0.005
1
47
Wavelength Channel
A
0.214
-0.009
1
47
Wavelength Channel
B
0.037
0.000
1
47
Wavelength Channel
C

Figure 4.43.

Experiment 1.1 were also fit to Experiment 2.1. We thus have for Experiment 2.1 two estimates of the rotation matrix $\underline{U}$, corresponding to the two combinations of static spectra for absorbers 1 and 2, with column 3, 4, and 5 in both matrices the same. Both estimates of $\underline{U}$ give the same concentration profiles for Absorbers 3, 4, and 5 when Equation (3.13) is solved for $\underline{V}$. Thus, the static spectra and concentration profiles for Absorbers 3, 4, and 5 are again insensitive to Absorbers 1 and 2.

Figure 4.44 shows the concentration profiles of Absorbers 3, 4, and 5 in Experiment 2.1. Note that the concentration profiles for these absorbers are nearly identical in Experiments 1.1 and 2.1. Recall that Experiments 1.1 and 2.1 have the same initial concentrations, but different premixing orders of substrates and enzyme (Table 4.1). Thus we conclude that in these experiments LADH and NDMA do not reach without NADH in a way that measurably alters the course of the reaction after NADH is added.

Experiment 3.1. Figure 4.45 shows the M analysis fits of the static spectra of Absorbers 3, 4, and 5, obtained from the analysis of Experiment 1.1. The concentration profiles obtained for Absorbers 3, 4, and 5 are shown in Figure 4.46. The decay of Absorber 4 (NDMA + $NADH_{340\ nm}$) occurs more rapidly in Experiment 3.1 than in Experiments 1.1 and 2.1, which have lower initial concentration of LADH than Experiment 3.1. Otherwise, the concentration

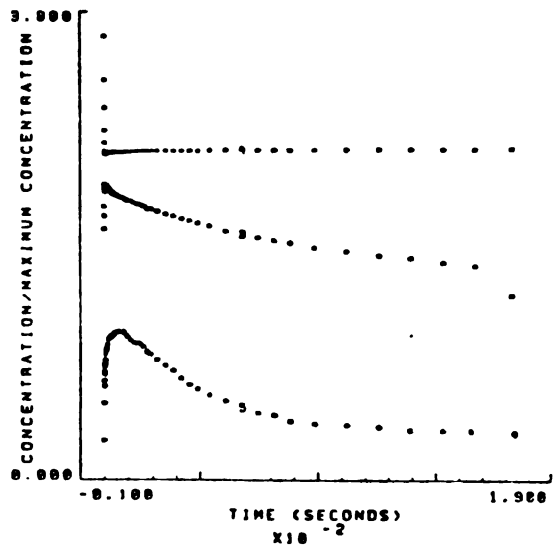

A

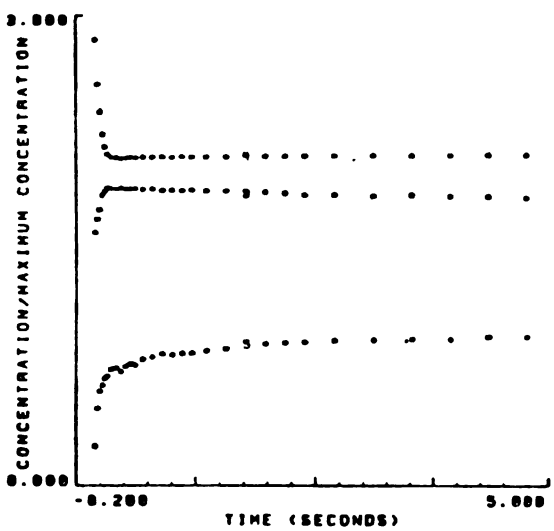

B

Figure 4.44. Concentration profiles of Absorbers 3, 4, and 5 in Experiment 2.1, $E_{7.39}N_{15.0}S_{13.4}$, (N+S) with (E). A. Full time course. B. Early time course.

Figure 4.45. M analysis fits of Absorbers 3, 4, and 5 to Experiment 3.1, $E_{18.6}N_{15.0}S_{13.4}$, (N+S) with (E). Vertical scales in arbitrary absorbance units.

A. Absorber 3.

B. Absorber 4.

C. Absorber 5.

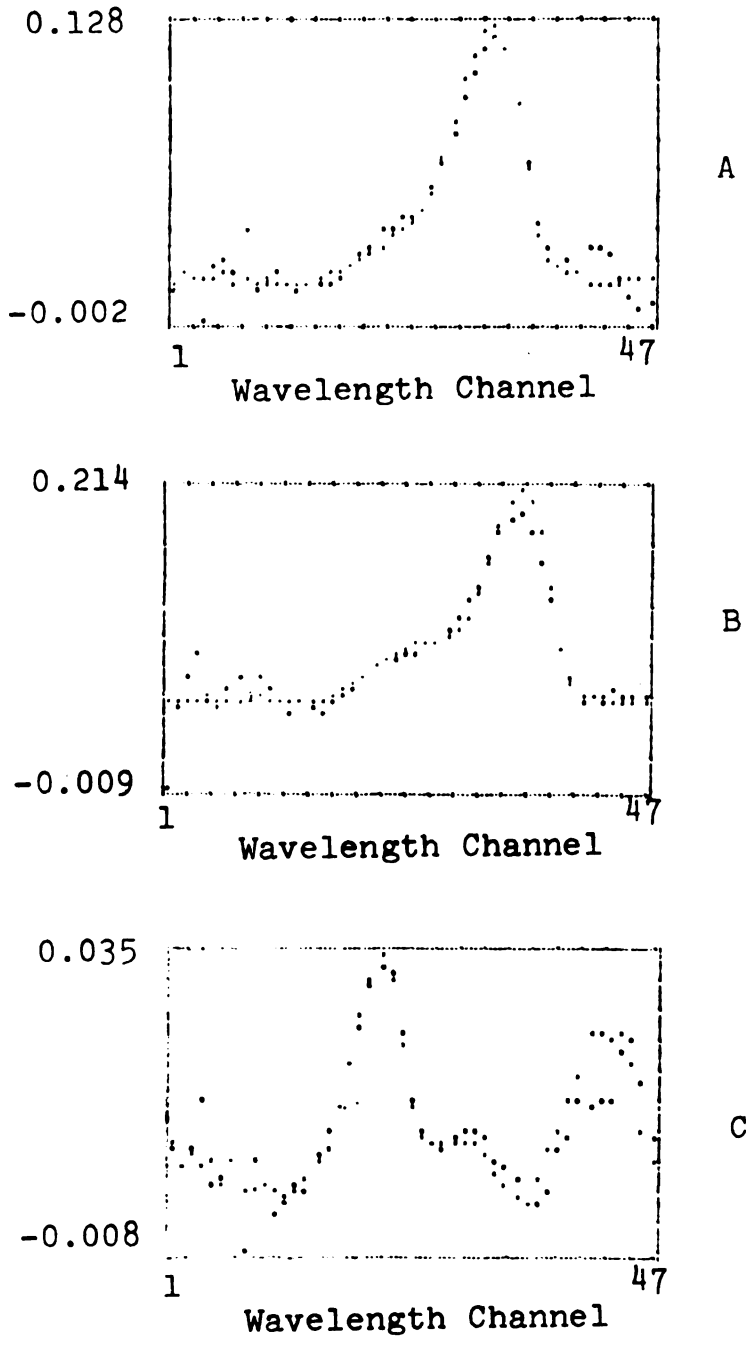
0.128
-0.002
1
47
Wavelength Channel
A
0.214
-0.009
1
47
Wavelength Channel
B
0.035
-0.008
1
47
Wavelength Channel
C

Figure 4.45.

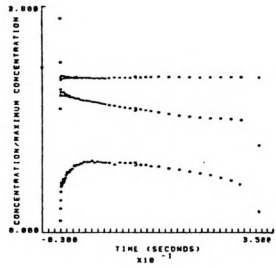

A

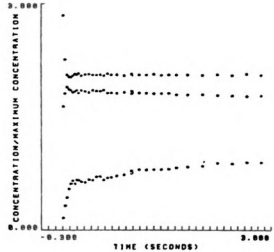

B

Figure 4.46. Concentration profiles of Absorbers 3, 4, and 5 in Experiment 3.1, $E_{18.6}N_{15.0}S_{13.4}$, (N+S) with (E). A. Full time course. B. Early time course.

profiles are qualitatively similar in these three experiments.

Experiment 4.1. In this case there are six linearly independent absorbers. We assume that Absorbers, 1, 2, 3, and 5 are the same as in Experiments 1.1, 2.1, and 3.1. Figure 4.47 shows the M analysis fits of Absorbers 3 and 5 to Experiment 4.1. For Absorber 4, we use the measured static spectrum of NDMA, which fit the M analysis eigenvectors for Experiment 4.1 without giving a shoulder at 340 nm (Figure 4.21). For Absorber 6, we use the 340 nm absorbance band of NADH, which fit as one of the six linearly independent absorbers (Figure 4.28).

Figure 4.48 shows the concentration profiles for Absorbers 3, 4, 5, and 6 in Experiment 4.1. The NDMA concentration profile is a biphasic decay. $NADH_{340\ nm}$ exhibits a rapid decay to zero concentration that corresponds to the rapid portion of the biphasic NDMA decay Moreover, the concentration profile of $NADH_{340\ nm}$ is qualitatively similar to the concentration profiles of (NDMA + $NADH_{340\ nm}$) in Experiments 1.1, 2.1, and 3.1. Experiment 4.1 is the only experiment that has a higher initial concentration of NDMA than of NADH. The presence of excess NDMA apparently decouples the concentration profiles of NDMA and $NADH_{340\ nm}$ in Experiment 4.1. The concentration of Absorber 3 grows biphasically with both parts correlated to the fast and slow portions of the

Figure 4.47. M analysis fits of Absorbers 3 and 5 to Experiment 4.1. Vertical scales in arbitrary absorbance units.

A. Absorber 3.

B. Absorber 5.

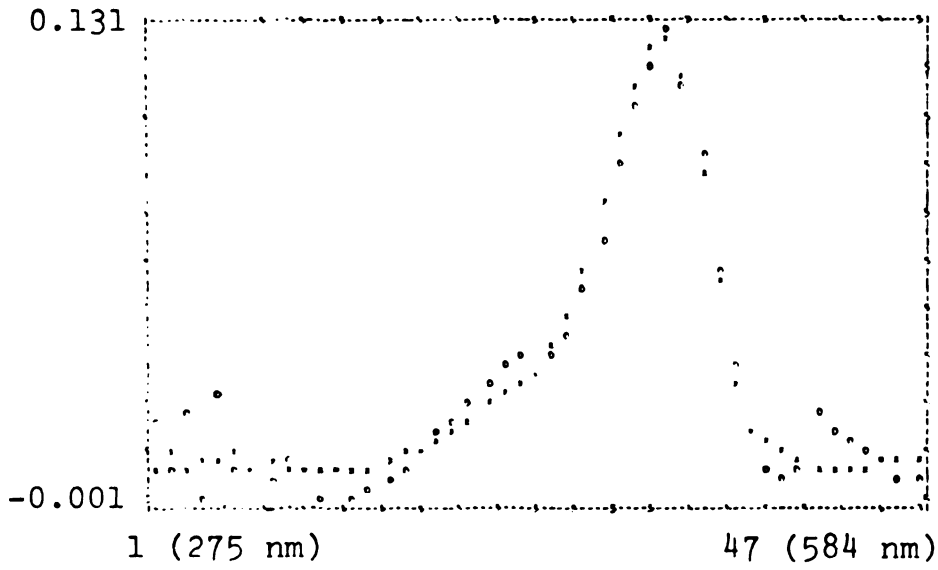
0.131
-0.001
1 (275 nm)
47 (584 nm)
Wavelength Channel
A

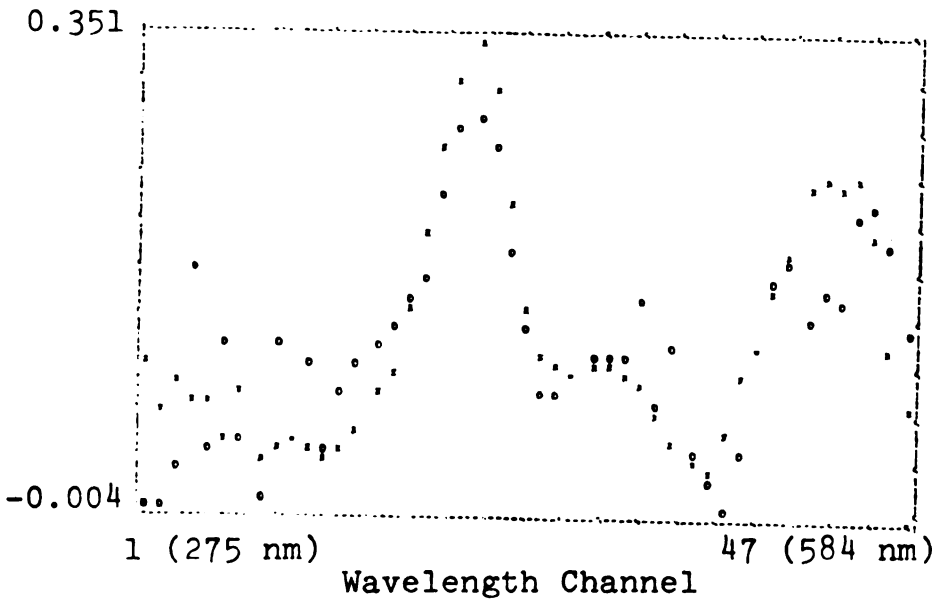
0.351
-0.004
1 (275 nm)
47 (584 nm)
Wavelength Channel
B

Figure 4.47.

Figure 4.48. Concentration profiles of Absorbers 3, 4, 5 and 6 in Experiment 4.1, $E_{7.39}N_{6.0}S_{13.4}$. A. Full time course. B. Early time course

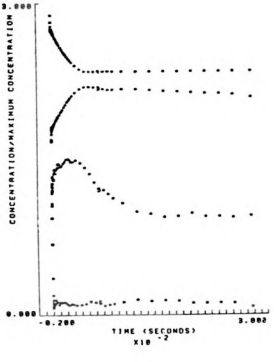

A

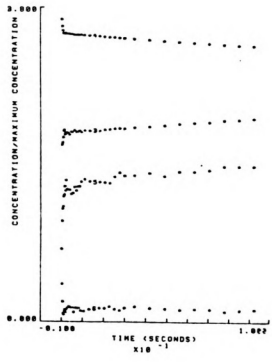

B

Figure 4.48.

NDMA biphasic decay. The concentration of Absorber 3 then very slowly decreases after reaching its maximum concentration. As in Experiments 1.1, 2.1, and 3.1, Absorber 5 has a biphasic growth followed by a slow decay in Experiment 4.1.

Table 4.12 summarizes the absorbance changes of Absorbers 3, 4, 5, and (Experiment 4.1) 6 in Experiments 1.1, 2.1, 3.1, and 4.1 at their wavelengths of maximum absorbance.

0. Scanning Experiments from 250 nm to 300 nm

Principal component analysis of Experiments 1.1 - 4.1 gives incomplete information about absorbers in the wavelength range 275 nm - 300 nm. The static spectrum of LADH and the 260 nm absorbance band of NADH-NAD^+ does not fit as belonging to absorbers in these experiments even though the initial concentrations of LADH and NADH were sufficiently large to contribute to absorbances measured in the 275 nm - 300 nm range. Principal component analysis reveals that Experiments 1.1 - 4.1 have two absorbers, Absorbers 1 and 2, in the range 275 nm - 300 nm (Subspace I). According to the solution bands for their normalized static spectra (Figure 4.32), the absorbance maxima of Absorbers 1 and 2 may occur below 275 nm, which is out of the range of the scan. Moreover, the 275 nm - 300 nm range includes only the high wavelength wings of the LADH

Table 4.12. Summary of Absorbers 3-6 in Experiments 1.1 - 4.1.

Experiment	Abbreviation	Absorber	Peak Wavelength Channel	λ_{max}/nm	A_{max}/OD	$\Delta A(\lambda_{max})$/OD
1.1	$E_{7.4}N_{15.0}S_{13.4}$ (N) vs (E+S)	3	32	403±5	0.261	0.229
		4	35	436±5	0.508	0.506
		5	21	324±3	0.079	0.068
2.1	$E_{7.4}N_{15.0}S_{13.4}$ (N+S) no (E)	3	32	403±5	0.233	0.211
		4	35	436±6	0.448	0.429
		5	21	324±3	0.077	0.063
3.1	$E_{18.6}N_{15.0}S_{13.4}$	3	32	403±5	0.196	0.186
		4	35	436±6	0.167	0.167
		5	21	324±3	0.070	0.070

Table 4.12. Continued

Experiment	Abbreviation	Absorber	Peak Wavelength Channel	λ_{max}/nm	A_{max}/OD	$\Delta A(\lambda_{max})$/OD
4.1	$E_{7.4}N_{6.0}S_{13.4}$	3	32	403±5	0.233	0.212
		4	35	436±6	0.776	0.735
		5	21	324±3	0.028	0.027
		6	24	340±3	0.036	0.036

and 260 nm NADH-NAD^+ absorbance spectra.

In order to characterize Absorbers 1 and 2 in Experiments 1.1 - 4.1 and to determine the spectral contributions of LADH and the 260 nm band of NADH-NAD^+, we performed a scanning experiment with a scan range of 250 nm - 300 nm. This range includes the low as well as the high wavelength wings of the LADH and 260 nm NADH-NAD^+ absorbance spectra. The initial concentrations were $E_{18.0}N_{15.0}S_{13.4}$, and the mixing order was (N+S) vs (E), these were also the initial conditions of Experiment 2.1. The absolute absorbance surface for Experiment 5.1 is shown in Figure 4.49. It contains 28 wavelength channels and 64 consecutive spectra. Weighted M and S analyses of the whole experiment five an (m,s) pair of (3,2). Thus, Experiment 5.1 has three linearly independent absorbers, of which at least two change concentration.

Figures 4.50 and 4.51 show the M analysis fits of the measured static spectra of, respectively, LADH and NADH (which represents the 260 nm band of NADH-NAD^+). The LADH static spectrum fits well except near the absorbance maximum, which is shifted to a lower wavelength in the calculated spectrum than occurs in the measured spectrum. A possible interpretation is that LADH is an absorber whose absorbance spectrum during the reaction is shifted to lower wavelengths (blue-shifted) by its interaction with the substrates and products. The measured static spectrum of NADH fits well, except for some

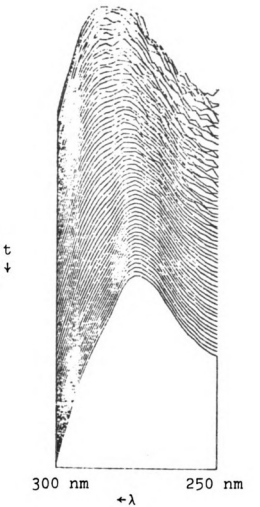

Figure 4.49. Experimental absolute absorbance surface A, Experiment 5.1, $E_{18.6}N_{15.0}S_{13.4}$, (N+S) with (E), wavelength range 250 nm - 300 nm, Rear view.

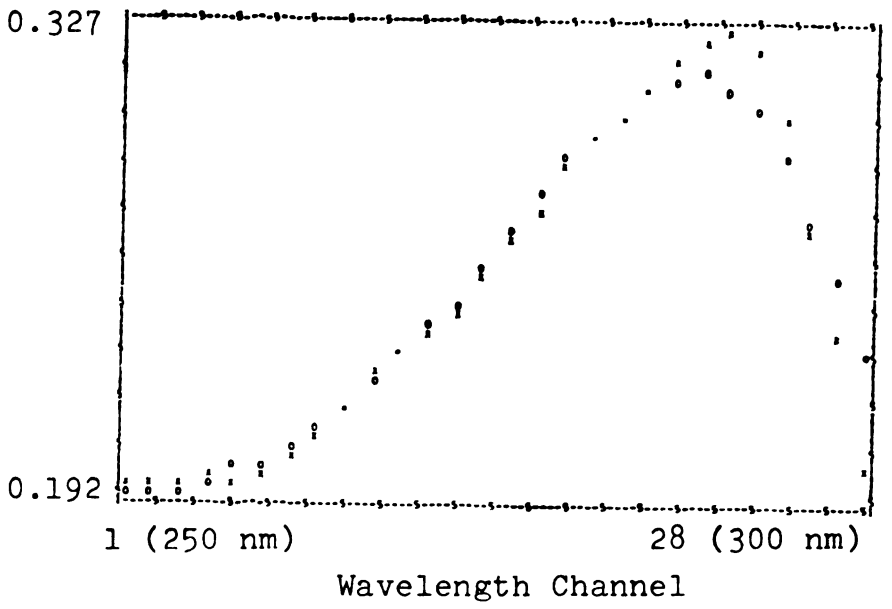

Figure 4.50. M analysis fit of the measured LADH static spectrum to Experiment 5.1. X = measured, O = calculated. Vertical scale in arbitrary absorbance units.

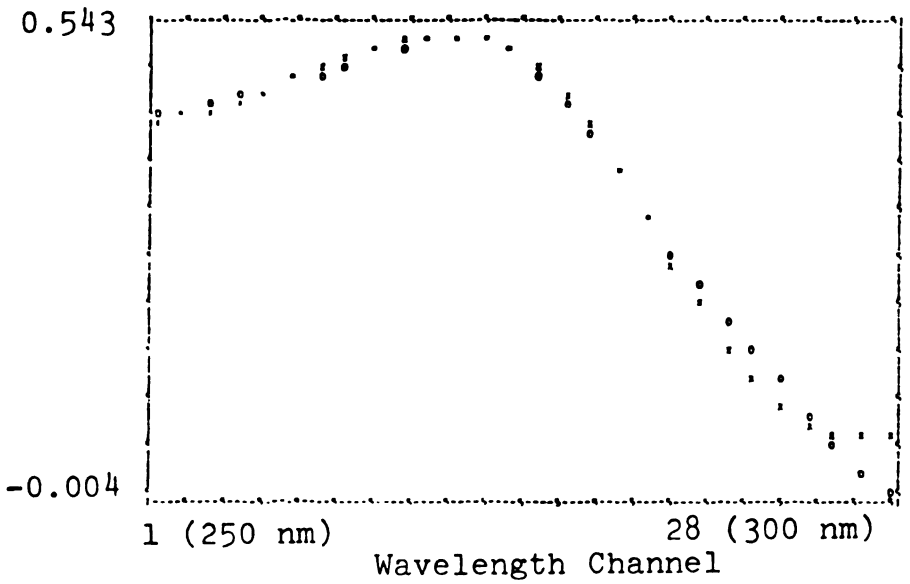

Figure 4.51. M analysis fit of the NADH-NAD^+ 260 nm absorbance band to Experiment 5.1. X = measured. O = calculated. Vertical scale in arbitrary absorbance units.

small systematic error in the high wavelength wing near 300 nm. We conclude that the 260 nm absorbance band of NADH-NAD^+ is one of the three linearly independent absorbers in Experiment 5.1.

The third absorber in Experiment 1.1 must be either a transient intermediate or a product for which we have no measured static spectrum. To resolve the whole experiment, we examine two wavelength subspaces; I (250 nm - 273 nm, channels 1-16), and II (275 nm - 300 nm, channels 17-28). The (m,s) pairs for Subspaces I and II are (3,2), and (2,1) respectively. Since LADH and NADH absorb across the entire spectral range 250 nm - 300 nm, we conclude that the third absorber absorbs only in Subspace I, and that only LADH and NADH-NAD^+ absorb in Subspace II. Moreover, since Subspace II in Experiment 5.1 covers the same wavelength range as Subspace I of Experiments 1.1 - 4.1, we conclude that Absorbers 1 and 2 in the latter experiments are blue-shifted LADH and the 260 nm NADH-NAD^+ band. The measured static spectrum of LADH does not fit Experiments 1.1 - 4.1 because LADH is blue-shifted in the reaction. The range 275 nm - 584 nm range of Experiments 1.1 - 4.1 includes only the tail of the 260 nm band of NADH-NAD^+, which is apparently why these experiments did not contain sufficient information to distinguish NADH-NAD^+ as an absorber.

We resolve Subspace II of Experiment 5.1 by using the static spectra of LADH and NADH-NAD^+. By fitting to

Subspace II the static spectra of LADH and NADH-NAD^+ that were obtained for the whole experiment, we obtain the (2x2) matrix $\underline{U}$ for Subspace II. From $\underline{U}$ we obtain $\underline{V}$ using Equation (3.13). The resultant concentration profiles of LADH and NADH-NAD^+ calculated from Subspace II are shown in Figures 4.52A and 4.52B. Note that the rates of LADH and NADH-NAD^+ are linearly dependent (s=1 in Subspace II); i.e., as the 260 nm bnad of NADH-NAD^+ grows, LADH decays.

We use the three absorber simplifications of Chapter 3, Section E to obtain the contribution of the third absorber in Experiment 5.1. Let Absorbers 1, 2, and 3 in Experiment 5.1 be, respectively, LADH, NADH-NAD^+, and the as yet unknown absorber. We first fit the concentration profiles of LADH and NADH-NAD^+ that we obtained from Subspace II to the M analysis eigenvectors for the whole experiment. This gives the two columns of $\underline{V}$ in the whole experiment that correspond to LADH and NADH-NAD^+; i.e., $\underline{v}_1$ and $\underline{v}_2$. Equation (3.27) then gives for $\underline{u}_3$

$$\underline{u}_3 = [1/\det(\underline{V})]\underline{\Omega}_{(3)}(\underline{v}_1 x \underline{v}_2),$$

where $\underline{\Omega}_{(3)}$, $\underline{v}_1$, and $\underline{v}_2$ are known, and where $1/\det(\underline{V})$ is arbitrarily set to unity. The static spectrum of Absorber 3 is then given by the equation

$$\hat{\underline{f}}_3 = (\underline{L}^{-1}\underline{\Phi}_{(3)})\underline{u}_3,$$

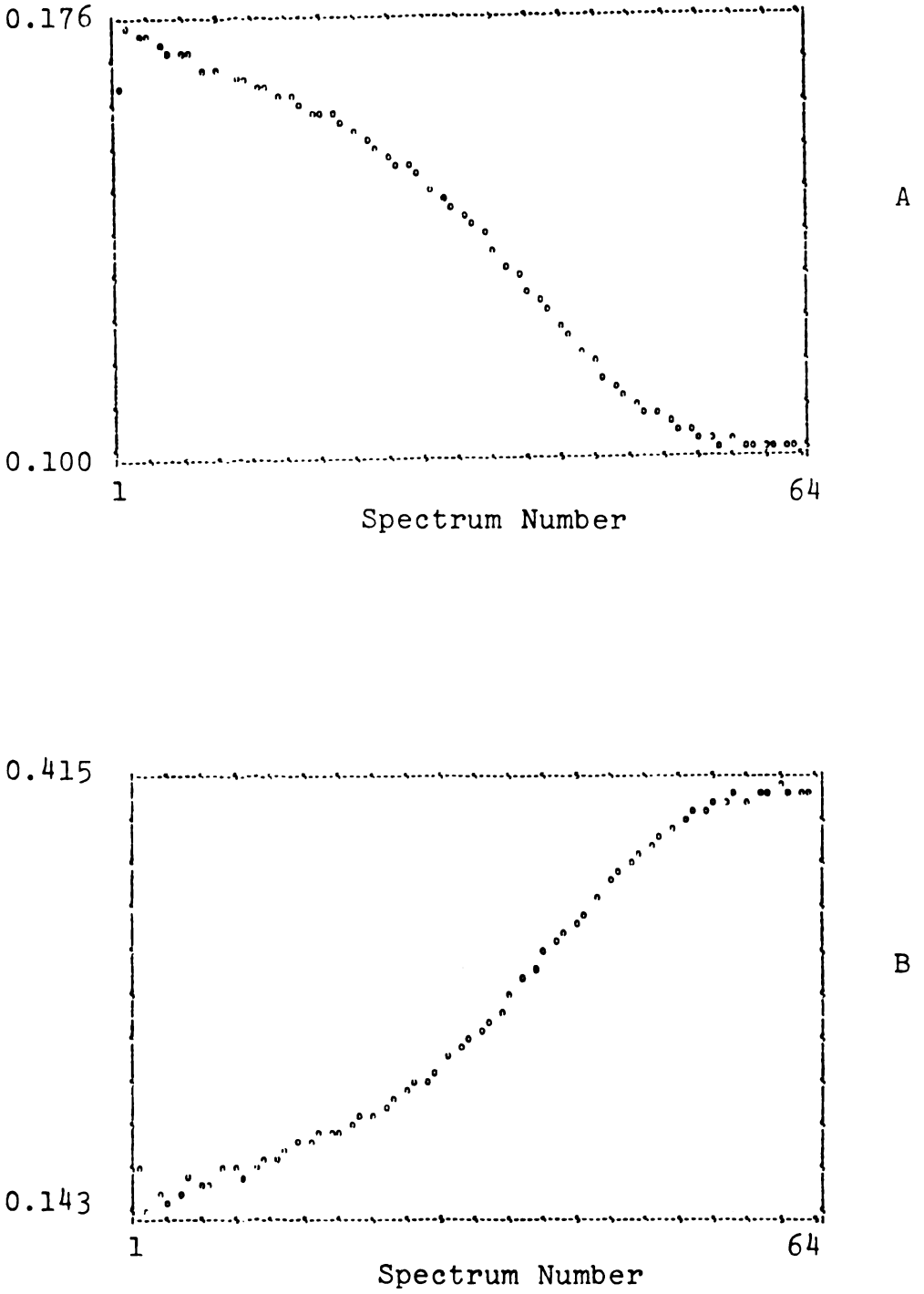

Figure 4.52. Concentration profiles from wavelength channels 17-28 of Experiment 5.1. A. "LADH". B. 260 nm band of NADH-NAD^+. Vertical scales in arbitrary absorbance units.

and is shown in Figure 4.53A.

We obtained the first two columns of $\underline{U}$ for the whole experiment when the measured static spectra of LADH and NADH-NAD^+ were fitted to the M analysis eigenvectors for the whole experiment. With the third column $\underline{u}_3$ obtained above for Absorber 3, $\underline{U}$ for the whole experiment is complete. Therefore, the concentration profiles of all three absorbers are obtained by calculating $\underline{V}$ from $\underline{U}$ using Equation (3.13). The resultant concentration profiles of Absorbers 1 and 2 (LADH and NADH-NAD^+) are the same as already shown in Figures 4.52A and 4.52B. The concentration profile of Absorber 3 is shown in Figure 4.53B The third absorber has its maximum absorbance near channel 1 (250 nm), and its concentration decays after remaining nearly constant for the first 30 consecutive spectra (3 sec).

In summary, Experiment 5.1 has three linearly independent absorbers. The static spectra and concentrations of blue-shifted LADH are shown in Figures 4.50 and 4.52A, respectively. The results for the 260 nm band of NADH-NAD^+ are shown in Figures 4.51 and 4.52B and the results for the third, unidentified absorbers are shown in Figures 4.53A and 4.53B. Table 4.13 summarizes the absorbance changes of Absorbers 1, 2, and 3 in Experiment 5.1.

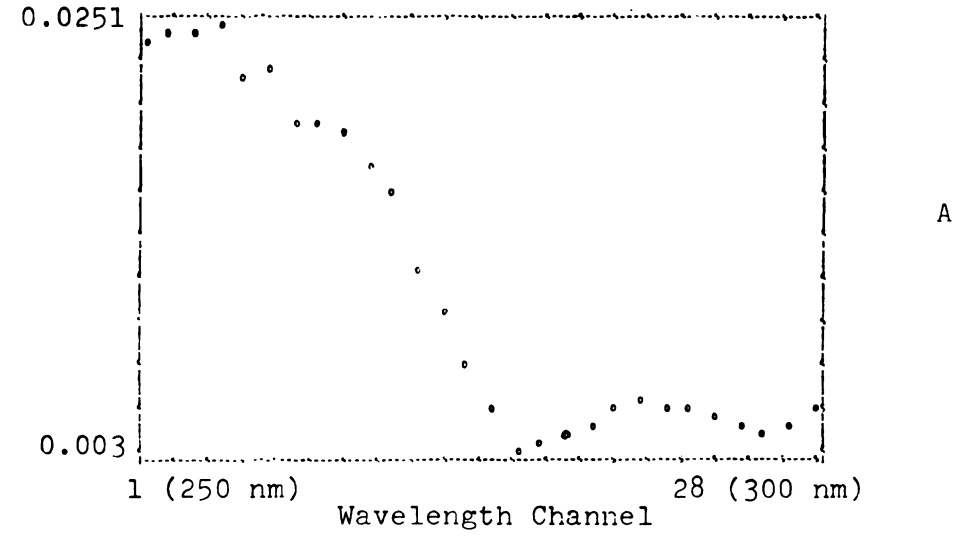

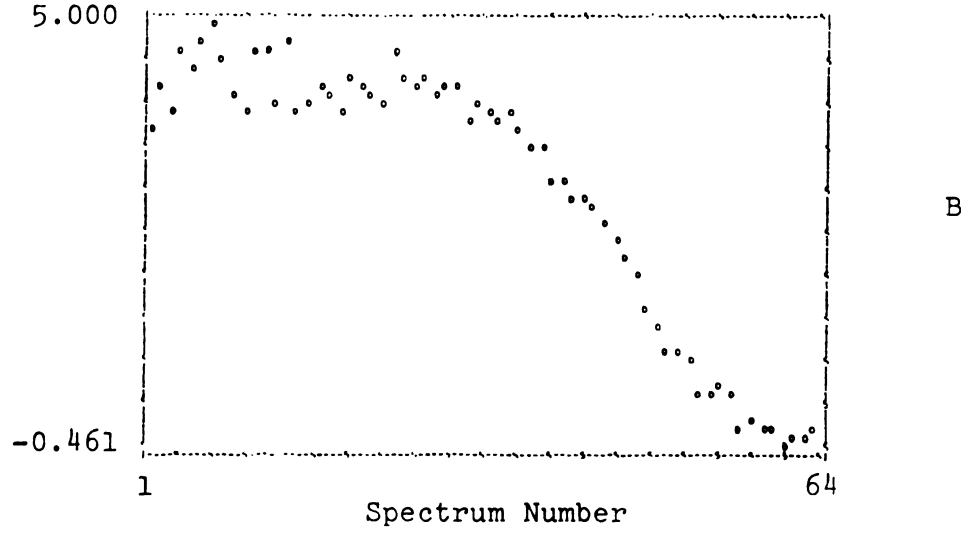

Figure 4.53. Third absorber in Experiment 5.1. A. Static spectrum. Arbitrary absorbance units. B. Concentration profile. Arbitrary concentration units.

Table 4.13. **Absorbers in Experiment 5.1 (250 nm - 300 nm).** $E_{18.6}N_{15.0}S_{13.4}$, (N+S) **vs** (E).

	Absorber	Peak Wavelength Channel	λ_{max}/nm	A_{max}/O.D.	$\Delta A(\lambda_{max})$/O.D.
1	(Shifted LADH)	22	275	1.579	0.678
2	260 nm NADH-NAD^+	13	260	0.933	0.607
3	Unidentified	1-4	250-255	0.126	0.121

P. Discussion

1. Summary of Results

Independently of any mechanistic hypotheses and of any assumptions about spectral shapes, weighted principal component analysis reveals that in the range 275 nm - 584 nm Experiments 1.3 - 3.1 have five linearly independent absorbers, of which four have linearly independent rates, while Experiment 4.1 in the same wavelength range has six linearly independent absorbers, of which five have linearly independent rates. Application of the seven-step strategy of Chapter 3 gives solution bands for the normalized static spectra and concentration profiles of Absorbers 1 and 2 in Experiment 1.1 (Figures 4.32 and 4.33), and gives the static spectra and concentration profiles of Absorbers 3, 4, and 5 in Experiments 1,1, 2.1, and 3.1 (Figures 4.40-4.44, and 4.46) and of Absorbers 3, 4, 5, and 6 in Experiment 4.1 (Figures 4.22, 4.28, 4.47, and 4.48). In this subsection we summarize the spectral and kinetic characteristics of these absorbers, and we suggest chemical identities for some of them.

In Experiments 1.1, 2.1, and 3.1, where the initial concentrations of NDMA (13.4 μM) and NADH (15.0 μM) are almost equal, the 440 nm band of NDMA and the 340 nm band of NADH are lumped together as one absorber, Absorber 4. This is because the concentrations of $NDMA_{440\ nm}$ and

$NADH_{340\ nm}$ are linearly dependent on each other in Experiments 1.1, 2.1, and 3.1. $NDMA_{440\ nm}$ and $NADH_{340\ nm}$ rapidly decay together to near zero concentration in these experiments.

In contrast, $NDMA_{440\ nm}$ and $NADH_{340\ nm}$ make separate contributions to Experiment 4.1 as Absorber 4 and Absorber 6, respectively. In Experiment 4.1, where the initial concentration of NDMA (13.4 μM) is greater than the initial concentration of NADH (6.0 μM), $NADH_{340\ nm}$ still decays rapidly to zero as it did in Experiments 1.1 - 3.1, but $NDMA_{440\ nm}$ decays biphasically. The total decay of $NADH_{340\ nm}$ is complete by the end of the rapid first portion of the biphasic $NDMA_{440\ nm}$ decay. This suggests that the rapid portion of the $NDMA_{440\ nm}$ decay and the entire rapid decay of $NADH_{340\ nm}$ in Experiment 4.1 correspond to the same fast process as the concomitant decays of $NDMA_{440\ nm}$ and $NADH_{340\ nm}$ in Experiments 1.1 - 3.1. The slow portion of the biphasic $NDMA_{440\ nm}$ decay in Experiment 4.1 is then a step that occurs after $NADH_{340\ nm}$ has decayed to zero concentration.

Absorber 3 has the same static spectrum in Experiments 1.1 - 4.1. It is the combination of a band with a peak at 403 nm and a shoulder near 320 nm. Note that the 403 nm band of Absorber 3 has a shape similar to the 440 nm band of NDMA (Figure 4.40). Note also that in Experiments 1.1 - 4.1 the growth portion of the growth and decay of Absorber 3 mirrors the decay of $NDMA_{440\ nm}$. These

observations suggest that Absorber 3 may be an intermediate form of NDMA that is formed upon the disappearance of $NDMA_{440\ nm}$. There is a striking difference between the behavior of Absorber 3 in Experiments 1.1 - 3.1 and in Experiment 4.1. In Experiments 1.1 - 3.1, Absorber 3 grows rapidly as $NDMA_{440\ nm}$ and $NADH_{340\ nm}$ decay to zero, and then Absorber 3 slowly decays to zero. In Experiment 4.1, Absorber 3 grows rapidly during the fast $NADH_{340\ nm}$ decay and the rapid portion of the biphasic $NDMA_{440\ nm}$ decay, but then, instead of slowly decaying as in Experiments 1.1 - 3.1, Absorber 3 continues a slow growth corresponding to the slow portion of the $NDMA_{440\ nm}$ decay.

Absorber 5, which has the same static spectrum in Experiments 1.1 - 4.1, is a combination of a 320 nm band and a 550 nm band. Absorber 5 accounts for most of the absorbance changes at 540 nm, and can thus be identified as the intermediate hypothesized by Schack and Dunn (1972) and Suelter, et al. (1975) to account for the growth and decay of absorbance at 540 nm. Principal component analysis gives the new information that the 540 nm intermediate also has a band at 320 nm. In Experiments 1.1 - 3.1, Absorber 5 is still growing when Absorber 3 has begun to decay. The growth of Absorber 5 is biphasic in Experiments 1.1 - 4.1.

Principal component analysis of Experiment 5.1, in the range 250 nm - 300 nm, suggests that Absorbers 1 and 2 in Experiments 1.1 - 4.1 are, respectively, the 260 nm

band of NAD^+-NADH and the static spectrum of LADH, blue-shifted from 280 nm to 275 nm. The rates of Absorbers 1 and 2 are linearly dependent in all the scanning experiments; i.e., as the 260 nm band of NAD^+-NADH grows, (as NADH is oxidized to NAD^+) the shifted LADH spectrum decays. The total absorbance change of Absorber 2 at 275 nm is 0.678 O.D. in Experiment 5.1. Fisher, Adija and Cross (1969) report small peaks (0.01 O.D.) at 275 nm - 295 nm in difference spectra measured for the binding of NADH to LADH. They attribute these changes to blue or red shifts of tyrosyl and tryptophanyl residues in LADH. The large absorbance change (0.670 O.D.) that we observe for Absorber 2 in Experiment 5.1 would seem to require a direct interaction such as a charge transfer complex formation between the enzyme chromophores and substrate or products, if we attribute all of the absorbance of Absorber 2 to enzyme chromophores.

There is an alternative explanation for Absorber 2. Absorber 2 may represent the chromophores on LADH plus a chromophore of a substrate or product intermediate whose spectral shape is coincidentally so similar to the spectral shape of the LADH chromophores that the LADH chromophores and the intermediate chromophore are lumped as one linearly independent absorber in the experiment. Since we cannot refute this possibility on the basis of the experiments reported here, further experiments are needed to determine the chemical identity of Absorber 2.

Principal component analysis of Experiment 5.1 also reveals an absorber with an absorbance maximum between 250 nm and 255 nm (Figures 4.54 and 4.55). Dunn and Bernhard (1971) proposed that the product P of Reaction II [see Section A] has an absorbance peak at 255 nm. However, the 255 nm absorber in Experiment 5.1 decays rather than grows, so that if it is the product proposed by Dunn and Bernhard (1971), it is only an intermediate product. Further scanning experiments in the 250 nm - 300 nm range are needed to charactize the 255 nm absorber. Table 4.14 lists the absorbers found in the range 250 nm - 584 nm. There are in all seven absorbers, of which three (2, 3, and 5) are transient intermediates in the sense that their concentrations grow and then decay. Table 4.14 also lists the figures in Chapter 4 that give final results for the static spectra and concentration profiles of these absorbers.

2. The "Half-of-the-Sites-Reactivity Mechanism"

The testing of Dunn and Bernhard's half-of-the-sites-reactivity mechanism (Mechanism III in Section A) is not the primary goal of this study. However, the resolved static spectra and concentration profiles from Experiments 1.1 - 4.1 provide new information concerning this mechanism.

For the conditions E < S < N, III predicts biphasic decay of S_{440}, with the fast portion using an amount of

Table 4.14. List of Absorbers in the LADH-NDMA-NADH Reaction.

Absorber Number	Absorbance Maxima.	Figures Giving Final Results
1	$(NAD^{+}\text{-}NADH)_{260\ nm}$	4.51, 4.52B
2	275 nm	4.50, 4.52A
3	403 nm	4.40, 4.41, 4.42
4	$(NADH_{340\ nm} + NDMA_{440\ nm})$ in Experiments 1.1 - 3.1 $NDMA_{440\ nm}$ in Exp. 4.1	4.44, 4.46, 4.48
5	320 nm 550 nm	
6	$NADH_{340\ nm}$ in Exp. 4.1	4.28, 4.48
7	255 nm	4.53

S equal to the enzyme site concentration E, and with the slow portion using the remainder of S_{440}. Dunn and Bernhard (1971) observed biphasic decay of <u>total absorbance</u> at 440 nm for the initial concentrations $E_{1.06}N_{15.0}S_{5.0}$. Attributing all the measured absorbance at 440 nm to S_{440}, they obtained results in agreement with III. In our Experiments 1.1 and 2.1, with initial concentrations $E_{7.39}N_{15.0}S_{13.4}$, we observe that, indeed, <u>total absorbance vs</u> time is a biphasic decay 400 nm to 450 nm (channels 31-36). However, principal component analysis reveals that there are <u>two</u> linearly independent absorbers contributing to the total absorbance at these channels. The <u>resolved concentration profile</u> of S_{440} in Experiments 1.1 and 2.1 is a single fast decay concomitant with the decay of N_{340}. The single fast decay $S_{440}N_{340}$ in Experiments 1.1 and 2.1 is incompatible with the half-of-the-sites reactivity mechanism.

In Experiment 3.1, with initial concentrations $E_{18.6}N_{15.0}S_{13.4}$, principal component analysis gives a single fast decay of S_{440} and N_{340}. Dunn and Bernhard (1971) assumed in Mechanism III that S is labile and is therefore free to find an E that is not inhibited by X. With this assumption, Mechanism III predicts for the conditions $S < N < E$, a single fast decay of S_{440}. Thus, Experiment 3.1 is compatible with Mechanism III. However, the single fast decay of S_{440} and N_{340} in Experiment 3.1 does not require that the sites of E interact with each other

and should therefore be compatible with many mechanisms that do not assume interaction between the sites.

For Experiment 4.1, with initial concentrations $E_{7.39}N_{6.0}S_{13.4}$, principal component analysis gives a biphasic decay of S_{440} and a single decay to zero of N_{340}. III predicts a biphasic decay of S_{440} when S > E > N, so that Experiment 4.1 and III qualitatively agree. However, III predicts that the fast and slow portions of the biphasic S_{440} decay each uses an amount of S equal to 1/2(S-N), so that the total S_{440} decay is (S-N). In Experiment 4.1 the resolved S_{440} decay uses a total amount of S $\sim$ 12.9 μM, which is almost the entire initial concentration S, and which is significantly greater than (S-N) = 7.4 μM, the prediction of III. Thus, although the S_{440} biphasic decay qualitatively agrees with III, the quantitative results are incompatible with III.

The significant conclusion from these results is that the qualitative observation of biphasic decay at 440 nm does not necessarily indicate biphasic decay of S_{440} since S_{440} is only one of two linearly independent absorbers at 440 nm. Our results are incompatible with the half-of-the-sites-reactivity mechanism of Dunn and Bernhard (1971). It is possible, of course, that our chemical system does not replicate the chemical system of Dunn and Bernhard (1971), so that in comparing our results to theirs, we are comparing observations on two different reaction systems. A closer examination of the half-of-the-

sites reactivity issue requires that the experiments of Dunn and Bernhard (1971) be repeated with principal component analysis of rapid scanning measurements covering at least the range 400 nm - 450 nm.

3. Speculation

The goal of this study has been to map out the static spectra and concentration profiles of the absorbing substrates, products, and transient intermediates without first invoking assumptions about the mechanism. Principal component analysis provides a mechanism-independent means of extracting the spectral and kinetic information from the experiments themselves. Having obtained the static spectra and concentration profiles independently of mechanistic hypotheses, the next step is to propose plausible mechanisms for the concentration profiles. In this subsection, as its title implies, we make no pretense of proposing a full kinetic mechanism for the LADH-NDMA-NADH reaction. Rather, we interpret our results and speculate on possible schemes (i.e., orders of events in the reaction) that might be used as starting points for developing and testing mechanisms in an extended study of this complex reaction.

We attempt to account for the behavior of Absorbers 3,4, 5, and 6 only since we have the static spectra and concentration profiles of these absorbers under four sets of initial conditions. We have the concentration profiles

of Absorbers 1, 2, and 7 only for Experiment 5.1, and we therefore do not attempt to account explicitly for these absorbers.

In Experiment 4.1 the concentration of $NDMA_{440\ nm}$ decays overall by 12.9 μM, which is significantly greater than 6.0 μM, the amount of $NADH_{340\ nm}$ available initially to reduce NDMA on the assumption of a 1:1 stoichiometry between NDMA and NADH. Dunn and Bernhard (1971) report 1:1 stoichiometry of NDMA and NADH under steady state conditions and under transient phase conditions. However, in their transient phase stopped flow experiments, as we have already noted, they assumed that all absorbance at 440 nm was attributable to $NDMA_{440\ nm}$. They thus seem to have underestimated the extent of disappearance of $NDMA_{440\ nm}$.

The apparent violation of 1:1 stoichiometry in Experiment 4.1 leads us to examine the possibility that ethanol not removed from LADH during dialysis recycles NAD^+ to NADH, which then reduces the excess NDMA. However, this seems unlikely for two reasons: (i) The initial concentration of ethanol in Experiment 4.1 would have to be at least 6.9 μM in order to account for the excess $NDMA_{440\ nm}$ decay. If we assume that 1 ml of 10% ethanol was carried over with the LADH precipitate into the first dialysis of LADH, that each of the 2000 ml dialysis steps reached equilibration with respect to ethanol, and that ethanol is not held in a tight complex with LADH, the initial concentration of ethanol in Experiment 4.1 would be of

the order 10^{-3} M, which is far too small to account for the excess $NDMA_{440\ nm}$ decay. (ii) The excess $NDMA_{440\ nm}$ decay in Experiment 4.1 results in more growth of Absorber 3. After the $NDMA_{440\ nm}$ decay is finished, the concentration of Absorber 3 remains nearly constant. If recycled NADH were responsible for the excess $NDMA_{440\ nm}$ decay, we would expect Absorber 3 to decay after the $NDMA_{440\ nm}$ decay is finished, as it does in Experiments 1.1 - 3.1. Thus, ethanol recycling NAD^+ to NADH does not explain the qualitative observation that Absorber 3 appears to be a dead end intermediate in Experiment 4.1, but not in Experiments 1.1 - 3.1.

A scheme that explains Experiments 1.1 - 5.1 should account for the following qualitative observations:

(1) When $[NDMA]_0 \geq [NADH]_0$, $NDMA_{440\ nm}$ and $NADH_{340\ nm}$ decay rapidly until all $NADH_{340\ nm}$ has disappeared.

(2) When $NDMA_{440\ nm}$ is initially in excess of $NADH_{340\ nm}$, the excess $NDMA_{440\ nm}$ decays via a slow process.

(3) The growth of Absorber 3 mirrors the decay of $NDMA_{440\ nm}$. When $NDMA_{440\ nm}$ is not initially in excess of $NADH_{340\ nm}$, Absorber 3 decays slowly following an initial rapid growth. When $NDMA_{440\ nm}$ is initially in excess of $NADH_{340\ nm}$, Absorber 3 continues to grow as the excess $NDMA_{440\ nm}$ slowly decays. Then Absorber 3 remains at a nearly constant concentration after the excess $NDMA_{440\ nm}$ decay is finished.

(4) Absorber 5 has a rapid biphasic growth followed by a slow decay in Experiments 1.1 - 4.1. In Experiments 1.1 - 3.1, Absorber 5 is still growing after Absorber 3 begins its decay. In Experiments 1.1 and 2.1 Absorber 3 is still decaying after Absorber 5 has finished decaying. The qualitative shape of Absorber five's concentration profile is not changed by having excess $NDMA_{440\ nm}$ over $NADH_{340\ nm}$ initially.

(5) $NDMA_{440\ nm}$ and $NADH_{340\ nm}$ both decay rapidly, even when both are initially in two-fold excess concentration of the total concentration of active enzyme sites (Experiments 1.1 and 2.1). Thus, the first and second turnovers of the enzyme sites are both rapid.

(6) In Experiment 5.1 ($E_{18.6}N_{15.0}S_{13.4}$) the growth of the NAD^+-NADH 260 nm band on forming NAD^+ is not complete until near the end of the experiment (35 sec), long after the initial decay of $NDMA_{440\ nm}$ and $NADH_{340\ nm}$ to zero concentration.

If Absorber 3 (403 nm) is enzyme-bound NDMA, shifted from 440 nm to 403 nm, the NDMA must bind only to a form of the enzyme that is induced by NADH or NAD^+, since premixing NDMA with the enzyme does not change the course of the reaction over premixing NDMA with NADH (Experiments 1.1 and 2.1).

The intermediates, Absorbers 3 and 5, decay slowly in Experiment 1.1 and 2.1, where two turnovers of $NDMA_{440\ nm}$ and $NADH_{340\ nm}$ are fast. This suggests that when Absorbers

3 and 5 decay either, (i) they are not enzyme bound, (ii) they are bound to an enzyme site other than an active site, or (iii) they are bound to one active site of each dimer, making that site inactive, but leaving the other site active.

We attempt to account for the qualitative observations above with the scheme shown in Figure 4.54. Of course, many other schemes could be proposed to account for these observations, and further experiments are required to test possible schemes and discriminate between them. In the scheme in Figure 4.54, we represent $NADH_{340\ nm}$ as N_{340}, $NDMA_{440\ nm}$ as S_{440}, and LADH as E or E' (two conformations) X, Y, and Z are intermediates. The subscript 403, 320 indicates a chromophore with the spectrum of Absorber 3, and 550, 320 represents a chromophore with the spectrum of Absorber 5. The formation of NAD^+_{260} is assumed to give the growth of absorbance in the 260 nm band of NAD^+-NADH.

We assume that all enzyme starts as the E conformation, with no E' conformation initially. N_{340} and S_{440} bind to E to give $EN_{340}S_{440}$, which rapidly reacts to form $E'X_{403,320}$. Thus, during its rapid growth, Absorber 3 is enzyme bound. $X_{403,320}$ rapidly dissociates from its enzyme complex, thus freeing the active enzyme site for a second rapid turnover of $N_{340}S_{440}$ to $X_{403,320}$. $X_{403,320}$ can then react further via either of two processes. In the first process, $X_{403,320}$ rapidly develops

the 550, 320 chromophore (Absorber 5). Then, in a slower step, $X^{550,320}_{403,320}$ loses the 403, 320 chromophore to give $X^{550,320}$, and finally, $X^{550,320}$ loses its 550, 320 chromophore to produce NAD^+_{260} and product P. In the second parallel process, $X_{403,320}$ can react to form NAD^+_{260} and P by first forming the intermediate $Y_{403,320}$. Thus, in this second process the 550, 320 chromophore never develops. These two parallel paths for the further reaction of $X_{403,320}$ are an attempt to account for the observation that in Experiments 1.1 and 2.1 Absorber 3 is still decaying after Absorber 5 has finished decaying.

On the first turnover E is converted to a different conformation E'. E' has the same catalytic activity as E, but E' has in addition the ability to slowly bind S_{440} without any coenzyme present to form a dead end complex $E'Z_{403,320}$. Thus, when S_{440} is initially in excess of N_{340}, the slow growth of $E'Z_{403,320}$ accounts for the slow growth of Absorber 3 during the slow portion of the biphasic S_{440} decay. Note that in this scheme the appearance of the 403, 320 chromophore requires the disappearance of S_{440}, either to form $E'X_{403,320}$ or $E'Z_{403,320}$.

More experiments with greater than two turnovers of the enzyme sites are needed to determine whether or not Absorber 3 and 5 are enzyme bound. Also needed are experiments to determine if NAD^+, NDMA, and LADH form a complex, and if this complex is Absorber 3 or Absorber 5. Of course, each additional experiment should be resolved by principal

component analysis. New absorbers may appear in the additional experiments, and species that were lumped by Experiments 1.1 - 4.1 as one absorber may be separated in the additional experiments. Once a given absorber has been shown by principal component analysis to appear in the additional experiments as well as the experiments reported here, the concentration-profiles of that absorber in both sets of experiments can be compared to obtain new mechanistic information.

$$EN_{340}S_{440} \text{ (or } E'N_{340}S_{440}) \xrightarrow{\text{fast}} E'X_{403,320} \xrightarrow{\text{fast}} E' + X_{403,320}$$

$$X_{403,320} \overset{\text{fast}}{\underset{\text{fast}}{\rightleftharpoons}} X^{550,320}_{403,320} \xrightarrow{\text{slow}} X^{550,320} \xrightarrow{\text{slow}} NAD^{+}_{260} + P$$

$$X_{403,320} \xrightarrow{\text{slow}} Y_{403,320} \xrightarrow{\text{slow}} NAD^{+}_{260} + P$$

$$E' + S_{440} \xrightarrow{\text{slow}} E'Z_{403,320}$$

Figure 4.54. Scheme to explain the qualitative observations in Experiments 1.1 - 5.1.

CHAPTER 5

FULL TIME COURSE ANALYSIS OF THE REVERSIBLE MICHAELIS-MENTEN MECHANISM

A. Introduction

The reversible, simple Michaelis-Menten mechanism is

$$E + S \underset{k_{-1}}{\overset{k_1}{\rightleftarrows}} C \underset{k_{-2}}{\overset{k_2}{\rightleftarrows}} E + P \qquad (I)$$

where E is enzyme, S is substrate, P is product, and C is the intermediate enzyme-substrate complex. The rate expressions for Mechanism (I) are coupled nonlinear differential equations that have so far eluded closed-form integration. To circumvent this mathematical difficulty, most enzyme kinetics studies treat only "initial velocity" data, using the familiar but approximate Michaelis-Menten equation (Michaelis and Menten 1913)

$$v_{mm} = V_{max}/\{1+(K_m/[S]_0)\}, \qquad (5.1)$$

where $[S]_0$ is the initial substrate molarity, v_{mm} is the initial velocity of disappearance of substrate or of appearance of product, and

$$V_{max} \equiv k_2[E]_0, \qquad (5.2)$$

$$K_m \equiv (k_{-1}+k_2)/k_1, \qquad (5.3)$$

where $[E]_0$ is the initial enzyme molarity.

Numerous more accurate but still approximate solutions have been proposed for Mechanism (I) and other closely related mechanisms. These include explicit algebraic (Morales and Goldman, 1955; Miller and Alberty, 1958; Wong, 1965; Hommes, 1962; Darvey, Proklovnik, and Williams, 1966; Maguire, Hijazi, and Laidler, 1974; Walter, 1974; Rubinow and Lebowitz, 1970; Heineken, Tsuchiya and Aris, 1967) as well as purely numerical solutions (Walter and Morales, 1964; Hommes, 1962; Hemker, 1972; Curtis and Chance, 1972). The numerical solutions have employed analog computers (Walter and Morales, 1964; Hommes, 1962) or special programs to integrate "stiff" differential equations on digital computers (Hemker, 1972; Curtis and Chance, 1972). Some of the algebraic solutions are restricted to the period before C has reached its steady-state level (Morales and Goldman, 1955; Darvey, Prokhovnik, and Williams, 1966; Maguire, Hijazi, and Laidler, 1974). Full time course algebraic solutions covering the pre-steady-state and steady-state periods have been obtained by perturbation methods (Miller and Alberty, 1956; Rubinow and Lebowitz, 1970; Heineken, Tsuchiya and Aris, 1967). Miller and Alberty (1958) used a perturbation about $(k_{-2}-k_1) = 0$ to obtain a solution to Mechanism (I). Their solution is not general, however, since $(k_{-2}-k_1)$ is not necessarily

small. Heineken, Tsuchiya and Aris (1967) obtained a solution to Mechanism (I) when $k_{-2} = 0$ by expanding about $([E]_0/[S]_0) = 0$ in a singular perturbation scheme. Since $([E]_0/[S]_0) << 1$ is a good approximation for the steady-state in most cases, their first order solution is quite useful. Rubinow and Lebowitz (1970) obtained only the zeroth order singular perturbation solution for a simple, irreversible, two substrate mechanism.

None of the works mentioned has included an examination of the accuracy of the Michaelis-Menten equation for the initial velocities determined and defined experimentally. In this chapter, after a thorough treatment of the steady-state rate expressions for the reversible, simple, Michaelis-Menten mechanism, we integrate the full-time-course rate expressions through first order in the singular perturbation scheme of Heineken, Tsuchiya and Aris (1967). We then use the results: (i) to examine the range of validity of initial product and substrate velocities predicted by Equation (5.1); (ii) to include explicitly the data obtained at the very beginning of the experiment; and (iii) to discuss optimal data collection and analysis in full-time-course experiments.

The chief purpose of this chapter is an analysis of the range of validity of Equation (5.1). To this end, we derive a more general result than Equation (5.1) and examine the circumstances in which the more general result reduces to Equation (5.1). In the usual experiment, unreacted

substrate, and the concentration of either substrate or product is monitored with time. The mass balances are

$$[E]_0 = [E] + [C], \quad [S]_0 = [S] + [P] + [C] \tag{5.4}$$

and the rate expressions for (I) are

$$[\dot{S}] = -k_1[S]([E]_0 - [C]) + k_{-1}[C], \tag{5.5}$$

$$[\dot{C}] = k_1[S]([E]_0 - [C]) + k_{-2}([E]_0 - [C])([S]_0 - [S] - [C]) - (k_{-1} + k_2)[C], \tag{5.6}$$

$$[\dot{P}] = k_2[C] - k_{-2}([E]_0 - [C])([S]_0 - [S] - [C]), \tag{5.7}$$

where $[\dot{S}] = (d[S]/dt)$, <u>etc</u>.

There are two experimental definitions for both the initial substrate velocity v_i^S and the initial product velocity v_i^P. Although Equation (5.1) applies for both definitions, it is derived differently in the two cases. The more common definition, called Method 1 in the remainder of this chapter, can be used if enough measurements are available to construct either a substrate or a product progress curve for small extent of reaction. The Method 1 initial velocity is defined as the magnitude of the slope of a line drawn tangent to the progress curve at time t, after a small extent of reaction, as in Figure 5.1.

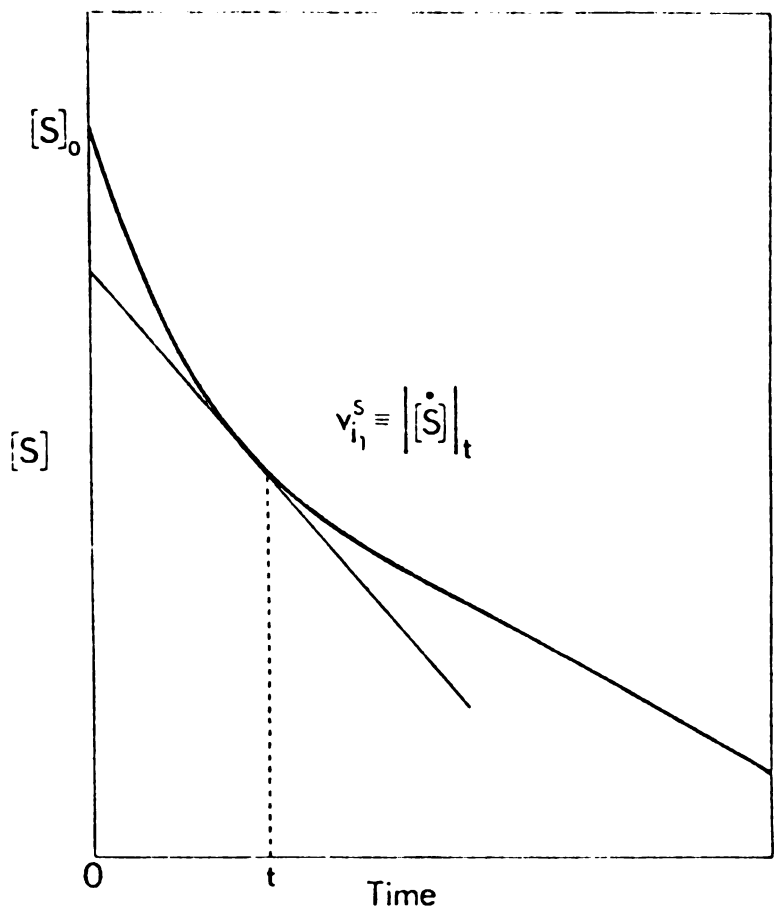

Figure 5.1. Definition of v_{i1}^s, the Method 1 initial substrate velocity.

$$v_{i1}^{S} \equiv \left\{\begin{matrix}\text{Method 1} \\ \text{initial substrate} \\ \text{velocity}\end{matrix}\right\} \equiv |\dot{[S]}|_t \tag{5.8}$$

$$v_{i1}^{P} \equiv \left\{\begin{matrix}\text{Method 1} \\ \text{initial product} \\ \text{velocity}\end{matrix}\right\} \equiv |\dot{[P]}|_t \tag{5.9}$$

Method 2 is less accurate, but it might be necessary to use it if product and substrate are difficult to assay and/or if few measurements are available. The Method 2 initial substrate and product velocities are defined by

$$v_{i_2}^{S} = ([S]_0 - [S]_t)/t, \tag{5.10}$$

$$v_{i_2}^{P} = [P]_t/t, \tag{5.11}$$

where $[S]_t$ and $[P]_t$ are measured a short time t after mixing, as in Figure 5.2.

The first two approximations in deriving Equation (5.1) are the same for Methods 1 and 2. They are made arbitrarily in this Section but they will be shown by the singular perturbation scheme in Section B to depend on the smallness of the ratio $([E]_0/[S]_0)$. First, make a steady state approximation on the complex C by setting $\dot{[C]} = 0$ in Equation (5.6). Then, omit all terms containing $[C]^2$ or $[C][E]_0$ from Equations (5.6) and (5.7). Rearrangement of the results to leave [S] as the only independent variable yields

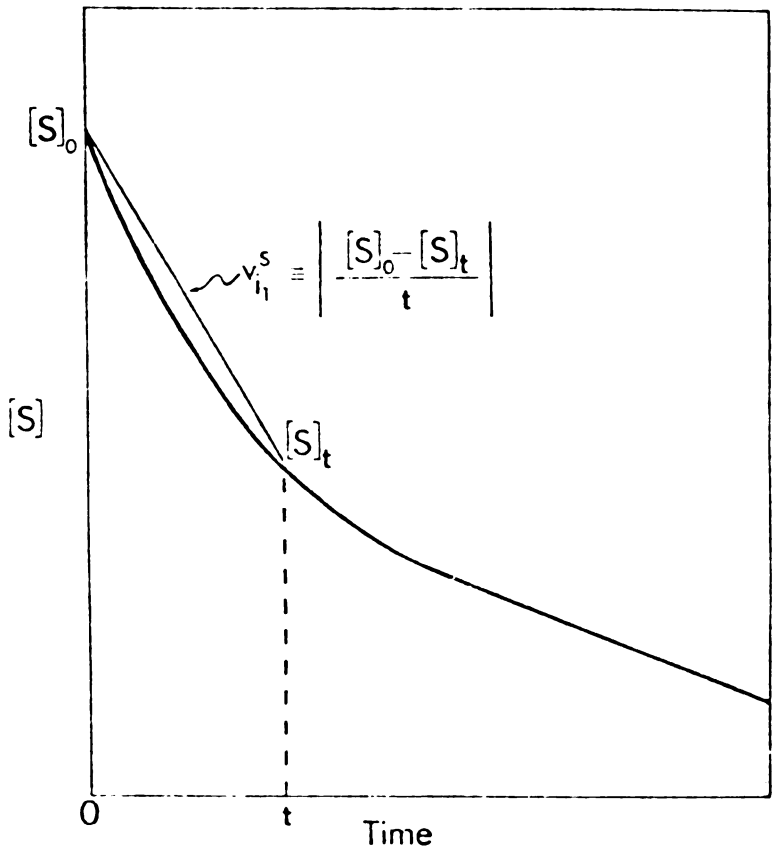

Figure 5.2. Definition of v_{12}^s, the Method 2 initial substrate velocity.

$$[\dot{S}] = -[\dot{P}] = [E]_0\{k_{-1}k_{-2}([S]_0-[S])-k_1k_2[S]\}/$$

$$\{k_{-1}+k_2+k_1[S]+k_{-2}([S]_0-[S])\} \qquad (5.12)$$

and

$$[C]=[E]_0\{k_{-2}([S]_0-[S])+k_1[S]\}/\{k_{-1}+k_2+k_1[S]+k_{-2}([S]_0-[S]\}. \qquad (5.13)$$

The further approximation $[S] \simeq [S]_0$ converts Equation (5.12) into Equation (5.1), in the form

$$v^S_{i_1} = \left|[\dot{S}]_t\right| = v^P_{i_1} = [\dot{P}]_t = V_{max}/\{1 + (K_m/[S]_0)\} \qquad (5.14)$$

[cf. Equations (5.8) and (5.9)]; these are the Method 1 Michaelis-Menten Equations.

In order to obtain the Method 2 Michaelis-Menten Equations, integrate Equation (5.12), whence

$$\frac{(k_{-2}-k_1)([S]_0-[S])}{(k_1k_2+k_{-1}k_{-2})} +$$

$$\frac{(k_2+k_{-1})(k_1k_{-2}[S]_0+k_1k_2+k_{-1}k_{-2})}{(k_1k_2+k_{-1}k_{-2})^2}.$$

$$\ln\left\{1 - \frac{(k_1k_2+k_{-1}k_{-2})([S]_0-[S])}{k_1k_2[S]_0}\right\} = -[E]_0t. \qquad (5.15)$$

If we assume

$$([S]_0-[S]) << k_1k_2[S]_0/(k_1k_2+k_{-1}k_{-2}), \qquad (5.16)$$

expand the logarithmic term in a Taylor's Series, and retain only the leading term, then Equation (5.15) becomes

$$(k_1[S]_0 + k_2+k_{-1})([S]_0-[S])/k_1k_2[S]_0 = [E]_0t. \qquad (5.17)$$

By Equations (5.2), (5.3), (5.10), (5.11), (5.12), and (5.17),

$$v^S_{i_2} = v^P_{i_2} = V_{max}/\{1 + (K_M/[S]_0)\} \qquad (5.18)$$

V_{max} and K_M are determined by fitting Equation (5.1) to a set of initial velocity measurements in which $[S]_0$ varies over the approximate range $0.2K_M \leq [S]_0 \leq 5K_M$. The roles of substrate and product can be reversed, and an additional pair of parameters, K'_M and V'_{max} can be determined from a similar series of experiments. These parameters are related to K_M and V_{max} by

$$V'_{max} - k_{-1}[E]_0 = (k_{-1}/k_2)\ V_{max} \qquad (5.2')$$

$$K'_M = (k_{-1}+k_2)/k_{-2} = (k_1/k_{-2})\ K_M \qquad (5.3')$$

All the approximations used in deriving the Michaelis-

Menten equation contribute to the errors of the predicted initial velocities. The steady-state approximation on the complex C causes greater errors at very small extents of reaction since the initial condition $[C]_{t=0} = 0$ is inconsistent with Equation (5.13), and some time is required after mixing for [C] to approach the value given by Equation (5.13). The errors from the approximation $[S] \tilde{=} [s]_0$ used in Method 1 and the similar approximation of Equation (5.16) for Method 2 increase with extent of reaction.

B. Singular Perturbation Solution

We now integrate the differential rate equations to first order in the singular perturbation scheme of Heineken, Tsuchiya and Aris (1967). The equations are first made dimensionless by the following definitions.

$$S \equiv [S]/[S]_0, \quad c \equiv [C]/[E]_0, \quad p \equiv [P]/[S]_0,$$

$$\epsilon \equiv [E]/[E]_0, \quad \mu \equiv [E]_0/[S]_0, \quad K \equiv (k_{-1}+k_2)/k_1[S]_0,$$

$$\lambda \equiv k_2/k_1[S]_0, \quad \gamma \equiv k_{-2}/k_1, \quad \tau \equiv k_1[E]_0 t \qquad (5.19)$$

The enzyme and substrate mass balance equations are, respectively,

$$1 = \epsilon + c \qquad (5.20)$$

$$1 = s + p + \mu c \tag{5.21}$$

Equations (5.20) and (5.21) reduce Equations (5.5) and (5.6) to a pair of differential equations to be solved for two concentration variables, s and c,

$$(ds/d\tau) = s(c-1) + (K-1)c = F(s,c,\tau,\mu) \tag{5.22}$$

$$\mu(dc/d\tau) = s(1-\gamma)(1-c) + \gamma - (\gamma+K)c + \mu\gamma c(c-1) = G(s,c,\tau,\mu) \tag{5.23}$$

with initial conditions

$$s(0) = 1, \quad c(0) = 0 \tag{5.24}$$

The pair of equations in p and c is

$$(dp/d\tau) = \lambda c - \gamma p(1-c) = U(p,c,\tau,\mu) \tag{5.25}$$

$$\mu(dc/d\tau) = (c-1)[1+(\gamma-1)p] - Kc + \mu c(c-1) = V(p,c,\tau,\mu) \tag{5.26}$$

with initial conditions

$$p(0) = 0, \quad c(0) = 0 \tag{5.27}$$

If an exact solution were obtainable for Equations (5.22) and (5.23), p could be calculated from the equation

$$p = 1-s - \mu c \tag{5.28}$$

However, μ is the perturbation parameter for our approximate solution. To maintain a well-ordered perturbation scheme for $\mu \neq 0$, it is necessary to obtain p from a separate solution to Equations (5.25) and (5.26). The solution of Equations (5.22) and (5.23) is described here. The same procedure is used to solve Equations (5.25) and (5.26), and their solutions are listed in Appendix H.

The perturbation parameter in our singular perturbation scheme is $\mu = ([E]_0/[S]_0)$, which is usually small compared to unity in steady-state kinetic studies. In the limit $\mu \to 0$, Equations (5.22) and (5.23) reduce to Equations (5.29) and (5.30), which are equivalent to the steady-state equations (5.12) and (5.13)

$$(ds/d\tau) = s(c-1) + (K-1)c = F(s,c,\tau,0) \tag{5.29}$$

$$0 = s(1-\gamma)(1-c)+\gamma-c(+K) = G(s,c,\tau,0) \tag{5.30}$$

Equation (5.30) is not satisfied by the initial conditions in Equation (5.24) since

$$G(s(0), c(0), 0, 0) = 1 \tag{5.31}$$

Another pair of differential equations is required that satisfies the initial conditions in the limit $\mu \to 0$. From Equation (5.23), in the limit $\mu \to 0$ at $\tau = 0$, we have

$$\lim_{\mu \to 0} (dc/d\tau)_{\tau=0} = \lim_{\mu \to 0} (\mu^{-1}) = \infty \tag{5.32}$$

This suggests the definition of an expanded time scale $\sigma = (\tau/\mu)$ to give a finite rate of complex production at $\tau = 0$.

$$\lim_{\mu \to 0} (dc/d\sigma)_{\sigma=0} = 1 \tag{5.33}$$

The differential equations in the σ time scale are called the inner equations. They can be integrated with the initial conditions $s(0) = 1$, $c(0) = 0$ in the limit $\mu \to 0$.

Inner Equations

$$(ds/d\sigma) = \mu[s(c-1) + (K-1)c] = \mu F(s,c,\tau,\mu) \tag{5.34}$$

$$(dc/d\sigma) = s(1-\gamma)(1-c) + \gamma - c(\gamma+K) + \mu\gamma c(c-1) = G(s,c,\tau,\mu) \tag{5.35}$$

The τ time scale equations are called the outer equations, where the bar over the concentration variables denotes "outer".

Outer Equations

$$(d\bar{s}/d\tau) = \bar{s}(\bar{c}-1 + (K-1)\bar{c} = F(\bar{s},\bar{c},\tau,\mu) \tag{5.36}$$

$$\mu(d\bar{c}/d\tau) = \bar{s}(1-\gamma)(1-\bar{c}) + \gamma-\bar{c}(\gamma+K) + \mu\gamma\bar{c}(\bar{c}-1) = G(\bar{s},\bar{c},\tau,\mu) \tag{5.37}$$

Equations (5.34) through (5.37) are nonlinear, and have no known closed form solutions. Hence, we take $\mu = 0$ as a zeroth order approximation to obtain solvable linear equations. An ordinary perturbation solution about $\mu = 0$ is obtained for the inner and outer equations,

$$s = \sum_{n=0}^{\infty} (1/n!)(\partial s/\partial \mu)_{\sigma,c}\mu^n = \sum_{n=0}^{\infty} s_n\mu^n, \tag{5.38}$$

and likewise for $\bar{c},\bar{s}$, and $\bar{c}$. The initial conditions of Equation (5.24) are applied to the inner equations without loss of generality as

$$s_0(0) = 1, \quad s_n(0) = 0, \; n \geq 1$$

$$c_n(0) = 0, \quad n \geq 0 \tag{5.39}$$

Initial conditions for the outer equations are derived by requiring the inner and outer solutions to match in a region where σ is large and τ is close to zero. The details of the matching procedure are described in Appendix I.

$$s_{(m)} \equiv \sum_{n=0}^{m} s_n \mu^n \tag{5.40}$$

$$\bar{s}_{(m)} \equiv \sum_{n=0}^{m} \bar{s}_n \mu^n \tag{5.41}$$

$$s_{(m)} \equiv \sum_{n=0}^{m} \frac{1}{n!} \left| \left(\mu \frac{\partial}{\partial \mu} + \tau \frac{\partial}{\partial \tau}\right)^n \bar{s} \right|_{(\mu=0, \tau=0)} \tag{5.42}$$

the total solution to order m in the parameter μ for substrate over the entire time course, $S_{(m)}$, is defined by Equation (5.43).

$$S_{(m)} \equiv s_{(m)} + \bar{s}_{(m)} - \hat{s}_{(m)} \tag{5.43}$$

Equations (5.40) and (5.41) are the m'th order inner and outer solutions, respectively. Equation (5.42) is the m'th order double Taylor's Series expansion of the outer solution about the point $\mu=0, \tau=0$. The role of $\hat{s}_{(m)}$ in Equation (5.43) is to subtract $\bar{s}_{(m)}$ from the right hand side on the inner time scale, and to subtract $s_{(m)}$ on the outer time scale. $C_{(m)}$, the total m'th order solution for the complex, is defined similarly by Equation (5.44).

$$C_{(m)} \equiv c_{(m)} + \bar{c}_{(m)} - \hat{c}_{(m)} \tag{5.44}$$

The zeroth and first order inner and outer equations and the total first order singular perturbation solution are given in Appendix H. The matching of the inner and

outer solutions is described in Appendix I.

C. Practical Results

In order to examine efficiently the accuracy of the Michaelis-Menten equation for initial velocities over a wide range of conditions, we must choose a compact set of variables to represent the four rate constants and two initial concentrations. The dimensionless differential equations (5.22) and (5.23) reduce these six quantities to the four independent parameters μ, K, λ, and γ. We therefore choose the dimensionless equations for our analysis.

In the dimensionless representation, the Michaelis-Menten equation for initial substrate and product velocities is

$$V_{mm} = \gamma/(1+K) \tag{5.45}$$

where upper case V's represent dimensionless initial velocities in the τ time scale. Since the first order singular perturbation equations agree with numerical integration of the differential equations for μ as high as 0.2, we use these solutions to represent the measured initial velocities V_1^s, V_2^s, V_1^P, and V_2^P. We define the ratios of these "measured" velocities to those predicted by the Michaelis-Menten equation as follows: For Method 1,

$$R_1^S \equiv (V_1^S/V_{mm}) = |dS_{(1)}/d\tau|_{\tau'}(1+K)\lambda^{-1} \qquad (5.46)$$

$$R_1^P \equiv (V_1^P/V_{mm}) = (dP_{(1)}/d\tau)_{\tau'}(1+K)\lambda^{-1} \qquad (5.47)$$

For Method 2,

$$R_2^S \equiv (V_2^S/V_{mm}) = (1-S_{(1)_{\tau'}})(1+K)\tau'^{-1}\lambda^{-1} \qquad (5.48)$$

$$R_2^P \equiv (V_2^P/V_{mm}) = P_{(1)_{\tau'}}(1+K)\tau'^{-1}\lambda^{-1}, \qquad (5.49)$$

where τ' is the time at which the initial velocity is measured. The initial velocity predicted by the Michaelis-Menten equations is exactly correct only when the appropriate ratio defined by Equation (5.46) through (5.49) equals 1.

We use the four independent combinations of μ, K, λ, and γ defined in Column 1 of Table 5.1 to examine R_1^S, R_1^P, R_2^S, and R_2^P. Column 2 of Table 5.1 lists these parameters as functions of the rate constants and initial concentrations. In practice some of the rate constants may be unknown. The Michaelis-Menten equation (5.1) gives only V_{max} and K_M from a single initial velocity study. If the reaction is irreversible ($k_{-2} = 0$), no further information is obtainable from steady-state initial velocities. If the reaction is reversible, we can measure the equilibrium constant $K_{eq} \equiv ([P]_{eq}/[S]_{eq})$. Column 3 of Table 5.1 lists

Table 5.1. Equivalent Expressions for the Dimensionless Parameters for the Analysis of the Michaelis-Menten Equation.

a	b	c	d
μ	$[E]_0/[S]_0$	$[E]_0/[S]_0$	$[E]_0[S]_0$
K	$(k_{-1}+k_2)(k_1[S]_0)^{-1}$	$K_m/[S]_0$	$K_m/[S]_0$
$\gamma[(K/\lambda)-1]$	$k_{-1}1_{-2}(k_1k_2)^{-1}$	K_{eq}^{-1}	$K_mV_m'K_m'^{-1}V_m^{-1}$
(λ/K)	$k_2(k_{-1}+k_2)^{-1}$	$V_m(K_mk_1[E]_0)^{-1}$	$V_m(V_m+V_m')^{-1}$

a. Dimensionless parameters for analysis of the Michaelis-Menten equation.

b. Equivalent expressions in rate constants and initial concentrations.

c. Equivalent expressions in K_m, K_{eq}, V_m, k_1, and the initial concentrations.

d. Equivalent expressions in initial concentrations and the forward-plus-reverse-direction Michaelis constants and maximum velocities.

the four dimensionless parameters in terms of K_M, V_{max}, $[S]_0$, $[E]_0$, K_{eq}, and k_1. The parameters μ, K, and $\gamma[(K/\lambda)-1]$ can be calculated even if k_1 is unknown. Their physical meaning is easily understood. To a large extent, μ determines the accuracy of the steady-state approximation, since it is the perturbing parameter in the perturbation scheme. K reflects the degree of saturation of the enzyme by substrate when the steady-state is obtained. In most initial velocity studies, K is varied from 0.2 to 5.0. $\gamma[(K/\lambda)-1]$ is the reciprocal of the overall equilibrium constant, K_{eq}. If the reaction is irreversible, $\gamma[(K/\lambda)-1] = 0$. (λ/K) requires a value for k_1, which cannot be determined from steady-state initial velocities in the forward direction only. However, (λ/K) is a function of rate constants only and is therefore independent of the initial concentrations. It lies in the open interval

$$0 < (\lambda/K) < 1. \tag{5.50}$$

From Inequality (5.50) we can derive a lower limit for k_1;

$$k_1 > (V_{max}/K_m[E]_0) \tag{5.51}$$

If the reaction is appreciably reversible, an initial velocity study in the reverse direction will yield V'_{max} and K'_m. All of the rate constant can be calculated from

V_{max}, V'_{max}, K_m, K'_m, $[E]_0$, and $[S]_0$ by

$$k_1 = (V_{max} + V'_{max})\,[E]_0^{-1}\,K_m^{-1} \tag{5.52}$$

$$k_{-1} = V'_{max}\,[E]_0^{-1} \tag{5.53}$$

$$k_2 = V_{max}\,[E]_0^{-1} \tag{5.54}$$

$$k_{-2} = (V_{max} + V'_{max})\,[E]_0^{-1}\,K'^{-1}_m \tag{5.55}$$

Column 4 of Table 5.1 lists the four dimensionless parameters in terms of V_{max}, V'_{max}, K_m, K'_m, $[E]_0$, and $[S]_0$.

We begin our analysis with a specific example to illustrate the use of the above definitions. The irreversible hydrolysis of acetyl-L-phenylalanine ethyl ester by chymotrypsin is consistent with Mechanism I with $K_m = 10^{-4}M$, and $V_{max} = 10^{-5}M^{-1}sec^{-1}$ (H. Gutfreund, 1955). Consider an initial substrate velocity determined by Method 1 with $[E]_0 = 10^{-6}M$, and $[S]_0 = 10^{-4}M$. Then $\mu = 10^{-3}$, $K = 1.0$, and $\gamma[(K/\gamma)-1] = 0$. Inequality (51) requires that $k_1 > 10^5\ M^{-1}sec^{-1}$. We use two hypothetical values of k_1 to calculate (λ/K). For $k_1 = 10^6\ M^{-1}sec^{-1}$, $(\lambda/K) = 10^{-1}$; and for $k_1 = 10^7\ M^{-1}sec^{-1}$, $(\lambda/K) = 10^{-2}$. Figure 5.3 shows that for $(\lambda/K) = 10^{-2}$, the measured initial substrate velocity (R_1^s is defined in Equation (5.46)) starts out 198 times as large as the velocity predicted by the Michaelis-Menten equation. For $(\lambda/K) = 10^{-1}$, R_1^s starts at 19.8.

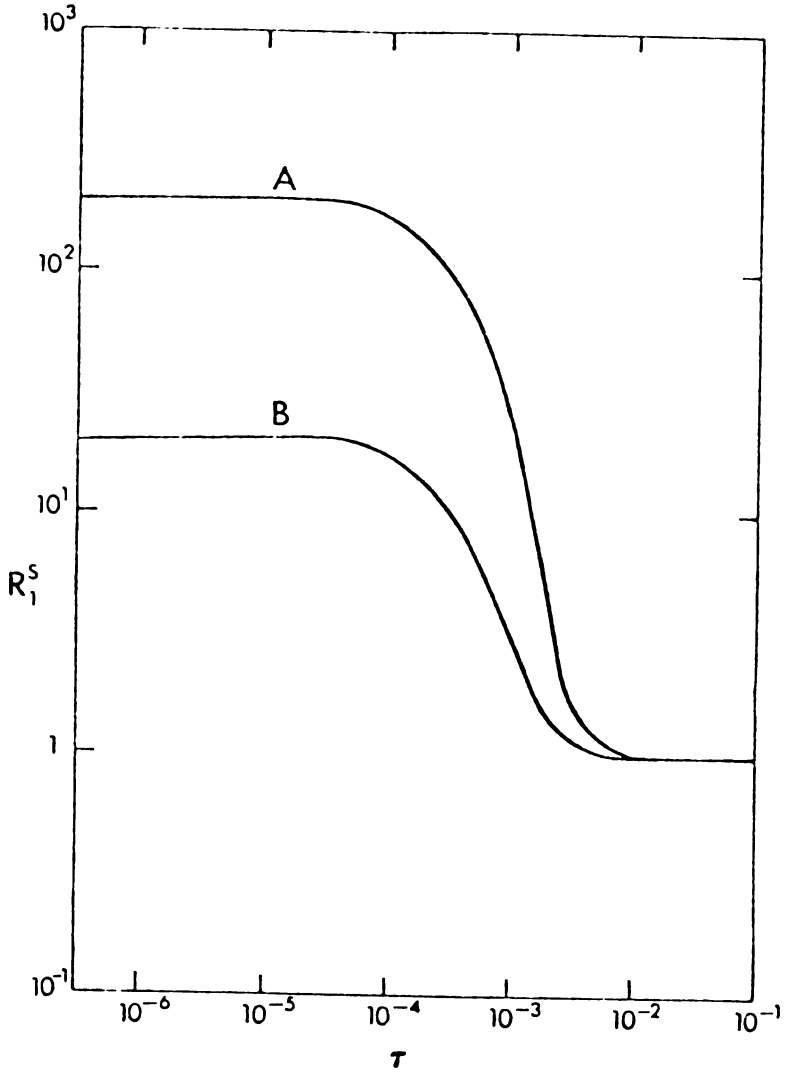

Figure 5.3. R_1^S versus time for irreversible hydrolysis of acetyl-L-phenylalanine ethyl ester by chymotrypsin. $(\lambda/K) = 10^{-2}$(A), 10^{-1}(B).

These large errors occur before the complex C has reached its steady-state level. At $\tau \cong 0.007$, R_1^s drops rapidly to values near 1 for both cases. As explained by Heineken, Tsuchiya and Aris (1967), this sudden drop is caused by the vanishing of the term $\exp[-(1+K)\tau\mu^{-1}]$ in the perturbation solution. The time t in seconds is related to τ by $t = k_1^{-1}[E]_0^{-1}\tau$. For $k_1 = 10^6\ M^{-1}sec^{-1}$, R_1^s reaches 1 in 7 msec, while for $k_1 = 10^7\ M^{-1}sec^{-1}$, R_1^s reaches 1 in 0.7 msec. Since k_1 is typically greater than $10^6\ M^{-1}sec^{-1}$, and initial velocities are usually measured at t > 5 msec, the majority of initial velocities require no pre-steady-state correction to the Michaelis-Menten equation. The pre-steady-state period can be lengthened by decreasing $[E]_0$ and $[S]_0$.

We now examine the influence of μ, K, $[(K/\lambda)-1]$, and (λ/K) on R_1^s, R_1^p, R_2^s, and R_2^p. For this analysis it is more informative to plot the ratios versus the extent of reaction instead of time. For product velocities the extent of reaction is defined as $P_{(1)}$, and for substrate velocities, as $1-S_{(1)}$.

Effect of $\mu = ([E]_0/[S]_0)$. Figure 5.4 shows the effect of on R_1^s at small extents of reaction. In each case R_1^s decreases to 1 at $(1-S_{(1)}) < \mu$. A Method 1 initial substrate velocity measured at an extent of reaction much less than μ is considerably greater than the Michaelis-Menten value because the complex C has not reached its steady-state concentration. Figure 5.5 shows that, even at extents of reaction greater than μ, the Michaelis-Menten equation underestimates Method 2 initial substrate

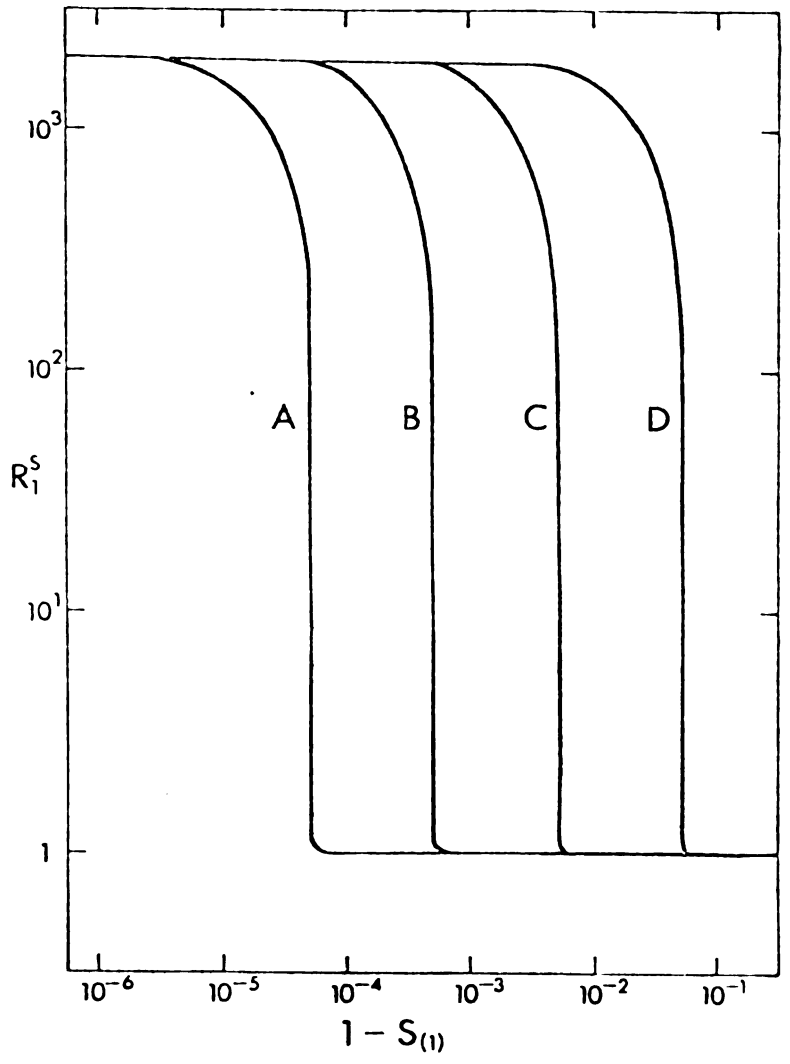

Figure 5.4. Effect of μ on R_1^S at small extents of reaction. $\mu = 10^{-4}$ (A), 10^{-3}(B), 10^{-2}(C), 10^{-1}(D). For all curves, $(\lambda/K) = 10^{-3}$, $K = 1.0$, $\gamma[(K/\lambda)-1] = 0$.

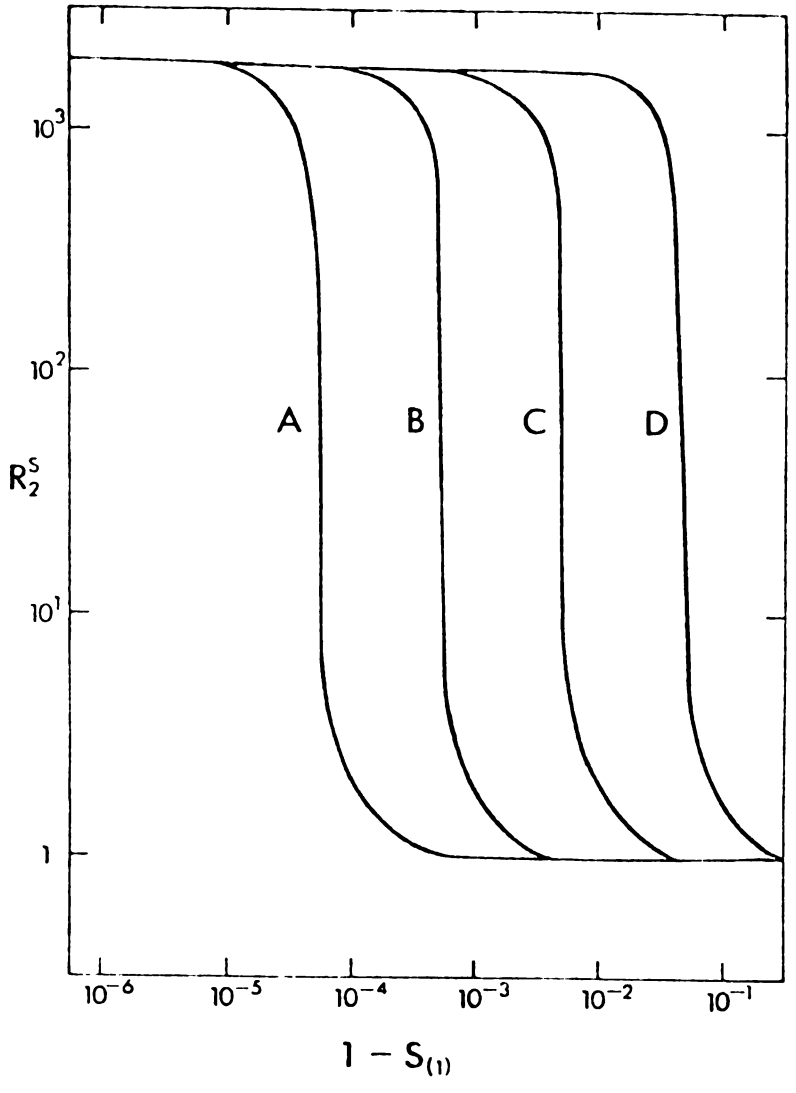

Figure 5.5. Effect of μ on R_2^S at small extents of reaction. $\mu = 10^{-4}$(A), 10^{-3}(B), 10^{-2}(C), 10^{-1}(D). For all curves, $(\lambda/K) = 10^{-3}$, $K = 1.0$, $\gamma[(K/\lambda)-1] = 0$.

velocities. The degree of underestimation is described approximately by

$$R_2^s \cong (1-S_{(1)})(1+K)[(1-S_{(1)})(1+K)-\mu]^{-1}. \qquad (5.56)$$

Equation (5.56) was obtained from the first order perturbation solution with the assumptions

$$(1-S_{(1)}) << 1,\ \mu << 1,\ \lambda << (K+1)\exp[-(1+K)\tau\mu^{-1}] \qquad (5.57)$$

Figures 5.6 and 5.7 show that the initial product velocities by the two methods are overestimated by the Michaelis-Menten equation at extents of reaction less than μ.

Excepting the lag shown by R_2^s, μ does not significantly affect the accuracy of the Michaelis-Menten equations at extents of reaction greater than μ for $\mu \leq 10^{-2}$. If $\mu \leq 10^{-2}$ and $(1-S_{(1)}) > \mu$, the zeroth order outer terms dominate the perturbation solution, and the following limiting equations, equivalent to the steady-state integrated Equation (5.15), can be used.

$$R_1^s = R_1^P \cong \{\gamma(\gamma-K)+[\lambda+\gamma(K-\gamma)\bar{s}_0][K+\gamma+(1-\gamma)\bar{s}_0]^{-1}(1+K)\lambda^{-1} \qquad (5.58)$$

$$R_2^P \cong \bar{p}_0\ (1+K)\tau^{-1}\lambda^{-1} \qquad (5.59)$$

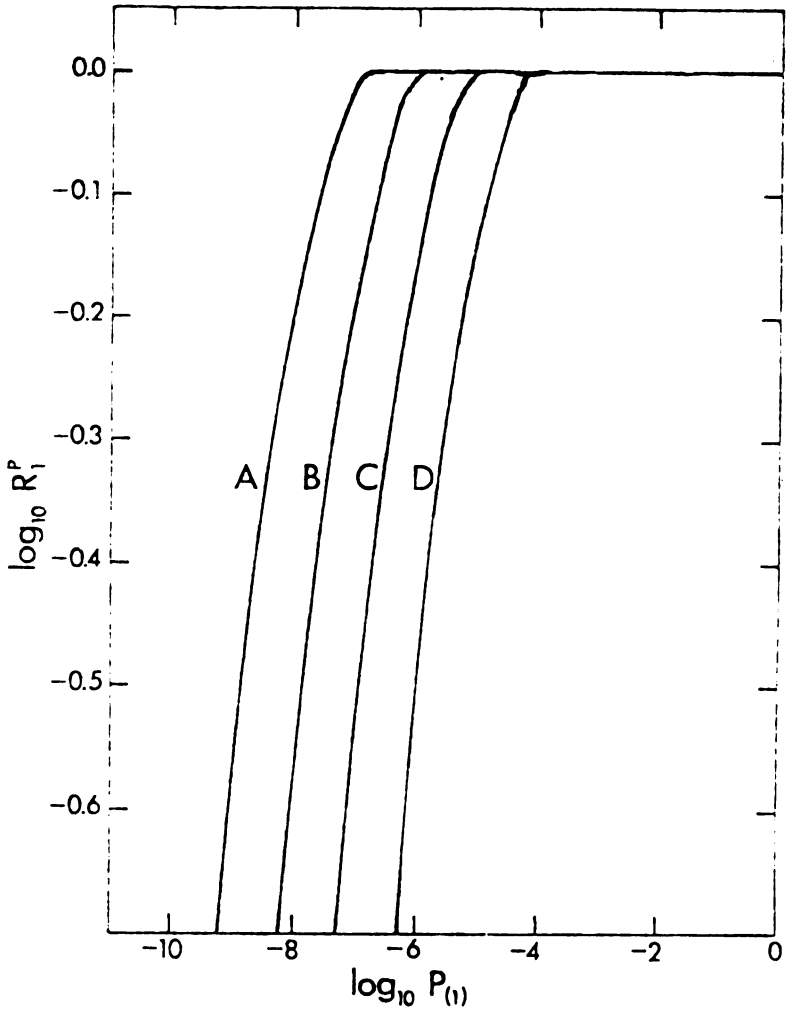

Figure 5.6. Effect of μ on R_1^p at small extents of reaction. $\mu = 10^{-4}$(A), 10^{-3}(B), 10^{-2}(C), 10^{-1}(D). For all curves, $(\lambda/K) = 10^{-3}$, $K = 1.0$, $\gamma[(K/\lambda)-1] = 0$.

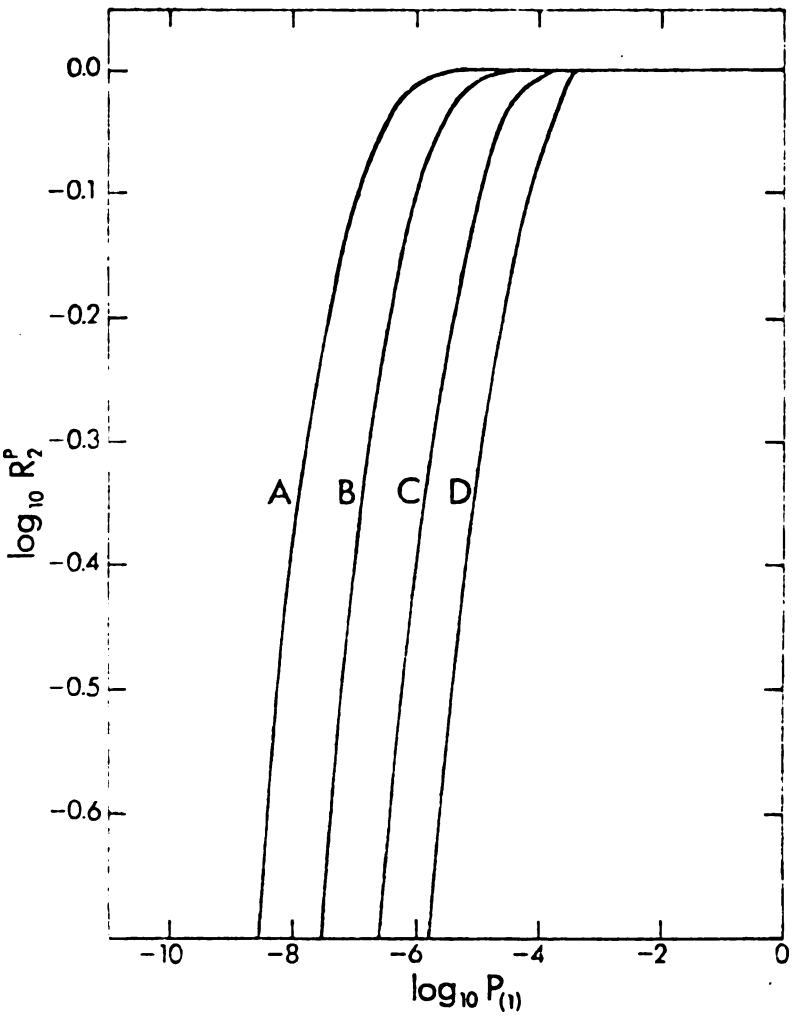

Figure 5.7. Effect of μ on R_2^p at small extents of reaction. $\mu = 10^{-4}$(A), 10^{-3}(B), 10^{-2}(C), 10^{-1}(D). For all curves, $(\lambda/K) = 10^{-3}$, $K = 1.0$, $\gamma[(K/\lambda)-1] = 0$.

where

$$\tau = \frac{(\gamma-1)\,\bar{p}_0}{[\gamma(\lambda-K)-\lambda]} - \frac{K[\gamma(1+K-\lambda)+\lambda]}{[\gamma(\lambda-K)-\lambda]^2}\,\ell n\,\frac{[\gamma(K-\lambda)-\lambda]\,\bar{p}_0+\lambda}{\lambda} \qquad (5.60)$$

If $(1-S_{(1)})(1+K)[(1-S_{(1)})(1+K)-\mu]^{-1} \cong 1$ and $\mu \leq 10^{-2}$, then

$$R_2^s = (1-\bar{s}_0)(1+K)\tau^{-1}\lambda^{-1}. \qquad (5.61)$$

Figure 5.8 shows that, for the relatively high value $\mu = 0.1$, R_1^s approaches 1 for only a small portion of the reaction. For μ much greater than 10^{-2}, the full first order perturbation solutions should be used.

Effect of $K = (K_M/[S]_0)$. Figure 5.9 illustrates the effect of K on R_1^s at small extents of reaction. The effect on R_2^s is qualitatively the same. As K increases, R_1^s approaches 1 at lower extents of reaction. Figure 5.10 shows the effect of K on R_1^p at small extents of reaction. R_2^p behaves similarly. When K is increased from 10^{-2} to 1, R_1^p approaches 1 at greater extents of reaction. As K increases beyond 1, the trend reverses and R_1^p approaches 1 at lower extents of reaction.

Figure 5.11 illustrates the effect of K on R_1^s and R_1^p at large extents of reaction for $\mu \leq 10^{-2}$, where Equation (5.58) is a good approximation. As K increases, R_1^s and R_1^p decrease more rapidly with extent of reaction. R_2^s and R_2^p behave similarly. The sources of this trend are the

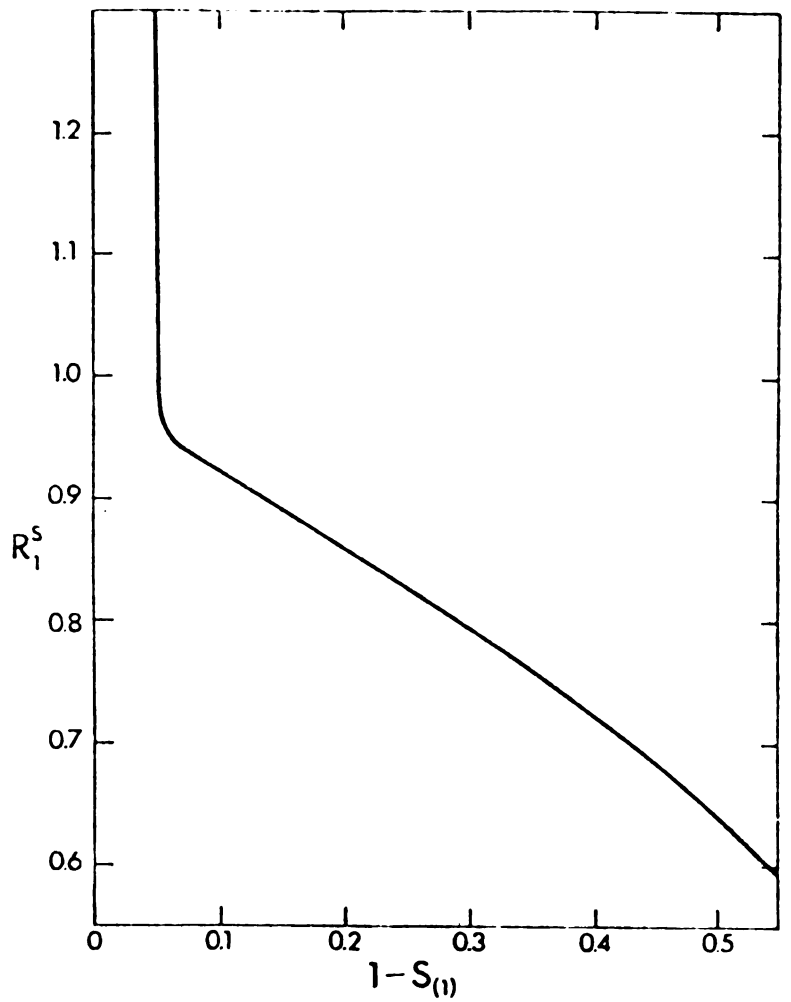

Figure 5.8. R_1^S versus extent of reaction for $\mu = 0.1$, $K = 1.0$, $(\lambda/K) = 10^{-3}$, $\gamma[(K/\lambda)-1] = 0$.

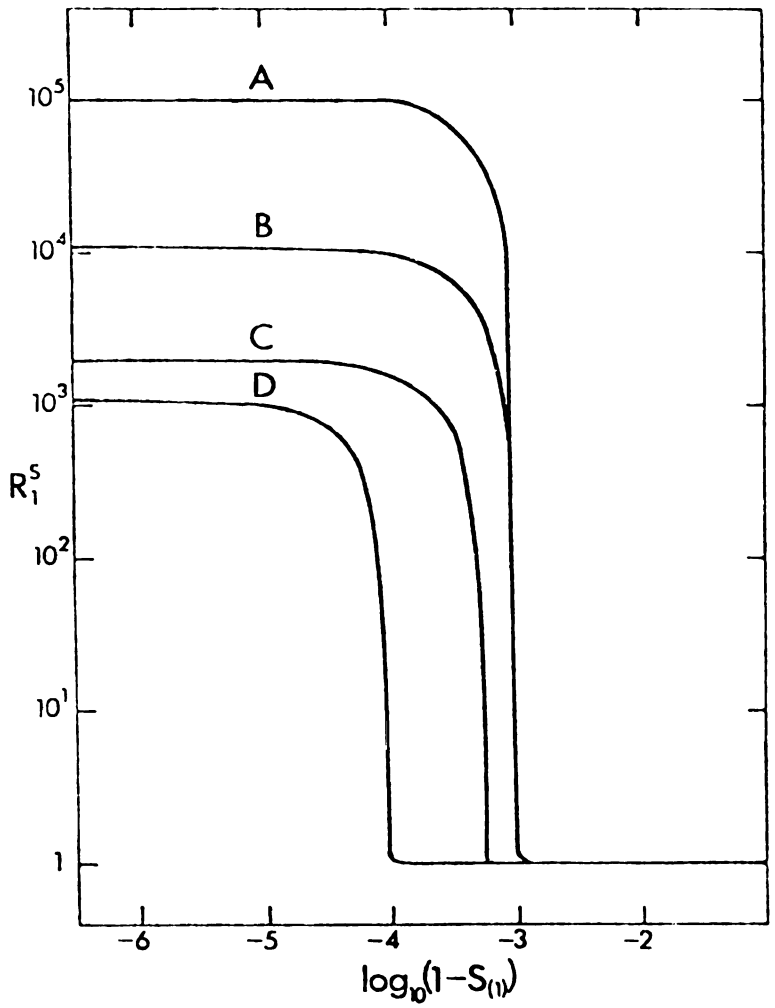

Figure 5.9. Effect of K on R_1^s at small extents of reaction. K = 10^{-2}(A), 10^{-1}(B), 1.0(C), 10.0 (D). For all curves $\mu = 10^{-3}$, $(\lambda/K) = 10^{-3}$, $\gamma[(K/\lambda)-1] = 0$.

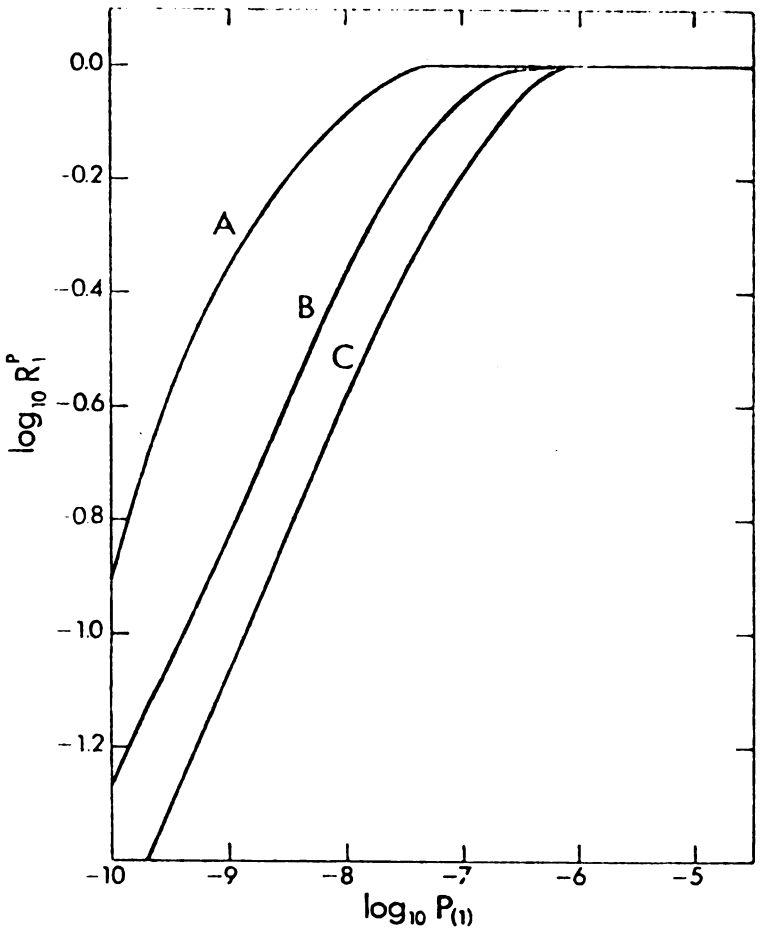

Figure 5.10. Effect of K on R_1^p at small extents of reaction. K = 10^{-2}(A), 10^{-1}(B), 1.0(C), 10.0(B). For all curves, $\mu = 10^{-3}$, $(\lambda/K) = 10^{-3}$, $\gamma[(K/\lambda)-1] = 0$.

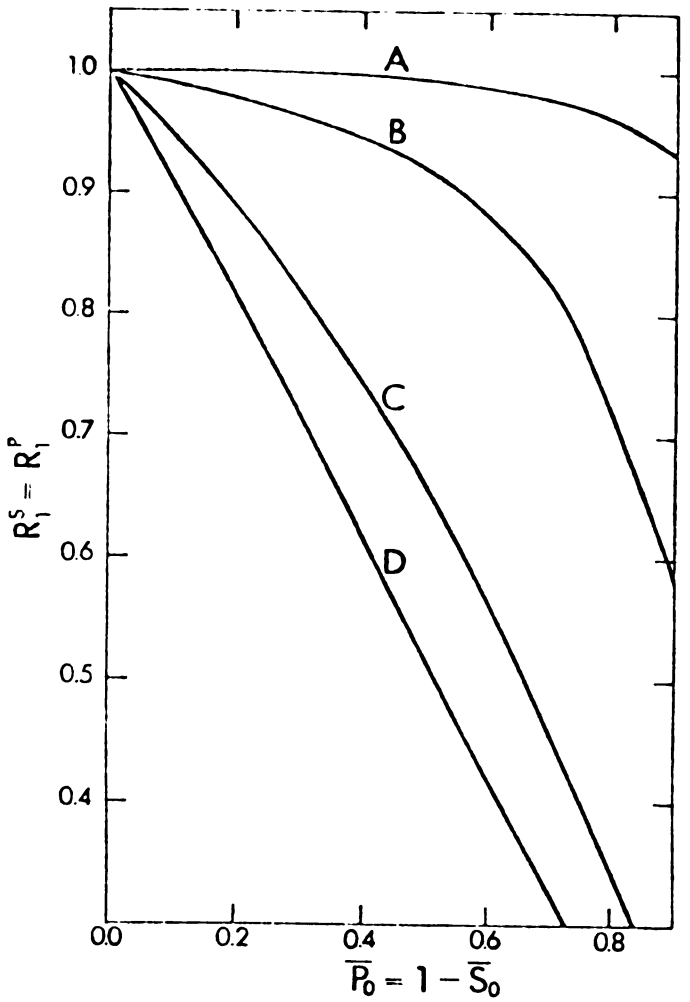

Figure 5.11. Effect of K on R_1^s and R_1^p at large extents of reaction. K = 10^{-2}(A), 10^{-1}(B), 1.0(C), 10.0(D). For all curves $\mu = 10^{-3}$, $(\lambda/K) = 10^{-3}$, $\gamma[(K/\lambda)-1] = 0$.

increasing errors of the Method 1 approximation $[S] \cong [S]_0$ and the Method 2 approximation $\log (1+\gamma) \cong 1+\gamma$ as $[S]_0$ is decreased.

Effect of (λ/K). Figure 5.12 shows the effect of (λ/K) on the initial behavior of R_1^s. The effect on R_2^s is qualitatively the same. As (λ/K) decreases (i.e., as k_1, which is usually unknown, increases), R_1^s starts at higher values, but drops to 1 at an extent of reaction insensitive to (λ/K). Figure 5.13 shows that R_1^P approaches 1 at lower extents of reaction as (λ/K) decreases. R_2^P behaves similarly.

If the reaction is irreversible, Equations (5.58) through (5.61) reduce to

$$R_1^P = R_1^s = \bar{s}_0(1+K)(K+\bar{s}_0)^{-1} \tag{5.62}$$

$$R_2^s = R_2^P = \bar{p}_0(1+K)\,[\bar{p}_0 - K\,\ell n\,(1-\bar{p}_0)]^{-1} \tag{5.63}$$

Since the right hand sides of Equations (5.62) and (5.63) are independent of (λ/K), (λ/K) has no effect on the irreversible reaction after the steady state is obtained if $\mu \leq 10^{-2}$. For high values of μ, however, (λ/K) affects the accuracy of the Michaelis-Menten equations at fairly high extents of reaction, as illustrated in Figure 5.14 for R_1^s.

If the reaction is reversible, (λ/K) affects even the steady-state results of Equations (5.58) through (5.61).

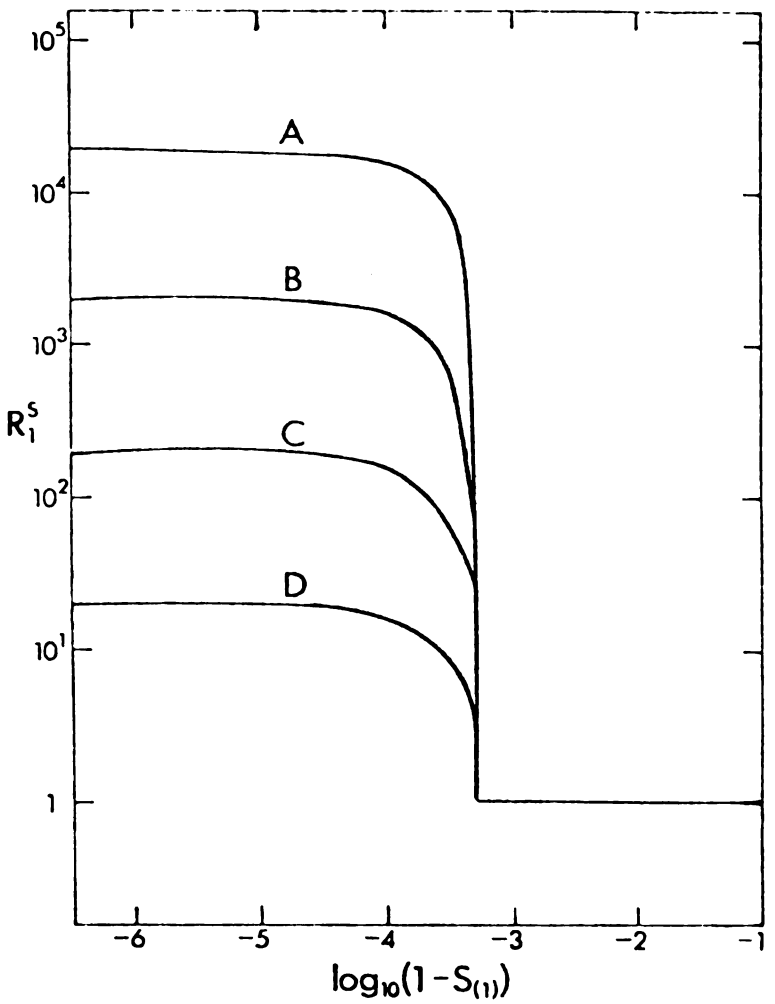

Figure 5.12. Effect of (λ/K) on R_1^s at small extents of reaction. $(\lambda/K) = 10^{-4}$(A), 10^{-3}(B), 10^{-2}(C), 10^{-1}(D). For all curves $\mu = 10^{-3}$, $K = 1.0$, $\gamma[(K/\lambda)-1] = 0$.

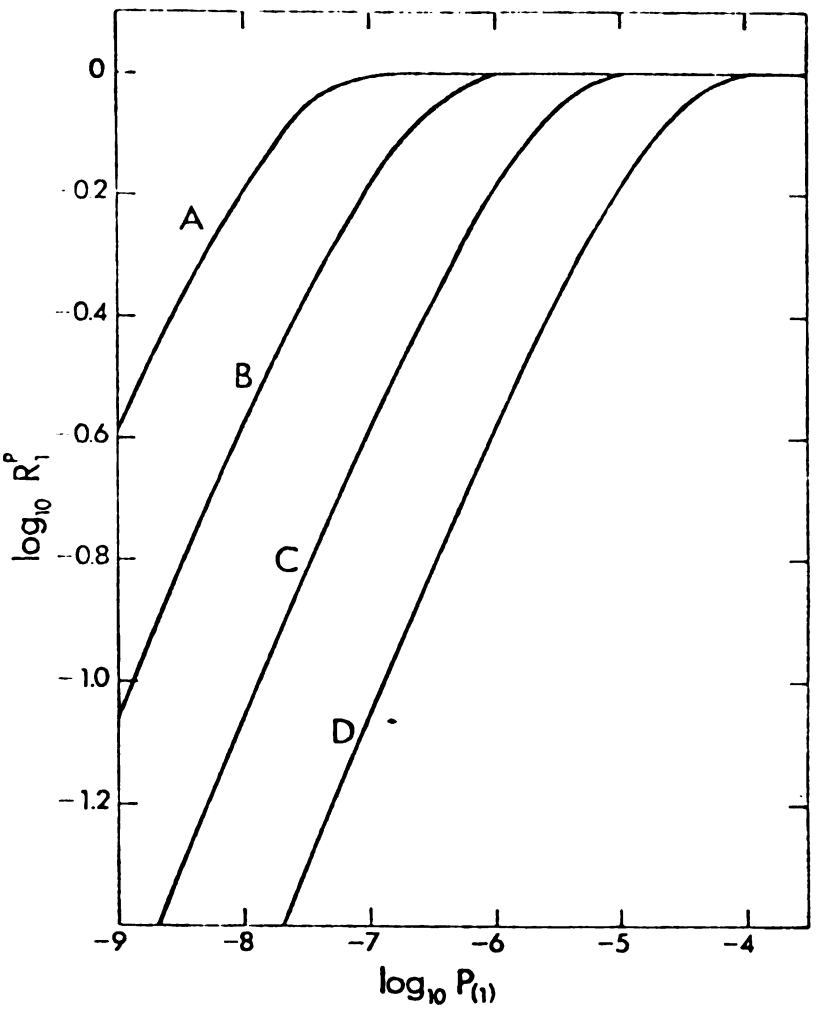

Figure 5.13. Effect of (λ/K) on R_1^p at small extents of reaction. $(\lambda/K) = 10^{-4}$(A), 10^{-3}(B), 10^{-2}(C), 10^{-1}(D). For all curves $\mu = 10^{-3}$, $K = 1.0$ $\gamma[(K/\lambda)-1] = 0$.

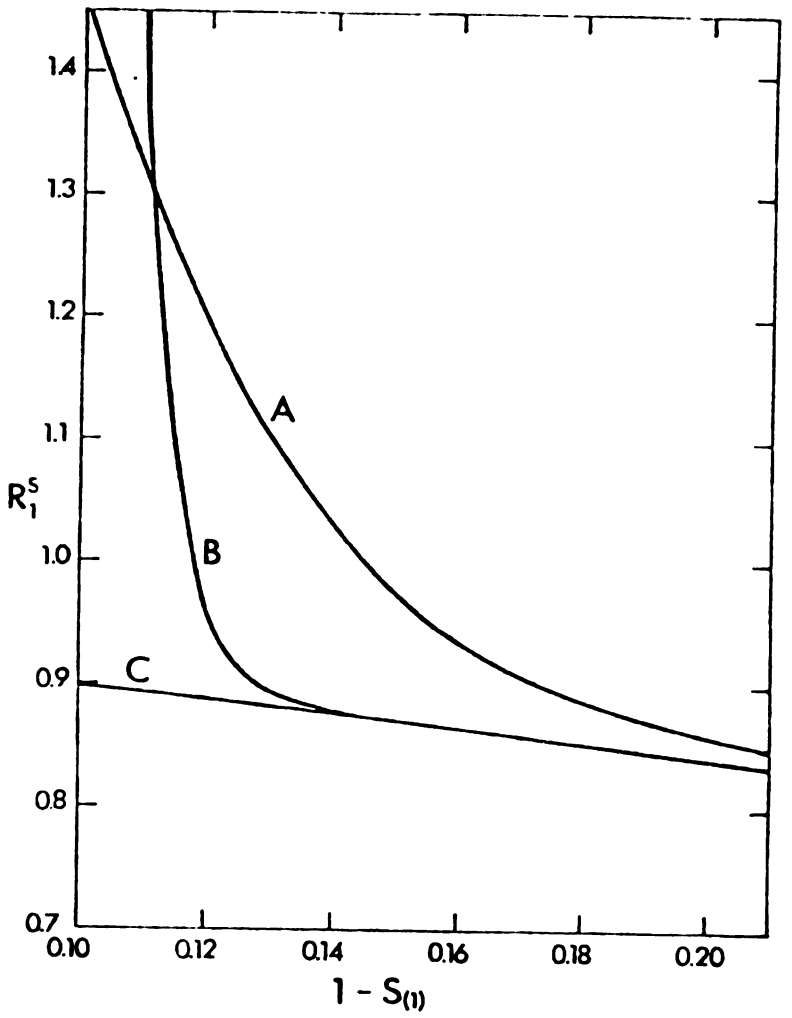

Figure 5.14. Effect of (/K) on R_1^s at large extents of reaction for $\mu = 0.2$ $(\lambda/K) = 0.5$(A), 0.1 (B), 0.01(C). For all curves K = 1.0, $\mu = 0.2$, $\gamma[(K/\lambda)-1] = 0$.

Figure 5.15 shows that as (λ/K) increases, R_1^s and R_1^P decrease faster with increasing extent of reaction.

Effect of $\gamma[(K/\lambda)-1] = K_{eq}^{-1}$. $\gamma[(K/\lambda)-1]$ does not significantly affect the pre-steady-state accuracy of the Michaelis-Menten equation. Figure 5.16 illustrates the effect of $\gamma[(K/\lambda)-1]$ on R_1^s and R_1^P during the steady-state period for small μ, where Equations (5.58) through (5.61) apply. The effect on R_2^s and R_2^P is similar.

D. Discussion

In the preceding section we have examined the accuracy of the Michaelis-Menten equation for Mechanism (I). The following recommendations can be formulated from the results.

1. For the usual initial velocity study, where $\mu \leq 10^{-2}$, the Michaelis-Menten equation predicts Method 1 substrate and product initial velocities and Method 2 product initial velocities most accurately at extents of reaction slightly greater than μ. At other extents of reaction, the equation for R_1^s, R_1^P, or R_2^P can be used to correct the measured initial velocities so that the Michaelis-Menten equation can still be used to interpret the results. For example, the Michaelis-Menten equation initial velocity can be calculated from a Method 1 initial substrate velocity by the equation

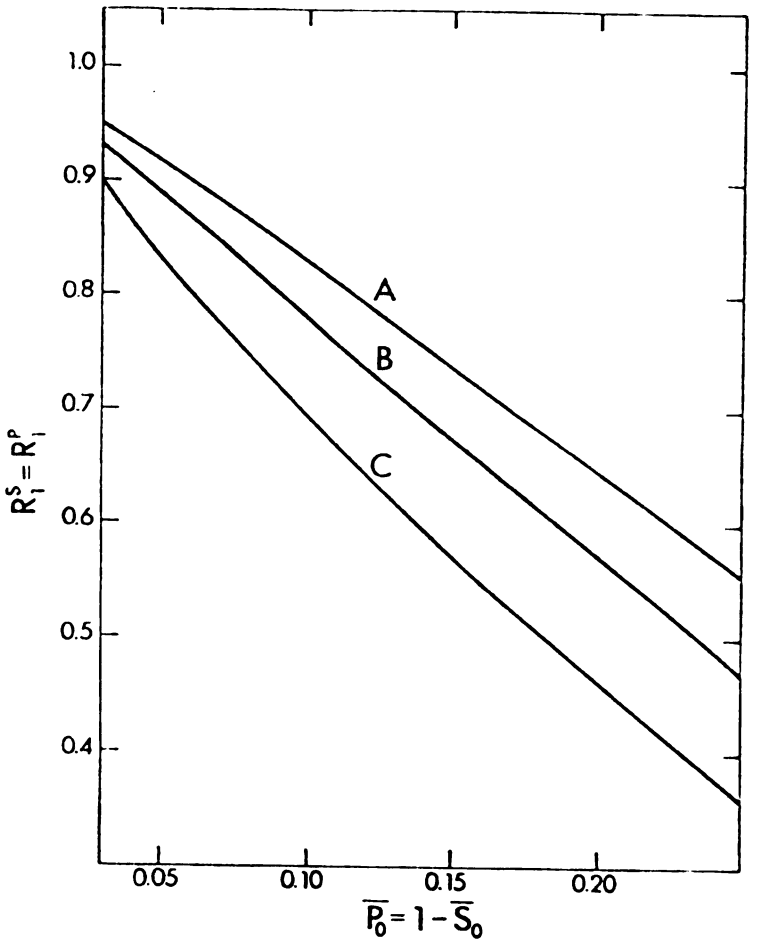

Figure 5.15. Effect of (λ/K) on R_1^s and R_1^p at large extents of reaction where $k-2 \neq 0$. $(\lambda/K) = 0.2(A)$, $0.6(B)$, $0.8(C)$. For all curves $\mu = 10^{-3}$, $K = 1.0$, $\gamma[(K/\lambda)-1] = K_{eq}^{-1} = 1.0$.

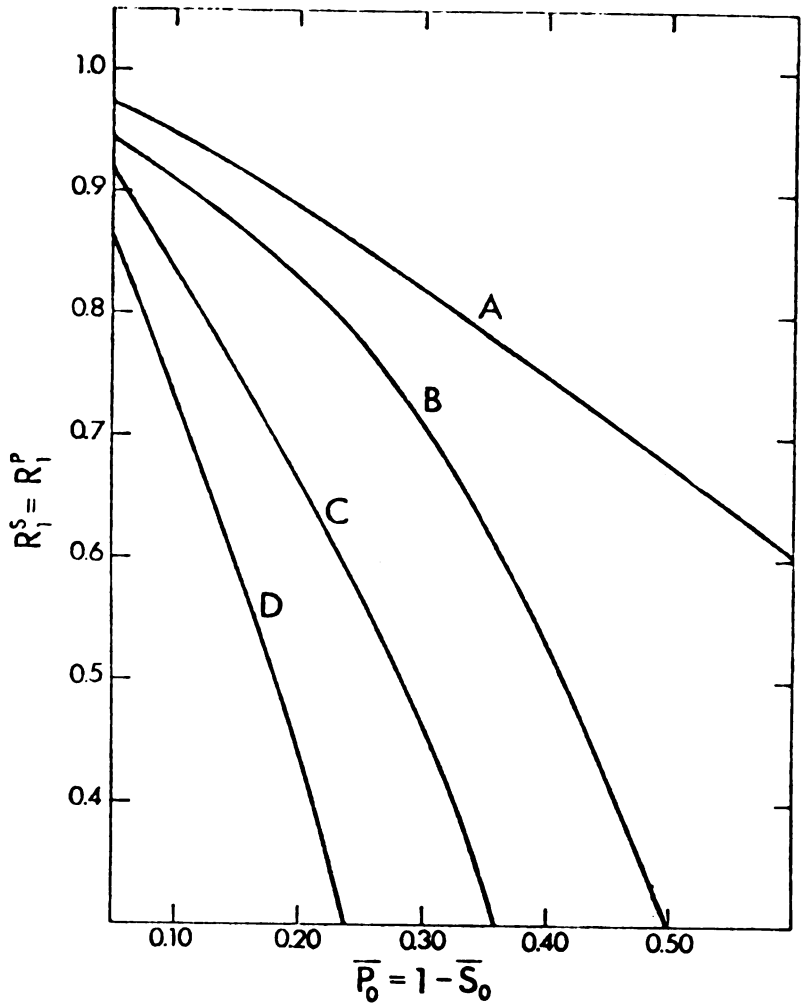

Figure 5.16. Effect of $\gamma[(K/\lambda)-1] = K_{eq}^{-1}$ on R_1^s and R_1^p at large extents of reaction. $\gamma[(K/\lambda)-1] = K_{eq}^{-1} = 0.0(A), 0.50(B), 0.99(C), 1.98(D)$.

$$v_{mm} = R_1^s \times \text{(measured initial velocity)}$$

For extents of reaction less than μ, R_1^s, R_1^P, and R_2^P should be calculated from Equations (5.46), (5.47), and (5.48) using the full first order solutions in Appendix H. At high extents of reaction where $\mu \leq 10^{-2}$, Equations (5.58) and (5.59) can be used.

2. Method 2 initial substrate velocities require the full first order perturbation solutions for extents of reaction less than μ. One can use the simplified Equation (5.57) for extents of reaction slightly greater than μ. Equation (5.61) holds at high extents of reaction where $\mu \leq 10^{-2}$.

3. For μ significantly larger than 10^{-2} but less than 0.2, the full first order perturbation solutions in Appendix H should be used.

Since the first order perturbation solutions in Appendix H depend on all four rate constants in the simple Michaelis-Menten Mechanism (I), experiments that require the perturbation solutions are richer with information than experiments that require only the Michaelis-Menten equation. The full first order solutions do not lend themselves to graphical analysis as easily as the Michaelis-Menten equation. However, nonlinear least squares curvefitting programs such as the KINFIT program (Dye and Nicely, 1971) make graphical fitting unnecessary. The entire substrate or product progress curve can be fit to the equations in Appendix H.

All that is required are the equations, enough smooth data to determine the parameters in the equations, and reasonable initial estimates of the parameters.

Heineken, Tsuchiya and Aris (1967) have shown how the singular perturbation formalism can be extended to more complicated enzyme mechanisms. By combining singular perturbation solutions with non-linear least squares fitting, pre-steady-state experiments, such as those of Maguire, Hijazi and Laidler (1974) on α-chymotrypsin catalyzed reactions of pseudosubstrates, can be expanded to full time course experiments covering the steady-state period as well. Furthermore, one is not restricted to $([E]_0/[S]_0) \leq 10^{-2}$, as with the Michaelis-Menten equation. This is particularly advantageous when larger $([E]_0/[S]_0)$ ratios are needed to observe directly enzyme-substrate and enzyme-product complexes, as in some experiments with horse liver alcohol dehydrogenase (Shore and Gutfreund, 1970; Bernhard, Dunn, Luisi, and Shack, 1970).

CHAPTER 6

SUGGESTIONS FOR FURTHER WORK

This chapter contains two sections: (A) suggestions for further experiments on the LADH-NADH-NDMA system, and (B) suggestions for the further development of principal component analysis in kinetics. The numerical order within each section is arbitrary and does not represent priorities.

A. LADH-NADH-NDMA System

1. In any experiment with LADH, assay each LADH preparation for ethanol (or any other reductant of NADH). Mix NAD^+ and the LADH preparation and measure the growth of NADH. The concentration of LADH in the assay should be $\sim$(5-15) μN, the concentration range used in transient phase experiments. Assay NDMA for reductants of NAD^+ by mixing NDMA, NAD^+ and a low concentration of LADH ($\sim 10^{-3}$ μN).

2. Perform scanning kinetics experiments with low initial concentrations of LADH ($<10^{-1}$ μN) and high initial concentrations of NADH and NDMA ($\sim$10-20 μM). Determine by principal component analysis whether the same intermediates are observed under these conditions as in the high LADH concentration experiments of Chapter 4. If the same

intermediates are present and reach approximately the same absorbance levels in high and low enzyme concentration experiments, they may be intermediates of substrates and products without enzyme.

3. Use principal component analysis to study the changes in the absorbance spectra of NADH, LADH, and NAD^+ in mixtures of these species. How many enzyme-bound species occur in the 340 nm - 320 nm NADH shift? Does NADH or NAD^+ perturb the absorbance spectrum of LADH at 280 nm? Since the spectra of NADH, NAD^+ and LADH are broad and highly overlapping in the range 250 nm - 300 nm, the latter question cannot be conclusively answered by simple difference spectra such as used by Fisher, Adija, and Cross (1969). It is ideally suited for attack by principal component analysis.

4. Investigate by rapid scanning stopped flow experiments with principal component analysis whether the spectrum of LADH is perturbed during the reduction of acetaldehyde by NADH.

5. Perform rapid scanning experiments with the same initial concentrations of LADH-NADH-NDMA for which Dunn and Bernhard (1971) proposed the "half-of-the-sites reactivity mechanism". Resolve the 400 nm - 480 nm range via principal component analysis, and determine whether the resolved NDMA concentrations agree with the "half-of-the-sites reactivity mechanism".

6. Add various initial concentrations of NAD^+ to the

LADH-NADH-NDMA reactions system in scanning stopped flow experiments. How does NAD^+ affect the amounts and rates of the intermediates that grow without NAD^+? Do new absorbers appear?

7. Determine whether LADH, NDMA, and NAD^+ form a complex with an absorbance spectrum distinguishable from the free species. If they do, may this intermediate be related to Absorber 3 ($X_{320,403}$) assuming Scheme 3 in Chapter 4?

8. Proceed to Step 4 of the strategy of Figure 1.1, but only after performing additional scanning experiments resolved via principal component analysis.

B. Principal Component Analysis

1. Derive confidence interval statistical criteria for determining the essential ranks of $\underline{M}_W$ and $\underline{S}_W$. To do this, the probability distribution must be deduced for the eigenvalues and eigenvectors given a probability distribution of the random measurement errors. Anderson (1963) should provide assistance. Addition of confidence interval testing would make the principal component description of an ideal experiment (*i.e.*, one with the assumed probability distribution for its errors) more complete. However, since real experiments are never ideal, the examination of plots of $\hat{\underline{A}}_{(r)}$ and $\underline{A}$ will continue to be most useful for determining the essential ranks.

2. Devise a weighting scheme for principal component analysis of experiments with arbitrary measurement error variances σ_{ij}^2 (see comments at end of Appendix C).

3. Derive a statistical criterion to help decide when a proposed static spectrum or concentration profile fits an experiment. The requirements for the derivation of this criterion are similar to those for the confidence interval statistical criteria mentioned in suggestion B.1 above.

4. Derive solution bands for the normalized static spectra and concentration profiles of three or more absorbers analogous to the solution bands for two absorbers presented in Chapter 3. With three or more absorbers, obtaining the solution bands may require nonlinear optimization.

5. Apply principal component analysis to rapid scanning fluorescence kinetics experiments.

APPENDICES

APPENDIX A

Demonstration that $\hat{\underline{A}}_{(r_M)} = \underline{A}$ For an Errorless Experiment

In this appendix we show that, for an errorless experiment, $\hat{\underline{A}}_{(4)}$ defined by Equation (2.4)

$$\hat{\underline{A}}_{(r)} = \underline{\Phi}_{(r)} \underline{\Phi}^{T}_{(r)} \underline{A} \tag{2.4}$$

is an exact reconstruction of the experimental absorbance matrix $\underline{A}$ when r equals r_M, the rank of $\underline{M}$; i.e., we derive the equation

$$\underline{A} = \underline{\Phi}_{(r_M)} \underline{\Phi}^{T}_{(r_M)} \underline{A} \tag{A.1}$$

By similar reasoning, one can show that Equations (2.9), (2.25), and (2.26) give exact reconstructions of the experimental absorbance matrix for an errorless experiment when r equals the rank of $\underline{S}$, $\underline{M}_W$, and $\underline{S}_W$, respectively.

Recall that in Chapter 2, Section B, we introduced the second moment matrix of $\underline{A}$ as $\underline{M}$, defined by Equation (2.2) as

$$\underline{M} = (1/N) \underline{A} \underline{A}^{T} \tag{2.2}$$

and that we considered the eigenvalue equations

$$\underline{M}\,\underline{\phi}_j = \underline{\phi}_j \delta_j, \quad j = 1,2,\ldots,p \tag{A.3}$$

where $\delta_1 \geq \delta_2 \geq \ldots \geq \delta_p$, and

$$\underline{\phi}_j^T \underline{\phi}_j = 1, \quad \underline{\phi}_j^T \underline{\phi}_k = 0, \text{ if } j \neq k$$

Here we shall be more specific and call $\underline{M}$ the outer second moment matrix of $\underline{A}$. The inner second moment matrix of $\underline{A}$ is called $\underline{M}'$, and is defined by the equation

$$\underline{M}' = (1/p)\underline{A}^T\underline{A} \tag{A.4}$$

The eigenvalue equations for $\underline{M}'$ are

$$\underline{M}'\underline{\psi}_j = \underline{\psi}_j \gamma_j, \quad j = 1,2,\ldots,N \tag{A.5}$$

where $\gamma_1 \geq \gamma_2 \geq \ldots \geq \gamma_N$, and

$$\underline{\psi}_j^T \underline{\psi}_j = 1, \quad \underline{\psi}_j^T \underline{\psi}_k = 0 \text{ if } j \neq k.$$

As byproducts of deriving Equation (A.1) we shall obtain the relationships between the eigenvectors and eigenvalues of $\underline{M}$ and $\underline{M}'$.

Define a matrix $\underline{Y}$ by the equation

$$\underline{Y}^{[(N+p)\times(N+p)]} = \begin{bmatrix} \underline{0}^{(N\times N)} & \underline{A}^{T(N\times p)} \\ \underline{A}^{(N\times p)} & \underline{0}^{(p\times p)} \end{bmatrix} \tag{A.6}$$

and consider its associated eigenvalue equations

$$\underline{Y}\ \underline{\theta}_j = \underline{\theta}_j\ \omega_j, \quad j = 1,2,\ldots(N+p) \tag{A.7}$$

where $\omega_1 \geq \omega_2 \geq \cdots \underline{\omega}_{(N+p)}$ and

$$\underline{\theta}_j^T\underline{\theta}_j = 2, \quad \underline{\theta}_j^T\underline{\theta}_k = 0 \text{ if } j \neq k$$

We partition each eigenvector $\underline{\theta}_j$ by the equation

$$\underline{\theta}_j^{[(N+p)\times 1]} = \begin{bmatrix} \underline{\psi}_j''^{(N\times 1)} \\ \underline{\psi}_j''^{(p\times 1)} \end{bmatrix} \tag{A.8}$$

where the double prime symbol is used at this point to distinguish $\underline{\psi}_j''$ from $\underline{\psi}_j$ and $\underline{\phi}_j''$ from $\underline{\phi}_j$. In expanded form, Equation (A.7) becomes

$$\begin{bmatrix} \underline{0}^{(N\times N)} & \underline{A}^{T(N\times p)} \\ \underline{A}^{(p\times N)} & \underline{0}^{(p\times p)} \end{bmatrix} \begin{bmatrix} \underline{\psi}_j''^{(N\times 1)} \\ \underline{\phi}_j''^{(p\times 1)} \end{bmatrix} = \begin{bmatrix} \underline{\psi}_j''^{(N\times 1)} \\ \underline{\phi}_j''^{(p\times 1)} \end{bmatrix} \omega_j \tag{A.9}$$

$$, \quad j = 1,2,\ldots,(N+p)$$

Upon multiplication of the matrices, Equation (A.9) reduces to the pair of equations

$$\underline{A}^T \underline{\phi}_j'' = \underline{\psi}_j'' \omega_j \qquad (A.10)$$

$$j = 1,2,\ldots(N+p)$$

$$\underline{A}\ \underline{\psi}_j'' = \underline{\phi}_j'' \omega_j \qquad (A.11)$$

Multiplying Equation (A.11) by (ω_j/N), we obtain

$$(1/N)\underline{A}(\underline{\psi}_j''\omega_j) = \underline{\phi}_j''(\omega_j^2/N). \qquad (A.12)$$

When the L.H.S. of Equation (A.10) is substituted for the quantity $(\underline{\psi}_j''\omega_j)$ in Equation (A.12), we obtain

$$[(1/N)\underline{A}\ \underline{A}^T]\underline{\phi}_j'' = \underline{\phi}_j'' = \underline{\phi}_j''(\omega_j^2/N) \qquad (A.13)$$

By comparing Equation (A.13) to Equation (A.3) and noting that $[(1/N)\underline{A}\ \underline{A}^T] = \underline{M}$, we obtain the following relationships

$$\underline{\phi}_j'' = \underline{\phi}_j \qquad (A.14)$$

$$(\omega_j^2/N) = \delta_j \qquad j = 1,2,\ldots,p \qquad (A.15)$$

Similar steps starting with Equation (A.10) give the relationships

$$\underline{\Psi}_j'' = \underline{\Psi}_j \qquad j = 1,2,\ldots,N \tag{A.16}$$

$$(\omega_j^2/p) = \gamma_j \tag{A.17}$$

Thus, the nonzero eigenvalues of $\underline{M}$ and $\underline{M}'$ are related by the equation

$$(\delta_j/\gamma_j) = (p/N) \tag{A.18}$$

Equations (A.10), (A.11), (A.14) and (A.16) give for nonzero ω_j the following relationships between the eigenvectors of $\underline{M}$ and $\underline{M}'$

$$\underline{\Psi}_j = (1/\omega_j)\ \underline{A}^T \underline{\Phi}_j \tag{A.19}$$

$$\underline{\Phi}_j = (1/\omega_j)\ \underline{A}\ \underline{\Psi}_j \tag{A.20}$$

In general, p and N are not the same, but both must be larger than r_M if principal component analysis is to be used to determine the minimum number of absorbers in the experiment. Introduce an integer k, whose value depends on which of p or N is larger

$$k \begin{cases} = p \text{ if } p \leq N \\ = N \text{ if } p > N \end{cases} \tag{A.21}$$

With Equations (A.14), (A.16), and (A.21), we can write Equations (A.10) and (A.11) as

$$\underline{A}^T \underline{\Phi}_{(k)} = \underline{\Psi}_{(k)} \underline{\Omega}_{(k)} \tag{A.22}$$

$$\underline{A} \underline{\Psi}_{(k)} = \underline{\Phi}_{(k)} \underline{\Omega}_{(k)} \tag{A.23}$$

where

$$\underline{\Phi}_{(k)} = (\underline{\phi}_1, \underline{\phi}_2, \ldots, \underline{\phi}_k) \tag{A.24}$$

$$\underline{\Psi}_{(k)} = (\underline{\psi}_1, \underline{\psi}_2, \ldots, \underline{\psi}_k) \tag{A.25}$$

$$\underline{\Omega}_{(k)} = \text{diag}(\omega_1, \omega_2, \ldots, \omega_k) \tag{A.26}$$

For the case where k equals N, right sided multiplication of Equation (A.23) by $\underline{\Psi}^T_{(k)}$ gives the result

$$\underline{A} = \underline{\Phi}_{(k)} \underline{\Omega}_{(k)} \underline{\Psi}^T_{(k)} \tag{A.27}$$

For the case where k equals p, right sided multiplication of Equation (A.22) by $\underline{\Phi}^T_{(k)}$, followed by transposition of the results, also gives Equation (A.27). Since only the first r_M eigenvalues of $\underline{M}$ or $\underline{M}'$ are nonzero, we have, using Equation (A.15)

$$\omega_{r_{M+1}}, \omega_{r_{M+2}}, \ldots, \omega_k = 0 \tag{A.28}$$

Therefore, Equation (A.27) can be reduced to

$$\underline{A} = \underline{\Phi}(r_M)\ \underline{\Omega}(r_M)\underline{\Psi}^T(r_M) \tag{A.29}$$

where

$$\underline{\Omega}(r_M) = \text{diag}\ (\omega_1,\omega_2,\ldots,\omega_{r_M}) \tag{A.30}$$

From Equation (A.22), we have

$$\underline{\Omega}(r_M)\ \underline{\Psi}^T(r_M) = \underline{\Phi}^T(r_M)\underline{A} \tag{A.31}$$

which substituted into Equation (A.29) gives

$$\underline{A} = \underline{\Phi}^T(r_M)\ \underline{\Phi}^T(r_M)\ \underline{A} \tag{A.32),A.1}$$

Thus, for an errorless experiment $\hat{\underline{A}}(r)$ defined by Equation (2.4) equals $\underline{A}$ when r equals r_M.

Moreover, Equations (A.22) and (A.23) can be used to derive the following identities, which are used in Chapter 3, and hold for any value of r

$$\hat{\underline{A}}(r) = \underline{\Phi}(r)\ \underline{\Phi}^T(r)\ \underline{A} \tag{A.33}$$

$$= \underline{A}\ \underline{\Psi}(r)\ \underline{\Psi}^T(r) \tag{A.34}$$

$$= \underline{\Phi}(r)\ \underline{\Omega}(r)\ \underline{\Psi}^T(r) \tag{A.35}$$

APPENDIX B

The Least Squares Significance of $\hat{\underline{A}}_{(r)}$

This appendix demonstrates the least squares significance of $\hat{\underline{A}}_{(r)}$, the r principal component reconstruction of $\underline{A}$, defined by

$$\hat{\underline{A}}_{(r)} = \underline{\Phi}_{(r)} \underline{\Phi}^{T}_{(r)} \underline{A} \qquad (2.4)$$

Specifically, we show that $\hat{\underline{A}}_{(r)}$ is, in an ordinary least squares sense, the best fit of the experimental matrix $\underline{A}$ that can be constructed by taking a linear combination of the first r eigenvectors of $\underline{M}$. This result is valid for any value of r, and does not require that the experimental matrix $\underline{A}$ be errorless. The least squares significance of Equations (2.9), (2.25), and (2.26) can be demonstrated by the same reasoning used here to demonstrate the least squares significance of Equation (2.4).

We construct a model absorbance matrix called $\underline{Y}_{(r)}$, where each column of $\underline{Y}_{(r)}$ is a linear combination of the first r eigenvectors of $\underline{M}$. The matrix $\hat{\underline{A}}_{(r)}$ is obtained as the particular value of $\underline{Y}_{(r)}$ that is the best ordinary least squares fit of the experimental matrix $\underline{A}$.

We partition $\underline{A}$, $\underline{Y}_{(r)}$ and $\hat{\underline{A}}_{(r)}$ into column vectors, as

follows

$$\underline{A} = (\underline{A}_1, \underline{A}_2, \ldots, \underline{A}_N) \tag{B.1}$$

$$\underline{Y}_{(r)} = (\underline{Y}_{(r)_1}, \underline{Y}_{(r)_2}, \ldots, \underline{Y}_{(r)_N}) \tag{B.2}$$

$$\hat{\underline{A}}_{(r)} = (\hat{\underline{A}}_{(r)_1}, \hat{\underline{A}}_{(r)_2}, \ldots, \hat{\underline{A}}_{(r)_N}) \tag{B.3}$$

The j'th vector $\underline{Y}_{(r)_j}$ is given by the linear model

$$\underline{Y}_{(r)_j} = \underline{\Phi}_{(r)}\ \underline{B}_j,\ j = 1,2,\ldots,N \tag{B.4}$$

where $\underline{B}_j$ is a vector of coefficients whose values are as yet unspecified. The ordinary least squares loss function that relates the models vector $\underline{Y}_{(r)_j}$ to the experimental vector $\underline{A}_j$ is Q_j, defined by

$$Q_j = (\underline{A}_j - \underline{\Phi}_{(r)}\underline{B}_j)^T(\underline{A}_j - \underline{\Phi}_{(r)}\underline{B}_j) \tag{B.5}$$

Define $\hat{\underline{A}}_{(r)_j}$ by the equation

$$\hat{\underline{A}}_{(r)_j} = \underline{\Phi}_{(r)}\ \underline{b}_j, \quad j = 1,2,\ldots,N \tag{B.6}$$

where $\underline{b}_j$ is the particular value of $\underline{B}_j$ in Equation (B.4) that minimizes Q_j; i.e., $\underline{b}_j$ is the ordinary least squares estimate of $\underline{B}_j$ obtained by fitting the model absorbances $\underline{Y}_{(r)_j}$ to the experimental absorbances $\underline{A}_j$.

To minimize Q_j with respect to $\underline{B}_j$, we first operate on Equation (B.4) with $\underline{\nabla}_{B_j}$, defined by

$$\underline{\nabla}_{B_j} = \begin{bmatrix} \partial/\partial B_{j_1} \\ \partial/\partial B_{j_2} \\ \partial/\partial B_{j_r} \end{bmatrix} \tag{B.7}$$

We obtain

$$\underline{\nabla}_{B_j} Q_j = 2[\underline{\nabla}_{B_j}(\underline{A}_j - \underline{\Phi}_{(r)}\underline{B}_j)][\underline{A}_j - \underline{\Phi}_{(r)}\underline{B}_j]$$

$$= -\underline{\Phi}^T_{(r)}(\underline{A}_j - \underline{\Phi}_{(r)}\underline{B}_j) \qquad j = 1,2,\ldots N \tag{B.8}$$

Q_j is minimized with respect to $\underline{B}_j$ when $\underline{\nabla}_{B_j} Q_j = \underline{0}$. Setting $\underline{\nabla}_{B_j} Q_j$ equal to $\underline{0}$ and substituting $\underline{b}_j$ for $\underline{B}_j$, we obtain

$$\underline{0} = -\underline{\Phi}^T_{(r)}\underline{A}_j + \underline{\Phi}_{(r)}\underline{\Phi}^T_{(r)}\,\underline{b}_j, \quad j = 1,2,\ldots,N \tag{B.9}$$

Multiplying Equation (B.9) by $(\underline{\Phi}^T_{(r)}\underline{\Phi}_{(r)})^{-1}$ and rearranging, we obtain for $\underline{b}_j$

$$\underline{b}_j = (\underline{\Phi}^T_{(r)}\underline{\Phi}_{(r)})^{-1}\underline{\Phi}^T_{(r)}\underline{A}_j, \quad j = 1,2,\ldots,N \tag{B.10}$$

By the orthonormality of the eigenvectors of $\underline{M}$, we have $(\underline{\Phi}^T_{(r)}\underline{\Phi}_{(r)})^{-1} = \underline{I}$, so that Equation (B.10) can be

simplified to

$$\underline{b}_j = \underline{\Phi}^T_{(r)}\underline{A}_j, \quad j = 1,2,\ldots,N \qquad \text{(B.11)}$$

Substituting $\underline{b}_j$ from Equation (B.11) into Equation (B.9), we obtain for the j'th column of $\hat{\underline{A}}_{(r)}$ the equation

$$\hat{\underline{A}}_{(r)_j} = \underline{\Phi}_{(r)}\underline{\Phi}^T_{(r)}\underline{A}_j, \quad j = 1,2,\ldots,N \qquad \text{(B.12)}$$

Therefore, $\hat{\underline{A}}_{(r)}$, the ordinary least squares reconstruction of $\underline{A}$ using the first r eigenvectors of $\underline{M}$ is given by the equation

$$\hat{\underline{A}}_{(r)} = \underline{\Phi}_{(r)}\underline{\Phi}^T_{(r)}\underline{A} \qquad \text{(B.1),(2.4)}$$

APPENDIX C

Expected Values, Variances, Covariances, and Weights for Principal Component Analysis

This appendix amplifies the discussion of error models and weights in Sections D and E of Chapter 2. After reviewing the definitions and some properties of expected values, variances, and covariances of random variables, we derive Equation (2.27) and discuss its significance.

The following background material concerning expected values, variances, and covariances, is taken from Chapter 2 of Beck and Arnold (1975). These concepts are also discussed in most mathematical statistics textbooks and their significance in principal component analysis is discussed in the paper by Anderson (1963) and the multivariate statistics textbooks of Anderson (1958) and Morrison (1967).

The expected value of a discrete random variable X is denoted by E(X), and is defined as the sum of the products of all possible values of X with their individual probabilities. If X can take on only n discrete values, (x_i, i = 1,2,...,n), E(X) is defined by

$$E(X) = \sum_{i=1}^{n} x_i P(X=x_i) \qquad (C.1)$$

where $P(X=x_i)$ is the probability that X has the value x_i. If X is a continuous variable, then E(X) is defined by

$$E(X) = \int_{-\infty}^{+\infty} xf(x)dx \qquad (C.2)$$

where f(x) is the probability density function of X. The expected value of X has the following significance: if we were to measure independently the value of X a large number of times, we would expect the arithmetic average of these independent measurements to approach the value E(X) as the number of measurement increases. In the words of Beck and Arnold (1975), E(X) is an "idealization of an arithmetic average".

The Operator E( ) has the following three important properties:

1. E( ) is a linear operator. Hence,

$$E(X+Y) = E(X) + E(Y)$$

2. E( ) leaves unchanged any constants or nonrandom variables. Thus, if X is a random variable, K is a constant, and F is a nonrandom variable, we have

$$E(K) = K$$
$$E(KX) = KE(X)$$
$$E(F) = F$$
$$E(FX) = FE(X)$$

3. If two random variables X and Y are uncorrelated, then

$$E(XY) = [E(X)][E(Y)]$$

The variance of X, denoted var(X), is defined by

$$\text{var}(X) = E[(X - E(X))^2] = \sigma_X^2 \qquad (C.3)$$

where σ_X is the standard deviation of X. Equation (C.3) can be simplified to

$$\text{var}(X) = E(X^2) - [E(X)]^2 \qquad (C.4)$$

Unlike E( ), var( ) is <u>not</u> a linear operator. Equation (C.3) shows the important property that, if X is real,

$$\text{var}(X) \geq 0.$$

The covariance of two random variables X and Y, denoted cov(X,Y), is defined by

$$\text{cov}(X,Y) = E[(X-E(X))(Y-E(Y))] \qquad (C.5)$$

Equation (C.5) can be simplified to

$$\text{cov}(X,Y) = E(XY) - [E(X)][E(Y)] \qquad (C.6)$$

Thus, if X and Y are uncorrelated random variables, cov(X,Y) = 0. Comparison of Equations (C.3) and (C.6) reveals that the variance of X is actually the covariance of X with itself

$$\text{var}(X) = \text{cov}(X,X)$$

The covariance operator is not a linear operator.

In Chapter 2, Section D, we introduced the following model for the measured absorbance matrix $\underline{A}$

$$\underline{A} = \underline{F}\ \underline{C}^T + \underline{\varepsilon} \qquad (C.7)$$

where all the random measurement errors are contained in $\underline{\varepsilon}$, and the matrices $\underline{F}$ and $\underline{C}$ are regarded as nonrandom (errorless). Thus,

$$E(\underline{F}\ \underline{C}^T) = \underline{F}\ \underline{C}^T \qquad (C.8)$$

We assumed that the errors in $\underline{\varepsilon}$ vary randomly about zero; i.e.,

$$E(\underline{\varepsilon}) = \underline{0} \qquad (C.9)$$

We therefore have

$$E(\underline{A}) = \underline{F}\ \underline{C}^T \qquad (C.10)$$

Each measurement error ε_{ij} was assumed to be uncorrelated to all other measurement errors,

$$E(\varepsilon_{ij}\varepsilon_{k\ell}) = 0 \qquad \text{if } i \neq k \text{ or } j \neq \ell \qquad \text{(C.11)}$$

$$\text{cov}(\varepsilon_{ij},\varepsilon_{k\ell}) = 0$$

In general the variance of ε_{ij} is given by

$$\text{var}(\varepsilon_{ij}) = E(\varepsilon_{ij}^2) - [E(\varepsilon_{ij})]^2 = E(\varepsilon_{ij}^2) = \sigma_{ij}^2 \qquad \text{(C.12)}$$

where σ_{ij}^2 may be different for every data point in $\underline{A}$. However, we emphasized the more restricted variance model

$$\text{var}(\varepsilon_{ij}) = \sigma_{ij}^2 = x_i z_j \qquad \text{(C.13)}$$

where σ_{ij}^2 is factorable into a function of the wavelength channel i and a function of the spectrum number j.

The motivation for developing weighted principal component analysis is the observation, shown by the example in Section D of Chapter 2, that, if $\text{var}(\varepsilon_{ij})$ deviates strongly from a single value for all channels and spectra, the random errors in $\underline{\varepsilon}$ can dominate the first few eigenvectors of $\underline{M}$. Consequently, we obtain an incorrect essential rank for $\underline{M}$ by the usual criterion of

reconstructing the absorbance surface. This problem arises because principal component analysis is sensitive to how the observations are scaled. Our model for $\underline{A}$ has a nonrandom part $\underline{F}\,\underline{C}^T$ and a random part $\underline{\varepsilon}$. The goal of the weighting scheme is to scale the observations so that the principal component eigenvectors are dominated as much as possible by the nonrandom part of the model.

We define a weighted absorbance matrix $\underline{A}_W$, given by wh

$$\underline{A}_W = \underline{L}\,\underline{A}\,\underline{T} \tag{C.14}$$

where $\underline{L}$ and $\underline{T}$ are nonsingular and diagonal. Note that $\underline{L}$ scales the rows of $\underline{A}$, that $\underline{T}$ scales the columns of $\underline{A}$, and that the ranks of $\underline{A}_W$ and $\underline{A}$ are the same, since $\underline{L}$ and $\underline{T}$ are nonsingular.

A reasonable criterion for assigning values for the weighting matrices $\underline{L}$ and $\underline{T}$ is to insist that, as the quantity of data increases, the effect of the random errors on the principal component analysis vanishes. Consider performing n independent replicate measurements of the matrix $\underline{A}$. We would have the n matrices, $(\underline{A}_i,\ i = 1,2,\ldots,n)$. The arithmetic average of these n matrices, $\underline{A}_{ave} = (1/n) \sum_{i=1}^{n} \underline{A}_i$ would approach the errorless expected value $E(\underline{A}) = \underline{F}\,\underline{C}^T$ as n becomes very large. However, the principal component reconstructions of $\underline{A}$ that are used to determine the essential rank m are not computed directly from $\underline{A}$, but indirectly, by the equation

$$\hat{\underline{A}}_{(r)} = \underline{L}^{-1}\underline{\Phi}_{(r)}\underline{\Omega}_{(r)}\underline{\Psi}^{T}_{(r)}\underline{T}^{-1} \qquad (C.15)$$

where $\underline{\Phi}_{(r)}$ and $\underline{\Psi}_{(r)}$ contain the eigenvectors of the weighted second moment matrices $\underline{M}_W = (1/N)\underline{A}_W\underline{A}_W^T$ and $\underline{M}'_W = (1/p)\underline{A}_W^T\underline{A}_W$, respectively. Consider computing $\underline{M}_W$ and $\underline{M}'_W$ for each of the n experiments, and then computing the arithmetic averages of the resulting n values of $\underline{M}_W$ and $\underline{M}'_W$. As n becomes very large, the average value of $\underline{M}_W$ would approach $E(\underline{M}_W)$, and the average value of $\underline{M}'_W$ would approach $E(\underline{M}'_W)$. We therefore choose the values of $\underline{L}$ and $\underline{T}$ so that the eigenvectors of $E(\underline{M}_W)$ and $E(\underline{M}'_W)$ are not influenced by the random measurement errors.

The expected value of $\underline{M}_W$ is given by

$$E(\underline{M}_W) = E[(1/N)\underline{A}_W\underline{A}_W^T] \qquad (C.16)$$

which may be expanded and simplified by inserting the definition of $\underline{A}_W$ and using the mathematical properties of the expected value operator. Substituting Equation (C.14) for $\underline{A}_W$, and noting that N is an integer constant, we obtain

$$E(\underline{M}_W) = (1/N)\ E(\underline{L}\ \underline{A}\ \underline{T}^2\ \underline{A}^T\ \underline{L}) \qquad (C.17)$$

Substituting Equation (C.8) for $\underline{A}$ in Equation (C.17) and expanding the result, we obtain

$$E(\underline{M}_W) = (1/N)[E(\underline{L}\ \underline{F}\ \underline{C}^T\underline{T}^2\underline{C}\underline{F}^T\underline{L}) + E(\underline{L}\ \underline{F}\ \underline{C}^T\underline{T}^2\underline{\varepsilon}^T\underline{L})$$

$$+ E(\underline{L}\ \underline{\varepsilon}\ \underline{T}^2\ \underline{C}\ \underline{F}^T\underline{L}) + E\ (\underline{L}\ \underline{\varepsilon}\ \underline{T}^2\ \underline{\varepsilon}^T\ \underline{L})] \qquad (C.18)$$

We now simplify one by one the four terms in Equation (C.18). Since the elements of $\underline{L}$, $\underline{F}$, $\underline{C}$ and $\underline{T}$ are non-random variables, we have

$$\begin{aligned} E(\underline{L}\ \underline{F}\ \underline{C}^T\ \underline{T}^2\ \underline{C}\ \underline{F}^T\ \underline{L}) &= \underline{L}\ \underline{F}\ \underline{C}^T\ \underline{T}^2\ \underline{C}\ \underline{F}^T\ \underline{L} \\ &= \underline{L}\ E(\underline{A})\underline{T}^2E(\underline{A})^T\underline{L} \end{aligned} \qquad (C.19)$$

The second term in Equation (C.18) may be simplified as follows,

$$\begin{aligned} E(\underline{L}\ \underline{F}\ \underline{C}^T\ \underline{T}^2\ \underline{\varepsilon}^T\ \underline{L}) &= \underline{L}\ \underline{F}\ \underline{C}^T\ \underline{T}^2\underline{E}(\underline{\varepsilon}^T\underline{L}) \\ &= \underline{L}\ \underline{F}\ \underline{C}^T\ \underline{T}^2[E(\underline{L}\ \underline{\varepsilon})]^T \\ &= \underline{L}\ \underline{F}\ \underline{C}^T\ \underline{T}^2[\underline{L}\ \underline{E}(\underline{\varepsilon})]^T \\ &= \underline{0} \end{aligned} \qquad (C.20)$$

where $E(\underline{\varepsilon}) = \underline{0}$ was used in the last step. Likewise, the third term in Equation (C.18) is

$$E(\underline{L}\ \underline{\varepsilon}\ \underline{T}^2\ \underline{C}\ \underline{F}^T\ \underline{L}) = \underline{L}\ E(\underline{\varepsilon})\underline{T}^2\underline{C}\ \underline{F}^T\ \underline{L} = \underline{0} \qquad (C.21)$$

Simplifying the fourth term in Equation (C.18) is easier if we consider its i, j'th element. We have

$$E(\underline{L}\ \underline{\varepsilon}\ \underline{T}^2\ \underline{\varepsilon}^T\ \underline{L}) = E(\sum_{k=1}^{N} L_i \varepsilon_{ik} T_k^2 L_j \varepsilon_{jk}) \tag{C.22}$$

$$= L_i L_j \sum_{k=1}^{N} T_k^2\ E(\varepsilon_{ik}\varepsilon_{jk})$$

Since we assumed that the errors are uncorrelated, we have, using Equations (C.11) and (C.12),

$$E(\underline{L}\ \underline{\varepsilon}\ \underline{T}^2\ \underline{\varepsilon}^T\ \underline{L})_{ij} = 0 \text{ if } i \neq j \tag{C.23}$$

$$E(\underline{L}\ \underline{\varepsilon}\ \underline{T}^2\ \underline{\varepsilon}^T\ \underline{L})_{ii} = L_i^2 \sum_{k=1}^{N} T_k^2 \sigma_{ik}^2 \tag{C.24}$$

Thus, $E(\underline{M}_W)$ has been simplified to the sum of two terms

$$E(\underline{M}_W) = (1/N)\ \underline{L}\ E(\underline{A})\ \underline{T}^2 E\ (\underline{A}^T)\ \underline{L} \tag{C.25}$$

$$+ (1/N)\ \text{diag}(L_1^2 \sum_{k=1}^{N} T_k^2\ \sigma_{1k}^2, \ldots, L_p^2 \sum_{k=1}^{N} T_k^2\ \sigma_{kp}^2)$$

The first term arises from the errorless Beer's Law contribution to $\underline{A}$, and the second term arises from the random measurement errors. The analogous derivation for $E(\underline{M}_W')$ gives the result

$$E(\underline{M}_W') = (1/p)\underline{T}\ E(\underline{A}^T)\underline{L}^2 E(\underline{A})\underline{T} \tag{C.26}$$

$$+ (1/p)\ \text{diag}(T_1^2 \sum_{k=1}^{p} L_k^2 \sigma_{k1}^2, \ldots, T_N^2 \sum_{k=1}^{p} L_k^2 \sigma_{kp}^2)$$

Equations (C.25) and (C.26) refer to the general

error variance model, where each σ_{ij}^2 is arbitrary. With the more restricted variance model given by Equation (C.13), we obtain the following simplifications of the sums in Equations (C.25) and (C.26)

$$L_i^2 \sum_{k=1}^{N} T_k^2 \sigma_{ik}^2 = L_i^2 x_i \sum_{k=1}^{N} T_k^2 z_k$$

$$T_j^2 \sum_{k=1}^{p} L_k^2 \sigma_{kj}^2 = T_j^2 z_j \sum_{k=1}^{p} L_k^2 x_k \qquad \text{(C.27)}$$

Note that in Equations (C.27) the quantities under the summation depend only on the index k. Therefore Equation (C.25) and (C.26) can be simplified to

$$E(\underline{M}_W) = (1/N)\, \underline{L}\, E(\underline{A})\, \underline{T}^2 E(\underline{A}^T)\underline{L}$$

$$+ (1/N)\, t_r(\underline{T}^2\underline{Z})\underline{L}^2\underline{X} \qquad \text{(C.28)}$$

and

$$E(\underline{M}_W') = (1/p)\underline{T}\, E(\underline{A}^T)\underline{L}^2\, E(\underline{A}^T)\underline{T}$$

$$+ (1/p)\, t_r(\underline{L}^2\underline{X})\underline{T}^2\underline{Z} \qquad \text{(C.29)}$$

where

$$\underline{X} = \text{diag}(x_1, x_2, \ldots, x_p)$$

$$\underline{Z} = \text{diag}(z_1, z_2, \ldots, z_N)$$

With these simplifications, we can easily choose the values of $\underline{L}$ and $\underline{T}$ so that the eigenvectors of $E(\underline{M}_W)$ and $E(\underline{M}'_W)$ are unperturbed by the random errors. We want the eigenvectors of $E(\underline{M}_W)$ and $E(\underline{M}'_W)$ to be eigenvectors of the errorless terms $(1/N)\underline{L}\ E(\underline{A})\underline{T}^2E(\underline{A}^T)\underline{L}$ and $(1/p)\underline{T}^2E(\underline{A}^T)\underline{L}^2E(\underline{A}^T)\underline{T}$, respectively. Thus, we assign $\underline{L}$ and $\underline{T}$ by the equations

$$\underline{L} = a^{1/2}\underline{X}^{-1/2}$$
$$\underline{T} = b^{1/2}\underline{Z}^{-1/2} \qquad (C.30)$$

where a and b are arbitrary positive constants. (Note that Equation (28) in the paper by Cochran and Horne (1977) should be corrected to agree with Equations (C.30); specifically, $\underline{L}$ and $\underline{T}$ should be defined with the arbitrary constants a and b taken to the positive one half power instead of the negative one half power. These corrections make the definitions of $\underline{L}$ and $\underline{T}$ consistent with the remainder of the paper and with this thesis.) $E(\underline{M}_W)$ and $E(\underline{M}'_W)$ become

$$E(\underline{M}_W) = (ab/N)\underline{X}^{-1/2}E(\underline{A})\underline{Z}^{-1}E(\underline{A}^T)\underline{X}^{-1/2} + ab\underline{I} \qquad (C.31)$$

$$E(\underline{M}'_W) = (ab/p)\underline{Z}^{-1/2}E(\underline{A}^T)\underline{X}^{-1}E(\underline{A})\underline{Z}^{-1/2} + ab\underline{I} \qquad (C.32)$$

where the error terms are reduced to scalar multiples of

the identity matrix in both cases. The eigenvectors of $E(\underline{M}_W)$ and $E(\underline{M}'_W)$ are the eigenvectors of the errorless first terms in Equations (C.31) and (C.32), respectively. This completes the derivation of the weighting scheme of Section E in Chapter 2.

Having successfully assigned the weights for the restricted error variance model, the next question is, given the unrestricted error variance model where σ^2_{ij} is arbitrarily different (but known) for each i and j, can the weights be assigned to accomplish the same purpose for $E(\underline{M}_W)$ and $E(\underline{M}'_W)$? We note that the error terms in Equations (C.25) and (C.26) can be made arbitrary scalar multiples of identity matrices by assigning the values of $\underline{L}$ and $\underline{T}$ to satisfy the following system of equations

$$L_i^2 \sum_{k=1}^{N} T_k^2 \sigma_{ik}^2 = K, \quad i = 1,2,\ldots p$$

$$T_j^2 \sum_{m=1}^{p} L_m^2 \sigma_{mj}^2 = K', \quad j = 1,2,\ldots N \qquad \text{(C.34)}$$

where K and K' are arbitrary real constants. Equations (C.34) form a set of (p+N) nonlinear coupled algebraic equations with (p+N) unknown. Therefore, $\underline{L}$ and $\underline{T}$ can always be chosen to satisfy these equations. However, Equations (C.34) are not restricted to have real roots. In fact, in the simple case where p=3 and N=2, it can be easily shown that T_1 and T_2 must be complex.

Thus, the derivation of a weighting scheme for the general error variance model is an area for future investigation. If the form $\underline{A}_W = \underline{L}\,\underline{A}\,\underline{T}$ is maintained, one may try relaxing the requirement that $\underline{L}$ and $\underline{T}$ be diagonal. However, the form of $\underline{L}$ and $\underline{T}$ must guarantee that they are nonsingular. Otherwise, $\underline{A}_W$ will not have the same rank as $\underline{A}$. An aesthetically pleasing property of principal component analysis that should be maintained in a more general weighting scheme is the unimportance of the order in which the rows and columns of $\underline{A}$ are arranged. When $\underline{L}$ and $\underline{T}$ are diagonal, the exchange of two rows in $\underline{A}$ can be accommodated by exchanging the same two rows in $\underline{L}$, $\underline{M}_W$, and $\underline{\Phi}$. The exchange of two columns of $\underline{A}$ can be accommodated by exchanging the corresponding two rows in $\underline{T}$, $\underline{M}_W'$, and $\underline{\Psi}$. This simplicity would be lost if $\underline{L}$ and $\underline{T}$ were, for example, tridiagonal matrices or upper or lower triangular matrices.

APPENDIX D

Derivation of Solution Bands for Two Absorber Experiments

In this appendix we derive the solution bands of the static spectra and concentration profiles in two absorber experiments. Lawton and Sylvestre (1971) present a derivation of solution bands for the static spectra in multicomponent equilibrium systems. Their derivation is based on geometrical arguments about the two dimensional space of the eigenvestors $\underline{\phi}_1$ and $\underline{\phi}_2$. The derivation presented here is equivalent to theirs, but emphasizes a more algebraical approach. We also extend the results to obtain the upper and lower bounds of the concentration profiles.

First we derive the solution bands for the static spectra. Then by taking advantage of the symmetry of the equation

$$\underline{F}\ \underline{C}^T = \underline{L}^{-1}\underline{\Phi}_{(2)}\underline{\Omega}_{(2)}\underline{\Psi}^T_{(2)}\underline{T}^{-1} \qquad (D.1)$$

we obtain the solution bands for the concentration profiles by inspection of the first results.

We make the following five assumptions to obtain the solution bands for the two static spectra:

1. The static spectra are normalized to unit length.

$$\sum_{i=1}^{p} \hat{f}'_{i1} = 1, \qquad \sum_{i=1}^{p} \hat{f}'_{i2} = 1 \tag{D.2}$$

2. The normalized static spectra $\hat{\underline{f}}'_1$ and $\hat{\underline{f}}'_2$ fit as linearly independent absorbers in the experiment.

$$\hat{\underline{f}}'_1 = (L^{-1}\underline{\Phi}_{(2)})\underline{u}'_1, \quad \hat{\underline{f}}'_2 = (\underline{L}^{-1}\underline{\Phi}_{(2)})\underline{u}'_2 \tag{D.3}$$

$$\hat{\underline{c}}_1 = (\underline{T}^{-1}\underline{\Psi}_{(2)})\underline{v}_1, \quad \hat{\underline{c}}_2 = (\underline{T}^{-1}\underline{\Psi}_{(2)})\underline{v}_2 \tag{D.4}$$

3. The static spectra and concentration profiles contain no negative elements. We have the inequalities

$$\begin{aligned} \hat{\underline{f}}'_1 \geq \underline{0}, \quad \hat{\underline{f}}'_2 \geq \underline{0} \\ \hat{\underline{c}}_1 \geq \underline{0}, \quad \hat{\underline{c}}_2 \geq \underline{0} \end{aligned} \tag{D.5}$$

4. The weighted second moment matrices $\underline{M}_W$ and $\underline{M}'_W$ have all nonnegative elements. This is automatically true if the absorbance matrix $\underline{A}$ has all nonnegative elements.

5. The determinants of $\underline{U}'$ and $\underline{V}$ are positive. This is merely a convention for identifying which absorber is one and which is two, since these determinants change sign when absorbers one and two are switched.

In expanded form, Equations (D.3) are

$$\hat{f}'_{i1} = L_i^{-1}(\phi_{i1}u'_{11} + \phi_{i2}u'_{21}), \quad i = 1,2,\ldots,p \tag{D.6}$$

$$\hat{f}'_{i2} = L_i^{-1}(\phi_{i1}u'_{12} + \phi_{i2}u'_{22}), \quad i = 1,2,\ldots,p \tag{D.7}$$

Deriving the solutions bands for $\hat{f}'_{i1}$ and $\hat{f}'_{i2}$ is equivalent to deriving all the constraints on u'_{11}, u'_{21}, u'_{12}, and u'_{22} that are implied by Assumptions 1 through 5 above.

We start by noting some restrictions on the signs of the eigenvectors of $\underline{M}_W$ and $\underline{M}'_W$. When Assumption 4 above holds, it can be shown that $\underline{\phi}_1$ and $\underline{\psi}_1$ have all nonnegative elements. The orthogonality conditions $\underline{\phi}_1^T\underline{\phi}_2 = 0$ and $\underline{\psi}_1^T\underline{\psi}_2 = 0$ then require that $\underline{\phi}_2$ and $\underline{\psi}_2$ each have a mixture of positive and negative elements.

Let us apply the sign constraints on $\underline{\phi}_1$ and $\underline{\phi}_2$ to Equations (D.6) and (D.7). All values of L_i and ϕ_{i1} are nonnegative, and some values of ϕ_{i2} must be positive and some must be negative. Therefore, for all values of $\hat{f}'_{i1}$ and $\hat{f}'_{i2}$ to be nonnegative, u'_{11} and u'_{12} must be positive. We have

$$u'_{11} > 0 \tag{D.8}$$

$$u'_{12} > 0 \tag{D.9}$$

As yet the signs of u'_{21} and u'_{12} are unspecified. However, the requirement that all values of $\hat{f}'_{11}$ and $\hat{f}'_{12}$ be non-negative gives for u'_{21} and u'_{22} the inequalities

$$-u'_{11} \min_{\phi_{i2}>0}\left(\frac{\phi_{i1}}{\phi_{i2}}\right) \leq u'_{21} \leq u'_{11} \min_{\phi_{i2}<0} \left|\frac{\phi_{i1}}{\phi_{i2}}\right| \tag{D.10}$$

$$-u'_{12} \min_{\phi_{i2}>0} \left(\frac{\phi_{i1}}{\phi_{i2}}\right) \leq u'_{22} \leq u'_{12} \min_{\phi_{i2}<0} \left|\frac{\phi_{i1}}{\phi_{i2}}\right| \tag{D.11}$$

By the same reasoning, application of the sign constraints for $\underline{\psi}_1$ and $\underline{\psi}_2$ plus the assumptions $\underline{\hat{c}}_1 \geq \underline{0}$, and $\underline{\hat{c}}_2 \geq \underline{0}$ to Equations (D.4) gives the inequalities

$$v_{11} > 0 \tag{D.12}$$

$$v_{12} > 0 \tag{D.13}$$

$$-v_{11} \min_{\psi_{j2}>0} \left(\frac{\psi_{j1}}{\psi_{j2}}\right) \leq v_{21} \leq v_{11} \min_{\psi_{j2}<0} \left|\frac{\psi_{j1}}{\psi_{j2}}\right| \tag{D.14}$$

$$-v_{12} \min_{\psi_{j2}>0} \left(\frac{\psi_{j1}}{\psi_{j2}}\right) \leq v_{22} \leq v_{12} \min_{\psi_{j2}<0} \left|\frac{\psi_{j1}}{\psi_{j2}}\right| \tag{D.15}$$

We can further restrict the elements of $\underline{U}'$ by recalling that $\underline{U}'$ and $\underline{V}$ must satisfy the equation

$$\underline{U}'\underline{V}^T = \underline{\Omega}_{(2)} \tag{D.16}$$

From Equation (D.16) we obtain the equations

$$v_{11} = \omega_1 u'_{22}/\det(\underline{U}') \tag{D.17}$$

$$v_{21} = -\omega_2 u'_{12}/\det(\underline{U}') \tag{D.18}$$

$$v_{12} = -\omega_1 u'_{21}/\det(\underline{U}') \tag{D.19}$$

$$v_{22} = \omega_2 u'_{11}/\det(\underline{U}') \tag{D.20}$$

where ω_1, ω_2 and $\det(\underline{U}')$ are all defined as positive. Equation (D.17) and Inequality (D.12) together give the new inequality,

$$u'_{22} > 0 \tag{D.21}$$

and Equation (D.13) and Inequality (D.19) together give

$$u'_{21} > 0 \tag{D.22}$$

Thus, the R.H.S. of Inequality (D.13) and the L.H.S. of Inequality (D.14) can be replaced by the stronger restrictions of Inequalities (D.21) and (D.22), giving

$$-u'_{11} \min_{\phi_{12}>0}\left(\frac{\phi_{11}}{\phi_{12}}\right) \leq u'_{21} < 0 \tag{D.23}$$

$$0 < u'_{22} \leq u'_{12} \min_{\phi_{i2}<0} \left|\frac{\phi_{i1}}{\phi_{i2}}\right| \tag{D.24}$$

Substituting Equations (D.17) and (D.18) into Inequality (D.14), we obtain

$$-\left(\frac{\omega_1}{\omega_2}\right)u'_{22} \min_{\psi_{j2}<0}\left|\frac{\psi_{j1}}{\psi_{j2}}\right| \leq u'_{12} \leq \left(\frac{\omega_1}{\omega_2}\right)u'_{22} \min_{\psi_{j2}>0}\left(\frac{\psi_{j1}}{\psi_{j2}}\right) \tag{D.25}$$

Since u'_{12} and u'_{22} are positive, the L.H.S. of Inequality (D.25) is already guaranteed to hold. The R.H.S. of Inequality (D.25) can be rearranged to give a new lower bound for u'_{22}.

$$\left(\frac{\omega_2}{\omega_1}\right)u'_{12} \max\left(\frac{\psi_{j2}}{\psi_{j1}}\right) \leq u'_{22} \tag{D.26}$$

Substituting Equations (D.19) and (D.20) into Inequality (D.15), we obtain

$$\left(\frac{\omega_1}{\omega_2}\right)u'_{12} \min_{\psi_{j2}>0}\left(\frac{\psi_{j1}}{\psi_{j2}}\right) \leq u'_{11} \leq -\left(\frac{\omega_1}{\omega_2}\right)u'_{21} \min_{\psi_{j2}<0}\left|\frac{\psi_{j1}}{\psi_{j2}}\right| \tag{D.27}$$

Since u'_{11} is positive and u'_{21} is negative, the L.H.S. of Inequality (D.27) is already guaranteed to hold. The R.H.S. of Inequality (D.27) can be rearranged to give a new upper bound for u'_{21},

$$u'_{21} \leq \left(\frac{\omega_2}{\omega_1}\right)u'_{11} \min\left(\frac{\psi_{j2}}{\psi_{j1}}\right). \tag{D.28}$$

In summary, Assumptions 2 through 5 require that the elements of $\underline{U}'$ satisfy the following inequalities,

$$u'_{11} > 0 \tag{D.29}$$

$$-\min_{\phi_{i2}>0}\left(\frac{\phi_{i1}}{\phi_{i2}}\right) \leq \frac{u'_{12}}{u'_{11}} \leq \left(\frac{\omega_2}{\omega_1}\right) \min\left(\frac{\psi_{j2}}{\psi_{j1}}\right) \tag{D.30}$$

$$u'_{12} > 0 \tag{D.31}$$

$$\left(\frac{\omega_2}{\omega_1}\right) \max\left(\frac{\psi_{j2}}{\psi_{j1}}\right) \leq \frac{u'_{22}}{u'_{12}} - \min_{\psi_{i2}<0}\left|\frac{\phi_{i1}}{\phi_{i2}}\right| \tag{D.32}$$

Assumption 1 gives the following two equations restricting the elements of $\underline{U}'$

$$u'_{11}\left(\sum_{i=1}^{p} L_i^{-1}\phi_{i1}\right) + u'_{21}\left(\sum_{i=1}^{p} L_i^{-1}\phi_{i2}\right) = 1 \tag{D.33}$$

$$u'_{12}\left(\sum_{i=1}^{p} L_i^{-1}\phi_{i1}\right) + u'_{22}\left(\sum_{i=1}^{p} L_i^{-1}\phi_{i2}\right) = 1 \tag{D.34}$$

Define $\underline{u}'_{jL}$ as the value of $\underline{u}'_j$ where the ratio (u'_{2j}/u'_{1j}) is a minimum, and define $\underline{u}'_{jH}$ as the value of $\underline{u}'_j$ where the ratio (u'_{2j}/u'_{1j}) is a maximum. Then Inequalities (D.29) through (D.32) and Equations (D.33) and (D.34) give for u'_{1L}, u'_{1H}, u'_{2L}, and u'_{2H} the expressions listed in Table 3.1. These are the extreme values for the elements of $\underline{U}'$. It follows that a normalized static spectrum $\underline{\hat{f}}'_j$ must fall within these extreme values. Thus $\underline{\hat{f}}'_j$ must fall on or

between $\underline{\hat{f}}'_{jL}$ and $\underline{\hat{f}}'_{jH}$, defined by

$$\underline{\hat{f}}'_{jH} = \underline{L}^{-1}\underline{\Phi}_{(2)}\underline{u}'_{jH} \tag{D.35}$$

To obtain the solution bands of the concentration profiles, we make the following five assumptions, which correspond to the assumptions made for the static spectra solution bands, but with the roles of $\underline{F}$ and $\underline{C}$ reversed.

1. Normalization:

$$\sum_{j=1}^{N} \hat{c}'_{j1} = 1, \qquad \sum_{j=1}^{N} \hat{c}'_{j2} = 1$$

2. Absorbers in the experiment:

$$\underline{c}'_1 = (\underline{T}^{-1}\underline{\Psi}_{(2)})\underline{v}'_1$$

$$\underline{\hat{c}}'_2 = (\underline{T}^{-1}\underline{\Psi}_{(2)})\underline{v}'_2$$

$$\underline{\hat{f}}_1 = (\underline{L}^{-1}\underline{\Phi}_{(2)})\underline{u}_1$$

$$\underline{\hat{f}}_2 = (\underline{L}^{-1}\underline{\Phi}_{(2)})\underline{u}_2$$

3. Nonnegative definiteness of concentrations and static spectra:

$$\underline{\hat{c}}_1' \geq \underline{0}, \quad \underline{\hat{c}}_2' \geq \underline{0}$$

$$\underline{\hat{f}}_1 \geq \underline{0}, \quad \underline{\hat{f}}_2 \geq \underline{0}$$

4. Nonnegative Definiteness of the Elements in $\underline{M}_W$ and $\underline{M}_W'$.

5. Determinant of $\underline{V}'$ is positive.

Noting the symmetry of Equation (D.1), we see that the solution bands for the concentration profiles presented in Table 3.1 can be obtained by rewriting the solution band equations for the static spectra with $\underline{\hat{c}}_j'$ substituted for $\underline{\hat{f}}_j'$, $\underline{\hat{f}}_j$ for $\underline{\hat{c}}_j$, ψ_{jk} for ϕ_{ik}, ϕ_{ik} for ψ_{jk}, and T_j for L_i.

Note that $\underline{\hat{f}}_{iL}'$ and $\underline{\hat{f}}_H'$ delineate regions of acceptability of $\underline{\hat{f}}_i'$. In general, $\underline{\hat{f}}_{iL}'$ and $\underline{\hat{f}}_{iH}'$ cross over, i.e., $\underline{\hat{f}}_{iL}'$ is not always less than $\underline{\hat{f}}_{iH}'$. The same situation obtains for $\underline{\hat{c}}_{iL}'$ and $\underline{\hat{c}}_{iH}'$. Examples may be found in Chapter 4.

APPENDIX E

Computer Transfer and Calibration of Stopped Flow Raw Data

This appendix gives instructions for (1) transferring stopped flow raw data from the PDP8I computer to the CDC-6500 computer, (2) estimating the wavelength of each wavelength channel in a scanning experiment, and (3) calculating absorbance versus time and wavelength channel from the raw data and storing the results in a form suitable for KINFIT and other data interpretation programs.

Figure E.1 is a flow diagram of steps (1) through (3) above. Stopped flow raw data can be transferred to the CDC-6500 computer via cards or tapes, and, since the procedures for steps (2) and (3) are different for the two methods of data transfer, the paths in Figure E.1 are labelled "cards", "tapes", or "cards and tapes" to indicate the data transfer method to which they apply. For each step in Figure E.1 in which a program is used, the name of the program is given in parentheses to the left of the box describing the step.

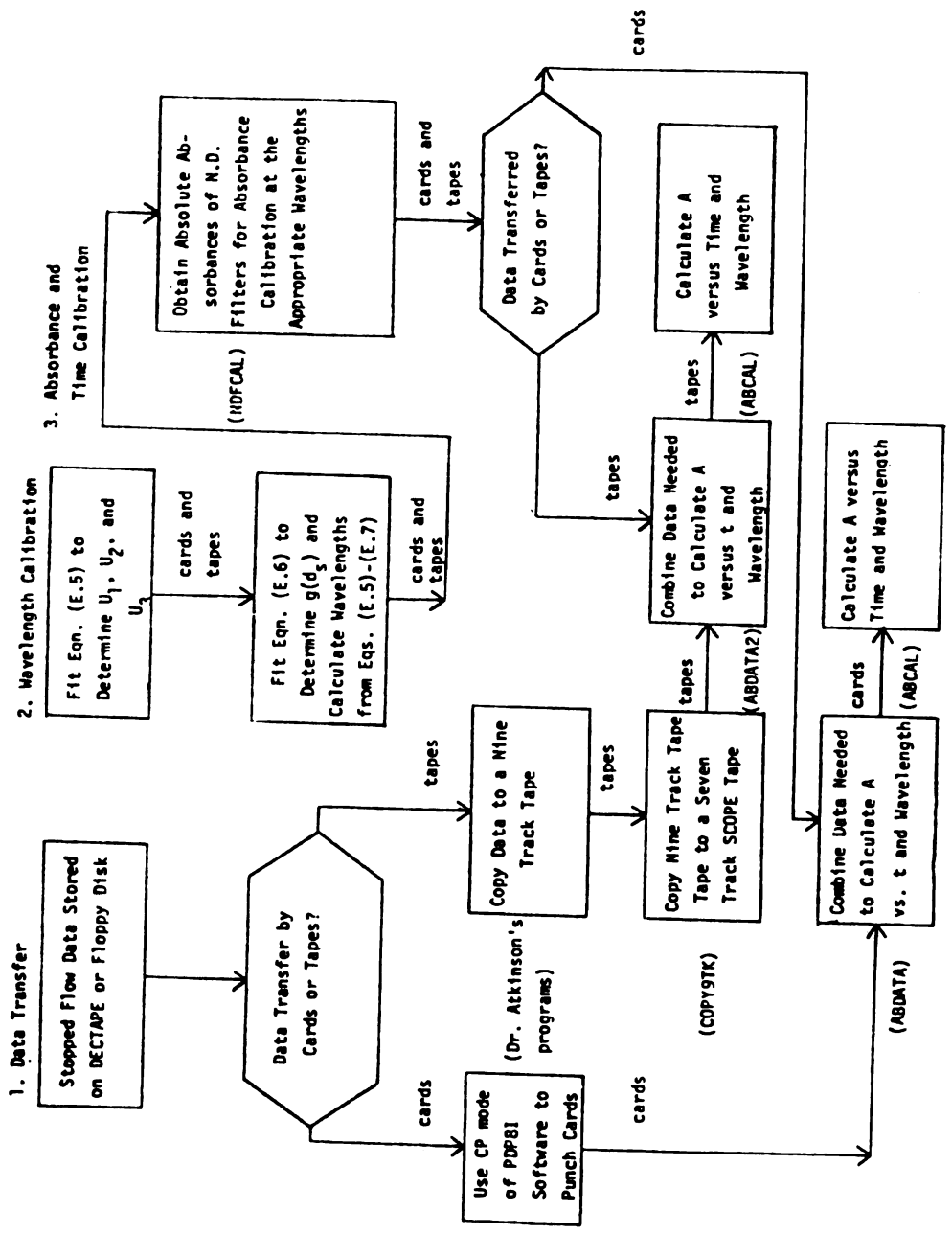

Figure E.1. Flow Diagram for Data Transfer and Calibration.

E.1. Data Transfer From the PDP8I to the CDC-6500

The instructions for using the CP mode of the stopped flow software to punch raw data onto cards are given by Papadakis (unpublished). Transferring data by tapes from the PDP8I computer to the CDC-6500 computer requires two steps. Raw data on a PDP8I floppy disk or a DECTAPE is first transferred to a nine track tape that can be read on the CDC-6500 computer. The programs for this step were developed by Dr. Tom Atkinson, and he shall provide written instructions for using them. Figure E.2 is a typical directory that lists the order of stopped flow data files on a nine track tape.

Although the CDC-6500 computer reads nine track tapes, the MSU Computer Center does not fully support them with software, and further use of the raw data is cheaper and more convenient if the contents of the nine track tape are copied onto a seven track SCOPE tape, and the SCOPE tape is used as the permanent record of the raw data for the CDC-6500 computer.

Dr. Donald Ward has provided a program named COPY9TK that copies the contents of a nine track tape onto a seven track SCOPE tape. One submits the data-filled nine track tape and a blank, zeroed seven track tape to the service window of the Computer Center, and then enters the following deck into the CDC-6500 computer.

```
MPIP VER 2.4 DIRECTORY  TAPE: 6200    28-FEB-77  13:57:43

FILE:     1 # REC =     17
   GWAOAA.RC
FILE:     2 # REC =     17
   GWAOAB.RC
FILE:     3 # REC =     17
   GWAOAC.RC
FILE:     4 # REC =     17
   GWAOAD.RC
FILE:     5 # REC =    209
   GWAOAE.RC
FILE:     6 # REC =    209
   GWAOAF.RC
FILE:     7 # REC =    209
   GWAOAG.RC
FILE:     8 # REC =    209
   GWAOAH.RC
FILE:     9 # REC =    209
   GWAOAI.RC
FILE:    10 # REC =    209
   GWAOAJ.RC
FILE:    11 # REC =    209
   GWAOAK.RC
FILE:    12 # REC =     43
   GWAOAL.RC
FILE:    13 # REC =     17
   GWAOAM.RC
FILE:    14 # REC =     17
   GWAOAN.RC
FILE:    15 # REC =     17
   GWAOAO.RC
FILE:    16 # REC =     17
   GWAOAP.RC
FILE:    17 # REC =     17
   GWAOAQ.RC
FILE:    18 # REC =     17
   GWAOAR.RC
FILE:    19 # REC =     17
   GWAOAS.RC
FILE:    20 # REC =     17
   GWAOAT.RC

TOTAL RECORDS =      1710.
```

Figure E.2. Directory showing first thirty data files on a nine track tape.

Example 1 Deck that Executes COPY9TK

```
 1.  Problem Number Card
 2.  Job Card---IDNAME,CM40000,T200,JC3000,NT1,MT1,RG1.
 3.  Password
 4.  REQUEST,TAPE1,VRN=9tk tape#,S,Z,HD,AS,RO.
 5.  REQUEST,TAPE2,VRN=7tk tape#, RW.
 6.  REWIND(TAPE1)
 7.  REWIND(TAPE2)
 8.  ATTACH(X,COPY9TK)
 9.  X.
10.  RETURN(TAPE1)
11.  RETURN(TAPE2)
12.  (7
       8
         9)
13.  Title, Number of files on the nine track tape,
     Format (A70,I10)
14   (6
       7
         8
           9)
```

The meaning of the control cards in Example 1 is described in The Computer Laboratory User's Guide, Vol. II, (1973) Chapters 2 through 7. The program COPY9TK records on the seven track tape in SCOPE format a facsimile of the information on the nine track tape.

The procedure for obtaining a particular data file from the seven track SCOPE tape is described in the Control Data SCOPE Reference Manual (1969), Section 10. The following example is a deck that reads files GWAOAC.RC and GWAOAT.RC from a seven track SCOPE tape and stores the information as permanent files GWAOAC and GWAOAT. In this example the seven track SCOPE tape with visual reel number 6200 contains twenty files, which are listed in Figure E.1. It was copied from a nine track tape having this directory. The files are identified on the tape by their numbers. Thus, GWAOAC.RC is file number

3, and GWAOAT.RC is file number 20.

Example 2 Deck that Retrieves Files GWAOAC.RC and GWAOAT.RC from the Seven Track SCOPE Tape 2412.

```
 1.  Problem Number Card
 2.  Job Card---IDNAME,CM40000,T100,JC250,MT1,RG2.
 3.  Password
 4.  REQUEST,T7,VRN=6200,RO.
 5.  REWIND(T7)
 6.  COPYCF(T7,X,2) copies the first two files onto
     local fileX.
 7.  COPYCF(T7,TAPE1,1) copies the third file onto
     local file TAPE1.
 8.  COPYCF(T7,X,17) copies files 4 through 19 onto
     local file X.
 9.  COPYCF(T7,TAPE2,1) copies file 20 onto local file
     TAPE2.
10.  CATALOG(TAPE1,GWAOAC,RP=10)
11.  CATALOG(TAPE2,GWAOAT,RP=10)
12.  RETURN(T7)
13.  (6
       7
         8
           9)
```

E.2. Wavelength Calibration

Each file on the seven track SCOPE tape contains the data collection parameters and the digitized output voltages of the Philbrick logarithmic amplifier for all the stored points in a single experiment. The purpose of the calibration programs is to calculate from these raw data the absolute Beer's Law absorbances, the wavelengths, and the times for all the stored data points, and to supply this information in a form suitable for use in KINFIT and other data interpretation programs.

The first calibration step for scanning experiments is to estimate the wavelength corresponding to each

wavelength channel in the scan. The computer programs used in this step are KINFIT and WAVE. The calibration data for this step are the (wavelength channel, wavelength) ordered pairs for the absorbance peaks of the holmium oxide and didymium oxide static spectra, collected with the same monochromator settings as the kinetic experiments.

Table E.1 lists these data for the LADH-NADH-NDMA reaction experiments discussed in Chapter 4. The instrumental conditions for these scanning experiments were drum setting = 1610.3, mirror nutation = 0.8615, mirror rotations/sec = 37.5, samples/point = 5, and stored points/spectrum = 54. In order to increase the resolution for the wavelength calibration, the holmium oxide and didymium oxide static spectra were measured with the same drum setting and mirror nutation as the kinetic experiments, but with mirror rotations/sec = 7.5, samples/point = 6, and stored points/spectrum = 226. The wavelength channel in the 54 point spectrum that corresponds to a given wavelength channel in the 226 point spectrum was calculated from the equation

$$\text{channel in 54 points spectrum} = (54.4/226.7) \times \text{channel in 226 point spectrum.} \qquad \text{(E.1)}$$

Equation (E.1) is derived from the facts that there are

$$\left(\frac{68 \text{ gear teeth}}{\text{forward scan}}\right) \times \left(\frac{4 \text{ samples}}{\text{gear tooth}}\right) \times \left(\frac{1 \text{ point}}{5 \text{ samples}}\right) = \frac{54.4 \text{ points}}{\text{forward scan}}$$

Table E.1. Holmium Oxide and Didymium Oxide Absorbance Peaks for the LADH-NADH-NDMA Experiments versus Wavelength Channel

m=Wavelength Channel in 54 pt. spectra	λ(nm)	$\bar{\nu}(cm^{-1})$
	Holmium Oxide Peaks	
6.0	279.0	35840
10.7	287.7	34760
22.9	334.1	29930
25.2	348.2	28720
27.1	361.0	27700
29.8	382.2	26160
30.2	386.2	25890
33.6	419.4	23840
36.0	446.2	22410
36.7	454.0	22030
37.2	460.6	21710
39.1	484.7	20630
43.0	536.9	18630
	Didymium Oxide Peaks	
41.0	514.0	19460
42.2	529.0	18900
46.1	573.0	17450
47.0	584.0	17120

in the scanning kinetic experiments, of which 54 are stored and 0.4 are wasted, and

$$\left(\frac{68 \text{ gear teeth}}{\text{forward scan}}\right) \times \left(\frac{20 \text{ samples}}{\text{gear tooth}}\right) \times \left(\frac{1 \text{ point}}{6 \text{ samples}}\right) = \frac{226.7 \text{ points}}{\text{forward scan}}$$

in the holmium oxide and didymium oxide static spectra, of which 226 are stored and 0.7 are wasted.

Calculating the wavelength of each wavelength channel could be viewed as the problem of interpolating between the observed holmium oxide and didymium oxide peaks. We could fit the data in Table E.1 with a polynomial and use the polynomial to calculate the wavelengths of all the channels for which there are no peaks. This would not be a satisfactory solution, however, because the polynomial would have to be extrapolated beyond the range of the peaks. For example, in Table E.1 the last channel out of 54 for which a calibration peak is observed is channel 47. A polynomial estimated by fitting the data in Table E.1 would contain no information about the wavelength of channels 48 through 54.

Rather than use an arbitrary polynomial to fit the wavelength calibration data, we shall use a model that describes the scanning monochromator. The Perkin Elmer scanning monochromator and the computer interface are so constructed, that, if the quartz prism's index of refraction were a linear function of wavelength, the relationship between $\bar{\nu}(cm^{-1})$, the wavenumber of light at the exit

slit, and m, the wavelength channel in the scan, would be

$$\bar{\nu}(cm^{-1}) = \beta_1 \sin [2\pi(m/n + \beta_3)] + \beta_2 \qquad (E.2)$$

where n is the total number of wavelength channels in the forward and backward scan (=108.8 for the data in Table E.1), β_1 is the half width of the forward scan in wavenumbers, β_2 is the center of the forward scan in wavenumbers, and β_3 is a phase angle (≈0.25).

For the ideal case of linear dependence of index of refraction on wavelength, we would estimate the three unknown parameters β_1, β_2, and β_3 by fitting Equation (E.2) in KINFIT to the $(m,\bar{\nu})$ pairs in Table E.1. However, the prism's index of refraction varies nonlinearly with wavelength, and, a better model is

$$\bar{\nu}(cm^{-1}) = f(\phi) \qquad (E.3)$$

where ϕ is the nutation angle of the rotating mirror, given by

$$\phi = \alpha_1 \sin [2\pi(m/n + \alpha_2)] \qquad (E.4)$$

and where α_1 is the half width of the scan in nutation angle of the mirror, and α_2 is a phase angle (≈0.25). Equation (E.2) is the special case of Equations (E.3)

and (E.4) where $\bar{\nu} = f(\phi) = \beta_2 + \beta_1\phi/\alpha_1$ and $\alpha_2 = \beta_3$. For nonlinear dependence of index of refraction on wavelength, $f(\phi)$ is some polynomial in ϕ of degree greater than one.

Rather than determine ϕ and $f(\phi)$, which would be experimentally difficult, we can include the nonlinear dependence of index of refraction on wavelength in the following way. We vary the angle with which the beam enters the prism, and hence the wavelength of light at the exit slit, by changing the drum setting with the mirror nutation angle set to zero. In this manner, we construct a table of holmium oxide and didymium oxide absorbance peak wavenumbers versus d_s, the drum setting at zero nutation. Table E.2 contains this information, measured on July 1, 1976 by Dr. Joseph Ceraso. We use this information in a wavelength calibration by assuming the model

$$d_s = U_1 \sin [2\pi(m/n + U_3)] + U_2 \qquad (E.5)$$

$$\bar{\nu}(cm^{-1}) = g(d_s) \qquad (E.6)$$

$$\lambda(nm) = 10^7/\bar{\nu}(cm^{-1}) \qquad (E.7)$$

where d_s is the drum setting at zero nutation angle, m is the wavelength channel number, U_1 is the half width of the scan in units of drum setting at zero nutation

Table E.2. Wavenumbers versus Drum Settings at Zero Mirror Nutation for Holmium Oxide and Didymium Oxide Absorbance Peaks.

d_s = Drum Setting at Zero Mirror Nutation	$\bar{\nu}(cm^{-1})$
1792.5	35840
1763.3	34760
1754.2	34480
1635.4	29930
1622.8	29300
1614.7	29000
1607.4	28720
1586.3	27700
1574.0	27120
1555.6	26160
1548.7	25890
1542.2	25560
1510.7	23840
1503.9	23500
1486.2	22410
1481.0	22030
1475.4	21710
1468.1	21080
1462.5	20630
1455.4	20470
1428.4	18630
1407.3	17120
1411.4	17450
1431.6	18900
1440.4	19460

angle, U_2 is the center of the scan in units of drum setting at zero nutation angle, U_3 is a phase angle ($\simeq 0.25$), n is the total number of wavelength channels in the forward and backward scans, and $g(d_s)$ is a polynomial in d_s.

Note that Equations (E.5) through (E.7) relate the wavelength λ to the channel number m. Equations (E.5) and (E.6) contain parameters to be estimated by least squares fitting the calibration data. Equation (E.7) is true by the definitions of λ and $\bar{\nu}$. The first step in using this model is to estimate U_1, U_2, and U_3 by fitting the (m,d_s) ordered pairs for the holmium oxide and didymium oxide static spectra to Equation (E.5) with KINFIT. The (m,d_s) ordered pairs for the LADH-NADH-NDMA experiments are listed in Table E.3, in which each d_s value is the one from Table E.2 whose wavenumber corresponds to the holmium oxide or didymium oxide peak from Table E.1. Given the data in Table E.3, estimated variances of m and d_s equal to one, and the residual function R defined by

$$R = d_{s_{observed}} - U_1 \sin [2\pi(m/n + U_3)] + U_2, \qquad (E.8)$$

KINFIT estimated the values $U_1 = 208.5 \pm 0.7$, $U_2 = 1604.3 \pm 1.4$, and $U_3 = 0.265 \pm 0.002$.

The next step is to estimate by least squares the polynomial $g(d_s)$ in Equation (E.6). This step, and the final step of calculating from Equations (E.5) through

Table E.3. Drum Settings at Zero Mirror Nutation versus Wavelength Channel for the Holmium Oxide and Didymium Oxide Calibration Spectra (Information Combined from Tables 1 and 2).

m = Wavelength Channel in 54 pt. Spectrum	d_s = Drum Setting At Zero Nutation	$\bar{\nu}(cm^{-1})$
	Holmium Oxide Peaks	
6.0	1792.5	35840
10.7	1763.3	34760
22.9	1635.4	29930
25.2	1607.4	28720
27.1	1586.3	27700
29.8	1555.6	26160
30.2	1548.7	25890
33.6	1510.7	23840
36.0	1486.2	22410
36.7	1481.0	22030
37.2	1475.4	21710
39.1	1462.5	20630
43.0	1428.4	18630
	Didymium Oxide Peaks	
41.0	1440.4	19460
42.2	1431.6	18900
46.1	1411.4	17450
47.0	1407.3	17120

(E.7) a table of wavelengths for all the wavelength channels, is performed by the program WAVE. WAVE has a subroutine called ORTHPOL that uses ordinary least squares to fit the data in Table E.2 to the equation

$$\bar{v} = g(d_s) = \beta_0 P_0(d_s) + \beta_1 P_1(d_s) + \ldots + \beta_5 P_5(d_s), \quad (E.9)$$

where P_0 through P_5 are orthogonal polynomials, chosen subject to the restrictions that $g(d_s)$ has no inflection points over the range of the d_s values in Table E.2, and that each term in Equation (E.9) is statistically significant at the 95% confidence level. More details about ORTHPOL are given in Appendix F. The program WAVE then uses Equations (E.5) through (E.6) to calculate a table of wavelengths for all the wavelength channels in the experiment. It prints this table and writes the information on a local file called TAPE8 that can be cataloged as a permanent file to be used in the next calibration step. The following deck executes the program WAVE.

Example 3 Deck that Executes the Program WAVE and Stores TAPE8 as Permanent File WCALIB.

Control Cards

```
1.  Problem Number Card
2.  Job Card---IDNAME,CM40000,T50,JC250,RG2.
3.  Password
4.  ATTACH(WAVE,WAVE)
5.  WAVE.
6.  CATALOG(TAPE8,WCALIB,RP=100)
7.  (78
    9)
```

Data Cards

8. NPTS,NCHAN
(2I5)

NPTS	Number of $(d_s,\bar{\nu})$ order pairs to be used in estimating the parameters in Equation (E.5).
NCHAN	Number of wavelength channels in a single forward scan of the experiment.

9. (U(I),I=1,2,3)
(3E10.4)

U(I)	U_1,U_2 and U_3 values estimated by KINFIT for Equation (E.5)

10. (X(I),Y(I), I = 1,NPTS)
(2E10.4).

X(I)	d_s, drum setting at zero nutation.
Y(I)	$\bar{\nu}(cm^{-1})$, wavenumber observed for d_s.

11. ($6_{7_{8_{9}}}$)

TAPE8 has written on it (WL(I), I = 1, NCHAN), Format (5X,E10.4), where WL(I) is the wavelength in nanometers of the I'th wavelength channel.

Given the data in Table E.2, ORTHPOL chose a third degree polynomial for $g(d_s)$. Table 4.3 lists the wavelength assignments of the 54 wavelength channels in the LADH-NADH-NDMA experiments. Figure 4.1 is a plot of the wavelength versus wavelength channel calibration.

E.3. Calculation of Absorbance versus Time and Wavelength Channel

The program WAVE defines the wavelength scale of a scanning experiment. The program ABCAL calculates absorbance versus time and wavelength channel for a scanning

experiment from the wavelength calibration information, data collection parameters, neutral density filter calibration data, and the digitized output voltages of the Philbrick logarithmic amplifier. ABCAL also calculates absorbance versus time for a fixed wavelength experiment and absorbance versus wavelength channel for a static spectrum. Several auxiliary programs, NDFCAL, ABDATA, and ABDATA2, are used to feed the neutral density filter data, kinetic raw data, and data collection parameters into ABCAL. Before describing their use, we shall briefly discuss the calculations performed in ABCAL.

Time

ABCAL and its subroutine TIMER calculate the time of each absorbance point in a scanning or fixed wavelength kinetic experiment from the data collection parameters (SAVEPAGE), the flow time, the stopping time, and the distances between certain flags and the plunger stopping plate.

Figure E.3 schematically shows the location of the timing flags for a scanning kinetic experiment. In this example it is assumed that the stop flag D was used to trigger data collection. Data collection would actually begin at point G, where the first beginning of scan pulse occurs after D. The zero of the time scale calculated

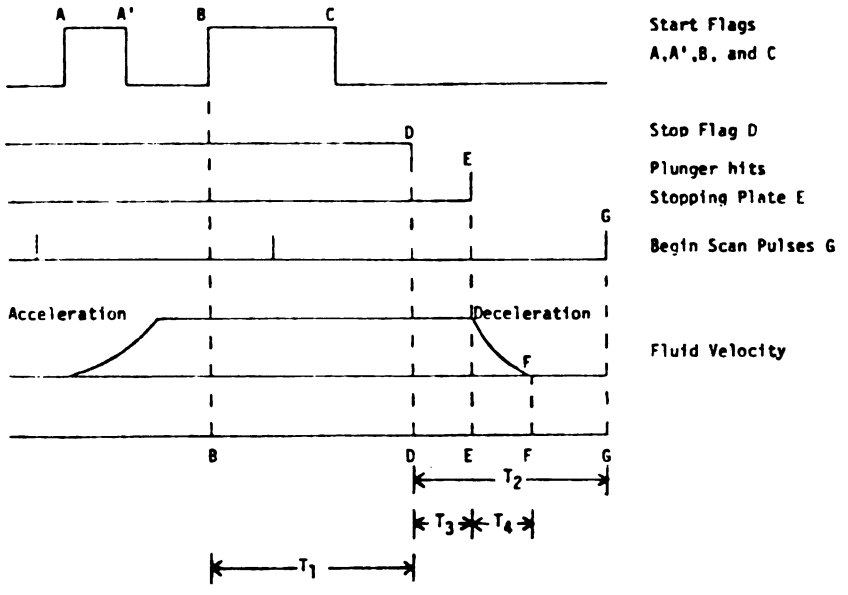

Figure E.3. Schematic diagram of timing flags for a scanning experiment triggered by the stop flag. T_1 = flow time, T_2 = time shift, T_3 = stop flag to plunger stop, T_4 = stopping time.

by TIMER is where the data collection begins, i.e., at point G in this example. ABCAL then adjusts the time scale to begin where the fluid flow has ended, i.e., point F in Figure E.3. This adjustment is calculated from the following four numbers:

1. T_1, the "flow time", which is the time elapsed between one of the start flags (A, B, or C), and the stop flag, D. The start flag used should be the earliest flag by which constant flow velocity has been reached, i.e., flag B in Figure E.4.

2. T_2, the "time shift", which is the time elapsed between the data collection trigger and the first beginning of scan pulse; i.e., between points D and G in Figure E.4.

3. T_3, the time elapsed between the stop flag D and point E, where the plunger hits the stopping plate.

4. T_4, the "stopping time", which is the time elapsed between the stopping of the plunger at point E and the end of fluid flow at point F.

For the example shown in Figure E.3, if T is the time scale calculated in TIMER that starts at point G, then T', the adjusted time scale calculated by ABCAL that starts at point F, is given by

$$T' = T + T_2 - T_3 - T_4 \qquad \text{(E.10)}$$

We shall briefly summarize the other cases. If data collection in a scanning experiment is triggered from a start flag, say flag B, then

$$T' = T - T_1 + T_2 - T_3 - T_4 \qquad \text{(E.11)}$$

In a fixed wavelength experiment the data collection begins at the flag chosen to trigger data collection, since there is no need to wait for a beginning of scan pulse. Therefore, there is no time shift, T_2. For a fixed wavelength experiment triggered by a start flag, we have

$$T' = T - T_1 - T_3 - T_4 \tag{E.12}$$

and for a fixed wavelength experiment triggered by the stop flag, we have

$$T' = T - T_3 - T_4 \tag{E.13}$$

T_1, T_2, T_3, and T_4 are obtained as follows. T_1, the flow time, is measured during the experiment and is entered into the calibration programs on a data card typed by the user. T_2, the time shift, is one of the AVEPAGE parameters stored by the PDP8I computer with each file. T_3, the time between the stop flag and the plunger stop, is computed by ABCAL from the equation

$$T_3 = xT_1/y \tag{E.14}$$

where x is the vertical distance displaced by the plunger between the stop flag and the plunger stopping plate, and y is the vertical distance displaced by the plunger between

the start flag used to measure T_1 and the stop flag. Equation (E.14) assumes that the fluid velocity is constant between point B and E in Figure E.3. The stopping time, T_4, is the time taken for the fluid velocity to reach zero after the plunger stops moving, and is usually estimated to be 0.5 msec.

Absorbance

For a given wavelength channel, ABCAL calculates the absolute absorbance of each data point from an equation of the form

$$A = A(V) = \beta_0 P_0(V) + \beta_1 P_1(V) + \ldots + \beta_5 P_5(V) \qquad (E.15)$$

where A is the absolute absorbance, V is the digitized output voltage of the Philbrick amplifier, β_0 through β_5 are parameters to be estimated by ordinary least squares, and $P_0(V)$ through $P_5(V)$ are orthogonal polynomials, each of degree in V equal to its subscript. The terms included in Equation (E.15), and the values of their coefficients, are determined in the subroutine ORTHPOL, which fits the absolute absorbances and voltages for the neutral density filter calibration data to Equation (E.15).

A detailed description of ORTHPOL is given in Appendix F. In using ABCAL, it is important to know that the terms chosen in Equation (E.15) must pass two tests:

(1) the terms must be significant at the 95% confidence level, and, (2) Equation (E.15) must have no unwanted inflection points. These tests exclude polynomials that fit the random errors in the calibration data by changing direction to go through every data point. The user supplies values for the variables MFLAG,KFLAG,LFLAG,NINC, VMAX, and JFLAG, defined in Appendix F, that control how the terms in Equation (E.15) are chosen.

The Philbrick logarithmic amplifier circuit has 11 output voltage gain settings. When the gain settings for the experiment and the neutral density filter calibration data are different, ABCAL assumes that the output voltage is linear with gain, and makes the following adjustment. The user enters on a data card the ratio R_g, defined

$$R_g = \text{gain during experiment/gain during calibration}$$

If V is the voltage measured during the experiment, ABCAL calculates the absorbance from $A = A(V')$, where $V' = V/R_g$ and $A(V')$ is given by Equation (E.15).

E.4 Instructions for Using ABCAL

In addition to various control parameters, flag distances, etc., ABCAL requires the following three blocks of data:

1. The data collection parameters and digitized Philbrick amplifier voltages for the experiment.
2. The digitized Philbrick amplifier voltages for the neutral density filter calibration data.
3. The absolute absorbances of the neutral density filters at the wavelengths corresponding to the wavelength channels of the experiment.

Blocks (1) and (2) are the DECTAPE files for the experiment and the neutral density calibration, respectively. The absolute absorbances of the neutral density filters are measured on the Cary 17 spectrometer. To calibrate one wavelength channel in a scanning experiment, ABCAL requires at the appropriate wavelength the absolute absorbance of each neutral density filter used in the calibration experiment. For example, in a 54 wavelength channel experiment for which 8 neutral density filters were used, ABCAL needs 54 x 8 = 432 absolute absorbances from the spectra of the neutral density filters. We can extract these absorbances from the spectra by hand, or, if the wavelengths fall between 250 nm and 610 nm, we can use the program NDFCAL, written by Mr. David June and adapted by R. Cochran, to interpolate the absorbances from a 770 point lookup table.

The program NDFCAL reads the wavelength calibration information from TAPE8 of the program WAVE, and linearly interpolates the absolute absorbances of the neutral density filters from a lookup table on a permanent file

called NFDAT2, which contains absorbances from the Cary 17 spectra of the neutral density filters at 5 nm intervals over the range 250 nm to 610 nm. Alternatively, the wavelength calibration information can be read from cards. NDFCAL prints the absolute absorbances of the neutral density filters for each wavelength, and writes this information on a local file called TAPE9, that can be used directly in the next step for calibrating data from a seven track SCOPE tape. The deck structure for executing NDFCAL follows.

Example 4. Deck that Executes NDFCAL and Stores the Absolute Absorbances on a Permanent File Named ABSOLUTE

Control Cards

1. Problem Number Card
2. Job Card---IDNAME,CM40000,T50,JC350,RG2.
3. Password
4. ATTACH(TAPE8,WCALIB)
   (If IOPT ≠ 1 on data card #1, TAPE8 should contain the array (WL(I),I=1,NCHAN) from the program WAVE)
5. ATTACH(TAPE7,NFDAT2)
6. ATTACH(NDFCAL,NDFCAL)
7. NDFCAL.
8. CATALOG(TAPE9,ABSOLUTE,RP=100)
9. (7 8 9)

Data Cards

10. IOPT (=1, wavelength versus wavelength channel information to be read from cards, ≠1, to be read from TAPE8)(I5)

Data cards (11) and (12) are used only if IOPT=1 above

(11) NWLC (Number of wavelength channels in the experiment) (I5)

(12) (XWVLTH(I),I=1,NWLC)
(5X,E10.4)
XWVLTH(I) Wavelength in nanometers of wavelength channel I.

13. NND Number of neutral density filters per wavelength channel in the calibration experiments (I5)

14. (ISELEC(I),I=1,NND)
(16I5)
ISELEC(I) is a code for the order in which the neutral density filters are stored in the calibration file.

ISELEC(I)	Nominal Optical Density of the I'th N.D. filter in the Calibration File
1	0.02
2	0.10
3	0.20
4	0.30
5	0.60
6	0.70
7	0.80
8	1.00
9	1.30
10	solvent vs. solvent

15. (6 7 8 9)

The local file TAPE9 contains the absolute absorbances of the neutral density filters for wavelength channels 1 through NWLC in the following form:

(XNDFIL(ISELEC(I)),I=1,NND) (8E10.4)

where XNDFIL(ISELEC(I)) is the absolute absorbance of neutral density filter ISELEC(I).

The program ABCAL obtains its input data from one of two programs; from ABDATA if the data were transferred

by tapes. The following example gives the deck structure for executing, in succession, ABDATA and ABCAL. Note that all of the raw data are entered on cards. Two local files, TAPE8 and TAPE9, contain the absorbance versus time and wavelength channel information in different forms. TAPE8 is intended for storage as a permanent file or as an APLIB file, and TAPE9 is intended to be punched as data cards for KINFIT. These files are described at the end of this section.

Example 5. Deck that Executes ABDATA, then ABCAL, Stores TAPE8 as a Permanent File, and Punches TAPE9 as Cards for KINFIT

Control Cards

```
 1. Problem Number Card
 2. Job Card---IDNAME,CM55000,T200,JC450,RG2.
 3. Password
 4. ATTACH(ABDATA,ABDATA)
 5. ABDATA.
 6. REWIND(TAPE10)
 7. COPYCF(TAPE10,TAPE6)
 8. REWIND(TAPE6)
 9. ATTACH(ABCAL,ABCAL)
10. CATALOG(TAPE8, Name of P. File, RP=10)
11. REWIND(TAPE9)
12. DISPOSE,TAPE9,PC.
13. (7
     8
     9)
```

Data Cards

```
14. VARTIM,VARABS,NWLC,SRFLAG,ITRIG
    (2F10.9,3I5)
```

VARTIM	Variance of time measurement errors in seconds
VARABS	Variance of absorbance measurement errors of Group 1 in absorbance units.
NWLC	Number of wavelength channels being calibrated in this run of ABCAL

*SRFLAG Spike Routine Flag (1 = yes, 0 - no) (leave blank)

ITRIG (=1, collection triggered from stop flag, ≠ 1, collection triggered from a start flag)

15. NAME, NUMS
(A8,I6)

NAME Name of experiment data file on DECTAPE

NUMS Number of save-page parameters for this run.

16. (SAVPAGE(K), K = 1, NUMS)
(6X, 12I6)

SAVPAGE(K) Save-page parameters for this kinetic run.

17. FLTIME,PHILR,TIMSKP,PNSK,SSFDIS,SFPLSD,STPTIM
(3F6.4,I6,3F6.4)

FLTIME Flow time in msec. (T_1 in Figure E.3)

PHILR Philbrick gain during experiment/Philbrick gain during calibrations

*TIMSKP Time to skip to assure good data (leave blank)

*PNSK Points to skip. (Leave blank.)

SSFDIS Distance between start/stop flag in mm (y in Equation 4.13)

SFPLSD Stop flag to plunger stop in mm (x in Equation 4.13)

STPTIM Stopping time in msec. (T_4 in Figure E.3).

18. MFLAG,KFLAG,LFLAG,NINC,VMAX,JFLAG,IPDLT
(4I5,E10.4,I5,5X,I5)

MFLAG (1, ORTHPOL automatically chooses a linear fit; ≠ 1, ORTHPOL considers adding terms to the linear function up to 5'th degree)

KFLAG (1, ORTHPOL requires ≥ 2 inflections within calibration range to reject a polynomial; ≠ 1, ORTHPOL requires ≥ 1 inflections within calibration range to reject a polynomial).

LFLAG (1, ORTHPOL checks for inflections from solvent versus solvent to VMAX; ≠ ORTHPOL checks for inflections from solvent versus solvent to highest N.D. calibration point).

NINC Number of intervals into which inflection point search region is divided.

VMAX If LFLAG = 1, ORTHPOL checks for inflections in A versus V from $V_{solvent}$ to V_{max}.

JFLAG (1, No inflection testing is performed; ≠ 1, inflection testing is performed).

IPDLT (=1, the absorbance versus time tables and parameters estimated in ORTHPOL are delected from the printed output, ≠ 1, everything is printed).

19. NDNAM
(A8)
NDNAM Name of Calibration file on DEC data tape.

20. Data Deck for Neutral Density Filter Calibration
(as it comes from PDP8I cardpunch)
For each wavelength channel:

(A) Card with number of wavelength channels, number of N.D. points, etc. (this card is not used in ABCAL, but appears in the PDP8I cardpunch deck).

(B) (VOLT(I), I = 1, # Calibration points)
(6X,12I6)
VOLT(I) Output voltage of Philbrick amplifier as digitized by the interface for each calibration point.

21. For each wavelength channel

(NDABS(I), I = 1, # of calibration points)
(6X,8F6.3)
NDABS(I) Absolute absorbances measured on Cary 17 for each calibration point.

22. For each wavelength channel,

(A) NUM, N, ISTART, IEND, IAINF, ISOLV
(2I6, 2I8, 2I6)

(B) (IDATA(I), I = 1,N)

NUM Wavelength channel number
N Number of Time points in the kinetic run.
ISTART Start Time in msec
IEND Final time in msec
IAINF Infinity voltage at wavelength channel NUM.
ISOLV Solvent versus solvent voltage at this wavelength channel. (If stored on this file.)
IDATA(I) Digitized voltage during experiment at wavelength channel NUM in spectrum number I.

23. (7_{8_9})

Data Cards for ABCAL

24. NND (I5) — NND = number of neutral density filters per wavelength channel
25. ($6_{7_{8_{9}}}$)

*ABCAL was adapted from the program ABSTIM. The variables SRFLAG, TIMSKP and PNSK are vestiges from ABSTIM, and can be ignored (left blank).

The deck structure for executing ABDATA2 and ABCAL, follows. Note that only control parameters and flag distances are read from cards.

Example 6 Deck that Executes ABDATA2 and ABCAL, Stores TAPE8 as a Permanent File and Punches TAPE9 as Cards for KINFIT

Control Cards

1. Problem Number Card
2. Job Card---IDNAME,CM55000,T200,JC450,RG2.
3. Password
4. ATTACH(TAPE11, Name of Experiment File from 7 track tape)
5. ATTACH(TAPE12, Name of N.D. File from 7 Track Tape)
6. ATTACH(TAPE13, Name of File Containing TAPE9 from NDFCAL)
   (Insert Card 6 only if NDFLAG ≠ 1 in Entry #20 below)
7. ATTACH(ABDATA2,ABDATA2)
8. ABDATA2.
9. REWIND(TAPE10)
10. COPYCF(TAPE10,TAPE6)
11. REWIND(TAPE6)
12. ATTACH(ABCAL,ABCAL)
13. ABCAL.
14. CATALOG(TAPE8, Name of P. File, RP = 100)
15. REWIND(TAPE9)
16. DISPOSE,TAPE9,PC.
17. ($7_{8_{9}}$)

Data Cards for ABDATA2

18. NAME (A9) — DECTAPE Name of the Experiment file; e.g., GULABD.RC.

19. NDNAME (A9) — DECTAPE Name of the neutral density filter calibration file; e.g., GULAAG.RC.

(NOTE: ABDATA2 checks NAME and NDNAME against the DECTAPE names stored as the first records of TAPE11 and TAPE12, respectively. If they do not match, program execution stops).

20. ITYPE, NND, IWLF, NWLC, NDFLAG
(5I5)

ITYPE	(=1, TAPE11 contains a static spectrum, =2, TAPE11 contains a fixed wavelength experiment, ≠1 or 2, TAPE11 contains a scanning kinetic experiment)
NND	Number of neutral density filters in the calibration file on TAPE12.
IWLF	When ITYPE=2, IWLF is the wavelength channel in the neutral density calibration file on TAPE12 whose wavelength is closest to the wavelength of the experiment.
NWLC	Number of wavelength channels in the neutral density calibration file on TAPE12.
NDFLAG	(=1, N.D. filter absolute absorbances are on TAPE13, ≠1, N.D. filter absolute absorbances are read from cards)

21. VARTIM, VARABS, SRFLAG, ITRIG
(2E10.4, 2I5)

22. FLTIME, PHILR, TIMSKP, PNSK, SSFDIS, SFPLSD, STPTIM
(3F6.4, I6, 3F6.4)

23. MFLAG, KFLAG, LFLAG, NINC, VMAX, JFLAG, IPDLT
(4I5,E10.4,I5,5X,I5)

(24) (NDABS(I,J),J=1,NND),I=1,NWLC)
(8E10.4)
Entry (24) appears only if NDFLAG ≠ 1

NDABS(I,j)	Absolute absorbance of the J'th neutral density filter at the I'th wavelength channel.

25. (7 8 9)

Data Card for ABCAL

26. NND
(I5)

27. ($6_{7_{8_{9}}}$)

ABCAL output file TAPE8 has the following structure:

1. NAME,ICOR
(A9,I5)

NAME	DECTAPE name of the experimental file; e.g., GULABD.RC
ICOR	A flag that is set equal to zero here. (Zero means that the absorbances have not been interpolated across each spectrum to correspond to a single time and have not been corrected for scattered light)

(Entries 2, 3, and 4 appear once for each wavelength channel in a scanning experiment or static spectrum starting with wavelength channel 1.)

2. NUM,N
(2I6)

NUM	Wavelength channel number
N	Number of Absorbances at wavelength channel NUM, not counting the absorbance of the infinity spectrum.

3. (TIME(J), VARTIM, ABSORB(J), VA(J), J ==1,N)
(4020)

TIME(J)	Time elapsed since end of fluid flow for the J'th stored point at wavelength channel NUM (in seconds)
VARTIM	Value entered on a data card in ABDATA or ABDATA2
ABSORB(J)	Absorbance of the J'th measurement at wavelength channel NUM.
VA(J)	VA(J) = VARABS/(g^{n-1}) where g = grouping factor, n = group number in which measurement J occurs.

4. TIMINF, VARTIM, AINFIN, VARINF
(4020)

TIMINF	Set equal to 1 x 10^6 seconds
AINFIN	Absorbance of channel NUM in the finitity spectrum.
VARINF	VARINF = VARABS/256

(NOTE: If TAPE12 has a static spectrum, entry 4 contains meaningless numbers. If TAPE12 has a fixed wavelength experiment, entries 2, 3, and 4 occur once each, and NUM=1)

TAPE9 of ABCAL has the following structure, repeated once for each wavelength channel in a scanning kinetic experiment.

1. NUM
   (1X, 'WAVELENGTH CHANNEL NUMBER', I5)
2. (TIME(J), VARTIM, ABSORB(J), VA(J), J=1,N)
   (8E10.4)
3. TIMINF, VARTIM, AINFIN, VARINF
   (8E10.4)

Instead of punching KINFIT data cards from TAPE9, the user can store TAPE9 as a permanent file or as an APLIB tape file.

APPENDIX F

Subroutine ORTHPOL

ORTHPOL is a subroutine of the program ABCAL (Appendix E) that fits absorbance A versus voltage V with the equation

$$A = A(V) = b_0P_0 + b_1P_1(V) +,\ldots, + b_5P_5(V) \qquad (F.1)$$

subject to certain restrictions regarding inflection points and statistical significance of the terms. In Equation (F.1) $P_0 \ldots P_5$ are orthogonal polynomial terms, each with degree in V equal to its subscript, and $b_0 \ldots b_5$ are parameters whose values are to be determined by ordinary least squares estimation. The orthogonal polynomials are defined by the following recursion equations (Himmelblau, 1970).

$$P_0 (V) = 1$$
$$P_j (V) = (V-\alpha_j)P_{j-1} - \gamma_j P_{j-2}, \quad j=1,2,\ldots,5$$

where

$$\alpha_0 = \gamma_0 = \gamma_1 = 0$$

$$\alpha_j = \sum_{k=1}^{N} V_k P_{j-1}^2(V_k) / \sum_{k=1}^{N} P_{j-1}^2(V_k), \quad j=1,2,\ldots,5$$

$$\gamma_j = \sum_{k=1}^{N} P_{j-1}^2(V_k) / \sum_{k=1}^{N} P_{j-2}^2(V_k), \quad j=2,3,\ldots,5$$

N = number of calibration points.

These polynomials have the orthogonality property

$$\sum_{k=1}^{N} P_j(V_k)\, P_i(V_k) = 0, \quad i \neq j \text{ for } i, j=0,1,\ldots,5. \quad (4.2)$$

The use of orthogonal polynomials gives a simple equation for estimating each b_j in Equation (4.1).

$$\hat{b}_j = \sum_{k=1}^{N} A_k P_j(V_k) / \sum_{k=1}^{N} P_j^2(V_k), \quad j=0,1,\ldots,5 \quad (4.3)$$

Note that $\hat{b}_j$ depends only on the values of A and P_j for the N calibration points. This means that the parameters are completely uncoupled; $\text{cov}(b_i, b_j) = 0$, if $i \neq j$, (see Appendix C). The estimated variance of each b_j is

$$\text{var}(b_j) = R_{LS} / [(N-M) \sum_{k=1}^{N} P_j^2(V_k)]$$

where M is the number of polynomial terms being used, and where R_{LS} is the least squares loss function defined by

$$R_{LS} = \sum_{k=1}^{N} (\hat{A}_k - A_k)^2$$

$$\hat{A}_k = \hat{b}_0 P_0 + \hat{b}_1 P_1(V_k) + \ldots \hat{b}_M P_M(V_k)$$

The advantage of orthogonal polynomials is that we can add and drop terms in Equation (F.1) without reestimating the remaining terms. Following is a summary of the procedure in ORTHPOL for determining what polynomial terms to use in Equation (F.1).

Let the parameters be written as a vector

$$\underline{b}^T = (b_1, b_2, \ldots, b_5).$$

ORTHPOL determines $\hat{\underline{b}}$ once. It then assumes that the relationship between A and V is at least of first degree in V. Thus $\hat{b}_0$ and $\hat{b}_1$ are always included in the equation. It then considers adding a third term from those that remain. (i.e., from $\hat{b}_2, \hat{b}_3, \hat{b}_4$, and $\hat{b}_5$). It determines which term, when added to Equation (4.1), gives the greatest improvement of the fit. The best new term is not automatically used, however. It must pass two tests. First an F test is performed to determine if the improvement of the fit is significant at the 95% confidence level. The F statistic is defined by the equation

$$F \equiv [R_{LS}(q) - R_{LS}(q+1)]/[R_{LS}(q+1)(N-q-1)]$$

where $R_{LS}(q)$ and $R_{LS}(q+1)$ are the ordering least squares loss functions for q and (q+1) parameters, respectively. If all calibration points have uniform variance normally distributed random measurement errors with expectation

value 0, then F has the F(1,N-q-1) distribution. The new term passes first test only if $F \geq F(1,N-q-1)$, in which case the new term is significant at the 95% confidence level.

The second test is a search for inflection points in A versus V over the range of the calibration data. If the degree of the polynomial is less than 3 there is no need to test for inflections. If the polynomial passes the inflection test (i.e., no inflections are found) ORTHPOL considers adding yet another term. Thus, ORTHPOL returns to the point in the loop where another term is added. If the polynomial fails the inflection test, ORTHPOL drops the term it was considering and tests the next best term. The final equation is chosen when either the list of terms to be added has been exhausted or the equation has one less parameter than the number of experimental points.

Tests 1 and 2 assure that:

1. The terms in the final equation are statistically significant at the 95% confidence level; and
2. There are no unwanted inflection points in the final equation.

On point 2 above, ORTHPOL has flags with which the user can decide to reject polynomials with only one inflection point, more than one inflection point, or to bypass the inflection test altogether. The flags are:

1. MFLAG (1, ORTHPOL automatically chooses a linear fit; ≠ 1, ORTHPOL considers adding terms to the linear function up to 5'th degree).
2. KFLAG (1, ORTHPOL requires ≥ 2 inflections within calibration range to reject a polynomial; ≠ 1, ORTHPOL requires ≥ 1 inflections within calibration range to reject a polynomial).
3. LFLAG (1, ORTHPOL checks for inflections from solvent versus solvent to VMAX; ≠ 1, ORTHPOL checks for inflections from solvent versus solvent to highest N.D. calibration point).
4. NINC Number of divisions into which inflection point search is divided.
5. VMAX If LFLAG = 1, ORTHPOL checks for inflections in A versus V from $V_{solvent}$ to V_{max}.
6. JFLAG (1, No inflection testing is performed; ≠ 1, inflection testing is performed).

APPENDIX G

Documentation of Principal Component Computer Programs

This Appendix gives instructions for using the computer programs with which the principal component calculations in Chapter 4 were performed. These programs are written in FORTRAN IV to run on the CDC 6500 computer at Michigan State University.

The following ten programs were used to perform the calculations in Chapter 4:

1. INTERP - Corrects absorbance-wavelength channel-time data from ABCAL (Appendix E) for the finite scan speed of the monochromator. INTERP can also use cutoff filter data to correct absorbances in the ultraviolet range for scattered visible light.

2. WEIGHTS - Estimates from a scanning experiment that has no reaction occurring and no spectral averaging the standard deviation of the random absorbance measurement errors at each wavelength channel.

3. RESOLV1 - Selects from an ABCAL or INTERP output file the absorbance-wavelength channel-time data that is to be used in a principal component analysis, reads principal component wavelength and time weights from cards, sets up this information for the solution of the eigenvalue

equations in RESOLV2, and provides three-dimensional plotting files of the matrix $\underline{A}$ and $(\underline{A} - \underline{\bar{A}})$ for the selected wavelengths and times.

4. RESOLV2 - Reads from the output file of RESOLV1 the absorbances and weights for the selected wavelengths and times, and solves the eigenvalue equation for weighted M analysis or weighted S analysis, depending on the value of a flag. RESOLV2 lists the eigenvalues and the mean of the nonessential eigenvalues. The output file of RESOLV2 contains the absorbances, weights, eigenvalues, and eigenvectors for the principal component analysis. The output file of RESOLV2 is an input file in programs that use these eigenvectors and eigenvalues.

5. RESOLV3 - Computes from the information on the output file of RESOLV2 the function $Q_r/(N-r)(p-r)$ for $r=1,2,\ldots,7$. RESOLV3 lists this function by individual wavelength channels and for all of the wavelength channels. RESOLV3 also provides files for three-dimensional plotting of $\underline{\hat{A}}_{(r)}$, $(\underline{\hat{A}}_{(r)} - \underline{\bar{A}})$, or weighted residuals for r=1,2,3,4, and n, where n is selected by the user.

6. RESOLV4 - Computes from the information in the output file of RESOLV2 the point-by-point values of $\underline{\hat{A}}_{(r)}$ and the weighted residuals for selected wavelength channels and values of r. The user has the option to obtain line printer plots of $\underline{\hat{A}}_{(r)}$ and $\underline{A}$ versus spectrum number and/or weighted residuals versus spectrum number for the selected wavelength channels.

7. STATIC - Performs an M or S analysis fit of a proposed static spectrum to the eigenvectors and eigenvalues from the output file of RESOLV2.

8. CONC - Performs an M analysis fit of a proposed concentration profile to the eigenvectors and eigenvalues from the output file of RESOLV2.

9. LIMIT2 - Computes from the information in the output file of RESOLV2 the solution bands for the normalized static spectra and concentration profiles of a two-absorber experiment or a two-absorber subspace of an experiment.

10. RESOLV6 - Reads from cards either the complete (mxm) rotation matrix U or the complete (mxm) rotation matrix V: RESOLV6 then computes V from U, or U from V, and the static spectra and concentration profiles of the m linearly independent absorbers.

The instructions for using these ten programs follows.

INTERP

INTERP uses, in addition to data cards, two input files, called TAPE10 and TAPE11. TAPE10 contains the calibrated absorbances and times for the scanning experiment that is to be corrected. TAPE11 contains the calibrated absorbances and times for a scanning experiment with the same conditions as the scanning experiment that is to be corrected, but with a cutoff filter that absorbs ultraviolet light inserted in the sample optical path. Both TAPE10 and TAPE11 come from the output file TAPE8 of the calibration program ABCAL (see Appendix E).

INTERP has one output file called TAPE12, that has the corrected absorbance-wavelength channel-time data in the following format, which is similar to the format of TAPE8 from ABCAL:

1. NAME, KFLAG, NAMCOR (A9,I5,A9)

   NAME - the DECTAPE name of the experimental file that has been corrected.

   KFLAG - (=1 if the data is corrected only for finite scan speed; = 2 if data is also corrected for scattered light).

   NAMCOR - the DECTAPE name of the experimental file that contains the cutoff filter information used to correct for scattered light.

(Entries 2 and 3 appear once for each wavelength channel)

2. I,NN (2I6)

   I - wavelength channel number

   NN - number of consecutive spectra (not including the infinity spectrum.

3. TCOR(J),ACOR(I,J),J=1,N (O20,20X,O20)

   TCOR(J) - corrected time of the J'th consecutive spectrum

   ACOR(I,J) - corrected absorbance at channel I in the J'th spectrum.

The following input deck executes INTERP:

Control Cards

1. ATTACH(TAPE10, Experiment file to be corrected)
2. ATTACH(TAPE11, Experiment file with cutoff filter)
3. ATTACH(INTERP,INTERP)
4. INTERP.
5. CATALOG(TAPE12, pfname)

Data Cards

1. NWLC,ICUT,NWLCOR (3I5)

   NWLC - number of wavelength channels in the scanning experiment.

   ICUT - (=0 if experiment is not to be corrected for scattered light; = 1 if experiment is to be corrected for scattered light)

   NWLCOR - number of wavelength channels starting with channel 1 that are to be corrected for scattered light if ICUT=1.

2. AFILT(I),I=1,NWLCOR (10X,E10.4)

   AFILT(I) - absorbance of the cutoff filter at wavelength channel I.

WEIGHTS

WEIGHTS requires an input file called TAPE9, which is the output file TAPE8 from ABCAL of a scanning experiment with no reaction occurring and with no spectral averaging (grouping factor =1).

The user specifies NWLC, the number of wavelength channels in the experiment. The following input deck executes WEIGHTS:

Control Cards

1. ATTACH(TAPE9,TAPE8 from ABCAL)
2. ATTACH(WEIGHTS,WEIGHTS)
3. WEIGHTS.

Data Cards

1. NWLC (I5)

RESOLV1

In addition to data cards, RESOLV1 requires an input file called TAPE9, which contains the absorbance-wavelength channel-time data for a scanning experiment, and comes from either TAPE12 of INTERP or from TAPE8 of ABCAL (if absorbance is not corrected by INTERP).

RESOLV1 prepares the absorbance data from selected wavelength channels and spectra for the solution of the eigenvalue problem in RESOLV2. The user specifies on data cards the selected wavelength channels and spectra and assigns values for the wavelength and time weights.

The input variables are as follows:

NWLC - number of wavelength channels in the complete experiment.

NOPCA - number of principal component calculations to be set up in this run of RESOLV1. (As originally programmed, NOPCA could be greater than one. However, as presently programmed, NOPCA should always be assigned the value 1).

KINF - (=0, input data on TAPE9 include the infinity spectrum; =1, input data on TAPE9 do not include the

infinity spectrum).

(As presently programmed, TAPE8 of ABCAL and TAPE12 of INTERP include the infinity spectrum, so that KINF=0 should be used.)

WL(I), I=1,NWLC - the wavelength weight for the I'th wavelength channel; i.e., WL(I)=L_i.

WT(J),J=1,N - the time weight for the J'th consecutive spectrum; i.e., WT(J)=T_j. N is the number of consecutive spectra in the complete experiment, including the infinity spectrum if KINF=0.

NW - number of wavelength channels to be used for the principal component calculation.

NT - number of spectra to be used for the principal component calculation.

LAM(I),I=1,NW - LAM(I) is the wavelength channel from the complete experiment that becomes the I'th wavelength channel used in the principal component calculation. If NW=NWLC all wavelength channels are selected for the principal component calculation and the LAM(I) array need not be specified by the user. However, if NW < NWLC, the user determines which wavelength channels are selected by specifying the LAM(I) array. For example, if NWLC=50, NW=5, and the wavelength channels 46-50 of the complete experiment are to be used for the principal component calculation, the user specifies LAM(1)=46, LAM(2)=47, LAM(3)=48, LAM(4)=49, and LAM(5)=50. In subsequent programs wavelength channel 1 in

the principal component analysis will correspond to wavelength channel 46 in the complete experiment.

ITIME(J),J=1,NT - ITIME(J) is the spectrum from the complete experiment that becomes the J'th spectrum used in the principal component analysis. ITIME(J) is treated analogously to LAM(I). Thus, the ITIME array is specified by the user only if NT < N.

RESOLV1 has three output files called TAPE10, TAPE11, and TAPE12. TAPE10 contains the data for solving the eigenvalue equation in RESOLV2. The structure of TAPE-10 is as follows:

1. NAME (A9)
2. NAMCOR (A9)
3. NOPCA (I5)
4. NW,NT(2I5)
5. LAM(I),I=1,NW (16I5)
6. ITIME(J),J=1,NT (16I5)
7. WL(LAM(I)),I=1,NW (6020)
8. WT(ITIME(J)),J=1,NT (6020)
9. A(LAM(I),ITIME(J)),J=1,NT (6020) (for each channel, I=1,NW)

TAPE11 contains the experimental data $\underline{A}$ for subsequent three dimensional plotting. TAPE11 has, for each wavelength channel I=1,NW,

A(LAM(I),ITIME(J)),J=1,NT (4020).

TAPE12 contains the experimental data matrix ($\underline{A} - \underline{\bar{A}}$) for subsequent three dimensional plotting. TAPE12 has for each wavelength channel I=1,NW.

A(LAM(I),ITIME(J)) - AVE(LAM(I)),J=1,NT (4020)

The following input deck executes RESOLV1:

Control Cards

1. ATTACH(TAPE9, TAPE8 from ABCAL or TAPE12 from INTERP)
2. ATTACH(RESOLV1,RESOLV1)
3. RESOLV1.
4. CATALOG(TAPE10,Pfname)
5. CATALOG(TAPE11,Pfname)
6. CATALOG(TAPE12,Pfname)

Data Cards

1. Two cards with messages for output (40A2)
2. NWLC,NOPCA,KINF (8E10.4)
3. WL(I),I=1,NWLC (8E10.4)
4. WT(J),J=1,N (8E10.4)
5. NW,NT (2I5)
6. LAM(I),I=1,NW (16I5)

(Entry 6 does not appear if NW=NWLC)

7. ITIME(J),J=1,NT (16I5)

(Entry 7 does not appear if NT=N)

RESOLV2

RESOLV2 requires an input data file called TAPE13, which is the output file TAPE10 from RESOLV1. The user determines whether RESOLV2 performs an M or S analysis by setting the value of a flag variable called IFLAG. If IFLAG=1, an M analysis is performed, and if IFLAG=0, an S analysis is performed.

RESOLV2 produces an output file called TAPE14, which contains the absorbance data, the weights, and the M or S analysis eigenvectors. TAPE14 is an input data file for each program that uses the M or S analysis eigenvectors. The structure of TAPE14 follows:

1. NAME (A9)
2. NAMCOR (A9)
3. NW,NT,IFLAG (3I5)
4. LAM(I),I=1,NW (16I5)
5. ITIME(J),J=1,NT (16I5)
6. WL(I),I=1,NW (6020)
7. WT(J),J=1,NT (6020)
8. A(I,J),J=1,NT,I=1,NW (6020)
9. B(I,J),J=1,NT,I=1,NW (6020)

(If IFLAG=1, then B(I,J) is the I,J'th element of $\underline{\Phi}$; if IFLAG=0, then B(I,J) is the I,J'th element of $\underline{B}$.)

10. EIG(I),I=1,NW (6020)

(The EIG array contains the M or S analysis eigenvalues, depending on the value of IFLAG.)

11. AVE(I),I=1,NW (6020)

(AVE(I)=0.0 if IFLAG=1; AVE(I) is the average absorbance at wavelength channel I if IFLAG=0.)

The following input deck executes RESOLV2:

Control Cards

1. ATTACH(TAPE13, TAPE10 from RESOLV1)
2. ATTACH(RESOLV2,RESOLV2)
3. RESOLV2.
4. CATALOG(TAPE14, Pfname)

Data Cards

1. Two cards with messages for output (40A2)
2. IFLAG (I5)

RESOLV3

RESOLV3 requires an input file called TAPE12, which is the output file TAPE14 from RESOLV2. RESOLV3 has five output files which contain the reconstructed absorbance data in a format for three dimensional plotting. These files are as follows:

TAPE1 - one eigenvector reconstruction

TAPE2 - two eigenvector reconstruction

TAPE3 - three eigenvector reconstruction

TAPE4 - four eigenvector reconstruction

TAPE5 - KQ eigenvector reconstruction, where KQ is set by the user

The type of surface represented in these files is determined by the flag variable JPLOT, which is set by the user. If JPLOT = 0, the reconstructed absolute absorbance $\underline{\hat{A}}_{(r)}$ is represented. If JPLOT=1, the reconstructed difference surface $\underline{\hat{A}}_{(r)} - \underline{\bar{A}}$ is represented, and if JPLOT =2, the residual surface $\underline{\hat{A}}_{(r)} - \underline{A}$ is represented. Each output file has the format

```
X(I,J),J=1,NT,I=1,NW (4020)
```

where X is the appropriate matrix for the surface designated by the value of JPLOT.

The following input deck executes RESOLV3:

Control Cards

1. ATTACH(TAPE12,TAPE14 from RESOLV2)
2. ATTACH(RESOLV3, RESOLV3)
3. RESOLV3.

Data Cards

1. Two cards with messages for output (40A2)
2. JPLOT,KQ (2I5)

RESOLV4

RESOLV4 requires the input file TAPE11, which is the output file TAPE14 of RESOLV2. By assigning values for

the following input variables, the user determines the wavelength channels and number of eigenvectors for which RESOLV4 computes the reconstructed absorbances and residuals.

NCP - the number of wavelength channels for which reconstructed absorbances and residuals are to be computed (NCP $\leq$ NW).

NCASE - the number of cases to be shown for each of the NCP wavelength channels. Each case corresponds to a certain number of eigenvectors, specified below.

JFLAG - (=0, no two dimensional plots; =1, calculated and experimental absorbance versus spectrum number plotted for each channel and each case; =2, weighted residuals versus spectrum number plotted for each case; =3, calculated and experimental absorbances and weighted residuals plotted for each case).

ICP(I),I=1,NCP - Each ICP(I) is one of the wavelength channel numbers for which absorbances and residuals are calculated. These wavelength channel numbers correspond to the enumeration of wavelength channels for the principal component calculation and are not necessarily the same as the wavelength channel numbers for the complete experiment (see instructions for RESOLV1 above).

IQ(I),I=1,NCASE - Each IQ(I) is a number of eigenvectors for which RESOLV4 computes the reconstructed absorbances and residuals.

The following input deck executes RESOLV4:

Control Cards

1. ATTACH(TAPE11, TAPE14 from RESOLV2)
2. ATTACH(RESOLV4, RESOLV4)
3. RESOLV4.

Data Cards

1. Two cards with messages for output (40A2)
2. NCP,NCASE,JFLAG (3I5)
3. ICP(I),I=1,NCP (16I5)
4. IQ(I),I=1,NCASE (16I5)

STATIC

STATIC requires the input file TAPE10, which is the output file TAPE14 from RESOLV2. STATIC fits a proposed static spectrum to the M or S analysis eigenvectors, depending on which type of eigenvectors TAPE10 contains. The user has the option of reading the proposed static spectrum from an input file called TAPE11, which has the same format as the ABCAL output file TAPE8 for a measured static spectrum. Alternatively, the user can enter the proposed static spectrum by cards.

Recall that in Equation (3.16) the term W_{fi} is set equal to unity if there is a proposed value for channel i and is set equal to zero otherwise. In STATIC, the user has the option of setting the nonzero W_{fi}'s equal to positive values other than unity. This would correspond to a weighted least squares fit of the proposed static spectrum.

The input variables for STATIC are as follows:

NWS - the total number of wavelength channels in the proposed static spectrum.

NWSU - the number of wavelength channels in the proposed static spectrum that are to be fit to the M or S analysis eigenvectors (NWSU < NWS)

NN - set equal to one.

NQ - the number of eigenvectors to be used in fitting the proposed static spectrum (should be set equal to the essential rank m)

IWT - (=0, all nonzero W_{fi} or W_{si} set equal to unity; =1, values of nonzero W_{fi} or W_{si} are set by the user)

IREAD - (=0, the proposed static spectrum is read from input file TAPE11; =1, the proposed static spectrum is read from cards).

IS(I),IR(I),I=1,NWSU - These arrays are specified by the user only when NWSU < NW, where NW is the number of wavelength channels used in the principal component calculation. IS(I) is the number of the wavelength channel in the proposed static spectrum that corresponds to wavelength channel IR(I) in the enumeration of wavelength channels for the principal component calculation.

WEIGHT(I),I=1,NWSU - This array is specified by the user only if IWT=1 above. WEIGHT(I) is the nonzero weight to be used for the I'th wavelength channel of the proposed static spectrum if IWT=1. If IWT=0, STATIC sets each element of the WEIGHT array equal

to unity.

FJ(I),I=1,NWS - This array is specified by the user only if IREAD=1. FJ(I) is the value for the I'th wavelength channel of the proposed static spectrum.

The following input deck executes STATIC:

Control Cards

1. ATTACH(TAPE10, output file TAPE14 from RESOLV2)
2. ATTACH(TAPE11, file containing proposed static spectrum if IREAD=0)
3. ATTACH(STATIC,STATIC)
4. STATIC.

Data Cards

1. Two cards with messages for output (40A2)
2. NWS,NWSU,NN,NQ,IWT,IREAD (6I5)

(Entry 3 appears only when NWSU < NW)

3. IS(I),IR(I),I=NWSU (2I5)

(Entry 4 appears only when IWT=1)

4. WEIGHT(I),I=1,NWSU (10x,E10.4)

(Entry 5 appears only when IREAD=1)

5. FJ(I),I=1,NWS (8E10.4)

CONC

CONC requires an input data file called TAPE10, which is the output file TAPE14 from RESOLV2. TAPE10 should contain M analysis eigenvectors. The proposed concentration profile may be read from an input file called TAPE11 or from cards. If TAPE11 is used, its format should be

CONC(J),J=1,NT (5X,E10.4)

where CONC(J) is the proposed concentration in the J'th consecutive spectrum.

Recall that in Equation (3.19) the nonzero W_{ci}'s were all set equal to unity. In CONC the user has the option of setting the nonzero W_{ci}'s equal to positive values other than unity. This would correspond to weighted least squares fitting of the proposed concentration vector.

CONC has an output file called TAPE12 that has the following structure:

CEST(J),J=1,NT (5X,E10.4)

where CEST(J) is the estimated concentration in the J'th consecutive spectrum.

The input variables for CONC are as follows:

NQ - the number of eigenvectors used to fit the proposed concentration profile.

IWT - (=0, all nonzero W_{ci} set equal to unity; =1, user specifies values for the nonzero W_{ci})

IREAD - (=0, proposed concentration profile is read from input file TAPE11; =1, proposed concentration profile is read from cards)

CONC(J),J=1,NT - the proposed concentration in consecutive spectrum J.

WEIGHT(J),J=1,NT - This array is specified only if IWT=1. WEIGHT(J) is the nonzero weight used for the proposed concentration in the J'th consecutive spectrum.

The following input deck executes CONC:

Control Cards

1. ATTACH(TAPE10, output file TAPE14 from RESOLV2)
2. ATTACH(TAPE11, file containing proposed concentration profile if IREAD=0)
3. ATTACH(CONC,CONC)
4. CONC.

Data Cards

1. Two cards with messages for output (40A2)
2. NQ,IWT,IREAD (3I5)

(Entry 3 appears only if IREAD=1)

3. CONC(J),J=1,NT (5X,E10.4)

(Entry 4 appears only if IWT=1)

4. WEIGHT(J),J=1,NT (8E10.4)

LIMIT2

LIMIT2 requires an input file called TAPE10, which is the output file TAPE14 from RESOLV2. TAPE10 should contain the M analysis eigenvectors of an experiment or subspace of an experiment for which the essential rank m equals 2.

The following input deck executes LIMIT2.

Control Cards

1. ATTACH(TAPE10, output file TAPE14 from RESOLV2)
3. ATTACH(LIMIT2,LIMIT2)
3. LIMIT2.

Data Cards

1. Two cards with messages for output (40A2)

RESOLV6

RESOLV6 requires an input file called TAPE10, which is the output file TAPE14 from RESOLV2. TAPE10 should

contain M analysis eigenvectors.

The user supplies either the complete (mxm) rotation matrix U or the complete (mxm) rotation matrix V. RESOLV6 then extracts from the M analysis eigenvectors the estimated static spectra and the concentration profiles for the m linearly independent absorbers.

The input variables for RESOLV6 are as follows:

NQ - the essential rank m.

JOPT - (=0, the matrix U is specified by the user; =1, the matrix V is specified by the user).

U(I,J),I=1,NQ,J=1,NQ - If JOPT=0, the user specifies one column at a time the rotation matrix U.

V(I,J),I=1,NQ,J=1,NQ - If JOPT=1, the user specifies one column at a time the rotation matrix V.

The following input deck executes RESOLV6:

Control Cards

1. ATTACH(TAPE10, output file TAPE14 from RESOLV2)
2. ATTACH(RESOLV6,RESOLV6)
3. RESOLV6.

Data Cards

1. Two cards with messages for output (40A2)
2. NQ,JPOT (2I5)
3. If JPOT=0, then for each column J=1,NQ, U(I,J), I=1,NQ (8E10.4)
4. If JPOT=1, then for each column J=1,NQ, V(I,J), I=1,NQ (8E10.4)

APPENDIX H

Simple Michaelis Menten Mechanism Singular Perturbation Solutions

1. First Order Singular Perturbation Solutions to Equations (5.22) and (5.23)

Zeroth Order Inner Equations

$$(ds_0/d\sigma) = 0$$

$$(dc_0/d\sigma) = (1-\gamma)s_0 + (\gamma-1)c_0s_0 + \gamma - (\gamma+K)c_0 \qquad (H.1)$$

First Order Inner Equations

$$(ds_1/d\sigma) = - s_0 + s_0c_0 + (K-\lambda)c_0$$

$$(dc_1/d\sigma) = (1-\gamma)s_1 + (\gamma-1)c_0s_1 + (\gamma-1)c_1s_0$$

$$+ \gamma - (\gamma+K)c_1 + \gamma c_0(c_0-1) \qquad (H.2)$$

Zeroth Order Outer Equations

$$(d\bar{s}_0/d\tau) = - \bar{s}_0 + \bar{c}_0\bar{s}_0 + (K-\lambda)\bar{c}_0$$

$$0 = (1-\gamma)\bar{s}_0 + (\gamma-1)\bar{c}_0\bar{s}_0 + \gamma - (\gamma+K)\bar{c}_0 \qquad (H.3)$$

First Order Outer Equations

$$(d\bar{s}_1/d\tau) = \bar{s}_1 + \bar{c}_0\bar{s}_1 + \bar{c}_1\bar{s}_0 + (K-\lambda)\bar{c}_1$$

$$(d\bar{c}_0/d\tau) = (1-\gamma)\bar{s}_1 + (\gamma-1)\bar{c}_0\bar{s}_1 + (\gamma-1)\bar{c}_1\bar{s}_0$$

$$+ \gamma - (\gamma+K)\bar{c}_1 + \gamma(\bar{c}_0-1)\bar{c}_0 \qquad (H.4)$$

$S_{(1)}$ and $C_{(1)}$ are the total first order singular perturbation solutions for the entire time course of the reaction,

$$S_{(1)} = s_{(1)} + \bar{s}_{(1)} - \hat{s}_{(1)} = s_0 + \bar{s}_0 + \mu(s_1 + \bar{s}_1) - \hat{s}_{(1)}$$

$$C_{(1)} = c_{(1)} + \bar{c}_{(1)} - \hat{c}_{(1)} = c_0 + \bar{c}_0 + \mu(c_1 + \bar{c}_1) - \hat{c}_{(1)} \qquad (H.5)$$

where

$$s_0 = 1 \qquad (H.6)$$

$$c_0 = (1+K)^{-1}(1-\{\exp[-(1+K)\tau\mu^{-1}\}) \qquad (H.7)$$

$$s_1 = -\lambda\tau\mu^{-1}(1+K)^{-1} + (1+K-\lambda)(1+K)^{-2}\{\exp[-(1+K)\tau\mu^{-1}]\}$$

$$+ (\lambda-1-K)(1+K)^{-2} \qquad (H.8)$$

$$c_1 = \{\gamma[-(1+K)^3 + \gamma(1+K) + \gamma K(1+K)]$$

$$- (1-\gamma)[-(\lambda/2)(1+K)^2\tau^2\mu^{-2} + (1+K)(1+K-\lambda)(K-1)\tau\mu^{-1}$$

$$+ 1+2K-\lambda-2K\lambda+K^2]\}(1+K)^{-4}\exp[-(1+K)\tau\mu^{-1}]$$

$$+ [\gamma(2K+2-\lambda) + (\lambda-K-1)](1+K)^{-4}\exp(-2(1+K)\tau\mu^{-1}]$$

$$+ [(1-\gamma)(1+K)K\lambda\tau\mu^{-1} + (1-\gamma)K(1+K-2\lambda)$$

$$+ \gamma(1+K)^3 - \gamma K(1+K)](1+K)^{-4} \qquad (H.9)$$

$\bar{s}_0$ is the solution of the transcendental equation

$$(1-\gamma)[\gamma(\lambda-K)-\lambda]^{-1}(s_0-1)$$

$$- K(\gamma(1+K+\lambda) +\lambda][\gamma(\lambda-K)-\lambda]^{-2} \ell n \{(-\lambda)^{-1}[\bar{s}_0(\gamma(\lambda-K)-\lambda)$$

$$(K-\lambda)\gamma] = \tau \qquad (H.10)$$

$\bar{c}_0$, $\bar{s}_1$ and $\bar{c}_1$ are expressed as functions of $\bar{s}_0$.

$$\bar{c}_0 = [(1-\gamma)s_0 + \gamma][(1-\gamma)s_0 + \gamma + K]^{-1} \qquad (H.11)$$

$$\bar{s}_1 = T_1(1+K-\lambda)[\lambda(1+K) + T_3]^{-1} + X_1 + X_2 + X_3 + X_4 + X_5$$

$$+ X_6 + X_7 + X_8 \qquad (H.12)$$

$$\bar{c}_1 = T_3^{-4} K(1-\gamma)T_3^3\bar{s}_1 + \gamma T_3^4 - \gamma K(T_3 - K)T_3^2 + K(\gamma-1)T_1 \qquad (H.13)$$

with

$$T_1 = \gamma(K-\lambda) + \bar{s}_0[\gamma(\lambda-K)-\lambda]$$

$$T_2 = [\gamma(\lambda-K)-\lambda]$$

$$T_3 = \gamma + K + (1-\gamma)\bar{s}_0$$

$$T_4 = K[\gamma(1+K-\lambda) + \lambda]$$

$$T_5 = \gamma(1+K) + K - \lambda$$

$$T_6 = \gamma(1+\lambda-K) + K-\lambda$$

$$T_7 = \lambda(\gamma-1) + \gamma(1+K)$$

$$T_8 = \log\{(-\lambda)^{-1}[(K-\lambda)\gamma + (\gamma(\lambda-K)-\lambda)\bar{s}_0]\}$$

$$T_9 = \log\{(1+K)^{-1}[\gamma + K + \bar{s}_0(1-\gamma)]\}$$

$$T_{10} = \log\{(-\lambda)[\gamma+K+(1-\gamma)\bar{s}_0](K+1)^{-1}[(K-\lambda)\gamma+[\gamma(\lambda-K)-\lambda]\bar{s}_0]\}$$

$$X_1 = \gamma T_1 T_2^{-2} T_3^{-1} T_5\{T_8 + \gamma(K-\lambda)\ (T_1^{-1} + \lambda^{-1})\}$$

$$X_2 = \gamma(1-\gamma)T_1 T_2^{-3} T_3^{-1}\{T_1 + \lambda - 2\gamma(K-\lambda)T_8 - \gamma^2(K-\lambda)^2 (T_1^{-1} + \lambda^{-1})\}$$

$$X_3 = \gamma(\gamma+K)\ (T_1+\lambda)T_2^{-1}T_3^{-1}$$

$$X_4 = \gamma K(\gamma-1)T_1 T_3^{-1}\{\gamma^2(K-\lambda)^2 T_2^{-2}T_4^{-1}(T_1^{-1}+\lambda^{-1})\}$$
$$+ \gamma(K-\lambda)T_2^{-2}T_8[\gamma[\gamma(K-\lambda) + K(2K+1-2\lambda) + \lambda] + 2K\lambda]$$
$$+ \gamma K T_1 T_3^{-1} T_4^{-2} T_9\ (\gamma+K)^2$$

$$X_5 = -\gamma K T_1 T_3^{-1} T_6\{\gamma(\lambda-K)T_2^{-1}T_4^{-1}(T_1^{-1} + \lambda^{-1}) - (\gamma+K)T_4^{-2}T_{10}\}$$

$$X_6 = \gamma^2(\lambda-K)T_1 T_3^{-1} T_4^{-1}\{T_1^{-1} + \lambda^{-1} + (1-\gamma)T_4^{-1}T_{10}\}$$

$$X_7 = T_1 T_3^{-1}\{K(\gamma+K)T_4^{-1}[(K+1)^{-1} - T_3^{-1}] - K\gamma(K-\lambda)(1-\gamma) T_4^{-2}T_{10}\}$$

$$X_8 = KT_1T_3^{-1}T_4^{-1}(1-\gamma)(K-\lambda)\{T_3^{-1} - (1+K)^{-1} + T_2T_4^{-1}T_{10}\}$$

$$\hat{s}_{(1)} = 1 - \lambda\tau(1+K)^{-1} + \mu(\lambda-K-1)(1+K)^{-2} \qquad \text{(H.14)}$$

$$\hat{c}_{(1)} = (1+K)^{-1} + K\lambda(\gamma-1)\tau(1+K)^{-3} \qquad \text{(H.15)}$$

$$+ \mu[K(\gamma-1)(1+K-2\lambda) + \gamma(1+K)^3 - \gamma K(1+K)](1+K)^{-4}$$

2. First Order Singular Perturbation Solutions to Equations (5.25) and (5.26)

$P_{(1)}$ and $C_{(1)}$ are total first order singular perturbation solutions for the entire time course of the reaction.

$$P_{(1)} = p_{(1)} + \bar{p}_{(1)} - \hat{p}_{(1)}$$

$$C_{(1)} = c_{(1)} + \bar{c}_{(1)} - \hat{c}_{(1)} \qquad \text{(H.16)}$$

where

$$p_0 = 0 \qquad \text{(H.17)}$$

$$c_0 = (1+K)^{-1}(1-\{\exp[-(1+K)\tau\mu^{-1}]\}) \qquad \text{(H.18)}$$

$$p_1 = -\lambda(1+K)^{-1}\tau\mu^{-1} + \lambda(1+K)^{-2}(-1+\{\exp[-(1+K)\tau\mu^{-1}]\}) \qquad \text{(H.19)}$$

$$c_1 = \{(K-1)[\lambda(\gamma-1) + K+1](K+1)^{-3}\tau\mu^{-1}$$

$$+ \lambda(\gamma-1)2^{-1}(1+K)^{-2}\tau^2\mu^{-2} - [\lambda(1-\gamma) - (1+K)](1+K)^{-4}$$

$$+ K\lambda(\gamma-1)(1+K)^{-4} - [\lambda K(1-\gamma) + (K+1)((K+1)K+1])(1+K)^{-4}\}$$

$$\{\exp[-(1+K)\tau\mu^{-1}]\}$$

$$+ [\lambda(1-\gamma) - (1+K)](1+K)^{-4}\{\exp[-2(1+K)\tau\mu^{-1}]\}$$

$$+ K\lambda(\gamma-1)(1+K)^{-4}[(1+K)\tau\mu^{-1}-1]$$

$$+ \{\lambda K(1-\gamma) + (K+1)[(K+1)K+1]\}(1+K)^{-4} \qquad \text{(H.20)}$$

$\bar{p}_0 = 1-\bar{s}_0$ where $\bar{s}_0$ is given by Equation (H.10)

$$\bar{p}_1 = T_1T_3^{-1}(1+K)^{-1} + Y_1 + Y_2 + Y_3 + Y_4 + Y_5 + Y_6 + Y_7 + Y_8 \qquad \text{(H.21)}$$

$$\bar{c}_1 = T_3^{-1}\{K(\gamma-1)T_3^{-1}\bar{p}_1+1-K(1+(\gamma-1)\bar{p}_0]T_3^{-2}-K(1-\gamma)T_1T_3^{-3}\} \qquad \text{(H.22)}$$

where

$$Y_1 = -\gamma(\gamma-1)T_1T_3^{-1}T_2^{-3}\{T_2\ \bar{p}_0$$

$$- 2\lambda T_8 + \lambda^2T_1^{-1} + \lambda\}$$

$$Y_2 = -T_1T_7T_3^{-1}T_2^{-2}\{T_8-\lambda T_1^{-1} - 1\}$$

$$Y_3 = -T_1\lambda(1+K)T_3^{-1}T_2^{-1}\{\lambda^{-1} + T_1^{-1}\}$$

$$Y_4 = -T_1 K\gamma(1-\gamma)T_3^{-1}\{-\lambda^2 T_4^{-1}T_2^{-2}T_1^{-1}$$

$$- \lambda T_4^{-1}T_2^{-2} + T_4^{-2}[(1+K)^2(\gamma-1)^{-1}T_9$$

$$+ \lambda[\lambda(1-\gamma) + 2\ T_4]T_2^{-2}T_8\}$$

$$Y_5 = T_1 K(T_7-\gamma K)T_3^{-1}\{+\lambda T_4^{-1}T_2^{-1}T_1^{-1}$$

$$+ T_4^{-1}T_2^{-1} - (1+K)T_4^{-2}T_{10}\}$$

$$Y_6 = \lambda K T_1 T_4^{-1}T_3^{-1}\{-T_1^{-1}-\lambda^{-1}$$

$$+ (\gamma-1)T_4^{-1}T_{10}\}$$

$$Y_7 = K\lambda(1-\gamma)T_1 T_3^{-1}T_4^{-1}\{T_3^{-1} - (1+K)^{-1}$$

$$+ T_2 T_4^{-1}T_{10}\}$$

$$Y_8 = -\gamma K(1-\gamma)T_1 T_3^{-1}\{(1+K)(\gamma-1)^{-1}T_4^{-1}T_3^{-1}$$

$$- (\gamma-1)^{-1}T_4^{-1} + \lambda T_4^{-2}T_{10}\}$$

$$\hat{p}_{(1)} = -\lambda\mu(1+K)^{-2} + \lambda\tau(1+K)^{-1} \qquad \text{(H.24)}$$

$$\hat{c}_{(1)} = (1+K)^{-1} + \mu[2K\lambda(1-\gamma)(1+K)^{-4} + (1+K)^{-1}$$

$$- K(1+K)^{-3}] + \tau K\lambda(\gamma-1)(1+K)^{-3} \qquad \text{(H.25)}$$

APPENDIX I

Matching of the Inner and Outer Singular Perturbation Solutions

The initial conditions for the outer solution are obtained by matching the inner and outer solutions. We note that in the limit $\mu \to 0$, $\sigma = (\tau/\mu) \to \infty$, even for τ close to zero. Thus, σ is very large near the beginning of the outer solution. We assume that the inner and outer solutions match where σ is large enough that exponential terms in Equations (H.6) through (H.9) vanish, but that $\tau \simeq 0$.

For σ very large,

$$s_{(1)\ \sigma \text{ very large}} = 1 + \mu(1+K)^{-1}[-\lambda\sigma + (\lambda-1-K)(1+K)^{-1}] \tag{I.1}$$

$$c_{(1)\ \sigma \text{ very large}} = (1+K)^{-1} + \mu(1+K)^{-4}\{K(1+K)[\lambda\sigma(1-\gamma)-\gamma] + K(1+K-2\lambda)(1-\gamma) + \gamma(1+K)^3\} \tag{I.2}$$

In the τ time scale, Equations I.1) and (I.2) are

$$s_{(1)} = 1 - \lambda\tau(1+K)^{-1} + \mu(\lambda-1-K)(1+K)^{-2} \tag{I.3}$$

$$c_{(1)} = (1+K)^{-1} + K\lambda\tau(1-\gamma)(1+K)^{-3}$$

$$+ \mu(1+K)^{-4}[K(1+K-2\lambda)(1-\lambda)$$

$$+ \gamma(1+K)(1+K+K^2)] \qquad (I.4)$$

When $\tau = 0$, Equations (I.3) and (I.4) become

$$s_{(1)\ \sigma \text{ very large}\ \tau=0} = 1 + \mu(\lambda-1-K)(1+K)^{-2} \qquad (I.5)$$

$$c_{(1)\ \sigma \text{ very large}\ \tau=0} = (1+K)^{-1} + \mu(1+K)^{-4}[K(1+K-2\lambda)(1-\gamma)$$

$$+ \gamma(1+K)(1+K+K^2)] \qquad (I.6)$$

Matching requires

$$\bar{s}_{(1)} = s_{(1)\ \sigma \text{ very large}\ \tau=0} = 1 + \mu(\lambda-1-K)(1+K)^{-2}$$

$$= \bar{s}_0(0) + \mu\bar{s}_1(0) \qquad (I.7)$$

and

$$\bar{c}_{(1)}(0) = c_{(1)\ \sigma \text{ very large}\ \tau=0} = (1+K)^{-1}$$

$$+ \mu(1+K)^{-4}[K(1+K-2\lambda)(1-\gamma)$$

$$+ \gamma(1+K)(1+K+K^2)] = \bar{c}_0(0) + \mu\bar{c}_1(0) \qquad (I.8)$$

Equations (I.7) and (I.8) are satisfied without loss of

generality by Equations (I.9)

$$\bar{s}_0(0) = 1$$

$$\bar{s}_1(0) = (\lambda-1-K)(1+K)^{-2}$$

$$\bar{c}_0(0) = (1+K)^{-1}$$

$$\bar{c}_1(0) = K(1+K-2\lambda)(1-\gamma)(1+K)^{-4}$$

$$+ \gamma(1+K)^{-3}(1+K+K^2) \qquad \text{(I.9)}$$

REFERENCES

REFERENCES

Anderson, T. W., Ann. of Math. Stat., 34, 122 (1963).

Atkinson, Anthony C., and William G. Hunter, Technometrics, 10(2), 271 (1968).

Beck, James V. and Kenneth J. Arnold, Parameter Estimation in Engineering and Science, Preliminary Edition, March 1975 Revision (Michigan State University, East Lansing, MI, 1975).

Bellman, R., Introduction to Matrix Analysis, Second Edition (McGraw-Hill Book Company, New York, 1970).

Bernhard, S. A., M. F. Dunn, P. L. Luisi, and P. Shack, Biochemistry, 9(1), 185 (1970).

Box, G. E. P., and H. L. Lucas, Biometrika, 46, 77 (1959).

Box, G. E. P., and W. J. Hill, Technometrics, 9(1), 57 (1967).

Bränden, Carl-Ivar, Hans Jovnvall, Hans Eklund, and Bo Furugren, "Alcohol Dehydrogenases", The Enzymes, 3rd Ed., Vol. 11, Paul D. Boyer, Ed., (Academic Press, New York, 1975).

Brooks, Robert L., Joseph D. Shore, and H. Gutfreund, The Journal of Biological Chemistry, 247(8), 2382 (1972).

Bulmer, J. T. and H. F. Shurvell, J. Phys. Chem., 77, 256 (1973).

Cleland, W. W., "Steady State Kinetics", The Enzymes, 3rd ed., Vol. 2, Paul D. Boyer, Ed., (Academic Press, New York, 1970).

Control Data 6400/6500/6600 Computer Systems SCOPE Reference Manual (1969). Palo Alto, California.

Coolen, Richard B., Ph.D. Thesis, Michigan State University, 1974.

Coolen, R. B., N. Papadakis, J. Avery, C. G. Enke, and J. L. Dye, Anal. Chem., 47, 1649 (1975).

Cukier, R. I., C. M. Fortuin, K. E. Shuler, A. G. Petsckek, and J. H. Schaibly, J. Chem. Phys., 59(8) 3873 (1973).

Cukier, R. I., J. H. Schaibly, and K. E. Shuler, J. Chem. Phys., 63(3), 1140 (1975).

Curtis, A. R. and E. M. Chance, Analysis and Simulation of Biochemical Systems, Vol. 25, H. C. Hemker and B. Hess, Eds., F.E.B.S., 39 (1972).

Dalziel, K., Biochem. J., 80, 440 (1961).

Dalziel, K., and F. M. Dickinson, Biochem, J., 100, 34 (1966).

Dalziel, Keith, "Kinetics and Mechanism of Nicotinamide-Nucleotide-Linked Dehydrogenases", The Enzymes, 3rd Ed., Vol. 11, Paul D. Bayer, Ed., (Academic Press, New York, 1975).

Darvey, I.G., S. J. Prokhornik, and J. F. Williams, J. Theoret. Biol., 11, 459 (1966).

Dunn, M. F., and Sidney A. Bernhard, Biochemistry, 10, No. 24, 4569 (1971).

Dunn, Michael F., and J. Scott Hutchinson, Biochemistry, 12, No. 24, 4882 (1973).

Dunn, Michael F., Biochemistry, 13, NO. 6, 1146 (1974).

Dunn, Michael F., Jean-Francois Biellmann, and Guy Branlant, Biochemistry, 14, No. 14, 3176 (1975).

Dye, J. L., and L. H. Feldman, Rev. Sci. Instr., 37, 154 (1966).

Dye, J. L. and V. Nicely, J. Chem. Ed., 48, 443 (1971).

Fisher, Harvey F., Dismus L. Adija, and Dallas G. Cross, Biochemistry, 8(11), 4424 (1969).

Gear, C. W., Numerical Initial Value Problems in Ordinary Differential Equations, (Prentice-Hall, Inc., New Jersey, 1971).

Gutfreund, H., Disc. Farad. Soc., 20, 167 (1955).

Hammes, Gordon G., and Paul R. Schimmel, "Rapid Reactions and Transient States", The Enzymes, 3rd Ed., Vol. 2, Paul D. Bayer, Ed., (Academic Press, New York, 1970).

Heineken, F. G., H. M. Tsuchiya, and R. Aris, Mathematical Biosciences, 1, 95 (1967).

Hemker, P. W., Analysis and Simulation of Biochemical Systems, Vol. 25, A. C. Hemker and B. Hess, Eds., F.E.B.S., 59 (1972).

Hill, William J., William G. Hunter, and Dean W. Wichern, Technometrics, 10(1) 145 (1968).

Hill, William J., and William G. Hunter, Technometrics, 16(3), 425 (1974).

Himmelblau, David M., Process Analysis by Statistical Methods, (John Wiley and Sons, (1970)).

Holbrook, J. J., and H. Gutfreund, FEBS Letters, 31(2), 157 (1973).

Hollaway, M. R. and H. A. White, Biochem. J., 149, 221 (1975).

Hommes, F. A., Arch. Biochem. Biophys., 96, 28 (1962).

Hommes, F. A., Arch. Biochem. Biophys., 96, 32 (1962).

Hugus, Z. Z., Jr. and A. A. El-Awady, J. Phys. Chem., 75, 2954 (1971).

Hunter, William G., and Albey M. Reiner, Technometrics, 7(3), 307 (1965).

Kankare, J. J., Anal. Chem., 42, 1322 (1970).

Kaplan, Nathan O., "The Pyridine Coenzymes", The Enzymes, 2nd Ed., Vol. 3, Paul D. Boyer, Henry Lardy and Karl Myrbäck, Eds. (Academic Press, New York, 1960).

Lawton, W. H. and E. A. Sylvestre, Technometrics, 13, 617 (1971).

Luisi, Pier Luigi, and Robert Favilla, Biochemistry, 11, No. 12, 2303 (1972).

M.S.U. Computer Laboratory, Computer Laboratory User's Guide, Vol. II, (1973).

Maguire, R. J., N. H. Hijazi, and K. J. Laidler, Biochem. Biophys. Acta., 341, 1 (1974).

McFarland, James T., and Sidney A. Bernhard, Biochemistry, 11, No. 8, 1486 (1972).

Michaelis, L. and M. L. Menten, Biochem. Z., 49, 333 (1913).

Milano, M. J. and H. L. Pardue, Anal. Chem., 47, 25 (1975).

Miller, J. A., P. Levoir, J. C. Fontaine, F. Garnier, and J. E. Dubois, Anal. Chem., 47, 29 (1975).

Miller, W. G. and R. A. Alberty, J.A.C.S., 80, 5146 (1958).

Morales, M. F. and D. E. Goldman, J.A.C.S., 77, 6069 (1955).

Morrison, Donald F., Multivariate Statistical Methods (McGraw-Hill Book Company, New York, 1967).

P. L. Biochemicals, Inc., Ultraviolet Absorption Spectra of 5'-Ribonucleotides, Circular No. OR-10, Milwaukee, WI (1973).

Papadakis, Nicholas, Ph.D. Thesis, Michigan State University, 1974.

Papadakis, Nicholas, An Interactive Computer Interface for Rapid Scanning Stopped Flow Kinetics, Part II, The Software (unpublished).

Papadakis, N., R.B. Coolen, and J.L. Dye, Anal. Chem., 47, 1644 (1975).

Pietrusko, R., A. Clark, J. M. H. Graves, and H. J. Ringold, B.B.R.C., 23, 526 (1966).

Pietrusko, Regina, and Hugo Theorell, Archives of Biochemistry and Biophysics 131, 288 (1969).

Ritter, G. L., S. R. Lowry, T. L. Isenhour, and C. L. Wilkins, Anal. Chem., 48, 591 (1976).

Rozett, R. W. and E. McL. Petersen, Anal. Chem., 47, 1301 (1975).

Rubinow, S. I. and J. L. Lebowitz, J.A.C.S., 92, 3888 (1970).

Santini, R. E., M. J. Milano, and H. L. Pardue, Anal. Chem., 45, 915A (1973).

Schack, P. and M. F. Dunn, Abstracts 8th Meeting Fed. Eur. Biochem. Soc., #303 (1972).

Schaibly, John H. and Kurt E. Shuler, J. Chem. Phys. 59(8) 3879 (1973).

Shore, Joseph D., Biochemistry, 8(4), 1589 (1969).

Shore, J.D. and H. Gutfreund, Biochemistry, 9(24), 4655 (1970).

Shore, J. D., H. Gutfreund, R. L. Brooks, D. Santiago, and P. Santiago, Biochemistry, 13, No. 20, 4185, (1974).

Shore, Joseph D., and David Santiago, The Journal of Biological Chemistry, 250(6), 2008 (1975).

Suelter, C. H., R. B. Coolen, N. Papadakis, and J. L. Dye, Analytical Biochemistry, 69, 155 (1975).

Sund, H. and H. Theorell, "Alcohol Dehydrogenases", The Enzymes, 2nd ed., Vol. 7, Paul D. Boyer, Henry Lardy, and Karl Mybäck, Eds. (Academic Press, New York, 1960).

Sylvestre, E. A., W. H. Lawton, and M. S. Maggio, Technometrics, 16, 353 (1974).

Theorell, H., Å. Åkeson, B. Liszka-Kopéc, and C. DeZalenski, Archives of Biochemistry and Biophysics, 139, 241 (1970).

Vadasdi, K., J. Phys. Chem., 78, 816 (1974).

Walter, C. and M. F. Morales, J. B. C., 239(4), 1277 (1964).

Walter, C., J. Theoret. Biol., 44, 1 (1974).

Wong, J. Tze-Fei, J.A.C.S., 87, 1788 (1965).